Novel Applications of Surface Based Morphometry and Pattern Classification in Autism Spectrum Disorders

Andrews, Derek Sayre

Awarding institution:
King's College London

Novel Applications of Surface Based Morphometry and Pattern Classification in Autism Spectrum Disorders

Thesis for the Degree of Doctor of Philosophy

by

Derek Sayre Andrews, MSc

Department of Forensic and Neurodevelopmental Sciences
Sackler Institute for Translational Neurodevelopment
Institute of Psychology, Psychiatry, & Neuroscience

Supervised by Prof. Christine Ecker, Dr. Andre Marquand, and Dr. Eileen Daly

2017

Abstract

Autism spectrum disorder (ASD) is a lifelong, behaviorally defined neurodevelopmental condition that is characterized by deficits in social communication, interaction, and repetitive behaviors. These behavioral symptoms are associated with atypical brain structure, function, and connectivity. The studies that comprise this thesis employed structural magnetic resonance imaging (MRI) to address aims in three areas of ASD research. First, we examined a novel neuroimaging feature based on signal intensity contrast between grey and white matter to quantify atypical microstructure at the grey-white matter boundary in ASD. We found reduced tissue contrast at the grey-white matter boundary among adults with ASD when compared typically developing (TD) controls. This result indicates that measures of tissue contrast may serve as an *in vivo* proxy measure of atypical cortical microstructure that has previously been reported in histological studies. Second, we trained multivariate pattern recognition models to identify individuals with ASD based on measures of cortical morphometry, and examined the predictive value of these models in a representative clinical sample. We demonstrated that these models have modest ability to distinguish cases from controls in the research setting. Only one model that was based on measures of grey-white matter tissue contrast identified individuals with and without ASD diagnoses at high overall accuracy (81%) in the clinical setting. However, this model did not provide significant accuracies above chance in the research setting, and therefore these results should be considered as preliminary and suggestive only. Third, we established normative models of phenotypic diversity in brain structure associated with biological sex in a sample of TD males and females which was subsequently applied to males and females with ASD. Across different morphometric features, females with ASD displayed a significant shift towards a more male-typical presentation of the brain. Sample probabilities for ASD also increased with predicted probabilities for male-typical brain phenotypes across both sexes. These studies highlight advances in the field of structural neuroimaging research in areas of feature development, clinical translation, and efforts to understand the modulating role of biological sex on the prevalence of ASD. Taken together, the work presented within this thesis thus constitutes an important step toward establishing translational imaging tools for ASD that may one day be applied in the clinical setting.

Table of Contents

Abstract **2**

Table of Contents **3**

Table of Figures **7**

Table of Tables **9**

Acknowledgments **10**

Declaration of Authorship **11**

Abbreviations **12**

Chapter 1: Introduction **13**
1.1 Autism Spectrum Disorder 13
1.2 Sex Differences in Autism Spectrum Disorder 16
1.3 The Etiology of Autism Spectrum Disorder 18
1.3.1 Environmental Factors *18*
1.3.2 Genetic Factors *19*
1.3.3 Competing Aetiological Theories *20*
1.4 The Structure of the Brain in Autism Spectrum Disorder 22
1.4.1 Volumetric Differences in the Autistic Brain *24*
1.4.2 Cortical Morphometry of the Autistic Brain *25*
1.5 Beyond Group Differences: Pattern Recognition in Autism Spectrum Disorder 31
1.5.1 Multivariate Pattern Classification in Autism Spectrum Disorder *32*
1.5.2 Towards Translational Tools *37*
1.6 The Current Thesis: Aims and Hypotheses 37
1.6.1 Study 1: In Vivo Evidence of Reduced Integrity of the Grey-White Matter Boundary in Autism Spectrum Disorder *37*
1.6.2 Study 2: Clinical Validation of Pattern Classification Models for Autism Spectrum Disorder *38*
1.6.3 Study 3 and 4: Association Between the Probability of Autism Spectrum Disorder and Normative Sex-Related Phenotypic Diversity in Brain Structure *38*
1.7 References 40

Chapter 2: Magnetic Resonance Imaging and Analysis Methods **56**
2.1 Principles of Nuclear Magnetic Resonance 56
2.2 Magnetic Characteristics of Tissue 58
2.3 Magnetic Resonance Images 62
2.3.1 Basic Magnetic Resonance Imaging Pulse Sequences *62*
2.3.2 Spatial Encoding and Image Reconstruction of Magnetic Resonance Signal *65*
2.4 Driven Equilibrium Single Pulse Observation of T_1 and T_2 Mapping 66
2.5 Cortical Surface Reconstruction using Freesurfer Software 67
2.6 Mass Univariate Magnetic Resonance Imaging Analyses 70
2.6.1 The General Linear Model *70*
2.6.2 Correcting for Multiple Comparisons *73*
2.7 Multivariate Pattern Classification 74
2.7.1 The Support Vector Machine *76*
2.7.2 Gaussian Process Classifiers *79*
2.7.3 Model Performance and Validation for Multivariate Pattern Classification *85*
2.7.4 Feature Extraction and Selection *86*
2.7.5 Model Visualization *88*
2.8 References 90

Chapter 3: Grey to White Matter Percent Contrast as an in vivo Neuroimaging Feature in Autism Spectrum Disorder 94
3.1 Title/Authors 97
3.2 Abstract 97
3.3 Introduction 97
3.4 Materials and Methods 97
3.4.1 Participants 97
3.4.2 Structural MRI Data Acquisition 98
3.4.3 Cortical Reconstruction using FreeSurfer 98
3.4.4 Grey to White Matter Percent Contrast (GWPC) and Grey Matter Signal Intensity Measures 98
3.4.5 Statistical Analysis 99
3.5 Results 99
3.5.1 Particpant Demographics and Global Brain Measures 99
3.5.2 Between-Group Differeces in GWPC Across the Cortex 99
3.5.3 Between-Group Differences in Grey and White Matter tissue intensities 100
3.5.4 Main Effects of Sex and Group by Sex Interactions 101
3.6 Discussion 103
3.7 Funding/Notes 105
3.8 References 105

Chapter 4: Clinical Testing of Multivariate Pattern Classification Models for Autism Spectrum Disorder 106
4.1 Introduction 106
4.2 Methods 108
4.2.2 Clinical Group Demographics 109
4.2.3 MRI Data Acquisition: 110
4.2.4 Cortical Surface Reconstruction 111
4.2.5 Pattern Classification 111
4.2.6 Classification Using Feature Selection 113
4.3 Results 114
4.3.1 Classification of ASD and TD individuals in the research sample 114
4.3.2 Predicting ASD Diagnosis within Clinical Sample 119
4.4 Discussion 121
4.5 Conclusions 125
References 126

Chapter 5: Association Between the Probability of Autism Spectrum Disorder and Normative Sex-Related Phenotypic Diversity in Brain Structure 128
5.1 Title/Authors 132
5.2 Abstract 132
5.3 Introduction 133
5.4 Methods 133
5.4.1 Participants 133
5.4.2 MRI Data Acquisition 133
5.4.3 Cortical Reconstruction using FreeSurfer 134
5.4.4 Gaussian Process Classification 134
5.4.5 Estimation of ASD Probability 135
5.4.5 Vertexwise Between-Groups Comparision of Cortical Thickness 135
5.5 Results 135
5.5.1 Predicition of Biological Sex Based on Normative Variance in Cortical Thickness 135
5.5.2 Phenotypic Prediction of Biological Sex for Individuals with ASD 135

5.5.3 ASD Probability as a Function of Normative Sex-Related Phenotypic Variance in Brain Structure *135*
5.5.4 Biological Sex Significantly Modulates the Cortical Anatomy of ASD *136*
5.6 Discussion 137
5.7 Conclusion 139
5.8 Article Information 139
5.9 References 140

Chapter 6: Normative Sex-Related Phenotypic Diversity Across Multiple Measures of Brain Anatomy is Associated with Probability for Autism Spectrum Disorder . 139
6.1 Abstract 142
6.2 Introduction 143
6.3 Methods 148
6.3.1 Participants *148*
6.3.2 Structural MRI Data Acquisition *147*
6.3.3 Cortical Reconstruction using FreeSurfer *147*
6.3.4 Gaussian Process Classification *148*
6.3.5 Estimating ASD Probability *149*
6.3.6 Vertex-wise between-group comparison of cortical measures *150*
6.4 Results 154
6.4.1 Participant Demographics and Global Brain Measures *150*
6.4.2 Prediction of Biological Sex Based on Normative Variability in Cortical Morphometry *151*
6.4.3 Prediction of Biological Sex Among Individuals with ASD *153*
6.4.4 ASD Probability as a Function of Normative Sex Variability in Cortical Morphometry *153*
6.4.5 Cortical Morphometry in ASD is Modulated by Biological Sex *156*
6.5 Discussion 158
6.6 Conclusions 161
6.7 References 162
6.7 Acknowledgements: 165
6.8 Funding: 165
6.9 Statement of Disclosure: 166

Chapter 7: General Discussion 167
7.1 Summary and Key Findings 167
7.1.1 Study 1: Tissue Contrast as a Novel Imaging Marker in Autism Spectrum Disorder *167*
7.1.2 Study 2: Clinical Validation of Multivariate Pattern Classification Models for Autism Spectrum Disorder *168*
7.1.3 Studies 3 and 4: Association of Normative Sex-Related Phenotypic Diversity in Brain Structure with Probability for Autism Spectrum Disorder *169*
7.2 Discussion 170
7.2.1 The Development of Imaging Features for Autism Spectrum Disorders *170*
7.2.2 The Development of Diagnostic Imaging Tools for Autism Spectrum Disorder *172*
7.2.3 Neuro-Diversity Associated with Biological Sex and Probability for Autism Spectrum Disorder *173*
7.3 Strengths of the Current Studies 174
7.4 Limitations 175
7.5 Future Directions 176
7.5.1 Large Scale Studies and Heterogeneity *176*
7.5.2 Development and Implementation of Multi-Modal Methods *177*
7.5.3 Linking Imaging with Biology *177*

7.5 Conclusion 178
7.6 References 179
Appendix I: ICD-10 Criteria for "Childhood Autism" 182
Appendix II: Chapter 3 Supplementary Materials 184
Appendix III: Chapter 5 Supplementary Materials 193
Appendix IV: Chapter 6 Supplementary Materials 217
Appendix V: Chapter 6 Manuscript Proof 224

Table of Figures

Figure 1.1, The Autism Spectrum 14
Figure 1.2 Multifactorial Liability Model of Autism Spectrum Disorder 17
Figure 1.3, Brain Regions Indicated in Autism Spectrum Disorder 23
Figure 1.4, Development of the Human Cerebral Cortex. 26

Figure 2.1, Interactions between RF Energy and Magnetic Nuclei in a Magnetic Field. 59
Figure 2.2, Longitudinal Magnetization. 60
Figure 2.3, Transverse Magnetization. 61
Figure 2.4, Development of T_1 Contrast between Two Tissues. 62
Figure 2.5, Development of Image Contrast in a Spin-Echo Sequence. 64
Figure 2.6, Development of T_1 Contrast in an Inversion Recovery Sequence. 65
Figure 2.7, The Support Vector Machine 77
Figure 2.8, The Gaussian Process in a One Dimensional Regression Problem 82
Figure 2.9, The Gaussian Process Classifier 83
Figure 2.10, Nested Parameter Tuning via Cross Validation 89

Figure 3.1, Grey and White Matter Signal Intensity Sampling Procedure 100
Figure 3.2, Regions of Decreased Grey-to-White Matter Signal Intensity Percent Contrast in ASD. 101
Figure 3.3, Regional Differences in Grey and White Matter Signal Intensities in ASD. 103

Figure 4.1 Support Vector Machine Predictions Within the Training Set 117
Figure 4.2 Gaussian Process Classification Predictions within the Training Set 118
Figure 4.3 Support Vector Machine Predictions within the Training Set using GLM based Feature Selection 119
Figure 4..4, Gaussian Process Classification Predictions within the Training Set using GLM based Feature Selection 120
Figure 4.5, Support Vector Machine Predictions within the Testing Set 121
Figure 4.6, Gaussian Process Classification Predictions within the Testing Set. 122
Figure 4.7, Gaussian Process Classification Predictions within the Testing Set using measures of Tissue Contrast and GLM based Feature Selection 123
Figure 4.8, Accuracy as a Function of Number of Included Patients in the Classification of Psychiatric and Neurodevelopmental Conditions 123

Figure 5.1, Gaussian Process Classification of Biological Sex 136
Figure 5.2, Regions of Decreased Grey-to-White Matter Signal Intensity Percent Contrast in ASD. 137
Figure 5.3, Regional Differences in Grey and White Matter Signal Intensities in ASD. 138

Figure 6.1, Gaussian Process Classification of Biological Sex 155
Figure 6.2, Probability for ASD as a Function of Normative Sex-Related Phenotypic Variance in Brain Morphology. 157
Figure 6.3, Prediction Maps for High and Low ASD Probability Males and Females 158

Figure 6.4, Group by Sex Interaction Effects in Cortical Morphometry. 160

Table of Tables

Table 1.1, Multivariate Pattern Classification Studies of Autism Spectrum Disorder 34

Table 3.1, Participant Demographics 99
Table 3.2, Clusters of Significant Reductions in Grey White Matter Percent Contrast and Increases in Grey Matter Intensity in ASD 102

Table 4.1, Participant Demographics (Research Sample) 111
Table 4.2, Participant Demographics (Clinical Sample) 112
Table 4.3, Classification Accuracies within Subgroups of the Clinical Sample ... 122

Table 5.1, Participant Demographics 134

Table 6.1, Participant Demographics and Global Brain Measures 149

Acknowledgments

I would first like to acknowledge the invaluable contribution of each of my supervisors. Professor Christine Ecker, Dr Andre Marquand, and Dr Eileen Daly have each offered exceptional guidance and imparted invaluable wisdom throughout this PhD project. I would also like to acknowledge and thank Professor Declan Murphy for lending his expertise to this project.

Additional thanks to my fourth supervisor Dr. Maria Rosá for her input during the early stages of this PhD, the co-authors who contributed to the published works in this thesis, Leon Aksman for sharing his MATLAB and machine learning skills, all my colleagues and friends who contributed in various ways, including; Parker, Rob, James, Maria, Rich, Anna, Jamie, Andreina, Charlotte, Gráinne, Jonny, Brenda, Mick, Daniel and Vincent. And all those who provided logistical support throughout this project. Foremost, our incredible business manager Harriet Meteyard as well as the members of the educational support office.

I would like to thank those organizations who provided funding for this project: the National Institute for Health Research Biomedical Research Centre, the UK Medical Research Council, the Innovative Medicines Initiative Joint Undertaking, Autism Speaks, and the Sackler foundation.

A very special thank you to Erica, who was by my side while writing this thesis and has been a consistent source of reassurance and unconditional support.

I must also thank all the members of my family who showed me their love and support throughout this project, including; Mimi who supervised my first scientific experiments, Constance for being an inspiration, Larry whose life long calculator continues its service, and most of all my parents, Karen and Stuart, who have given me every opportunity to pursue my dreams.

Lastly, I would like to give the deepest thanks to all the participants and families who took part in this research.

Declaration of Authorship

I, Derek Andrews, declare that this thesis and the work presented in it are my own and have been generated by me as the result of my own original research.

I confirm that:

1. This work was done wholly or mainly while in candidature for a research degree at King's College London;
2. Where I have consulted the published work of others, this is always clearly attributed;
3. Where I have quoted from the work of others, the source is always given.;
4. I have acknowledged all main sources of help;
5. Parts of this work have been published or are currently in submission as: [see list references below]. In cases where I was not lead author my contribution to the work has been detailed.

Signed: 

Date: June 21st, 2017

Andrews, D., Avino, T., Gudbrandsen, M., Daly, E., Marquand, A., Murphy, C., Lai, MC., Lombardo, M, Ruigrok, A, Williams, S., Bullmore, E., MRC AIMS Consortium, Suckling J., Baron-Cohen S., Craig M., Murphy D. and Ecker C. 2017. In Vivo Evidence of Reduced Integrity of the Gray–White Matter Boundary in Autism Spectrum Disorder. *Cerebral Cortex* 2017; 27 (2): 877-887

Ecker C., Andrews D., Gudbrandsen C., Marquand A., Ginestet C., Daly E., Murphy C., Lai M., Lombardo M., Ruigrok A., Bullmore E., Suckling J., Williams S., Baron-Cohen S., Craig M., Murphy D., MRC AIMS Consortium. Association Between the Probability of Autism Spectrum Disorder and Normative Sex-Related Phenotypic Diversity in Brain Structure. *JAMA Psychiatry.* 2017;74(4):329-338

Andrews D., Marquand A., Ginestet C., Gudbrandsen C., Daly E., Murphy C., Lai M., Lombardo M., Ruigrok A., Bullmore E., Suckling J., Williams S., Baron-Cohen S., MRC AIMS Consortium, Craig M., Murphy D., Ecker C., Normative Sex-Related Phenotypic Diversity Across Multiple Measures of Brain Anatomy is Associated with Probability for Autism Spectrum Disorder: *American Journal of Psychiatry*: (In Submission)

Abbreviations

ADD: Attention-Deficit Disorder
ADI: Autism Diagnostic Interview
ADOS: Autism Diagnostic Observation Schedule
ADHD: Attention-deficit hyperactivity disorder
ASD: Autism Spectrum Disorder
CT: Cortical Thickness
CURV: Mean radian curvature
CV: Cross Validation
DSM: Diagnostic and Statistical Manual for Mental Disorders
DTI: Diffusion Tensor Imaging
FA: Fractional anisotropy
fMRI: Functional Magnetic Resonance Imaging
FWHM: Full width at half maximum
GLM: General linear model
GM: Grey Matter
GP: Gaussian Process
GPC: Gaussian Process Classification
GWR: Grey:White Matter signal contrast ratio
GWP: Grey:White Matter percent contrast
ICD: International Statistical Classification of Diseases
iPSCs: induced pluripotent stem cells
JACOB: jacobian metric distortion
lGI: Local gyrification index
LOO-CV: Leave one out cross validation
MD: Mean Diffusivity
MMR: Measles Mumps & Rubella
MRI: Magnetic Resonance Imaging
MRS: Magnetic Resonance Spectroscopy
MVPC: Multivariate pattern classification
OCD: Obsessive-compulsive disorder
ODD: Oppositional defiant disorder
RFT: Random Field Theory
ROI: Region of interest
rsMRI: Resting state Magnetic resonance imaging
SA: Surface Area
SBM: Surface Based Morphometry
SE: Sensitivity
SP: Specificity
sMRI: Structural Magnetic Resonance Imaging
SULC: Sulcal depth
SVM: Support Vector machine
TD: Typically Developing
VBM: Voxel Based Morphometry
WM: White Matter

Chapter 1: Introduction

Autism spectrum disorder (ASD) is a complex neurodevelopmental condition. While progress continues to be made in understanding the neurological origins of ASD the underlying neurodevelopmental mechanisms and biological markers of the condition remain unclear. The broad aim of this thesis is to advance our knowledge of ASD in a way that offers real world translational benefits to patients through applications of structural brain imaging. More specifically the studies that compose this work focus on *i*) novel ways to measure atypical brain structure in ASD, *ii*) testing the efficacy of measures of brain structure to identify ASD within the clinic, and *iii*) examining how biological sex/gender may modulate risk for the condition.

I begin this introductory chapter by introducing the behavioral ASD phenotype and associated diagnostic criteria. The role of biological sex/gender in ASD will then be discussed followed by current etiological theories for the condition. I will then discuss evidence for atypical brain structure in ASD with a focus on cortical magnetic resonance imaging (MRI) findings and review studies that apply particular types of 'machine learning' methods to classify ASD using MRI scans. Lastly, I will outline the aims of the three studies, which compose the body of this thesis.

1.1 Autism Spectrum Disorder

Autism spectrum disorder (ASD) is a lifelong behaviorally defined neurodevelopmental condition characterized by deficits in social interaction and communication in addition to the presentation of repetitive and/or restricted behaviors (World Health Organization, 2004). The earliest reports of the ASD phenotype are attributed to Kanner (1943) and Asperger (1944). In these foundational works Kanner and Asperger both detail case studies of children in which typical autistic behaviors are observed. By definition ASD is phenotypically heterogeneous, encapsulating a spectrum of individuals whose behavioral deficits range from severe impairment (e.g. learning disability, non-verbal) to high functioning (e.g. average or above average IQ, relatively minor impairments to social communication) (Wing, 1997). In addition to the core features, individuals with ASD experience high rates of comorbidity with other psychiatric and medical conditions including; social anxiety disorder, attention-deficit disorder (ADD), attention-deficit hyperactivity disorder (ADHD), oppositional defiant disorder (ODD), obsessive-compulsive disorder (OCD), specific phobia,

gastrointestinal problems, and epilepsy (Simonoff et al., 2008, Leyfer et al., 2006, Amiet et al., 2008) (Figure 1.1).

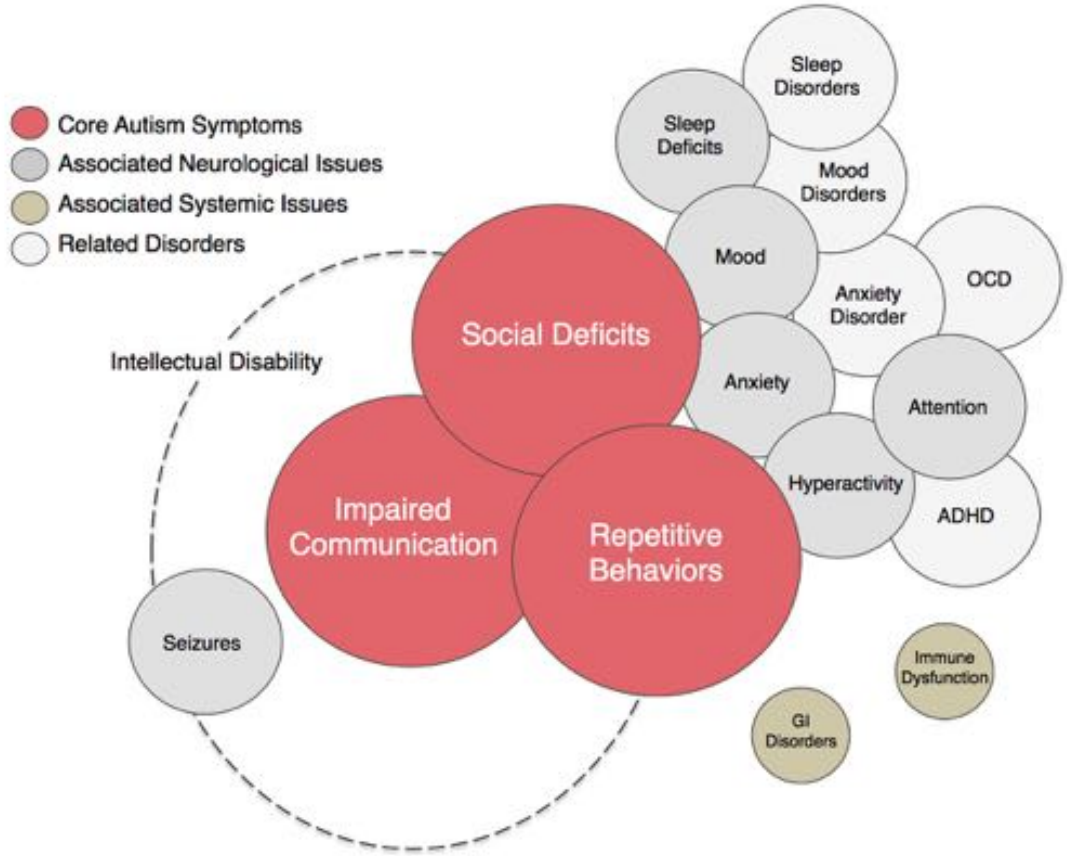

Figure 1.1, The Autism Spectrum (*autismspeaks*): Autism Spectrum Disorder (ASD) is defined by core symptoms (red circles). However, the condition is often accompanied by several associated neurological (dark grey circles) and systemic (gold circles) issues. Individuals with ASD also experience increased rates of related comorbid disorders (light grey circles) and intellectual disability (dotted line).

Large population studies carried out around the globe report ASD prevalence to range from 0.5% to 2% in the general population. Over the past few decades it has been widely speculated that ASD prevalence is increasing. However, empirical evidence suggests that these increases can largely be attributed to growing awareness of the condition and greater accessibility of diagnostic services (Mazumdar et al., 2013, Hansen et al., 2015).

As a behaviorally defined disorder the diagnosis of ASD is reliant on parental interviews and/or assessments and observations of patient's behaviors. A clinical ASD diagnosis can be granted by meeting the diagnostic criteria outlined in the

Diagnostic and Statistical Manual of Mental Disorders (DSM V) (American Psychiatric Association, 2013) or the *International Statistical Classification of Diseases, 10th Revision* (ICD-10) (World Health Organization, 2004), which is the standard criteria used within the United Kingdom. To reach a diagnosis for "childhood autism" under the ICD-10 atypical or impaired development in at least one of the following categories must be evident before the age of three years; *i*) "receptive or expressive language as used in social communication", *ii*) "the development of selective social attachments or of reciprocal social interactions", and *iii*) "functional or symbolic play". Furthermore, individuals must display at least six symptoms associated with ASD, with at least one of these falling under each of the categories of *i*) reciprocal social interaction, *ii*) qualitative abnormalities in communication, *iii*) and restricted, repetitive, and stereotyped patterns of behavior, interests, or activities. Lastly, the clinical phenotype must not be attributable to another pervasive developmental disorder or condition. Full ICD-10 criteria for childhood ASD are provided in Appendix I.

The clinical diagnostic criterion outlined by the ICD-10 encompasses significant phenotypic heterogeneity. While there is extensive evidence to suggest that ASD is associated with several genetic and neurobiological markers (Ruggeri et al., 2013, Ecker and Murphy, 2014) currently there are no reliable diagnostic biomarkers validated for clinical use in the condition. Therefore, two 'gold-standard' assessment tools may be used as additional confirmation of a diagnosis of ASD, namely the *Autism Diagnostic Interview-Revised* (ADI-R) (Lord et al., 1994) and *Autism Diagnostic Observation Schedule* (ADOS) (Lord et al., 2000). Both these measures require administration by an experienced clinical interviewer.

The ADI-R is a clinical structured caregiver interview appropriate for children and adults with a mental age of 18 or more months. The ADI-R provides a diagnostic algorithm for ASD as described by the ICD-10 and focuses on probing behaviors in the three main symptom areas of social interaction, communication, and repetitive/restricted behaviors. The 93-item interview covers the patient's full developmental history, and usual lasts 1-2 hours. Questions focus on current behavior as well as a period between the ages of 4 and 5 years when several behaviors associated with ASD are likely to be most evident. Exceptions to this are questions

regarding group play (4-10 years), reciprocal friendships (5+ years), and circumscribed interests (3+ years) that are appropriate only for particular ages. As ASD is a lifelong neurodevelopmental condition, meeting ADI-R criteria for a diagnosis is key for establishing a childhood origin of ASD, particularly in diagnoses of adults on the spectrum.

In contrast to the ADI-R, the ADOS involves a series of semi-structured assessments of communication, social interaction, play and/or imaginative thinking scenarios conducted with the patient. Four modules of the ADOS are available to allow for administration across the spectrum of impairment observed in ASD. The choice of module depends on the individual's competency in using phrase speech (i.e. non-echoed, meaningful word combinations that are spontaneous, contain at least three words, and sometimes a verb), verbal fluency, and age. As the ADOS is used to assess current symptom presentation it is considered a gold standard metric not only for diagnosis but also for quantification of current ASD symptoms.

1.2 Sex Differences in Autism Spectrum Disorder

Of significant note is the preponderance of males with ASD. Based on large-scale population studies conducted around the globe currently it is estimated that ASD is 2-5 times more prevalent in males than females (Lai et al., 2017). This male bias in ASD diagnoses may partly be related to differences in the ASD phenotype in females who have been shown to display less severe impairments in the repetitive behaviors domain and improved skills in coping with social deficits (Szatmari et al., 2012, Mandy et al., 2012). Such phenotypic differences between males and females with ASD have likely contributed to the historical view of ASD as a 'male condition' and subsequent under diagnosis of females on the spectrum.

However, as awareness of females with ASD increases population studies continue to show a male bias in prevalence, albeit in a lower range of 1.7-2.5 males for every 1 female with the condition (Kim et al., 2011, Mattila et al., 2011, Idring et al., 2012). This indicates that in addition to male biased diagnostic criteria and tools, sex differentiated developmental processes may have a modulating effect on the risk for ASD. For example, multifactorial liability models propose that liability for ASD is

distributed throughout the population with males and females experiencing different liability thresholds for the development of ASD (Werling and Geschwind, 2013) (Figure 1.2).

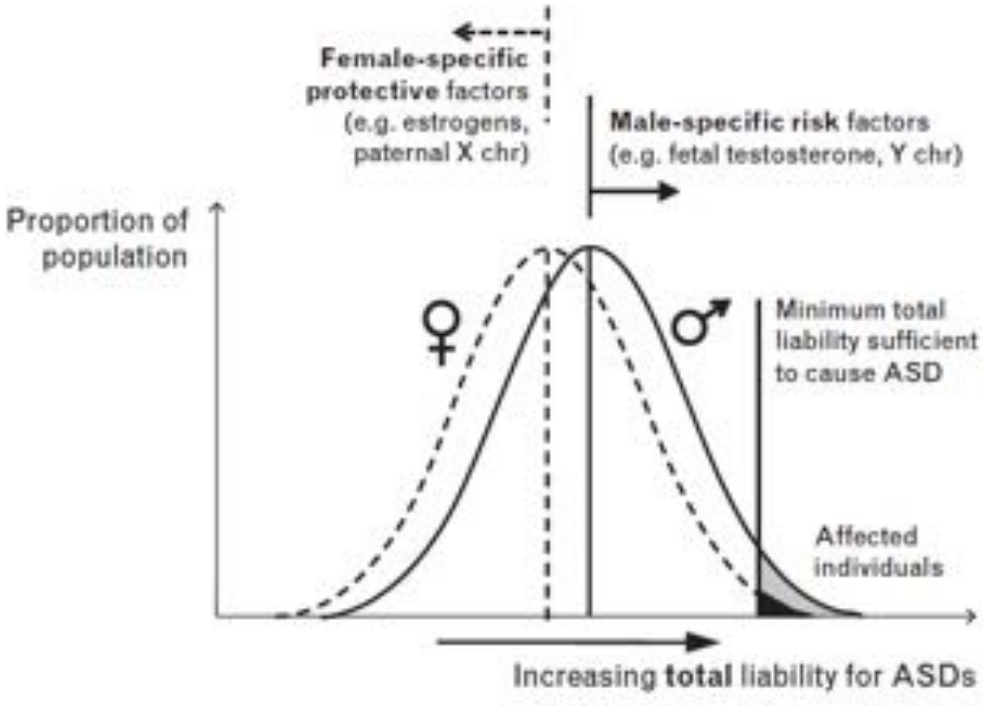

Figure 1.2 Multifactorial Liability Model of Autism Spectrum Disorder (Werling and Geschwind, 2013, Reich et al., 1975): Within this model liability for ASD is distributed throughout the population. However female specific 'protective factors' shift liability away from and male-specific 'risk factors' towards the minimum total liability needed for an individual to develop ASD.

Multifactorial liability models of ASD propose so-called 'male risk' and/or 'female protective' factors inherent to the sexes that shift liability toward or away the minimum liability threshold required for an ASD phenotype to manifest. Genetic studies have provided some evidence for a 'female protective effect' reporting increased genetic load for ASD risk genes among siblings of females with the condition than siblings of males with ASD (reviewed in (Werling, 2016)). Beyond well-established findings of increased brain size in males (Voigt & Pakkenburg, 1983), there is growing evidence that sex differences in brain structure exist (Jahanshad & Thompson, 2017). Several of these differences have been identified in brain regions indicated in ASD (for review see (Ruigrok et al., 2014)) suggesting diversity in brain structure associated with sex may modulate ASD risk. However, to date the role of sex differences in ASD liability has been largely understudied. Thus,

while there is some evidence that suggests differences between the sexes in both ASD clinical and biological phenotypes (Lai et al., 2017, Werling 2016), much work remains in understanding the role of sex related risk factors in ASD.

1.3 The Etiology of Autism Spectrum Disorder

Postmortem evidence indicates that ASD pathology is likely to first manifest during the early prenatal stages of development (Bauman and Kemper, 2005). For example, reduced numbers of cerebellar Purkinje cells have been observed in both childhood and adult ASD cases (Bailey et al., 1998, Duong et al., 1986, Arin et al., 1991). During fetal development axons climbing from the inferior olive region of the brainstem synapse with Purkinje cell dendrites within a transitory zone beneath the Purkinje cells known as the lamina dessicans (Rakic, 1971). Within human fetuses the lamina dessicans is no longer present after 28-30 weeks gestation (Rakic and Sidman, 1970). After this time, due to the strong connective relationship between Purkinje cells and olivary neurons, loss or damage to Purkinje cells causes retrograde losses of olivary neurons (Norman, 1940, Holmes and Stewart, 1908, Greenfield and Aring, 1954). Thus, findings of reduced Purkinje cells with persevered olivary neurons within ASD cases indicate that the development of ASD pathology occurs at some time prior to the resolution of the lamina dessicans at 28-30 weeks gestation.

Consensus thinking recognizes the role of complex interactions between several possible genetic, epigenetic, and environmental risk factors in the development and manifestation of an ASD phenotype (Sandin et al., 2014). It would be beyond the scope of this thesis to discuss all of these factors in detail. Here I will briefly highlight a selection of some of the factors known to be associated with increased risk for the development of ASD followed by a discussion of current etiological theory.

1.3.1 Environmental Factors

Various environmental factors have been implicated in ASD. Of these the most widely discussed is the idea that vaccinations (particularly the measles, mumps, and rubella [MMR] vaccination) cause ASD. Despite the large amount of attention paid to this potential relationship there is no empirical evidence that strongly supports this claim. In fact a large body of evidence shows no relationship between MMR

vaccination and increased risk for ASD (DeStefano et al., 2004, DeStefano et al., 2013, Smith and Woods, 2010, Klein et al., 2011, Klein et al., 2012, Klein and Diehl, 2004, Peltola et al., 1998, Taylor et al., 1999, Taylor et al., 2002, Kaye et al., 2001, Black et al., 2002, Farrington et al., 2001, Dales et al., 2001, Davis et al., 2001, Fombonne and Chakrabarti, 2001, Nejad et al., 2012, Lingam et al., 2003, Smeeth et al., 2004, Chen et al., 2004, Honda et al., 2005, Richler et al., 2006, Fombonne et al., 2006, D'Souza et al., 2006, Uchiyama et al., 2007, Baird et al., 2008, Hornig et al., 2008). Similar evidence refutes a relationship between thimerosal (a preservative historically used in vaccines) and ASD (Hviid et al., 2003, Jacquemont et al., 2006, Madsen et al., 2003, Stehr-Green et al., 2003, Andrews et al., 2004, Fombonne et al., 2006, Thompson et al., 2007, Pichichero et al., 2008, Schechter and Grether, 2008, Price et al., 2010, Mrozek-Budzyn et al., 2010). Taken together this evidence overwhelmingly suggests that childhood vaccinations do not lead to ASD.

Some environmental factors that have been associated with increased risk for ASD include; parental age (Gardener et al., 2009), low birth weight (Schendel and Bhasin, 2008), multiple births (Croen et al., 2002), maternal infections and illness during pregnancy (Sandin et al., 2014, Lichtenstein et al., 2010, Hallmayer et al., 2011a, Atladóttir et al., 2010, Lee et al., 2015) and exposure to toxins (Adams et al., 2009). However, each of these factors taken in isolation accounts for only a small minority of total ASD cases.

1.3.2 Genetic Factors

The role of genetics in ASD susceptibility has been highlighted by studies showing an increased recurrence risk of up to 20% in families with a child with ASD (Ozonoff et al., 2011). Early twin studies showed ASD to be a highly heritable condition with concordance rates of 82-92% amongst monozygotic twins compared to 1-10% in dizygotic twins (Bailey et al., 1995, Folstein and Rutter, 1977), although a more recent study revealed higher concordance rates (>20%) among dizygotic twins (Hallmayer et al., 2011b).

While there is a consensus that genetic factors contribute to ASD, extensive heterogeneity exists in the specific genetic pathways leading to the development of the condition. For example, in ~10% of ASD cases specific genetic conditions (e.g.

fragile X syndrome, Rett syndrome, 22q-11 deletion disorder etc.) can be identified (Tammimies et al., 2015, Carter and Scherer, 2013). These cases where ASD is a secondary diagnosis to a known genetic condition are referred to as 'syndromic' autism (as opposed to 'idiopathic' autism). Within ~10-20% of the ASD population chromosomal rearrangements as well as rare and de novo copy-number variants can be observed compared to 1-2% in the general population (Jacquemont et al., 2006, Sebat et al., 2007). Additionally significant increases in rare and de novo coding sequence mutations affecting neuronal genes have been observed in ASD and could account for approximately 5-10% of cases (Huguet et al., 2013). Several risk genes for ASD have only recently been identified (C Yuen et al., 2017) and add to the over 850 genes currently implicated in ASD (sfari.org/resources/sfari-gene). These genes largely focus around processes that effect neurogenesis and neuronal and synaptic homeostasis such as chromatin remodeling, metabolism, mRNA translation, and synaptic functioning (Huguet et al., 2013, Packer, 2016). However, much like known environment risk factors, each of these specific risk genes in isolation is more than likely to confer a small amount of risk for ASD and therefore account for a small proportion of cases within the total population.

1.3.3 Competing Aetiological Theories

1.3.3.1 The "Autisms"

The complex heterogeneity of ASD phenotypes and genotypes has led to competing aetiological theories for the condition. On one hand, it has been proposed that ASD is actually comprised of several disorders that are individually rare each having its own aetiology. This concept of ASD as the "Autisms" helps explain the heterogeneity of the condition in terms of both behavioral manifestation and apparent underlying casual mechanisms (Geschwind and Levitt, 2007).

1.3.3.2 Unitary Theory

Another contrasting view is that ASD is a unitary disorder resulting from a common cause. Support for this theory is hindered due to a failure to identify a common causal mechanism for ASD, the observed heterogeneity of the condition, and the ever-increasing list of environmental and genetic risk factors (Boucher, 2011). However, recently it has been proposed that ASD may arise from the single pathophysiological

mechanism, namely heterochronic division of germinal cells during early development leading to subsequent neural migration abnormalities (Casanova, 2014, Packer, 2016). Under this unitary theory differences in individual ASD phenotypes can be explained by the severity and nature of the initial triggering exogenous factor, differences in the neurodevelopmental period which the insult was experienced, and the genetic susceptibility of the patient (Casanova, 2007).

1.3.3.3 Atypical Brain Connectivity

A widely accepted hypothesis that accommodates both the "Autisms" and unitary aetiological theories attributes ASD behaviors to aberrant brain connectivity (Belmonte et al., 2004). Under this view atypical neural connectivity is described in two key facets, namely local over connectivity (i.e. within brain regions) and long-range under connectivity (i.e. between brain regions). Behaviorally, aspects of the ASD phenotype such as hyper-arousal, reduced selectivity, and increased computational noise have been linked to possible local over connectivity (Belmonte and Yurgelun-Todd, 2003). Respectively, under connectivity between distant cortical regions may explain deficits in information integration observed in the condition (i.e. weak "central coherence") (Geschwind and Levitt, 2007, Frith, 2004, Just et al., 2012).

Evidence for atypical connectivity in ASD has been provided by both postmortem and *in vivo* studies. For example, reports of increased neuronal dendritic spine counts in ASD (Tang et al., 2014, Hutsler and Zhang, 2010) are suggestive of excessive local connectivity in the condition. Structural imaging results also show reduced intrinsic wiring costs within cortical grey matter in ASD (Ecker et al., 2013b) that may represent a bias towards local over global information processing (Happé and Frith, 2006).

Poor connectivity between brain regions in ASD is supported by functional magnetic resonance imaging (fMRI) findings of lower degrees of synchronization across cortical networks responsible for language processing and executive functioning (Just et al., 2007, Just et al., 2004). Other studies of under connectivity have focused on white matter deficits, particularly in the corpus callosum due to its role in providing

long range connections between the brain's two hemispheres and potential mediation of inter-regional cortical synchronization (Uhlhaas et al., 2009). Within ASD, diffusion-imaging measures of lower fractional anisotropy and increased radial diffusivity in the corpus callosum have been reported (Alexander et al., 2007, Barnea-Goraly et al., 2004, Shukla et al., 2010). Studies using magnetic transfer imaging have also reported atypical myelin development in the structure (Gozzi et al., 2012). These results likely reflect underlying changes in myelination, density, and size of axons within the tract (Hong et al., 2011) which are likely to adversely affect long range connectivity in the ASD brain. Additional ways that atypical cortical structure observed in ASD might affect brain connectivity are discussed in section 1.4.2.

1.4 The Structure of the Brain in Autism Spectrum Disorder

Indications of abnormalities in the neuroanatomical structure of the autistic brain arose from some of the first documented observations of the condition, where Kanner (1943) noted ASD patients to have significantly larger head size than typically developing (TD) individuals. Since these early observations several different research techniques have been applied in order to better understand atypical neuroanatomical structure in ASD (Ecker and Murphy, 2014). These studies have led to the identification of several brain regions indicated in ASD behaviors (Figure 1.3).

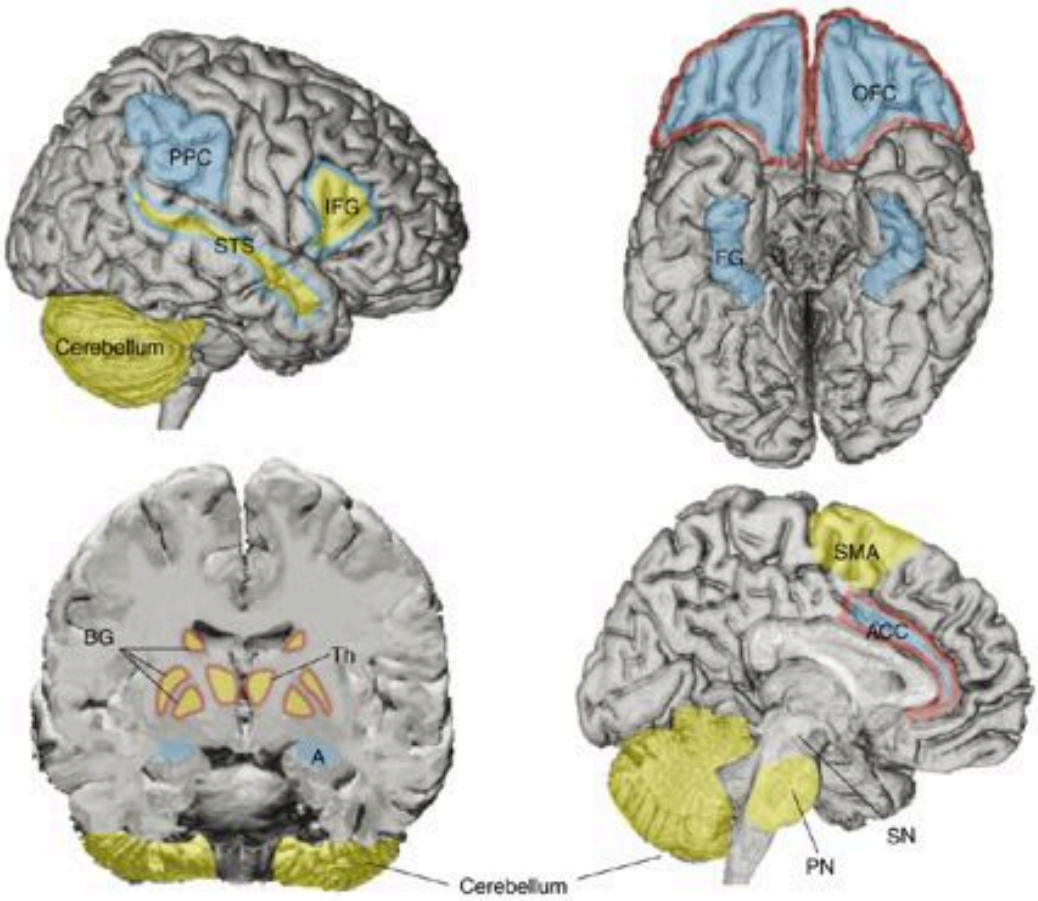

Social impairment	Communication deficits	Repetitive behaviors
OFC – Orbitofrontal cortex ACC – Anterior cingulate cortex FG – Fusiform gyrus STS – Superior temporal sulcus A – Amygdala mirror neuron regions IFG – Inferior frontal gyrus PPC – Posterior parietal cortex	IFG- Inferior frontal gyrus (Broca's area) STS – Superior temporal sulcus SMA – Supplementary motor area BG – Basal ganglia SN – Substantia nigra Th – Thalamus PN – Pontine nuclei cerebellum	OFC – Orbitofrontal cortex ACC – Anterior cingulate cortex BG – Basal ganglia Th – Thalamus

Figure 1.3, Brain Regions Indicated in Autism Spectrum Disorder (Amaral et al., 2008): Brain regions indicated in social (blue), communication (yellow), and repetitive and restricted behaviors (red) domains are highlighted.

This thesis focuses on applications of structural magnetic resonance imaging (MRI) methods, namely surface based morphometry (SBM) in order to *i*) identify novel ways to measure atypical brain structure in ASD, *ii*) test the efficacy of measures of brain structure to identify ASD within clinical samples, and *iii*) examining how normative variance in SBM measures associated with biological sex are associated with risk for the condition. Accordingly, the focus of this section will be a review of *in vivo* structural neuroimaging studies of the brain in ASD with a focus on SBM studies cortical structure.

1.4.1 Volumetric Differences in the Autistic Brain

Consistent with early observations (Kanner, 1943), findings of increased global brain size in ASD, particularly among younger patients, remains one of the most widely reported and cited neuroanatomical findings in the condition. Some of the first MRI studies in ASD showed patients to have significantly larger mid-sagittal brain areas apposed to healthy controls (Piven et al., 1992, Piven et al., 1996). Furthermore, it was revealed that these increases were not gross in nature, but rather differed between the frontal, temporal, parietal, and occipital lobes (Piven et al., 1996, Piven et al., 1995). In line with these MRI studies, findings using measures of head circumference have shown ASD patients to have higher rates of macrocephaly than the general population (Davidovitch et al., 1996, Woodhouse et al., 1996, Fidler et al., 2000, Miles et al., 2000, Dementieva et al., 2005).

Current evidence shows the ASD brain to have a nonlinear growth trajectory that when compared to TD controls experiences periods of precocious growth during the first few years of life, which are then followed by a deceleration leading to harder to distinguish differences in adolescence and later adulthood (Courchesne et al., 2011a). These early increases in brain volumes among young children with ASD appear to have an anterior to posterior growth gradient (Courchesne et al., 2004) showing the greatest GM differences in the frontal and temporal lobes (Carper et al., 2002). There is also some preliminary evidence to suggest that the observed enlargements in brain volumes in young children with ASD are driven by disproportional increases in WM compared to GM (Courchesne et al., 2001, Hazlett et al., 2005, Ben Bashat et al., 2007), yet it remains unclear if these WM increases persist into later life (Palmen et al., 2005, Hazlett et al., 2006, Barnea-Goraly et al., 2004). Furthermore, in line with the heterogeneous nature of the condition, recent evidence suggests that brain overgrowth in ASD may be specific to a subset of the ASD population (Libero et al., 2016).

Several MRI studies have used voxel based morphometry (VBM) methods (Ashburner and Friston, 2000) to explore regional differences in brain volumes (Nickl‐Jockschat et al., 2012). While these studies are largely consistent in reporting distributed patterns of volumetric differences in ASD (Ecker et al., 2012, Hyde et al.,

2010, McAlonan et al., 2005) they often differ on specific brain regions identified as well as the directionality of their findings. Some limitations common to all imaging studies of ASD contribute to the lack of replicability of VBM findings. These include *i*) heterogeneity of ASD phenotypes and genotypes *ii*) non linear changes in brain structure across developmental stages (Ecker et al., 2014, Courchesne et al., 2011a), and *iii*) small samples often drawn from homogenous subgroups of the autism spectrum (e.g. high functioning adult males, ect.). Despite inconsistencies, VBM studies have been valuable in linking regional atypical brain volumes to ASD symptomatology (Ecker et al., 2012) and highlighting anatomical heterogeneity across the spectrum (McAlonan et al., 2009, McAlonan et al., 2008).

1.4.2 Cortical Morphometry of the Autistic Brain

The pathological processes underlying volumetric abnormalities in ASD remain unclear. More recent studies of cortical structure have moved beyond measures of volume to investigations of the dimensions and shape (i.e. morphometry) of the cortex. Surface based morphometry (SBM) comprises a series of structural MRI methods that use tessellated reconstructions of the cortical surface to quantify a variety of morphological features relating to brain structure. These studies are particularly valuable in ASD for their potential to indicate developmental pathways in the condition that are associated with specific features of neural architecture, particularly in cortical grey matter (i.e. the cerebral cortex).

The cerebral cortex is organized according to different cellular layers and follows a columnar architecture. At their core, cortical minicolumns are comprised of radially oriented arrays of pyramidal projection neurons. Inputs and outputs from these pyramidal neurons are modulated by GABAergic interneurons that lie within the core and periphery of mini-columns allowing for area and task specific information processing (Kawaguchi and Kubota, 1997, Sanders et al., 2012, DeFelipe, 1997). Several types of progenitor cells and related molecular and genetic signaling pathways regulate the development of this cortical organization (Figure 1.4).

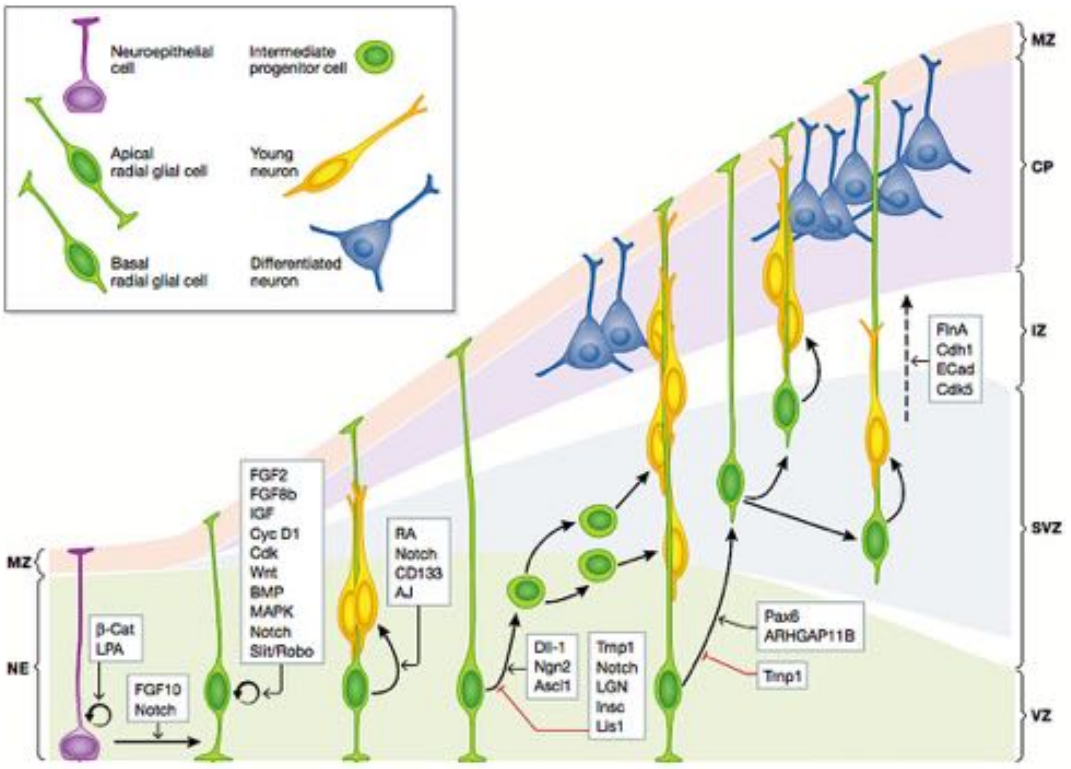

Figure 1.4, Development of the Human Cerebral Cortex (Fernández et al., 2016): This model depicts the main types of progenitor cells involved in the development of the cerebral cortex. Arrows indicate lineage relationships between cell types. During cortical expansion most neuroepithelial cells divide symmetrically to amplify their numbers and generate apical radial glial cells (aRGC). During neurogenesis these aRGCs divide into neuron cells directly or via intermediate progenitor cells (IPC). IPCs divide solely into neurons, allowing for rapid proliferation of cortical neurons. Neurons migrate along scaffolding provided by aRGC fibers to form cortical units known as minicolumns. Basal radial glial cells (bRGC) provide additional scaffolding for migrating neurons across convoluted cortical surfaces and are thought to be important to the development of cortical gyrification. Boxes highlight some of the many molecular and genetic pathways that regulate these processes. Marginal zone (MZ), cortical plate (CP), intermediate zone (IZ), subventricular zone (VZ), ventricular zone (VZ).

According to the radial unit hypothesis (Rakic, 1995) the quantity of neuron cells within each individual minicolumn is a main determinant of cortical thickness (CT) while cortical surface area (SA) is closely related to the number of minicolumns (i.e. radial units). It is now widely believed that intermediate progenitor cells (IPC) are a principle modulator of CT (Pontious et al., 2007). These cells divide solely into neurons (Miyata et al., 2004, Noctor et al., 2004) and are responsible for the vast proliferation of neuronal cells within the cortical sheet. These neuronal cells migrate from the ventricular zone along scaffolding fibers provided by apical radial glial cells (aRGC) leading to the formation of cortical minicolumns. Increases in SA have thus been linked to the length of symmetrical division cycles for neuroepithelial progenitor cells responsible for the expansion of aRGC (Pontious et al., 2007).

There is a large body of postmortem evidence that suggests disruptions to the above developmental processes in ASD. For example, individuals with ASD have been shown to have increased minicolumn density in frontal and temporal regions (Casanova et al., 2006, Casanova et al., 2002). Shorter distances between these cellular units could introduce hyper connectivity within local brain regions resulting in signal delays and metabolic inefficiencies in connecting disparate brain regions, potentially leading to ASD behaviors (Belmonte et al., 2004, Horwitz et al., 1988, Just et al., 2004, Casanova et al., 2003). As could be predicted by this increased column density, greater numbers of prefrontal neuron cells in young children with ASD have also been reported (Courchesne et al., 2011b). The presence of supernumerary neurons within white matter bellow the cortical sheet and poor definition of the grey-white matter boundary in ASD (Avino and Hutsler, 2010, Bailey et al., 1998) also point towards disruptions to neuronal migratory processes in the condition. Together these findings provide evidence for atypical cell division of neuronal progenitors and the subsequent migration of neuron cells to their target locations within the developing cortex in ASD (Casanova, 2014). Furthermore, it can be predicted that disruptions to these foundational developmental processes have lasting impact on the structural morphology of the cortex.

Several researchers have applied SBM methods to quantify differences in cortical features associated with diagnoses of ASD. To date CT is the most reported in the condition, although results have been mixed. Some studies have reported decreased CT in ASD (Hadjikhani et al., 2006, Scheel et al., 2011, Ekman et al., 1975), others no differences (Hazlett et al., 2011, Hutsler et al., 2007), and others still CT increases in the condition (Hardan et al., 2006). These inconsistent findings can likely be largely attributed to nonlinear changes in CT across developmental stages (Ecker et al., 2014). For example, within a large multi-centre study including individuals from 6-35 years of age, Khundrakpam et al. (2017) reported CT increases in young children with ASD were greatest around the age of ten. Due to accelerated cortical thinning these differences decreased into adolescence and adulthood such that little to no difference was observed at 35 years (Khundrakpam, 2017). These findings are supported by both histological (Hutsler et al., 2007) and longitudinal MRI findings (Hardan et al., 2009) reporting accelerated reductions in CT with age in ASD

compared to TD controls, which is consistent with the observed developmental trajectory of volume measures within the condition (Courchesne et al., 2011a).

However, imaging studies of both CT and SA have found closer links between SA expansion and observed early life volumetric increases in ASD (Hazlett et al., 2011, Hazlett et al., 2017). One recent study reported that accelerated SA expansion between 6 and 12 months predicted increased brain volumes at 24 months (Hazlett et al., 2017). Furthermore, Ecker et al. (2013a) found that 56% of a distributed pattern of volumetric differences in adults with ASD was driven by underlying changes in SA measures compared to 8% for CT, with only 5% shared between the two. The small degree of overlap between CT and SA findings highlights the need for studies that differentiate volumetric measures into these component measures. Furthermore, findings by Ecker et al. (2013a) and Hazlett et al. (2017) of a greater contribution of SA expansion to volumetric differences advance theories that processes governing SA expansion are a possible aetiological agent in ASD. However, it should be noted that Ecker at al. (2013a) was only able to highlight these underlying relationships through liberal statistical thresholding (uncorrected $p<0.05$). When corrected for multiple comparisons no significant differences in SA measures were observed, which is consistent with a few other reports (Wallace et al., 2013, Raznahan et al., 2009). Furthermore, another study has reported reduced cortical SA within the left fusiform and bilateral middle temporal cortices in ASD (Libero et al., 2014), which were also reported by Ecker et al. (2013a).

In addition to SA and CT, individuals with ASD have been shown to have atypical morphology associated with cortical folding. For example, an early MRI study conducted by Piven et al. (1990) found significantly more instances of cortical malformations relating to folding among ASD cases including; *i*) polymicrogyria (excessive small folding), *ii*) schizencephaly (clefts lined within the cortical grey matter) and *iii*) macrogyria (increased gyri size) (Piven et al., 1990). Other early MRI studies have reported atypical placement of major sulci within the frontal and temporal lobes (Levitt et al., 2003) and increased gyrification in frontal brain regions (Hardan et al., 2004) in children and adolescences with ASD.

More recent studies using MRI based gyrification index (GI) measures (Zilles et al., 1988, Su et al., 2013) to quantify cortical folding have reported decreased GI in ASD (Bos et al., 2015). Recently SBM studies using a vertex wise implementation of the GI, namely the local gyrification index (*l*GI) (Schaer et al., 2008), have reported decreased gyrification in inferior fronto-parietal and posterior medial cortical regions (Schaer et al., 2013) as well as the supramarginal gyrus (Libero et al., 2014). Others have reported regional patterns of increased *l*GI in ASD (Wallace et al., 2013, Ecker et al., 2016). Some studies have linked differences in gyrification in ASD to underlying changes in WM diffusion measures (Ecker et al., 2016, Bos et al., 2015, Schaer et al., 2013) which provides preliminary evidence for what are likely to be complex interrelations between white matter and grey matter development which may contribute to atypical intra- and inter-cortical connectivity in the condition.

In addition to gyrification other studies have sought to quantify various aspects of sulcal morphometry and the relationship between these features and ASD symptomology. For example, increased sulcal depths within ASD participants have been reported and found to correlate with ADOS social interaction scores (Auzias et al., 2014, Nordahl et al., 2007). Furthermore, abnormalities in sulcal length and SA have been noted in ASD (Shokouhi et al., 2012, Nordahl et al., 2007). Some of these abnormal findings appear to be larger within younger children on the spectrum suggesting a "normalization" of these measures into adolescence and adulthood similar to the trajectory observed in volumetric measures (Nordahl et al., 2007).

The mechanisms underlying and relating to cortical folding are numerous and complex (Fernández et al., 2016). Folding has been related to differential growth rates between outer and inner cortical layers (Richman et al., 1975, Kriegstein et al., 2006), proliferation of bRGCs (Nonaka‐Kinoshita et al., 2013, Reillo et al., 2011), axonal tension (Van Essen, 1997), and the neural complexity of a particular brain region (i.e. numbers of neurons, synaptic density, and/or dendritic arborization) (Welker, 1990). Studies of cortical folding are further complicated by large variances in the degree of gyrification across individuals in the normative population (Bartley et al., 1997). This is supported by findings of discordant folding patterns between monozygotic twins pairs where only one twin had a diagnosis of ASD (Kates et al., 2009). This is in

contrast to volumetric measures of the brain, which have been found to be highly concordant between twins (White et al., 2002). These twin studies and the lack of correlation between cortical folding and measures that are largely genetically determined such as total brain volume and body weight and length (Zilles et al., 1988, Rogers et al., 2010) indicate that measures of gyrification may be more sensitive to environmental factors than measures that are largely genetically determined (Zilles et al., 2013).

The identification of group differences in SBM measures such as CT, SA, sulcal depth and *l*GI are valuable for their ability to highlight different developmental pathways that may contribute to ASD pathology. In doing so these studies can narrow focus on or introduce novel etiological targets for the condition. For example, IPCs and the proliferation of neuron cells (Pontious et al., 2007), dendritic arborization (Huttenlocher, 1990), and myelination (Sowell et al., 2004) have all been attributed to changes in CT while the length of symmetrical division cycles for aRGC progenitor cells appear to correspond with proliferation of cortical minicolumns and SA (Pontious et al., 2007). Parsing out the deterministic mechanisms responsible for cortical folding abnormalities in ASD may be more difficult due to the potentially large contribution of environmental factors in the development of folding patterns (Zilles et al., 2013). However, current evidence suggests that cortical folding relates to bRGCs and differential expansion rates of the outer and inner cortical surface (Richman et al., 1975, Kriegstein et al., 2006, Nonaka‐Kinoshita et al., 2013, Reillo et al., 2011) thus, cortical folding may be related to processes governing the expansion of cortical SA.

To date, results reported by SBM studies in ASD have been somewhat inconsistent. In many cases this can be attributed to the complex developmental trajectories that morphometric cortical features undergo (Ecker et al., 2014). This is further complicated by relatively small samples sizes and the large degree of phenotypic heterogeneity among the ASD population. Several of these studies are likely underpowered due to such small samples as one power study estimated that 50 subjects per group are needed to detect a 0.25mm differences in CT between two groups (Pardoe et al., 2013). To date, most SBM studies fall below this number of

participants. Thus, work remains to be done in confirming differences in morphological phenotypes across the spectrum as well as untangling the numerous genetic and molecular pathways that regulate their development. Additionally, some atypical structural features that have been identified in postmortem studies of ASD brains, such as integrity of the grey-white matter boundary, have yet to be investigated *in vivo*.

1.5 Beyond Group Differences: Pattern Recognition in Autism Spectrum Disorder

Until recently, the majority of neuroimaging research in psychiatric conditions has employed mass-univariate statistical methods based the general linear model (GLM) (Friston et al., 1994). The GLM is a valuable tool for identifying mean differences between groups. However, these models are not suited to make predictions for individual cases based on multivariate patterns within the data (i.e. predictions regarding group membership or clinical outcome), and thus offer limited translational value to clinical applications. Alternatively, a class of 'machine learning' methods known as multivariate pattern classification (MVPC) can be applied to generate image-based predictive models that have the potential to be utilized as diagnostic tools and intervention outcome measures.

Within 'machine learning' an algorithm is said to learn from experience *E* with respect to some class of tasks *T* and performance measure *P*. Learning is said to occur when performance in task *T* improves with experience *E* as measured by performance *P* (Mitchell, 1997). Within this context classification poses a supervised learning problem in which examples from a training set of empirical data are mapped to a known output such as a class label. In brief MVPC algorithms differentiate cases between two or more classes in the following way. During a 'training phase' the model is initially trained using well-defined samples or data subsets (e.g. ASD and controls) to establish a mathematical criterion or decision function that best distinguishes between the groups. During the 'testing phase' the decision function is applied to predict the label of an unseen data point. Often MVPC model performance is validated within the same sample using cross-validation methods. However, gold

standard assessment of a predictive model's accuracy in distinguishing between classes is reliant on validation using completely independent testing data.

A variety of MVPC algorithms including the Support Vector Machine (SVM) (Vapnik, 1995) and Gaussian Process Classification (GPC) (Rasmussen and Williams, 2006) as well as numerous others (e.g. linear discriminant classifiers, logistic regression, decision trees, random forest, etc.) have been successfully trained using various structural and functional imaging data modalities to distinguish individuals diagnosed with various neuropsychiatric disorders from healthy controls and/or to predict treatment outcome or subjective states (Wolfers et al., 2015, Arbabshirani et al., 2016). These findings provide proof of concept for the development of safe, *in vivo* diagnostic and prognostic tools and biomarkers for a variety of psychiatric conditions. However, until these models undergo stringent validation on independent data sets that accurately reflect the clinical environment their potential translational value remains to be realized.

1.5.1 Multivariate Pattern Classification in Autism Spectrum Disorder

In a behaviorally defined disorder such as ASD the development of biologically based diagnostic and prognostic markers would represent an invaluable tool to clinicians. Furthermore, identification of a biomarker for ASD could provide pathways towards better understanding the casual mechanisms for the condition. While several genetic and neurobiological markers have been proposed, there are currently no reliable biomarkers that have been validated for clinical use in ASD (Ruggeri et al., 2013, Ecker and Murphy, 2014). Classification of ASD using MRI features is one pathway towards the development of a biomarker for the condition. To date several MVPC methods have been applied to a variety of neuroimaging data and psychiatric conditions (Wolfers et al., 2015, Arbabshirani et al., 2016). The results of MVPC studies in ASD are reviewed bellow and summarized in Table 1.1.

Table 1: Multivariate Pattern Classification Studies of Autism Spectrum Disorder

Modality	Features	Classifier	Number of Subjects	Biological Gender	ASD age	Overall Accuracy	Reference
sMRI	Cortical Thickness and Volumetric ROIs	SVM	TDC=325, ASD=325	Male and Female	17.8±7.4	59%	Sabuncu et al. (2014)
sMRI	Cortical Thickness and Volumetric ROIs	Multi-kernel SVM	TDC=59, ASD=58	Male and Female	10.8±4.0	96.3%	Wee et al. (2014)
sMRI	VBM GM and WM volume maps	SVM	TDC=24, ASD=24	Male and Female	13.2±0.6	92%	Uddin et al. (2011)
sMRI	Cortical Thickness	Logistic model trees	TDC=16, ASD=22	Male and Female	9.2±2.1	87%	Jiao et al (2010)
sMRI	VBM and SBM based ROI	SVM	TDC=20, ASD=21	Male	4.1±0.8	74%	Gori et al. (2015)
sMRI	GM volume map	SVM	TDC=40, ASD=52	Male and Female	14.4±1.7	80-85%	Segovia et al. (2014)
sMRI	VBM GM and WM volume maps	SVM	TDC=22, ASD=22	Male	27.0±7.0	77%	Ecker et al.(2010)
sMRI	Cortical Thickness, Surface Area, Sulcal depth, Curvature, Metric Distortion	SVM	TDC=20, ASD=20	Male	33.0±11.0	85%	Ecker et al.(2010)
sMRI	VBM GM volume maps	SVM	TDC=38, ASD=30	Female	4.4±1.5	80%	Calderoni et al. (2012)
sMRI	Volumetric measures	Discriminant function analysis	TDC=15, ASD=52	Male	3.4±0.7	92.3-95.8%	Akshoomoff et al. (2004)
sMRI	Age, Sex, Volume, Surface Area, and Cortical Thickness ROIs	Three-Stage Deep Learning Network	HRN = 145, ASD=34	Male and Female	6 and 12 months	94%	Hazlett et al. (2017)
sMRI	Extra-axial Cerebrospinal Fluid	Decision Tree	HRN = 174, ASD= 47	Male and Female	6 months	66-72%	Shen et al. (2017)
dMRI	FA and MD based ROI	SVM	TDC=30, ASD=45	Male and Female	10.5±2.5	80%	Ingalhalikar er al. (2011)
fMRI	Activation of selected voxels during social interaction task	Gaussian naïve Bayes	TDC=17, ASD=17	Male and Female	25.6±6.7	97%	Just et al. (2014)
fMRI	Language and theory of mind task based functional connectivity	Logistic regression	TDC=14, ASD=13	Male	21.4±3.9	96%	Murdaugh et al. (2012)
fMRI	Activation of selected voxels during social interaction task	SVM	TDC=14, ASD=15	Male and Female	28.6±1.8	92.3%	Chanel et al. (2016)
rsfMRI	rsfMRI ICA components	Logistic regression	TDC=20, ASD=20	Male and Female	9.9±1.5	78%	Uddin et al (2013)

Table 1: Multivariate Pattern Classification Studies of Autism Spectrum Disorder (continued)

Modality	Features	Classifier	Number of Subjects	Biological Gender	ASD age	Overall Accuracy	Reference
rsfMRI	ROI based functional connectivity	Random forest	TDC=126, ASD=126	Male and Female	14.8±1.6	79%	Chen et al. (2015)
rsfMRI	ROI based functional connectivity	Logistic regression and SVM	TDC=59, ASD=59	Male	17.66±2.7	77%	Plitt et al (2015)
rsfMRI	ROI based functional connectivity	Probabilistic neural network	TDC=328, ASD=312	Male and Female	13.2±3.1	90%	Iidaka (2015)
rsfMRI	ROI based functional connectivity	Thresholding	TDC=40, ASD=40	Male	22.7±7.4	79%	Anderson et al. (2011)
fMRI and dMRI	Functional connectivity and FA values	SVM	TDC=15, ASD=15	not reported	21.1±0.9	95.9%	Deshpande et al. (2013)
sMRI, dMRI and MRS	Cortical Thickness, FA and neurochemical concentration	Decision tree	TDC=18, ASD=19	Male and Female	27.1±1.3	91.9%	Libero et al. (2015)
sMRI and rsfMRI	rsfMRI, Cortical Thickness and Volume based graph theory metrics	Random forest	TDC=153, ASD=127	Male and Female	13.5±6.0	70%	Zhou et al. (2014)

Table 1, Multivariate Pattern Classification Studies of Autism Spectrum Disorder: Twenty-two MVPC studies that use magnetic resonance imaging (MRI) data to classify ASD are summarized. Ages are given in mean years ± standard deviation. sMRI = structural MRI, VBM = voxel based morphometry, SBM= surface based morphometry dMRI = diffusion MRI, FA = fractional anisotropy, MD = mean diffusivity, fMRI = functional MRI, rsfMRI = resting state functional MRI, MRS = magnetic resonance spectroscopy, SVM = support vector machine, TDC = typically developing controls.

The use of MVPC models based on brain imaging data in ASD was first reported by Akshoomoff et al. (2004). Using a discriminate function and pre-selected volumetric regions of interest (ROIs) from young children and TD controls a high classification accuracy (95%) was achieved. However, this rate was not based on a thorough cross validation but on reclassification of the entire sample and is therefore inherently circular. More recent studies employing SVM algorithms to classify ASD cases using volumetric GM and WM ROIs have reported overall classification accuracies ranging from 65-90% for different brain regions (Uddin et al., 2011, Segovia et al., 2014). In addition to these volumetric ROI studies whole brain VBM data has been shown to classify adult male ASD cases with a cross-validated accuracy of 81% (Ecker et al., 2010b).

When comparing structural MRI measures used to predict ASD diagnoses, models using SBM features such as CT have been generally shown to outperform those using volumetric features (Jiao et al., 2010). A study by Ecker et al. (2010a) investigating the predictive value of five SBM measures (CT, SA, sulcal depth, mean radial curvature, and metric distortion) used a SVM to classify adult males with ASD and matched controls. These studies revealed that CT measures in the left hemisphere produced the highest cross-validated prediction accuracy (90%). Other SVM studies using a variety of regional cortical volume and thickness features have also successfully classified ASD cases from controls albeit at lower discriminative accuracies (59-74%) (Gori et al., 2015, Sabuncu and Konukoglu, 2014). In addition to being able to classify cases from controls, measures of interregional CT covariance have also been shown to be predictive of current symptom measures among ASD patients (Sato et al., 2013).

In addition to volumetric and morphometric features both diffusion and functional MRI (fMRI) features have been used to classify ASD. To date, two studies investigating the predictive power of mean diffusivity and fractional anisotropy diffusion measures in ASD using a SVM have reported classification accuracies in line with the best performing SBM based models (~80%-89%) (Ingalhalikar et al., 2010, Ingalhalikar et al., 2011). Activation patterns during theory-of-mind and language fMRI tasks as well as resting state brain activity (rsMRI) have been used to classify individuals with ASD from controls with varying reported accuracies

(Deshpande et al., 2013, Murdaugh et al., 2012, Uddin et al., 2013, Anderson et al., 2011, Wee et al., 2016, Iidaka, 2015, Plitt et al., 2015).

Recent studies have begun to implement methodologies that combine multiple neuroimaging modalities into single predictive models. Decision tree algorithms have been used to combine selections of diffusion, morphometric, and MR spectroscopy features as inputs for ASD classification. Under this framework one model was able to achieve a 91.9% classification accuracy between ASD cases and controls. These findings also highlighted the potential utility for MVPC methods to aid in understanding ASD risk factors and etiology. For example, if certain favorable values among features within the decision tree were present an individual could be protected from an ASD classification, even in the presence of other unfavorable metrics (Libero et al., 2015). Other studies have combined diffusion MRI with auditory task based magnetoencephalography (MEG) data, resulting in the successful classification of ASD cases from TD controls at a CV accuracy of 83.3% (Ingalhalikar et al., 2014). Another recent study employed multi-kernel learning SVM methods to investigate the predictive capacity of combined vertex based surface measures (i.e. CT, grey and white matter surface volumes), subcortical volumetric ROI data, and interregional correlation measures. Using this methodology the researchers reported a CV accuracy over 96% (Wee et al., 2014).

Two recent studies have shown promise in predicting ASD diagnoses at 24 months based on MRI measures at 6 month, an age before diagnosis is possible using current gold standard criterion. The first of these studies used a three stage deep learning algorithm employing age and sex data along with volumetric, CT, and SA based ROIs. This study was able to classify high-risk infants who received an ASD diagnosis at 24 months from those who did not at accuracies of 95%. The second study utilized measures of extra-axial spinal fluid at 6 months to classify high-risk infants with ASD at 24 months (Shen et al., 2017). This study achieved a cross-validated classification accuracy of 69% within the training sample, as well as an accuracy of 72% when applied to an independent data set.

1.5.2 Towards Translational Tools

While the above studies provide proof of concept for imaging based diagnostic models in ASD, translating these tools from the research to 'real-world' clinical settings raises additional hurdles. To date no studies have tested classification models for ASD trained in the research environment on independent samples that are representative of the broader clinical population. This is important because several differences exist between research and clinical ASD cohorts. For example, individuals with ASD recruited within the research environment will generally be excluded if they have comorbid conditions, are taking certain medications, or fail to reach cut-offs on behavioral metrics such as the autism diagnostic interview (ADI) and/or autism diagnostic observation schedule (ADOS). As such, many individuals who would qualify for a clinical ASD diagnosis would not meet inclusion criteria for research. Thus, inherent differences in the clinical phenotype between individuals in research and clinical ASD samples are likely. Accordingly, if imaging-based prediction models are to be adopted in the clinical setting, a critical first step will be the testing of models trained in the research setting on separate (i.e. independent) samples that are representative of the clinical population.

1.6 The Current Thesis: Aims and Hypotheses

This chapter has outlined several advances that have been made in structural MRI studies of ASD. Broadly, this thesis aims to advance this literature in a way that offers the potential for real world benefits to patients and stakeholders. With regards to this aim this thesis includes fours studies that focus on *i*) the development of novel informative imaging features for ASD, *ii*) evaluating the efficacy of structural neuroimaging measures to predict ASD diagnosis within clinical samples, and *iii*) investigating the role of normative sex differentiation in brain structure on the probability for ASD.

1.6.1 Study 1: In Vivo Evidence of Reduced Integrity of the Grey-White Matter Boundary in Autism Spectrum Disorder

Reduced integrity of the grey-white matter boundary has previously been reported by postmortem studies in individuals with ASD (Avino and Hutsler, 2010). However, prior to this work no *in vivo* studies have examined this atypical structure in the condition. Here, we used structural MRI to examine differences in tissue contrast

between grey and white matter at the boundary between these tissue types as well as across different cortical layers. As individuals with ASD are thought to have a less well defined transition between grey and white matter we hypothesized that individuals with ASD would show significant reductions in measures of tissue contrast taken at and around the grey-white matter boundary.

1.6.2 Study 2: Clinical Validation of Pattern Classification Models for Autism Spectrum Disorder

Several proof of concept studies have shown promise in developing diagnostic imaging tools for ASD using multivariate pattern classification (MVPC) and SBM measures (see section 1.4.1 for review). However, to date these models have not been tested on samples that are representative of the clinical setting. Thus, this study first aimed to train SVM and GPC models to separate adult ASD patients from TD controls acquired in the research setting using a variety of morphological cortical features, including features that have not previously been reported (i.e. *l*GI and tissue contrast). The second and primary aim of this study was to then test the ability of classifiers trained within the research setting to make diagnostic predictions within an independent clinical sample consisting of individuals who had been referred for a specialist ASD diagnostic assessment.

1.6.3 Study 3 and 4: Association Between the Probability of Autism Spectrum Disorder and Normative Sex-Related Phenotypic Diversity in Brain Structure

Male preponderance is an understudied hallmark of ASD and other neurodevelopmental and psychiatric conditions. While some degree of male preponderance is likely attributable to sex differences in the ASD phenotype and male biased diagnostic tools, it has been purposed that variance in biology attributable to normative sex differences may modulate ASD risk (Werling, 2016). Thus, these studies sought to understand how biological sex/gender is associated with probability for ASD. The aims of these studies were three-fold; *i*) provide a phenotypic characterization of normative sex related diversity in brain structure, *ii*) determine how diversity in sex based neurophenotypes is associated with probability for ASD,

and *iii*) estimate how much ASD prevalence in the general population might vary as a function of normative sex-related phenotypic diversity in brain structure

1.7 References

ADAMS, J. B., BARAL, M., GEIS, E., MITCHELL, J., INGRAM, J., HENSLEY, A., ZAPPIA, I., NEWMARK, S., GEHN, E., RUBIN, R. A., MITCHELL, K., BRADSTREET, J. & EL-DAHR, J. M. 2009. The Severity of Autism Is Associated with Toxic Metal Body Burden and Red Blood Cell Glutathione Levels. *Journal of Toxicology,* 2009.

AKSHOOMOFF, N., LORD, C., LINCOLN, A. J., COURCHESNE, R. Y., CARPER, R. A., TOWNSEND, J. & COURCHESNE, E. 2004. Outcome classification of preschool children with autism spectrum disorders using MRI brain measures. *Journal of the American Academy of Child & Adolescent Psychiatry,* 43**,** 349-357.

ALEXANDER, A. L., LEE, J. E., LAZAR, M., BOUDOS, R., DUBRAY, M. B., OAKES, T. R., MILLER, J. N., LU, J., JEONG, E.-K. & MCMAHON, W. M. 2007. Diffusion tensor imaging of the corpus callosum in autism. *Neuroimage,* 34**,** 61-73.

AMARAL, D. G., SCHUMANN, C. M. & NORDAHL, C. W. 2008. Neuroanatomy of autism. *Trends in neurosciences,* 31**,** 137-145.

AMERICAN PSYCHIATRIC ASSOCIATION 2013. *Diagnostic and statistical manual of mental disorders V*.

AMIET, C., GOURFINKEL-AN, I., BOUZAMONDO, A., TORDJMAN, S., BAULAC, M., LECHAT, P., MOTTRON, L. & COHEN, D. 2008. Epilepsy in autism is associated with intellectual disability and gender: evidence from a meta-analysis. *Biological Psychiatry,* 64**,** 577-582.

ANDERSON, J. S., NIELSEN, J. A., FROEHLICH, A. L., DUBRAY, M. B., DRUZGAL, T. J., CARIELLO, A. N., COOPERRIDER, J. R., ZIELINSKI, B. A., RAVICHANDRAN, C. & FLETCHER, P. T. 2011. Functional connectivity magnetic resonance imaging classification of autism. *Brain,* 134**,** 3742-3754.

ANDREWS, N., MILLER, E., GRANT, A., STOWE, J., OSBORNE, V. & TAYLOR, B. 2004. Thimerosal exposure in infants and developmental disorders: a retrospective cohort study in the United Kingdom does not support a causal association. *Pediatrics,* 114**,** 584-591.

ARBABSHIRANI, M. R., PLIS, S., SUI, J. & CALHOUN, V. D. 2016. Single subject prediction of brain disorders in neuroimaging: Promises and pitfalls. *NeuroImage*.

ARIN, D., BAUMAN, M. & KEMPER, T. 1991. The distribution of Purkinje cell loss in the cerebellum in autism. *Neurology,* 41**,** 307.

ASHBURNER, J. & FRISTON, K. J. 2000. Voxel-Based Morphometry—The Methods. *NeuroImage,* 11**,** 805-821.

ASPERGER, H. 1944. Die „Autistischen Psychopathen" im Kindesalter. *European Archives of Psychiatry and Clinical Neuroscience,* 117**,** 76-136.

ATLADÓTTIR, H. Ó., THORSEN, P., ØSTERGAARD, L., SCHENDEL, D. E., LEMCKE, S., ABDALLAH, M. & PARNER, E. T. 2010. Maternal infection requiring hospitalization during pregnancy and autism spectrum disorders. *Journal of autism and developmental disorders,* 40**,** 1423-1430.

AUZIAS, G., VIELLARD, M., TAKERKART, S., VILLENEUVE, N., POINSO, F., FONSÉCA, D. D., GIRARD, N. & DERUELLE, C. 2014. Atypical sulcal anatomy in young children with autism spectrum disorder. *NeuroImage: Clinical,* 4**,** 593-603.

AVINO, T. A. & HUTSLER, J. J. 2010. Abnormal cell patterning at the cortical gray–white matter boundary in autism spectrum disorders. *Brain Research,* 1360**,** 138-146.

BAILEY, A., LE COUTEUR, A., GOTTESMAN, I., BOLTON, P., SIMONOFF, E. & YUZDA, E. 1995. Autism as a strongly genetic disorder: evidence from a British twin study. *Psychol Med,* 25**,** 63 - 77.

BAILEY, A., LUTHERT, P., DEAN, A., HARDING, B., JANOTA, I., MONTGOMERY, M., RUTTER, M. & LANTOS, P. 1998. A clinicopathological study of autism. *Brain,* 121**,** 889-905.

BAIRD, G., PICKLES, A., SIMONOFF, E., CHARMAN, T., SULLIVAN, P., CHANDLER, S., LOUCAS, T., MELDRUM, D., AFZAL, M. & THOMAS, B. 2008. Measles vaccination and antibody response in autism spectrum disorders. *Archives of disease in childhood,* 93**,** 832-837.

BARNEA-GORALY, N., KWON, H., MENON, V., ELIEZ, S., LOTSPEICH, L. & REISS, A. L. 2004. White matter structure in autism: preliminary evidence from diffusion tensor imaging. *Biological psychiatry,* 55**,** 323-326.

BARTLEY, A. J., JONES, D. W. & WEINBERGER, D. R. 1997. Genetic variability of human brain size and cortical gyral patterns. *Brain,* 120**,** 257-269.

BAUMAN, M. L. & KEMPER, T. L. 2005. Neuroanatomic observations of the brain in autism: a review and future directions. *International Journal of Developmental Neuroscience,* 23**,** 183-187.

BELMONTE, M. K., ALLEN, G., BECKEL-MITCHENER, A., BOULANGER, L. M., CARPER, R. A. & WEBB, S. J. 2004. Autism and abnormal development of brain connectivity. *The Journal of Neuroscience,* 24**,** 9228-9231.

BELMONTE, M. K. & YURGELUN-TODD, D. A. 2003. Functional anatomy of impaired selective attention and compensatory processing in autism. *Cognitive brain research,* 17**,** 651-664.

BEN BASHAT, D., KRONFELD-DUENIAS, V., ZACHOR, D. A., EKSTEIN, P. M., HENDLER, T., TARRASCH, R., EVEN, A., LEVY, Y. & BEN SIRA, L. 2007. Accelerated maturation of white matter in young children with autism: a high b value DWI study. *Neuroimage,* 37**,** 40-47.

BLACK, C., KAYE, J. A. & JICK, H. 2002. Relation of childhood gastrointestinal disorders to autism: nested case-control study using data from the UK General Practice Research Database. *Bmj,* 325**,** 419-421.

BOS, D. J., MERCHÁN-NARANJO, J., MARTÍNEZ, K., PINA-CAMACHO, L., BALSA, I., BOADA, L., SCHNACK, H., ORANJE, B., DESCO, M., ARANGO, C., PARELLADA, M., DURSTON, S. & JANSSEN, J. 2015. Reduced Gyrification Is Related to Reduced Interhemispheric Connectivity in Autism Spectrum Disorders. *Journal of the American Academy of Child & Adolescent Psychiatry,* 54**,** 668-676.

BOUCHER, J. 2011. Redefining the Concept of Autism as a Unitary Disorder: Multiple Causal Deficits ofa Single Kind? *The neuropsychology of autism***,** 469.

C YUEN, R. K., MERICO, D., BOOKMAN, M., L HOWE, J., THIRUVAHINDRAPURAM, B., PATEL, R. V., WHITNEY, J., DEFLAUX, N., BINGHAM, J., WANG, Z., PELLECCHIA, G., BUCHANAN, J. A., WALKER, S., MARSHALL, C. R., UDDIN, M., ZARREI, M., DENEAULT, E., D'ABATE, L., CHAN, A. J. S., KOYANAGI, S., PATON, T., PEREIRA, S. L., HOANG, N., ENGCHUAN, W., HIGGINBOTHAM, E. J., HO, K., LAMOUREUX, S., LI, W., MACDONALD, J. R.,

NALPATHAMKALAM, T., SUNG, W. W. L., TSOI, F. J., WEI, J., XU, L., TASSE, A.-M., KIRBY, E., VAN ETTEN, W., TWIGGER, S., ROBERTS, W., DRMIC, I., JILDERDA, S., MODI, B. M., KELLAM, B., SZEGO, M., CYTRYNBAUM, C., WEKSBERG, R., ZWAIGENBAUM, L., WOODBURY-SMITH, M., BRIAN, J., SENMAN, L., IABONI, A., DOYLE-THOMAS, K., THOMPSON, A., CHRYSLER, C., LEEF, J., SAVION-LEMIEUX, T., SMITH, I. M., LIU, X., NICOLSON, R., SEIFER, V., FEDELE, A., COOK, E. H., DAGER, S., ESTES, A., GALLAGHER, L., MALOW, B. A., PARR, J. R., SPENCE, S. J., VORSTMAN, J., FREY, B. J., ROBINSON, J. T., STRUG, L. J., FERNANDEZ, B. A., ELSABBAGH, M., CARTER, M. T., HALLMAYER, J., KNOPPERS, B. M., ANAGNOSTOU, E., SZATMARI, P., RING, R. H., GLAZER, D., PLETCHER, M. T. & SCHERER, S. W. 2017. Whole genome sequencing resource identifies 18 new candidate genes for autism spectrum disorder. *Nat Neurosci,* advance online publication.

CARPER, R. A., MOSES, P., TIGUE, Z. D. & COURCHESNE, E. 2002. Cerebral lobes in autism: early hyperplasia and abnormal age effects. *Neuroimage,* 16**,** 1038-1051.

CARTER, M. & SCHERER, S. 2013. Autism spectrum disorder in the genetics clinic: a review. *Clinical genetics,* 83**,** 399-407.

CASANOVA, M. F. 2007. The neuropathology of autism. *Brain Pathology,* 17**,** 422-433.

CASANOVA, M. F. 2014. Autism as a sequence: from heterochronic germinal cell divisions to abnormalities of cell migration and cortical dysplasias. *Medical hypotheses,* 83**,** 32-38.

CASANOVA, M. F., BUXHOEVEDEN, D. & GOMEZ, J. 2003. Disruption in the inhibitory architecture of the cell minicolumn: implications for autisim. *The Neuroscientist,* 9**,** 496-507.

CASANOVA, M. F., BUXHOEVEDEN, D. P., SWITALA, A. E. & ROY, E. 2002. Neuronal density and architecture (gray level index) in the brains of autistic patients. *Journal of child neurology,* 17**,** 515-521.

CASANOVA, M. F., VAN KOOTEN, I. A., SWITALA, A. E., VAN ENGELAND, H., HEINSEN, H., STEINBUSCH, H. W., HOF, P. R., TRIPPE, J., STONE, J. & SCHMITZ, C. 2006. Minicolumnar abnormalities in autism. *Acta neuropathologica,* 112**,** 287-303.

CHEN, W., LANDAU, S., SHAM, P. & FOMBONNE, E. 2004. No evidence for links between autism, MMR and measles virus. *Psychological medicine,* 34**,** 543-553.

COURCHESNE, E., CAMPBELL, K. & SOLSO, S. 2011a. Brain growth across the life span in autism: age-specific changes in anatomical pathology. *Brain research,* 1380**,** 138-145.

COURCHESNE, E., KARNS, C., DAVIS, H., ZICCARDI, R., CARPER, R., TIGUE, Z., CHISUM, H., MOSES, P., PIERCE, K. & LORD, C. 2001. Unusual brain growth patterns in early life in patients with autistic disorder An MRI study. *Neurology,* 57**,** 245-254.

COURCHESNE, E., MOUTON, P. R., CALHOUN, M. E., SEMENDEFERI, K., AHRENS-BARBEAU, C., HALLET, M. J., BARNES, C. C. & PIERCE, K. 2011b. Neuron number and size in prefrontal cortex of children with autism. *JAMA: The Journal of the American Medical Association,* 306**,** 2001-2010.

COURCHESNE, E., REDCAY, E. & KENNEDY, D. P. 2004. The autistic brain: birth through adulthood. *Current opinion in neurology,* 17**,** 489-496.
CROEN, L. A., GRETHER, J. K. & SELVIN, S. 2002. Descriptive epidemiology of autism in a California population: who is at risk? *Journal of autism and developmental disorders,* 32**,** 217-224.
D'SOUZA, Y., FOMBONNE, E. & WARD, B. J. 2006. No evidence of persisting measles virus in peripheral blood mononuclear cells from children with autism spectrum disorder. *Pediatrics,* 118**,** 1664-1675.
DALES, L., HAMMER, S. J. & SMITH, N. J. 2001. Time trends in autism and in MMR immunization coverage in California. *Jama,* 285**,** 1183-1185.
DAVIDOVITCH, M., PATTERSON, B. & GARTSIDE, P. 1996. Head circumference measurements in children with autism. *Journal of child neurology,* 11**,** 389-393.
DAVIS, R. L., KRAMARZ, P., BOHLKE, K., BENSON, P., THOMPSON, R. S., MULLOOLY, J., BLACK, S., SHINEFIELD, H., LEWIS, E. & WARD, J. 2001. Measles-mumps-rubella and other measles-containing vaccines do not increase the risk for inflammatory bowel disease: a case-control study from the Vaccine Safety Datalink project. *Archives of pediatrics & adolescent medicine,* 155**,** 354-359.
DEFELIPE, J. 1997. Types of neurons, synaptic connections and chemical characteristics of cells immunoreactive for calbindin-D28K, parvalbumin and calretinin in the neocortex. *Journal of chemical neuroanatomy,* 14**,** 1-19.
DEMENTIEVA, Y. A., VANCE, D. D., DONNELLY, S. L., ELSTON, L. A., WOLPERT, C. M., RAVAN, S. A., DELONG, G. R., ABRAMSON, R. K., WRIGHT, H. H. & CUCCARO, M. L. 2005. Accelerated head growth in early development of individuals with autism. *Pediatric neurology,* 32**,** 102-108.
DESHPANDE, G., LIBERO, L. E., SREENIVASAN, K. R., DESHPANDE, H. D. & KANA, R. K. 2013. Identification of neural connectivity signatures of autism using machine learning. *Frontiers in human neuroscience,* 7.
DESTEFANO, F., BHASIN, T. K., THOMPSON, W. W., YEARGIN-ALLSOPP, M. & BOYLE, C. 2004. Age at first measles-mumps-rubella vaccination in children with autism and school-matched control subjects: a population-based study in metropolitan Atlanta. *Pediatrics,* 113**,** 259-266.
DESTEFANO, F., PRICE, C. S. & WEINTRAUB, E. S. 2013. Increasing exposure to antibody-stimulating proteins and polysaccharides in vaccines is not associated with risk of autism. *The Journal of pediatrics,* 163**,** 561-567.
DUONG, T., ROBINSON, H., BA, D. G. & RITVO, A. 1986. Lower Purkinje cell counts in the cerebella of four autistic subjects: initial findings of the UCLA-NSAC Autopsy Research Report. *Am J Psychiatry,* 143**,** 862-866.
ECKER, C., ANDREWS, D., DELL'ACQUA, F., DALY, E., MURPHY, C., CATANI, M., DE SCHOTTEN, M. T., BARON-COHEN, S., LAI, M. & LOMBARDO, M. 2016. Relationship Between Cortical Gyrification, White Matter Connectivity, and Autism Spectrum Disorder. *Cerebral Cortex*.
ECKER, C., GINESTET, C., FENG, Y., JOHNSTON, P., LOMBARDO, M. V., LAI, M.-C., SUCKLING, J., PALANIYAPPAN, L., DALY, E. & MURPHY, C. M. 2013a. Brain Surface Anatomy in Adults With Autism - The Relationship Between Surface Area, Cortical Thickness, and Autistic Symptoms. *JAMA psychiatry,* 70**,** 59-70.

ECKER, C., MARQUAND, A., MOURÃO-MIRANDA, J., JOHNSTON, P., DALY, E. M., BRAMMER, M. J., MALTEZOS, S., MURPHY, C. M., ROBERTSON, D. & WILLIAMS, S. C. 2010a. Describing the brain in autism in five dimensions—magnetic resonance imaging-assisted diagnosis of autism spectrum disorder using a multiparameter classification approach. *The Journal of Neuroscience,* 30**,** 10612-10623.

ECKER, C. & MURPHY, D. 2014. Neuroimaging in autism - from basic science to translational research. *Nat Rev Neurol,* 10**,** 82-91.

ECKER, C., ROCHA-REGO, V., JOHNSTON, P., MOURAO-MIRANDA, J., MARQUAND, A., DALY, E. M., BRAMMER, M. J., MURPHY, C. & MURPHY, D. G. 2010b. Investigating the predictive value of whole-brain structural MR scans in autism: A pattern classification approach. *NeuroImage,* 49**,** 44-56.

ECKER, C., RONAN, L., FENG, Y., DALY, E., MURPHY, C., GINESTET, C. E., BRAMMER, M., FLETCHER, P. C., BULLMORE, E. T. & SUCKLING, J. 2013b. Intrinsic gray-matter connectivity of the brain in adults with autism spectrum disorder. *Proceedings of the National Academy of Sciences,* 110**,** 13222-13227.

ECKER, C., SHAHIDIANI, A., FENG, Y., DALY, E., MURPHY, C., D'ALMEIDA, V., DEONI, S., WILLIAMS, S. C., GILLAN, N., GUDBRANDSEN, M., WICHERS, R., ANDREWS, D., VAN HEMERT, L. & MURPHY, D. G. M. 2014. The effect of age, diagnosis, and their interaction on vertex-based measures of cortical thickness and surface area in autism spectrum disorder. *Journal of Neural Transmission,* 121**,** 1157-1170.

ECKER, C., SUCKLING, J., DEONI, S. C., LOMBARDO, M. V., BULLMORE, E. T., BARON-COHEN, S., CATANI, M., JEZZARD, P., BARNES, A., BAILEY, A. J., WILLIAMS, S. C., MURPHY, D. G. M. & CONSORTIUM, M. A. 2012. Brain Anatomy and Its Relationship to Behavior in Adults With Autism Spectrum Disorder. *Archives of General Psychiatry,* 69**,** 195-209.

EKMAN, P., FRIESEN, W. V. & PRESS, C. P. 1975. *Pictures of facial affect,* Consulting Psychologists Press.

FARRINGTON, C. P., MILLER, E. & TAYLOR, B. 2001. MMR and autism: further evidence against a causal association. *Vaccine,* 19**,** 3632-3635.

FERNÁNDEZ, V., LLINARES‐BENADERO, C., BORRELL, V., MICHL, J., ZIMMER, J. & TARSOUNAS, M. 2016. Cerebral cortex expansion and folding: what have we learned? *The EMBO journal,* 35**,** 1021-1044.

FIDLER, D. J., BAILEY, J. N. & SMALLEY, S. L. 2000. Macrocephaly in autism and other pervasive developmental disorders. *Developmental Medicine & Child Neurology,* 42**,** 737-740.

FOLSTEIN, S. & RUTTER, M. 1977. Infantile autism: a genetic study of 21 twin pairs. *Journal of Child psychology and Psychiatry,* 18**,** 297-321.

FOMBONNE, E. & CHAKRABARTI, S. 2001. No evidence for a new variant of measles-mumps-rubella–induced autism. *Pediatrics,* 108**,** e58-e58.

FOMBONNE, E., ZAKARIAN, R., BENNETT, A., MENG, L. & MCLEAN-HEYWOOD, D. 2006. Pervasive developmental disorders in Montreal, Quebec, Canada: prevalence and links with immunizations. *Pediatrics,* 118**,** e139-e150.

FRISTON, K. J., HOLMES, A. P., WORSLEY, K. J., POLINE, J. P., FRITH, C. D. & FRACKOWIAK, R. S. J. 1994. Statistical parametric maps in functional imaging: a general linear approach. *Human brain mapping,* 2**,** 189-210.

FRITH, C. 2004. Is autism a disconnection disorder? *The Lancet Neurology,* 3**,** 577.
GARDENER, H., SPIEGELMAN, D. & BUKA, S. L. 2009. Prenatal risk factors for autism: comprehensive meta-analysis. *The British Journal of Psychiatry,* 195**,** 7-14.
GESCHWIND, D. H. & LEVITT, P. 2007. Autism spectrum disorders: developmental disconnection syndromes. *Current opinion in neurobiology,* 17**,** 103-111.
GORI, I., GIULIANO, A., MURATORI, F., SAVIOZZI, I., OLIVA, P., TANCREDI, R., COSENZA, A., TOSETTI, M., CALDERONI, S. & RETICO, A. 2015. Gray matter alterations in young children with autism spectrum disorders: comparing morphometry at the voxel and regional level. *Journal of Neuroimaging,* 25**,** 866-874.
GOZZI, M., NIELSON, D. M., LENROOT, R. K., OSTUNI, J. L., LUCKENBAUGH, D. A., THURM, A. E., GIEDD, J. N. & SWEDO, S. E. 2012. A magnetization transfer imaging study of corpus callosum myelination in young children with autism. *Biological psychiatry,* 72**,** 215-220.
GREENFIELD, J. G. & ARING, C. D. 1954. *The Spino-Cerebellar Degenerations.(Edited by Charles D. Aring.)[With a Bibliography.]*, Blackwell Scientific Publications.
HADJIKHANI, N., JOSEPH, R. M., SNYDER, J. & TAGER-FLUSBERG, H. 2006. Anatomical differences in the mirror neuron system and social cognition network in autism. *Cerebral cortex,* 16**,** 1276-1282.
HALLMAYER, J., CLEVELAND, S., TORRES, A. ET AL. 2011a. Genetic heritability and shared environmental factors among twin pairs with autism. *Archives of General Psychiatry,* 68**,** 1095-1102.
HALLMAYER, J., CLEVELAND, S., TORRES, A., PHILLIPS, J., COHEN, B. & TORIGOE, T. 2011b. Genetic heritability and shared environmental factors among twin pairs with autism. *Arch Gen Psychiatry,* 68**,** 1095 - 102.
HANSEN, S. N., SCHENDEL, D. E. & PARNER, E. T. 2015. Explaining the increase in the prevalence of autism spectrum disorders: The proportion attributable to changes in reporting practices. *JAMA pediatrics,* 169**,** 56-62.
HAPPÉ, F. & FRITH, U. 2006. The weak coherence account: detail-focused cognitive style in autism spectrum disorders. *Journal of autism and developmental disorders,* 36**,** 5-25.
HARDAN, A., MUDDASANI, S., VEMULAPALLI, M., KESHAVAN, M. & MINSHEW, N. 2006. An MRI study of increased cortical thickness in autism. *American Journal of Psychiatry,* 163**,** 1290-1292.
HARDAN, A. Y., JOU, R. J., KESHAVAN, M. S., VARMA, R. & MINSHEW, N. J. 2004. Increased frontal cortical folding in autism: a preliminary MRI study. *Psychiatry Research: Neuroimaging,* 131**,** 263-268.
HARDAN, A. Y., LIBOVE, R. A., KESHAVAN, M. S., MELHEM, N. M. & MINSHEW, N. J. 2009. A preliminary longitudinal magnetic resonance imaging study of brain volume and cortical thickness in autism. *Biological psychiatry,* 66**,** 320-326.
HAZLETT, H. C., GU, H., MUNSELL, B. C., KIM, S. H., STYNER, M., WOLFF, J. J., ELISON, J. T., SWANSON, M. R., ZHU, H. & BOTTERON, K. N. 2017. Early brain development in infants at high risk for autism spectrum disorder. *Nature,* 542**,** 348-351.

HAZLETT, H. C., POE, M., GERIG, G., SMITH, R. G., PROVENZALE, J., ROSS, A., GILMORE, J. & PIVEN, J. 2005. Magnetic resonance imaging and head circumference study of brain size in autism: birth through age 2 years. *Archives of general psychiatry,* 62**,** 1366.

HAZLETT, H. C., POE, M. D., GERIG, G., SMITH, R. G. & PIVEN, J. 2006. Cortical gray and white brain tissue volume in adolescents and adults with autism. *Biological psychiatry,* 59**,** 1-6.

HAZLETT, H. C., POE, M. D., GERIG, G., STYNER, M., CHAPPELL, C., SMITH, R. G., VACHET, C. & PIVEN, J. 2011. Early brain overgrowth in autism associated with an increase in cortical surface area before age 2 years. *Archives of general psychiatry,* 68**,** 467-476.

HOLMES, G. & STEWART, T. G. 1908. ON THE CONNECTION OF THE INFERIOR OLIVES WITH THE CEREBELLUM IN MAN. *Brain,* 31**,** 125-137.

HONDA, H., SHIMIZU, Y. & RUTTER, M. 2005. No effect of MMR withdrawal on the incidence of autism: a total population study. *Journal of Child Psychology and Psychiatry,* 46**,** 572-579.

HONG, S., KE, X., TANG, T., HANG, Y., CHU, K., HUANG, H., RUAN, Z., LU, Z., TAO, G. & LIU, Y. 2011. Detecting abnormalities of corpus callosum connectivity in autism using magnetic resonance imaging and diffusion tensor tractography. *Psychiatry Research: Neuroimaging,* 194**,** 333-339.

HORNIG, M., BRIESE, T., BUIE, T., BAUMAN, M. L., LAUWERS, G., SIEMETZKI, U., HUMMEL, K., ROTA, P. A., BELLINI, W. J. & O'LEARY, J. J. 2008. Lack of association between measles virus vaccine and autism with enteropathy: a case-control study. *PLoS One,* 3**,** e3140.

HORWITZ, B., RUMSEY, J. M., GRADY, C. L. & RAPOPORT, S. I. 1988. The cerebral metabolic landscape in autism: intercorrelations of regional glucose utilization. *Archives of neurology,* 45**,** 749.

HUGUET, G., EY, E. & BOURGERON, T. 2013. The genetic landscapes of autism spectrum disorders. *Annual review of genomics and human genetics,* 14**,** 191-213.

HUTSLER, J. J., LOVE, T. & ZHANG, H. 2007. Histological and magnetic resonance imaging assessment of cortical layering and thickness in autism spectrum disorders. *Biological psychiatry,* 61**,** 449-457.

HUTSLER, J. J. & ZHANG, H. 2010. Increased dendritic spine densities on cortical projection neurons in autism spectrum disorders. *Brain research,* 1309**,** 83-94.

HUTTENLOCHER, P. R. 1990. Morphometric study of human cerebral cortex development. *Neuropsychologia,* 28**,** 517-527.

HVIID, A., STELLFELD, M., WOHLFAHRT, J. & MELBYE, M. 2003. Association between thimerosal-containing vaccine and autism. *JAMA,* 290**,** 1763-1766.

HYDE, K. L., SAMSON, F., EVANS, A. C. & MOTTRON, L. 2010. Neuroanatomical differences in brain areas implicated in perceptual and other core features of autism revealed by cortical thickness analysis and voxel-based morphometry. *Human Brain Mapping,* 31**,** 556-566.

IDRING, S., RAI, D., DAL, H., DALMAN, C., STURM, H., ZANDER, E., LEE, B. K., SERLACHIUS, E. & MAGNUSSON, C. 2012. Autism spectrum disorders in the Stockholm Youth Cohort: design, prevalence and validity. *PloS one,* 7**,** e41280.

IIDAKA, T. 2015. Resting state functional magnetic resonance imaging and neural network classified autism and control. *Cortex,* 63**,** 55-67.
INGALHALIKAR, M., KANTERAKIS, S., GUR, R., ROBERTS, T. P. & VERMA, R. 2010. DTI based diagnostic prediction of a disease via pattern classification. *Medical Image Computing and Computer-Assisted Intervention–MICCAI 2010.* Springer.
INGALHALIKAR, M., PARKER, D., BLOY, L., ROBERTS, T. P. L. & VERMA, R. 2011. Diffusion based abnormality markers of pathology: Toward learned diagnostic prediction of ASD. *NeuroImage,* 57**,** 918-927.
INGALHALIKAR, M., PARKER, W. A., BLOY, L., ROBERTS, T. P. & VERMA, R. 2014. Creating multimodal predictors using missing data: Classifying and subtyping autism spectrum disorder. *Journal of neuroscience methods,* 235**,** 1-9.
JACQUEMONT, M.-L., SANLAVILLE, D., REDON, R., RAOUL, O., CORMIER-DAIRE, V., LYONNET, S., AMIEL, J., LE MERRER, M., HERON, D. & DE BLOIS, M.-C. 2006. Array-based comparative genomic hybridisation identifies high frequency of cryptic chromosomal rearrangements in patients with syndromic autism spectrum disorders. *Journal of medical genetics,* 43**,** 843-849.
JAHANSHAD, N. and THOMPSON, P.M., 2017. Multimodal neuroimaging of male and female brain structure in health and disease across the life span. *Journal of neuroscience research*, *95*(1-2), pp.371-379.
JIAO, Y., CHEN, R., KE, X., CHU, K., LU, Z. & HERSKOVITS, E. H. 2010. Predictive models of autism spectrum disorder based on brain regional cortical thickness. *Neuroimage,* 50**,** 589-599.
JUST, M. A., CHERKASSKY, V. L., KELLER, T. A., KANA, R. K. & MINSHEW, N. J. 2007. Functional and anatomical cortical underconnectivity in autism: evidence from an FMRI study of an executive function task and corpus callosum morphometry. *Cerebral Cortex,* 17**,** 951-961.
JUST, M. A., CHERKASSKY, V. L., KELLER, T. A. & MINSHEW, N. J. 2004. Cortical activation and synchronization during sentence comprehension in high-functioning autism: evidence of underconnectivity. *Brain,* 127**,** 1811-1821.
JUST, M. A., KELLER, T. A., MALAVE, V. L., KANA, R. K. & VARMA, S. 2012. Autism as a neural systems disorder: a theory of frontal-posterior underconnectivity. *Neuroscience & Biobehavioral Reviews,* 36**,** 1292-1313.
KANNER, L. 1943. Autistic disturbances of affective contact. *Nervous child,* 2**,** 217-250.
KATES, W. R., IKUTA, I. & BURNETTE, C. P. 2009. Gyrification patterns in monozygotic twin pairs varying in discordance for autism. *Autism Research,* 2**,** 267-278.
KAWAGUCHI, Y. & KUBOTA, Y. 1997. GABAergic cell subtypes and their synaptic connections in rat frontal cortex. *Cerebral cortex,* 7**,** 476-486.
KAYE, J. A., DEL MAR MELERO-MONTES, M. & JICK, H. 2001. Mumps, measles, and rubella vaccine and the incidence of autism recorded by general practitioners: a time trend analysis. *BMJ,* 322**,** 460-463.
KHUNDRAKPAM, B. S. L., J.D.; KOSTOPOULOS, P.; CARBONELL, F.; EVANS, A.C. 2017. Cortical Thickness Abnormalities in Autism Spectrum Disorders

Through Late Childhood, Adolescence, and Adulthood: A Large-Scale MRI Study. *Cerebral Cortex*.
KIM, Y. S., LEVENTHAL, B. L., KOH, Y.-J., FOMBONNE, E., LASKA, E., LIM, E.-C., CHEON, K.-A., KIM, S.-J., KIM, Y.-K., LEE, H., SONG, D.-H. & GRINKER, R. R. 2011. Prevalence of Autism Spectrum Disorders in a Total Population Sample. *American Journal of Psychiatry,* 168**,** 904-912.
KLEIN, K. C. & DIEHL, E. B. 2004. Relationship between MMR vaccine and autism. *Annals of pharmacotherapy,* 38**,** 1297-1300.
KLEIN, N. P., AUKES, L., LEE, J., FIREMAN, B., SHAPIRA, S. K., SLADE, B., BAXTER, R. & SUMMAR, M. 2011. Evaluation of immunization rates and safety among children with inborn errors of metabolism. *Pediatrics***,** peds. 2010-3706.
KLEIN, N. P., LEWIS, E., BAXTER, R., WEINTRAUB, E., GLANZ, J., NALEWAY, A., JACKSON, L. A., NORDIN, J., LIEU, T. & BELONGIA, E. A. 2012. Measles-containing vaccines and febrile seizures in children age 4 to 6 years. *Pediatrics,* 129**,** 809-814.
KRIEGSTEIN, A., NOCTOR, S. & MARTÍNEZ-CERDEÑO, V. 2006. Patterns of neural stem and progenitor cell division may underlie evolutionary cortical expansion. *Nature Reviews Neuroscience,* 7**,** 883-890.
LAI, M. C., LERCH, J. P., FLORIS, D. L., RUIGROK, A. N., POHL, A., LOMBARDO, M. V. & BARON‐COHEN, S. 2017. Imaging sex/gender and autism in the brain: Etiological implications. *Journal of Neuroscience Research,* 95**,** 380-397.
LEE, B. K., MAGNUSSON, C., GARDNER, R. M., BLOMSTRÖM, Å., NEWSCHAFFER, C. J., BURSTYN, I., KARLSSON, H. & DALMAN, C. 2015. Maternal hospitalization with infection during pregnancy and risk of autism spectrum disorders. *Brain, behavior, and immunity,* 44**,** 100-105.
LEVITT, J. G., BLANTON, R. E., SMALLEY, S., THOMPSON, P., GUTHRIE, D., MCCRACKEN, J. T., SADOUN, T., HEINICHEN, L. & TOGA, A. W. 2003. Cortical sulcal maps in autism. *Cerebral Cortex,* 13**,** 728-735.
LEYFER, O. T., FOLSTEIN, S. E., BACALMAN, S., DAVIS, N. O., DINH, E., MORGAN, J., TAGER-FLUSBERG, H. & LAINHART, J. E. 2006. Comorbid psychiatric disorders in children with autism: Interview development and rates of disorders. *Journal of autism and developmental disorders,* 36**,** 849-861.
LIBERO, L. E., DERAMUS, T. P., DESHPANDE, H. D. & KANA, R. K. 2014. Surface-based morphometry of the cortical architecture of autism spectrum disorders: volume, thickness, area, and gyrification. *Neuropsychologia,* 62**,** 1-10.
LIBERO, L. E., DERAMUS, T. P., LAHTI, A. C., DESHPANDE, G. & KANA, R. K. 2015. Multimodal neuroimaging based classification of autism spectrum disorder using anatomical, neurochemical, and white matter correlates. *Cortex,* 66**,** 46-59.
LIBERO, L. E., NORDAHL, C. W., LI, D. D., FERRER, E., ROGERS, S. J. & AMARAL, D. G. 2016. Persistence of megalencephaly in a subgroup of young boys with autism spectrum disorder. *Autism Research,* 9**,** 1169-1182.
LICHTENSTEIN, P., CARLSTROM, E., RASTAM, M., GILLBERG, C. & ANCKARSATER, H. 2010. The genetics of autism spectrum disorders and related neuropsychiatric disorders in childhood. *Am J Psychiatry,* 167**,** 1357-63.

LINGAM, R., SIMMONS, A., ANDREWS, N., MILLER, E., STOWE, J. & TAYLOR, B. 2003. Prevalence of autism and parentally reported triggers in a north east London population. *Archives of Disease in Childhood,* 88**,** 666-670.
LORD, C., RISI, S., LAMBRECHT, L., COOK JR, E. H., LEVENTHAL, B. L., DILAVORE, P. C., PICKLES, A. & RUTTER, M. 2000. The Autism Diagnostic Observation Schedule—Generic: A standard measure of social and communication deficits associated with the spectrum of autism. *Journal of autism and developmental disorders,* 30**,** 205-223.
LORD, C., RUTTER, M. & COUTEUR, A. 1994. Autism Diagnostic Interview-Revised: a revised version of a diagnostic interview for caregivers of individuals with possible pervasive developmental disorders. *Journal of autism and developmental disorders,* 24**,** 659-685.
MADSEN, K. M., LAURITSEN, M. B., PEDERSEN, C. B., THORSEN, P., PLESNER, A.-M., ANDERSEN, P. H. & MORTENSEN, P. B. 2003. Thimerosal and the occurrence of autism: negative ecological evidence from Danish population-based data. *Pediatrics,* 112**,** 604-606.
MANDY, W., CHILVERS, R., CHOWDHURY, U., SALTER, G., SEIGAL, A. & SKUSE, D. 2012. Sex differences in autism spectrum disorder: evidence from a large sample of children and adolescents. *Journal of autism and developmental disorders,* 42**,** 1304-1313.
MATTILA, M., KIELINEN, M., LINNA, S., JUSSILA, K., EBELING, H. & BLOIGU, R. 2011. Autism spectrum disorders according to DSM-IV-TR and comparison with DSM-5 draft criteria: an epidemiological study. *J Am Acad Child Adolesc Psychiatry,* 50**,** 583 - 92.
MAZUMDAR, S., WINTER, A., LIU, K.-Y. & BEARMAN, P. 2013. Spatial clusters of autism births and diagnoses point to contextual drivers of increased prevalence. *Social science & medicine,* 95**,** 87-96.
MCALONAN, G., CHEUNG, C., CHEUNG, V., WONG, N., SUCKLING, J. & CHUA, S. 2009. Differential effects on white-matter systems in high-functioning autism and Asperger's syndrome. *Psychological Medicine,* 39**,** 1885-1893.
MCALONAN, G. M., CHEUNG, V., CHEUNG, C., SUCKLING, J., LAM, G. Y., TAI, K., YIP, L., MURPHY, D. G. & CHUA, S. E. 2005. Mapping the brain in autism. A voxel-based MRI study of volumetric differences and intercorrelations in autism. *Brain: A Journal of Neurology,* 128**,** 268-276.
MCALONAN, G. M., SUCKLING, J., WONG, N., CHEUNG, V., LIENENKAEMPER, N., CHEUNG, C. & CHUA, S. E. 2008. Distinct patterns of grey matter abnormality in high‐functioning autism and Asperger's syndrome. *Journal of Child Psychology and Psychiatry,* 49**,** 1287-1295.
MILES, J. H., HADDEN, L., TAKAHASHI, T. & HILLMAN, R. 2000. Head circumference is an independent clinical finding associated with autism. *American journal of medical genetics,* 95**,** 339-350.
MITCHELL, T. M. 1997. Machine learning. 1997. *Burr Ridge, IL: McGraw Hill,* 45**,** 37.
MIYATA, T., KAWAGUCHI, A., SAITO, K., KAWANO, M., MUTO, T. & OGAWA, M. 2004. Asymmetric production of surface-dividing and non-surface-dividing cortical progenitor cells. *Development,* 131**,** 3133-3145.
MROZEK-BUDZYN, D., KIELTYKA, A. & MAJEWSKA, R. 2010. Lack of association between measles-mumps-rubella vaccination and autism in children: A case-control study. *The Pediatric infectious disease journal,* 29**,** 397-400.

MURDAUGH, D. L., SHINKAREVA, S. V., DESHPANDE, H. R., WANG, J., PENNICK, M. R. & KANA, R. K. 2012. Differential deactivation during mentalizing and classification of autism based on default mode network connectivity. *PloS one,* 7**,** e50064.

MWANGI, B., TIAN, T. S. & SOARES, J. C. 2014. A review of feature reduction techniques in neuroimaging. *Neuroinformatics,* 12**,** 229-244.

NEJAD, A. B., MADSEN, K. H., EBDRUP, B. H., SIEBNER, H. R., RASMUSSEN, H., AGGERNÆS, B., GLENTHØJ, B. Y. & BAARÉ, W. F. C. 2012. Neural markers of negative symptom outcomes in distributed working memory brain activity of antipsychotic-naive schizophrenia patients. *The International Journal of Neuropsychopharmacology,* FirstView**,** 1-10.

NICKL‐JOCKSCHAT, T., HABEL, U., MARIA MICHEL, T., MANNING, J., LAIRD, A. R., FOX, P. T., SCHNEIDER, F. & EICKHOFF, S. B. 2012. Brain structure anomalies in autism spectrum disorder—a meta‐analysis of VBM studies using anatomic likelihood estimation. *Human brain mapping,* 33**,** 1470-1489.

NOCTOR, S. C., MARTÍNEZ-CERDEÑO, V., IVIC, L. & KRIEGSTEIN, A. R. 2004. Cortical neurons arise in symmetric and asymmetric division zones and migrate through specific phases. *Nature neuroscience,* 7**,** 136-144.

NONAKA‐KINOSHITA, M., REILLO, I., ARTEGIANI, B., MARTÍNEZ‐MARTÍNEZ, M. Á., NELSON, M., BORRELL, V. & CALEGARI, F. 2013. Regulation of cerebral cortex size and folding by expansion of basal progenitors. *The EMBO journal,* 32**,** 1817-1828.

NORDAHL, C. W., DIERKER, D., MOSTAFAVI, I., SCHUMANN, C. M., RIVERA, S. M., AMARAL, D. G. & VAN ESSEN, D. C. 2007. Cortical Folding Abnormalities in Autism Revealed by Surface-Based Morphometry. *The Journal of Neuroscience,* 27**,** 11725-11735.

NORMAN, R. 1940. Cerebellar atrophy associated with etat marbre of the basal ganglia. *Journal of neurology and psychiatry,* 3**,** 311-318.

OZONOFF, S., YOUNG, G., CARTER, A., MESSINGER, D., YIRMIYA, N. & ZWAIGENBAUM, L. 2011. Recurrence risk for autism spectrum disorders: a baby siblings research consortium study. *Pediatrics,* 128**,** e488 - 95.

PACKER, A. 2016. Neocortical neurogenesis and the etiology of autism spectrum disorder. *Neuroscience & Biobehavioral Reviews,* 64**,** 185-195.

PALMEN, S. J., HULSHOFF POL, H. E., KEMNER, C., SCHNACK, H. G., DURSTON, S., LAHUIS, B. E., KAHN, R. S. & VAN ENGELAND, H. 2005. Increased gray-matter volume in medication-naive high-functioning children with autism spectrum disorder. *Psychological medicine,* 35**,** 561-570.

PARDOE, H. R., ABBOTT, D. F. & JACKSON, G. D. 2013. Sample size estimates for well‐powered cross‐sectional cortical thickness studies. *Human brain mapping,* 34**,** 3000-3009.

PELTOLA, H., PATJA, A., LEINIKKI, P., VALLE, M., DAVIDKIN, I. & PAUNIO, M. 1998. No evidence for measles, mumps, and rubella vaccine-associated inflammatory bowel disease or autism in a 14-year prospective study. *The Lancet,* 351**,** 1327-1328.

PICHICHERO, M. E., GENTILE, A., GIGLIO, N., UMIDO, V., CLARKSON, T., CERNICHIARI, E., ZAREBA, G., GOTELLI, C., GOTELLI, M. & YAN, L. 2008. Mercury levels in newborns and infants after receipt of thimerosal-containing vaccines. *Pediatrics,* 121**,** e208-e214.

PIVEN, J., ARNDT, S., BAILEY, J. & ANDREASEN, N. 1996. Regional brain enlargement in autism: a magnetic resonance imaging study. *Journal of the American Academy of Child & Adolescent Psychiatry,* 35**,** 530-536.
PIVEN, J., ARNDT, S., BAILEY, J., HAVERCAMP, S., ANDREASEN, N. C. & PALMER, P. 1995. An MRI study of brain size in autism. *American Journal of Psychiatry,* 152**,** 1145-1149.
PIVEN, J., BERTHIER, M. L., STARKSTEIN, S. E., NEHME, E., PEARLSON, G. & FOLSTEIN, S. 1990. Magnetic resonance imaging evidence for a defect of cerebral cortical development in autism. *The American journal of psychiatry*.
PIVEN, J., NEHME, E., SIMON, J., BARTA, P., PEARLSON, G. & FOLSTEIN, S. E. 1992. Magnetic resonance imaging in autism: measurement of the cerebellum, pons, and fourth ventricle. *Biological Psychiatry,* 31**,** 491-504.
PLITT, M., BARNES, K. A. & MARTIN, A. 2015. Functional connectivity classification of autism identifies highly predictive brain features but falls short of biomarker standards. *NeuroImage: Clinical,* 7**,** 359-366.
PONTIOUS, A., KOWALCZYK, T., ENGLUND, C. & HEVNER, R. F. 2007. Role of intermediate progenitor cells in cerebral cortex development. *Developmental neuroscience,* 30**,** 24-32.
PRICE, C. S., THOMPSON, W. W., GOODSON, B., WEINTRAUB, E. S., CROEN, L. A., HINRICHSEN, V. L., MARCY, M., ROBERTSON, A., ERIKSEN, E. & LEWIS, E. 2010. Prenatal and infant exposure to thimerosal from vaccines and immunoglobulins and risk of autism. *Pediatrics***,** peds. 2010-0309.
RAKIC, P. 1971. Neuron‐glia relationship during granule cell migration in developing cerebellar cortex. A Golgi and electonmicroscopic study in Macacus rhesus. *Journal of Comparative Neurology,* 141**,** 283-312.
RAKIC, P. 1995. A small step for the cell, a giant leap for mankind: a hypothesis of neocortical expansion during evolution. *Trends in neurosciences,* 18**,** 383-388.
RAKIC, P. & SIDMAN, R. L. 1970. Histogenesis of cortical layers in human cerebellum, particularly the lamina dissecans. *Journal of Comparative Neurology,* 139**,** 473-500.
RASMUSSEN, C. E. & WILLIAMS, C. K. I. 2006. *Gaussian processes for machine learning*, MIT press Cambridge, MA.
RAZNAHAN, A., TORO, R., DALY, E., ROBERTSON, D., MURPHY, C., DEELEY, Q., BOLTON, P. F., PAUS, T. & MURPHY, D. G. 2009. Cortical anatomy in autism spectrum disorder: an in vivo MRI study on the effect of age. *Cerebral cortex*.
REICH, T., CLONINGER, C. R. & GUZE, S. B. 1975. The multifactorial model of disease transmission: I. Description of the model and its use in psychiatry. *The British Journal of Psychiatry,* 127**,** 1-10.
REILLO, I., DE JUAN ROMERO, C., GARCÍA-CABEZAS, M. Á. & BORRELL, V. 2011. A role for intermediate radial glia in the tangential expansion of the mammalian cerebral cortex. *Cerebral Cortex,* 21**,** 1674-1694.
RICHLER, J., LUYSTER, R., RISI, S., HSU, W.-L., DAWSON, G., BERNIER, R., DUNN, M., HEPBURN, S., HYMAN, S. L. & MCMAHON, W. M. 2006. Is there a 'regressive phenotype'of autism spectrum disorder associated with the measles-mumps-rubella vaccine? A CPEA study. *Journal of autism and developmental disorders,* 36**,** 299-316.

RICHMAN, D. P., STEWART, R. M., HUTCHINSON, J. & CAVINCSS JR, V. S. 1975. Mechanical mode of brain convolutional deve lopment. *Science,* 189**,** 18-21.
ROGERS, J., KOCHUNOV, P., ZILLES, K., SHELLEDY, W., LANCASTER, J., THOMPSON, P., DUGGIRALA, R., BLANGERO, J., FOX, P. T. & GLAHN, D. C. 2010. On the genetic architecture of cortical folding and brain volume in primates. *Neuroimage,* 53**,** 1103-1108.
RUGGERI, B., SARKANS, U., SCHUMANN, G. & PERSICO, A. M. 2013. Biomarkers in autism spectrum disorder: the old and the new. *Psychopharmacology***,** 1-16.
RUIGROK, A.N., SALIMI-KHORSHIDI, G., LAI, M.C., BARON-COHEN, S., LOMBARDO, M.V., TAIT, R.J. and SUCKLING, J., 2014. A meta-analysis of sex differences in human brain structure. *Neuroscience & Biobehavioral Reviews*, *39*, 34-50.
SABUNCU, M. R. & KONUKOGLU, E. 2014. Clinical Prediction from Structural Brain MRI Scans: A Large-Scale Empirical Study. *Neuroinformatics***,** 1-16.
SANDERS, S., MURTHA, M., GUPTA, A., MURDOCH, J., RAUBESON, M. & WILLSEY, A. 2012. De novo mutations revealed by whole-exome sequencing are strongly associated with autism. *Nature,* 485**,** 237 - 41.
SANDIN, S., LICHTENSTEIN, P., KUJA-HALKOLA, R., LARSSON, H., HULTMAN, C. M. & REICHENBERG, A. 2014. The familial risk of autism. *Jama,* 311**,** 1770-7.
SATO, J. R., HOEXTER, M. Q., DE MAGALHÃES OLIVEIRA, P. P., BRAMMER, M. J., MURPHY, D., ECKER, C. & CONSORTIUM, M. A. 2013. Inter-regional cortical thickness correlations are associated with autistic symptoms: a machine-learning approach. *Journal of psychiatric research,* 47**,** 453-459.
SCHAER, M., CUADRA, M. B., TAMARIT, L., LAZEYRAS, F., ELIEZ, S. & THIRAN, J. 2008. A surface-based approach to quantify local cortical gyrification. *Medical Imaging, IEEE Transactions on,* 27**,** 161-170.
SCHAER, M., OTTET, M.-C., SCARIATI, E., DUKES, D., FRANCHINI, M., ELIEZ, S. & GLASER, B. 2013. Decreased frontal gyrification correlates with altered connectivity in children with autism. *Frontiers in human neuroscience,* 7.
SCHECHTER, R. & GRETHER, J. K. 2008. Continuing increases in autism reported to California's developmental services system: mercury in retrograde. *Archives of General Psychiatry,* 65**,** 19-24.
SCHEEL, C., ROTARSKA-JAGIELA, A., SCHILBACH, L., LEHNHARDT, F. G., KRUG, B., VOGELEY, K. & TEPEST, R. 2011. Imaging derived cortical thickness reduction in high-functioning autism: Key regions and temporal slope. *Neuroimage,* 58**,** 391-400.
SCHENDEL, D. & BHASIN, T. K. 2008. Birth weight and gestational age characteristics of children with autism, including a comparison with other developmental disabilities. *Pediatrics,* 121**,** 1155-1164.
SEBAT, J., LAKSHMI, B., MALHOTRA, D., TROGE, J., LESE-MARTIN, C., WALSH, T., YAMROM, B., YOON, S., KRASNITZ, A. & KENDALL, J. 2007. Strong association of de novo copy number mutations with autism. *Science,* 316**,** 445-449.
SEGOVIA, F., HOLT, R., SPENCER, M., GÓRRIZ, J. M., RAMÍREZ, J., PUNTONET, C. G., PHILLIPS, C., CHURA, L., BARON-COHEN, S. & SUCKLING, J. 2014.

Identifying endophenotypes of autism: a multivariate approach. *Frontiers in computational neuroscience,* 8.
SHEN, M. D., KIM, S. H., MCKINSTRY, R. C., GU, H., HAZLETT, H. C., NORDAHL, C. W., EMERSON, R. E., SHAW, D., ELISON, J. T., SWANSON, M. R., FONOV, V. S., GERIG, G., DAGER, S. R., BOTTERON, K. N., PATERSON, S., SCHULTZ, R. T., EVANS, A. C., ESTES, A. M., ZWAIGENBAUM, L., STYNER, M. A., AMARAL, D. G. & PIVEN, J. 2017. Increased Extra-axial Cerebrospinal Fluid in High-Risk Infants who Later Develop Autism. *Biological Psychiatry*.
SHOKOUHI, M., WILLIAMS, J. H., WAITER, G. D. & CONDON, B. 2012. Changes in the sulcal size associated with autism spectrum disorder revealed by sulcal morphometry. *Autism Research,* 5**,** 245-252.
SHUKLA, D. K., KEEHN, B., LINCOLN, A. J. & MÜLLER, R.-A. 2010. White matter compromise of callosal and subcortical fiber tracts in children with autism spectrum disorder: a diffusion tensor imaging study. *Journal of the American Academy of Child & Adolescent Psychiatry,* 49**,** 1269-1278.
SIMONOFF, E., PICKLES, A., CHARMAN, T., CHANDLER, S., LOUCAS, T. & BAIRD, G. 2008. Psychiatric disorders in children with autism spectrum disorders: prevalence, comorbidity, and associated factors in a population-derived sample. *Journal of the American Academy of Child & Adolescent Psychiatry,* 47**,** 921-929.
SMEETH, L., COOK, C., FOMBONNE, E., HEAVEY, L., RODRIGUES, L. C., SMITH, P. G. & HALL, A. J. 2004. MMR vaccination and pervasive developmental disorders: a case-control study. *The Lancet,* 364**,** 963-969.
SMITH, M. J. & WOODS, C. R. 2010. On-time vaccine receipt in the first year does not adversely affect neuropsychological outcomes. *Pediatrics,* 125**,** 1134-1141.
SOWELL, E. R., THOMPSON, P. M., LEONARD, C. M., WELCOME, S. E., KAN, E. & TOGA, A. W. 2004. Longitudinal mapping of cortical thickness and brain growth in normal children. *The Journal of neuroscience,* 24**,** 8223-8231.
STEHR-GREEN, P., TULL, P., STELLFELD, M., MORTENSON, P.-B. & SIMPSON, D. 2003. Autism and thimerosal-containing vaccines: lack of consistent evidence for an association. *American journal of preventive medicine,* 25**,** 101-106.
SU, S., WHITE, T., SCHMIDT, M., KAO, C. Y. & SAPIRO, G. 2013. Geometric computation of human gyrification indexes from magnetic resonance images. *Human brain mapping,* 34**,** 1230-1244.
SZATMARI, P., LIU, X. Q., GOLDBERG, J., ZWAIGENBAUM, L., PATERSON, A. D., WOODBURY‐SMITH, M., GEORGIADES, S., DUKU, E. & THOMPSON, A. 2012. Sex differences in repetitive stereotyped behaviors in autism: implications for genetic liability. *American Journal of Medical Genetics Part B: Neuropsychiatric Genetics,* 159**,** 5-12.
TAMMIMIES, K., MARSHALL, C. R., WALKER, S., KAUR, G., THIRUVAHINDRAPURAM, B., LIONEL, A. C., YUEN, R. K., UDDIN, M., ROBERTS, W. & WEKSBERG, R. 2015. Molecular diagnostic yield of chromosomal microarray analysis and whole-exome sequencing in children with autism spectrum disorder. *Jama,* 314**,** 895-903.
TANG, G., GUDSNUK, K., KUO, S.-H., COTRINA, MARISA L., ROSOKLIJA, G., SOSUNOV, A., SONDERS, MARK S., KANTER, E., CASTAGNA, C., YAMAMOTO, A., YUE, Z., ARANCIO, O., PETERSON, BRADLEY S.,

CHAMPAGNE, F., DWORK, ANDREW J., GOLDMAN, J. & SULZER, D. 2014. Loss of mTOR-Dependent Macroautophagy Causes Autistic-like Synaptic Pruning Deficits. *Neuron*.
TAYLOR, B., MILLER, E., FARRINGTON, C., PETROPOULOS, M.-C., FAVOT-MAYAUD, I., LI, J. & WAIGHT, P. A. 1999. Autism and measles, mumps, and rubella vaccine: no epidemiological evidence for a causal association. *The Lancet,* 353**,** 2026-2029.
TAYLOR, B., MILLER, E., LINGAM, R., ANDREWS, N., SIMMONS, A. & STOWE, J. 2002. Measles, mumps, and rubella vaccination and bowel problems or developmental regression in children with autism: population study. *Bmj,* 324**,** 393-396.
THOMPSON, W. W., PRICE, C., GOODSON, B., SHAY, D. K., BENSON, P., HINRICHSEN, V. L., LEWIS, E., ERIKSEN, E., RAY, P. & MARCY, S. M. 2007. Early thimerosal exposure and neuropsychological outcomes at 7 to 10 years. *New England Journal of Medicine,* 357**,** 1281-1292.
UCHIYAMA, T., KUROSAWA, M. & INABA, Y. 2007. MMR-vaccine and regression in autism spectrum disorders: negative results presented from Japan. *Journal of autism and developmental disorders,* 37**,** 210-217.
UDDIN, L. Q., MENON, V., YOUNG, C. B., RYALI, S., CHEN, T., KHOUZAM, A., MINSHEW, N. J. & HARDAN, A. Y. 2011. Multivariate searchlight classification of structural magnetic resonance imaging in children and adolescents with autism. *Biological Psychiatry,* 70**,** 833-841.
UDDIN, L. Q., SUPEKAR, K., LYNCH, C. J., KHOUZAM, A., PHILLIPS, J., FEINSTEIN, C., RYALI, S. & MENON, V. 2013. Salience network–based classification and prediction of symptom severity in children with autism. *JAMA psychiatry,* 70**,** 869-879.
UHLHAAS, P. J., ROUX, F., SINGER, W., HAENSCHEL, C., SIRETEANU, R. & RODRIGUEZ, E. 2009. The development of neural synchrony reflects late maturation and restructuring of functional networks in humans. *Proceedings of the National Academy of Sciences,* 106**,** 9866-9871.
VAN ESSEN, D. C. 1997. A tension-based theory of morphogenesis and compact wiring in the central nervous system. *NATURE-LONDON-***,** 313-318.
VAPNIK, V. 1995. *The Nature of Statistical Learning Theory,* New York, Springer-Verlag.
VOIGT J, PAKKENBERG H. 1983. Brain weight of Danish children. A forensic material. *Acta Anat (Basel)* 116:290–301.
WALLACE, G. L., ROBUSTELLI, B., DANKNER, N., KENWORTHY, L., GIEDD, J. N. & MARTIN, A. 2013. Increased gyrification, but comparable surface area in adolescents with autism spectrum disorders. *Brain,* 136**,** 1956-1967.
WEE, C. Y., WANG, L., SHI, F., YAP, P. T. & SHEN, D. 2014. Diagnosis of autism spectrum disorders using regional and interregional morphological features. *Human brain mapping,* 35**,** 3414-3430.
WEE, C. Y., YAP, P. T. & SHEN, D. 2016. Diagnosis of Autism Spectrum Disorders Using Temporally Distinct Resting‐State Functional Connectivity Networks. *CNS Neuroscience & Therapeutics*.
WELKER, W. 1990. Why does cerebral cortex fissure and fold? *Cerebral cortex.* Springer.
WERLING, D. & GESCHWIND, D. 2013. Sex differences in autism spectrum disorders. *Curr Opin Neurol,* 26**,** 146 - 153.

WERLING, D. M. 2016. The role of sex-differential biology in risk for autism spectrum disorder. *Biology of Sex Differences,* 7**,** 58.
WHITE, T., ANDREASEN, N. C. & NOPOULOS, P. 2002. Brain volumes and surface morphology in monozygotic twins. *Cerebral cortex,* 12**,** 486-493.
WING, L. 1997. The autistic spectrum. *The lancet,* 350**,** 1761-1766.
WOLFERS, T., BUITELAAR, J. K., BECKMANN, C. F., FRANKE, B. & MARQUAND, A. F. 2015. From estimating activation locality to predicting disorder: A review of pattern recognition for neuroimaging-based psychiatric diagnostics. *Neuroscience & Biobehavioral Reviews,* 57**,** 328-349.
WOODHOUSE, W., BAILEY, A., RUTTER, M., BOLTON, P., BAIRD, G. & COUTEUR, A. 1996. Head circumference in autism and other pervasive developmental disorders. *Journal of Child Psychology and Psychiatry,* 37**,** 665-671.
WORLD HEALTH ORGANIZATION 2004. *International statistical classification of diseases and related health problems*, World Health Organization.
ZILLES, K., ARMSTRONG, E., SCHLEICHER, A. & KRETSCHMANN, H.-J. 1988. The human pattern of gyrification in the cerebral cortex. *Anatomy and embryology,* 179**,** 173-179.
ZILLES, K., PALOMERO-GALLAGHER, N. & AMUNTS, K. 2013. Development of cortical folding during evolution and ontogeny. *Trends in neurosciences,* 36**,** 275-284.

Chapter 2: Magnetic Resonance Imaging and Analysis Methods

I will begin this chapter by discussing the basic physical principles underlying Magnetic Resonance Imaging (MRI) (Lauterbur, 1973, Mansfield, 1977), as reviewed by Sprawls (1987). Details of basic MRI scanning sequences and those used to acquire structural images of the brain within this thesis will then be covered. Last, I will discuss methods for the analysis of MRI images including surfaced based (SBM) morphometry, the general linear model (GLM), and multivariate pattern classification (MVPC) (i.e. "machine learning") techniques.

2.1 Principles of Nuclear Magnetic Resonance

Magnetic resonance imaging (MRI) is made possible by interactions of atomic nuclei and radio waves that occur when objects are placed within a magnetic field. Under these conditions atoms take on a resonant characteristic whereby electromagnetic radiation is absorbed and rereleased at a particular frequency. This phenomena is generally known as Nuclear Magnetic Resonance (NMR) (Bloch, 1946, Purcell et al., 1946). The resonance frequency of materials (e.g. animal tissue) in a magnetic field typically occurs within the radio frequency (RF, ~3 kHz to 300GHz) of the electromagnetic spectrum. This allows for NMR RF signal to be captured using a radio-receiver coil and later displayed as images (i.e. MRI).

The magnetic properties and potential NMR RF signal of individual nuclei are reliant on their neutron-proton composition. Nuclei with an odd number of protons and neutrons act in themselves as small magnets with a magnetic dipole. Nuclei with this magnetic property have increased NMR susceptibility. Of all nucleotides, hydrogen-1 (^{1}H) is unique in that it occurs in relatively high concentrations in most human tissues and is highly sensitive to NMR. These properties make ^{1}H key to the efficacy of MRI in humans.

In order to produce NMR a magnetic nucleus (e.g. ^{1}H) must be placed within a static magnetic field denoted as B_0. MRI scanners use superconducting electrical coils to generate highly homogeneous magnetic fields in the range of 1.5 to 7 tesla (T), with 3T magnets being the standard at time of writing for clinical research. During

scanning, a patient lies within this electrical coil (i.e. bore) so that the magnetic field runs parallel to the individual's body.

During MRI scanning protocols NMR RF signal is captured across segmented three-dimensional volumetric units known as voxels. The RF signal intensity at each individual voxel is determined by characteristics of the tissue, namely 1) the concentration of chemical elements, 2) quantity of magnetic isotopes, and 3) the NMR sensitivity of the specific nuclides within the tissue. Signal from a voxel is emitted as the result of stimulation by short RF energy pulses applied during the imaging cycle. The NMR process involves a series of interactions involving the magnetic nuclei, the magnetic field, and these RF pulses and signals.

When not undergoing strong magnetic forces magnetic nuclei (e.g. ^{1}H) will be randomly oriented throughout the body. However, when placed within a magnetic field (B_0) these nuclei experience torque to bring their magnetic dipole in alignment with the direction of the field. Due to agitation caused by thermal energy only a small percentage of the total nuclei (on the order of a few out of a million) come into alignment during MRI scanning of the human body. The number of magnetic nuclei that align with the magnetic field is a function of the field strength of the MRI scanner.

Once aligned with B_0 nuclei are not static but precess (an oscillation similar to a spinning top wobbling) along the axis of the magnetic field (Figure 2.1 A). The precession of an atomic nucleus in a magnetic field occurs at a specific frequency making it susceptible to RF energy applied at the same frequency. This frequency is known as the resonant frequency, or Larmor frequency (ω),

$$\omega = (\gamma_i)B_0 \tag{2.1}$$

Where B_0 = the applied magnetic field strength, and γ = the gyromagnetic ratio or resonance quality of the nuclei i. When RF energy is applied at the Larmor frequency the absorption of this energy by the nuclei will cause it to flip its alignment away from the direction of B_0, resulting in a state of increased energy or excitation (Figure

2.1 B). In the excited state the nuclei experiences increasing force from B_0 to align with the main direction of the magnetic field. A nuclei in an excited state returns to alignment with B_0 by transferring energy to surrounding material in a process known as relaxation (Figure 2.1 C).

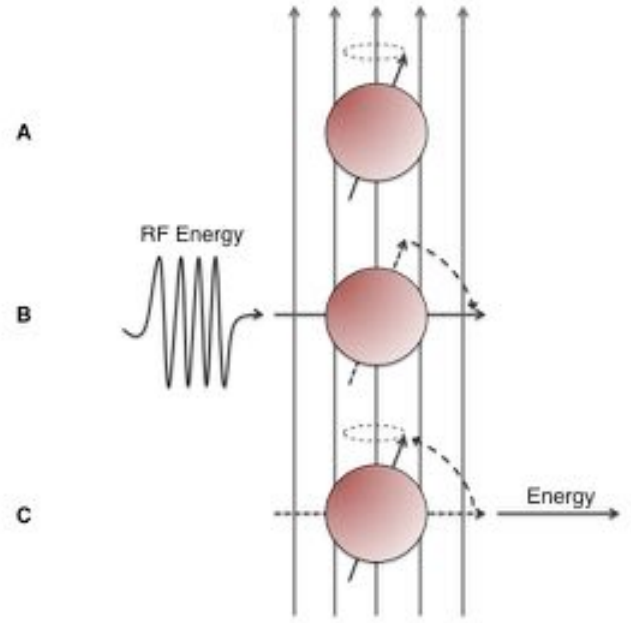

Figure 2.1, Interactions between RF Energy and Magnetic Nuclei in a Magnetic Field (Sprawls, 1987): Parallel vertical arrows indicate the direction of the main magnetic field (B_0). A.) When placed inside B_0 a magnetic nuclei (red sphere) will align B_0 and precess (i.e. spin) around its magnetic dipole (small arrow). B.) When RF energy is applied at the Larmor frequency the nuclei enters a state of increased energy causing alignment away from B_0. C.) A nuclei in this excited state will then transfer energy to surrounding material, returning to alignment with B_0 through a process known as relaxation.

Relaxation rates of individual nuclei are influenced by the structure surrounding them and differ across various tissues. These differing relaxation rates are a key component in producing the contrasts seen in MR images of the brain.

2.2 Magnetic Characteristics of Tissue

When tissue is placed within a magnetic field the nuclei of that tissue will align in parallel to the main direction of the field. Although only a small proportion of nuclei will come into alignment a net magnetization vector (M_0) is formed within the tissue voxel. An equilibrium state known as longitudinal magnetization occurs when M_0 is aligned with B_0. If nuclei are perturbed out of this state via application of RF energy they will seek to regain longitudinal magnetization through relaxation. This relaxation

occurs at an exponential rate. As a convention, the time needed for recovery of 63% of the maximum longitudinal magnetization energy is known as T_1 (Figure 2.2). The angle at which a nuclei aligns itself in relation to B_0 as a result of an RF pulse is know as the flip angle (FA) or α. Application of a 90 degree RF pulse (i.e. FA=90) results in longitudinal magnetization being reduced to zero. This unstable condition is known as saturation and will lead to longitudinal magnetization being recovered exponentially through relaxation.

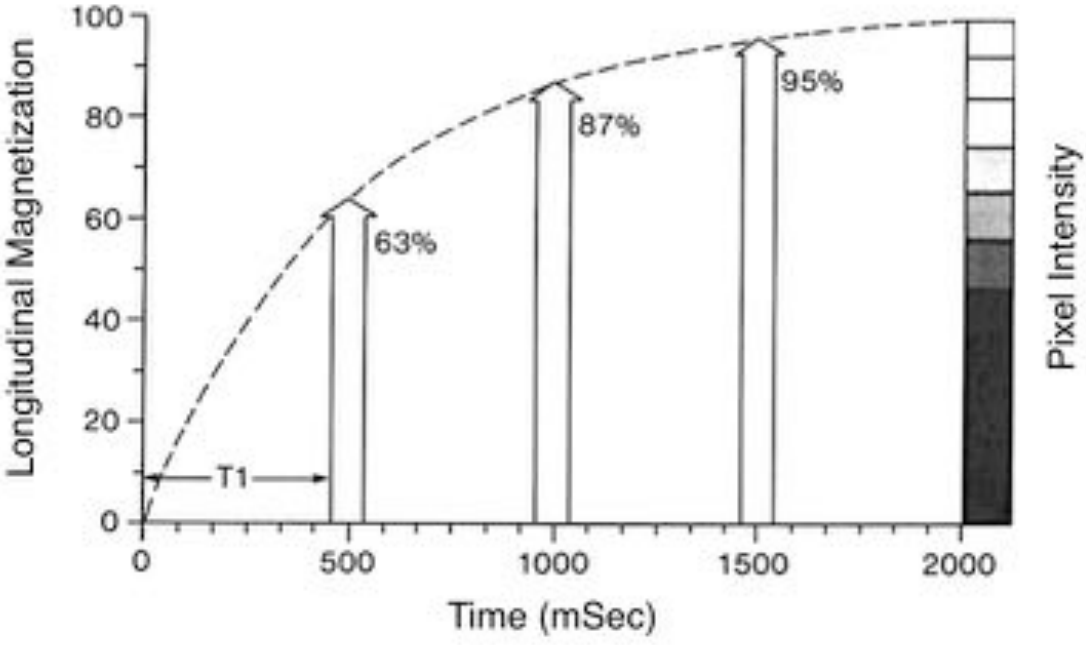

Figure 2.2, Longitudinal Magnetization (Sprawls, 1987): The rate at which longitudinal magnetization occurs is defined by T_1. One T_1 interval indicates the amount of time for a voxel to gain 63% of its maximum longitudinal magnetization. MRI images based on T_1 have increased signal intensity with time.

When RF energy is applied to nuclei they will enter an excited state in which M_0 is not aligned with B_0, this is known as transverse magnetization. This excited state is unstable and quickly decays via a relaxation process known as free induction decay (FID). The time required for 63% of the initial transverse magnetization to dissipate after excitation is known as T_2 (Figure 2.3). Due to its instability, transverse magnetization decay occurs much quicker that T_1 relaxation. Therefore, T_2 values are considerably less than T_1 values for a majority of tissue types.

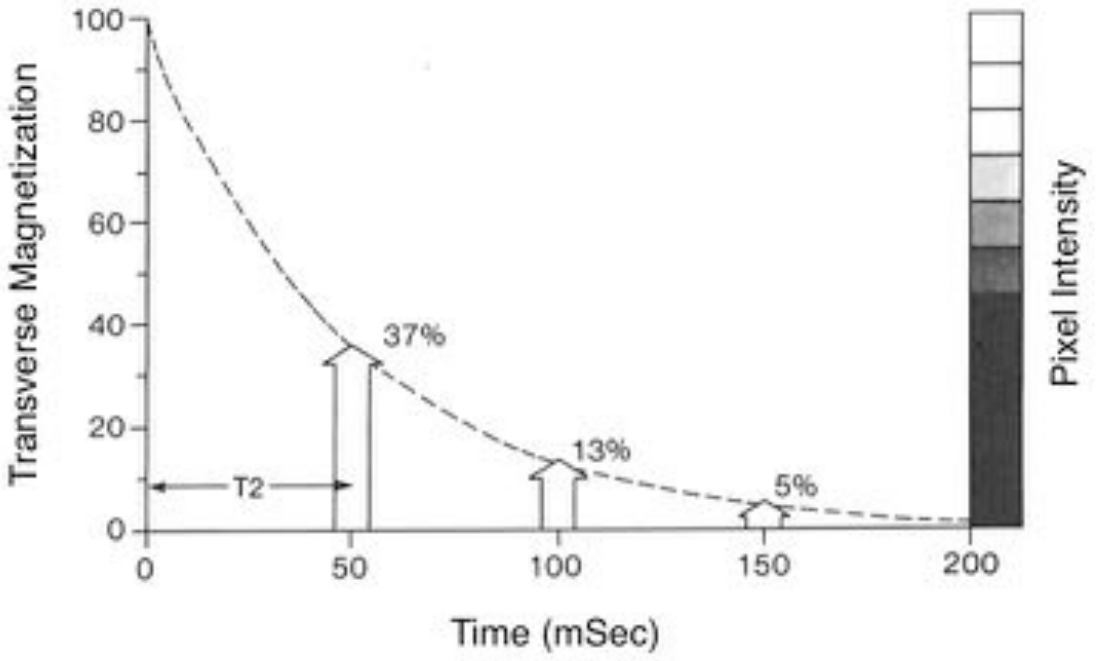

Figure 2.3, Transverse Magnetization (Sprawls, 1987): The rate of transverse magnetization decay is determined by T_2. One T_2 interval indicates when the transverse magnetization is at 37% of its original strength prior to decay. As transverse magnetization is not stable, MRI images based on T_2 have decreased signal intensity with time.

Differing T_1 and T_2 relaxation times across tissues are what lead to contrast within MRI images. In basic MRI sequences contrast is controlled via two factors Time of Repetition (TR) and Time to Echo (TE). TR is the length of one image acquisition cycle as well as the interval between the start of longitudinal relaxation and signal measurement. On the other hand, TE is the time interval between the beginning of transverse relaxation and signal measurement.

In addition to T_1 and T_2 the concentration of protons within a particular voxel (i.e. proton density) is a third factor that can influence MRI image contrast. Proton density contrast is relatively weak compared to T_1 contrast early in longitudinal relaxation. Therefore, proton density images are best captured with long TR times (e.g. three or more T_1 intervals) when longitudinal magnetization approaches its maximum value.

Images designed to maximize T_1 contrast are known as T_1 weighted, and are a commonly used form of structural MRI. T_1 weighted images can be formed by application of an RF pulse at the Larmor frequency resulting in excitation. From this state different tissues will recover longitudinal magnetization at different rates. The

physical composition of the voxel, the molecular size of the nuclei within that voxel, and the strength of the magnetic field combine to determine these T_1 values. For example, fluids (such as cerebral spinal fluid [CSF]) have relatively long T_1 values while the T_1 of lipids (i.e. fat) is relatively short.

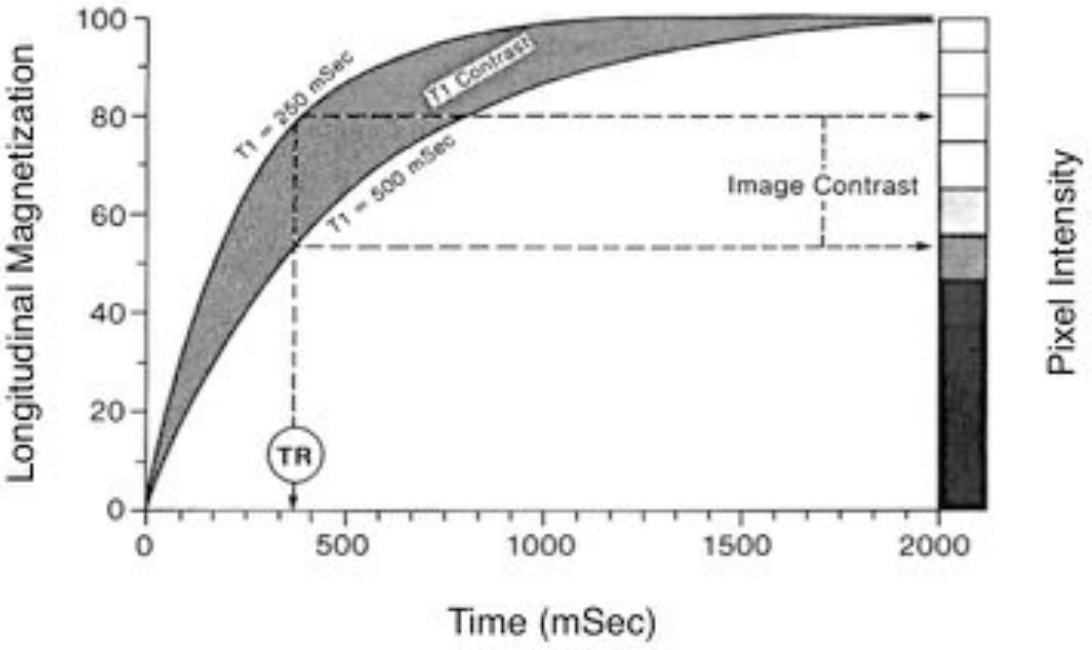

Figure 2.4, Development of T_1 Contrast between Two Tissues (Sprawls, 1987): After the application of a 90 degree RF pulse two tissues return to a state of equilibrium at different relaxation rates (250 and 500 mSec). TR is set to a time at which contrast between the two different tissues is maximized producing contrast in the pixel (i.e. voxel) intensities. Images that maximize T_1 contrast are often used in structural MRI research.

Setting a TR to capture RF signal at a point where T_1 contrast is significantly different across tissues, prior to a voxel fully regaining longitudinal magnetization, results in a T_1 weighted image (Figure 2.4). Within these images tissue with a short T_1 (e.g. white matter [WM]) will appear brighter than those with longer T_1 values (e.g. grey matter [GM]). The choice of flip angle (α) is an important factor in producing T_1 weighted images. For each value of T_1 the optimum flip angle for acquiring signal is known as the Ernst angle and is calculated as,

(2.2)

$$\alpha Ernst = arccos\left(e^{-\frac{TR}{T1}}\right)$$

Additional MRI contrasts can be produced by utilizing differences in transverse magnetization relaxation rates across tissues. These images are known as T_2 weighted,

with contrast being dependent on the TE selected by the user. Furthermore, inherent inhomogeneity of B_0 within each individual voxel will cause dephasing of transverse magnetization at a rate much faster than would be indicated by the intrinsic T_2 characteristics of the tissue. The actual transverse relaxation time taking into account this dephasing effect is known as T_{2*}, which is always less than T_2. Contrast resulting from T_{2*} is a key property in the imaging of changes in blood oxygenation, known as functional MRI (fMRI).

2.3 Magnetic Resonance Images

Magnetic resonance images are three-dimensional volumes comprised of individual units (i.e. voxels) that encode signal intensity resulting from emitted NMR RF energy. MRI protocols can be described in two main phases, namely signal acquisition and image reconstruction. During signal acquisition a particular sequence of RF pulses and magnetic field gradients (i.e. controlled inhomogenities in B_0) are applied. Differences between MRI methods are determined by these pulse sequences. Here I will describe some characteristics of basic MRI pulse sequences followed by spatial encoding of MR signal and MR image reconstruction.

2.3.1 Basic Magnetic Resonance Imaging Pulse Sequences

The process of MRI signal acquisition can be separated into longitudinal and transverse magnetization phases. Transition between these two phases is produced by the application of an RF pulse characterized by α, causing excitation. The transverse magnetization phase concludes with the echo event, which is produced by either the application of RF pulses (e.g. spin-echo, inversion recovery methods) or field gradient (i.e. gradient-echo methods) and results in the emission of RF signal.

Basic spin-echo pulse sequences are characterized by the application of a 90-degree excitation pulse followed by a 180-degree pulse that produces the echo event and RF signal (Figure 2.5). Spin-echo imaging methods can be used to produce T_1, T_2, or proton density weighted images by manipulating TR and TE. For example, T_1 weighted images require a short TR and TE, proton density images a long TR and short TE, and T_2 weighted images a long TR and TE.

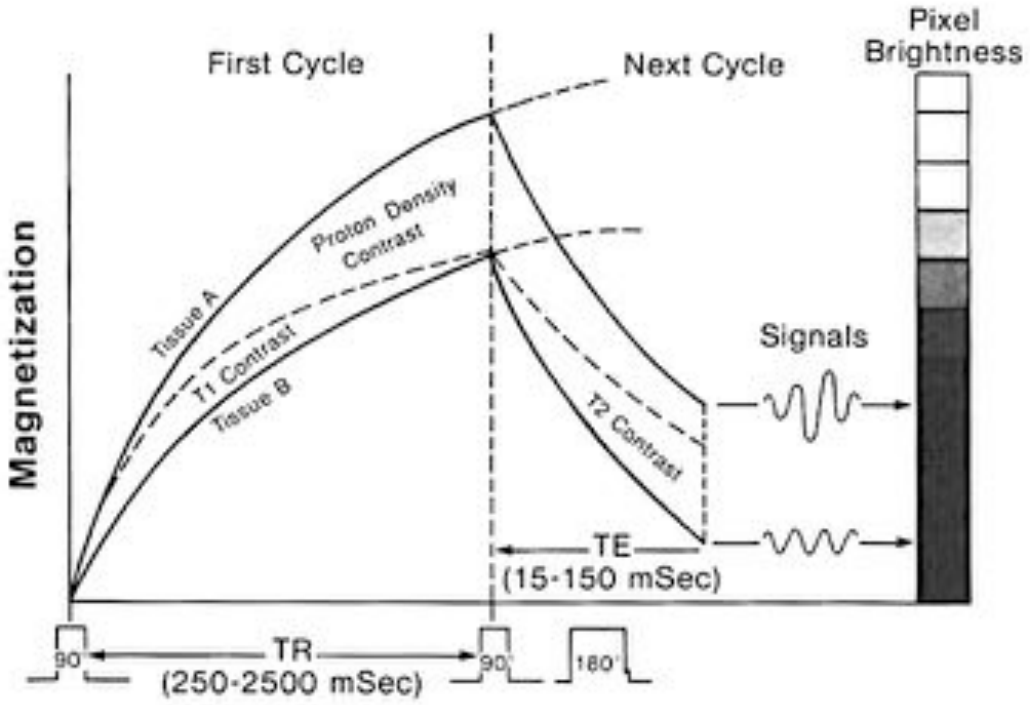

Figure 2.5, Development of Image Contrast in a Spin-Echo Sequence (Sprawls, 1987): Here the imaging cycle begins with the application of a 90 degree RF pulse. Tissue A and B then recover longitudinal magnetization at differing rates determined by their T_1, producing T_1 contrast. As longitudinal magnetization reaches its maximum, proton density becomes the key factor in contrast between tissues A and B. The end of this imaging cycle is indicated by the application of another 90-degree RF pulse, converting longitudinal magnetization to transverse magnetization. At the start of transverse relaxation tissue A and B have different magnetization as a result of differing T_1 and proton density characteristics. However, due to different T_2 properties between the tissues as transverse relaxation progresses T_2 contrast develops. At a time selected by the user an echo event is triggered by the application of a 180 degree RF pulse resulting in the emission of RF signal. Adjusting TR and TE times will result in different weighted images (i.e. T_1, T_2, proton density).

In addition to the 90-degree excitation pulse and 180-degree RF pulse used in basic spin-echo techniques, inversion recovery (IR) MRI protocols employ an additional 180-degree pulse at the beginning of the scanning sequence (Figure 2.6). The time between the initial 180-degree and 90-degree pulses is known as the inversion time (TI). There are two main benefits in the application of IR sequences that result from the longer longitudinal magnetization relaxation rates they provide. 1) IR sequences with a short TI can be used to nullify signal from tissues that have a relatively short T_1 (e.g. fat). 2) IR sequences with long TI give more time for T_1 contrast to develop. This makes IR MRI particularly well suited to produce T_1 weighted images commonly used in structural MRI analyses. The images used throughout this thesis are a form of synthetically calculated IR MRI (see section 2.4).

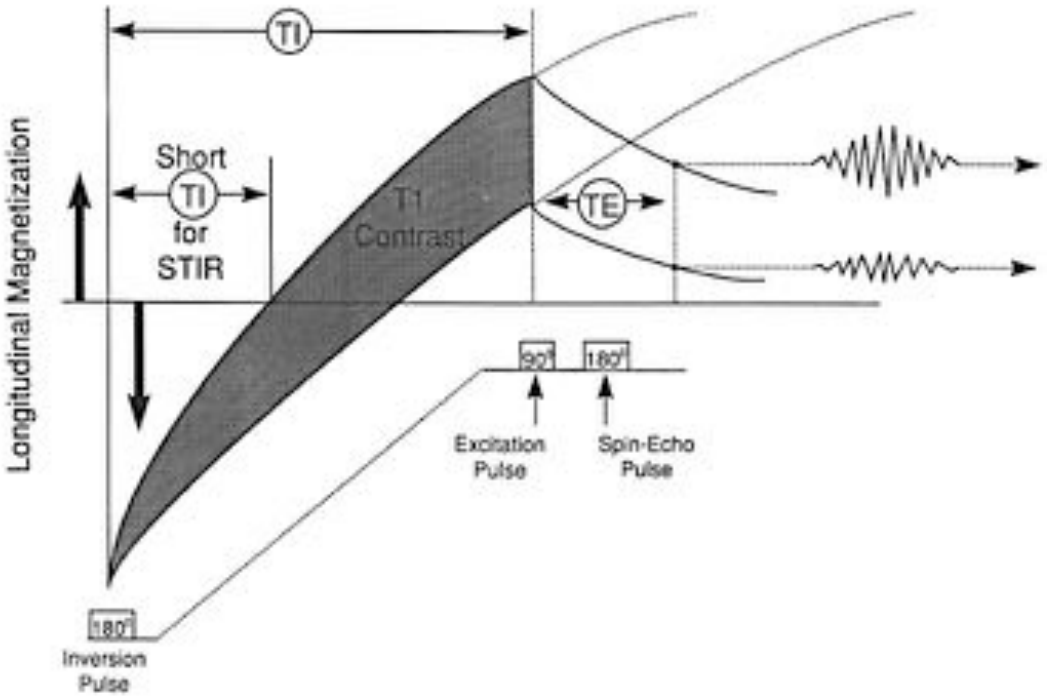

Figure 2.6, Development of T_1 Contrast in an Inversion Recovery Sequence (Sprawls, 1987): Inversion recovery (IR) sequences operate in a similar manner to spin-echo sequences but begin with the application of a 180 degree inversion recovery RF pulse. This causes increased longitudinal relaxation times as the process begins from a negative (inverted) value. Short inversion times (TI) (i.e. short time inversion recovery [STIR]) can be used to eliminate signal from tissues with short T_1 values (e.g. fat) while longer TI can be used to increase T_1 contrast.

Differing from spin-echo techniques, gradient-echo sequences are characterized by their application of a RF excitation pulse with a relatively small α (i.e. >90-degrees). Flip angles of less than 90-degrees cause less longitudinal magnetization to be converted into transverse magnetization. Therefore, over a short TR more longitudinal magnetization and less transverse magnetization signal intensity can be captured, with net signal intensity being the combination of the two. The relatively short TR needed to acquire these images gives the benefit of reduced total acquisition time.

Gradient-echo sequences employ a single RF energy pulse per imaging cycle in order to not affect the longitudinal magnetization. However, when TR is set to be only slightly longer than TE time it is possible for an echo event to be produced by each excitation pulse. Thus, transverse magnetization in a gradient-echo sequence has two components; free induction decay (T_{2*}) and the spin-echo event resulting from the previous RF pulse (T_2). By not applying a second RF pulse during each imaging cycle gradient-echo differs from spin-echo techniques in their handling of transverse magnetization.

In order to produce T_1 weighted images with a gradient-echo sequence the spin-echo component resulting from carryover transverse magnetization across imaging cycles is spoiled (i.e. eliminated) by altering the phase relationship of the RF excitation pulses or through the application of dephasing gradient pulses. Popular gradient-echo sequences used for structural MRI include gradient recalled acquisition in steady state (GRASS) and spoiled gradient recalled-echo (SGPR).

2.3.2 Spatial Encoding and Image Reconstruction of Magnetic Resonance Signal

During the acquisition phase NMR RF signal from a particular voxel is encoded with distinct frequency and phase properties in order to identify the spatial origin of the signal during image reconstruction. Frequency and phase encoding are achieved through the application of magnetic field gradients (i.e. controlled changes in field strength) at specific times along three orthogonal directions (i.e. x, y, and z) within a MRI scanner.

A gradient applied along the direction of B_0 can be used to selectively image a particular slice of tissue. Tissue across the gradient will experience minor differences in field strength and therefore have slightly different resonant frequencies. Thus, over the course of a single TR an excitation pulse can be applied at different frequencies to selectively excite and capture signal from each slice of tissue. A phase encoding gradient can then be applied in order to alter the precession rate in voxels across this gradient. The phase encoding gradient is only applied for a short amount of time leaving each voxel in a different phase (i.e. position) of precession (i.e. phase encoded). In order to produce a distinct phase relationship for each voxel in an image phase encoding must be repeated n times, where n = the number of voxels. Last, the application of a frequency encoding gradient at the time of the echo event when signal is captured is used to isolate signal from a particular column of voxels within a slice. The frequency encoding gradient causes magnetic nuclei to precess at different rates and therefore produce different signal frequencies across the gradient.

Combined effects of slice, phase, and frequency encoding gradients cause individual voxels to have unique differences in phase in one direction and frequency in another. Thus, while signal from all voxels within an MRI image are captured as a single composite signal and stored in what is known as *K* space a Fourier transformation can be used to isolate the spatial location of a particular voxel's signal from the composite signal. The spatial sorting of the composite RF signal captured by the MRI scanner in *K* space into an image via Fourier transformation comprises the most commonly applied form of MR image reconstruction.

Up to this point of the chapter I have described elements common to several standard structural MRI methods. I will now describe the quantitative relaxometry MRI technique used to produce synthetic T_1 weighted IR images described in this thesis, namely Driven Equilibrium Single Pulse Observation of T_1 and T_2 (DESPOT1 and DESPOT2) (Deoni et al., 2005, Deoni et al., 2003).

2.4 Driven Equilibrium Single Pulse Observation of T_1 and T_2 Mapping

Traditional structural MRI methods result in images that display qualitative differences in T_1 or T_2 contrast between tissue types. Alternatively intrinsic T_1 and T_2 relaxation times can be determined and mapped in a voxel-wise manner (Breger et al., 1986, Johnson et al., 1987, Kjær et al., 1987). MR sequences that quantify relaxation times are commonly referred to as relaxometry or quantitative mapping methods. These techniques offer several benefits over traditional structural MRI. For example, contrast within a synthetic T_1 weighted image produced using quantitative mapping is determined solely by differences in T_1 properties of the tissue being imaged with extraneous effects such as T_2 and proton density removed. Furthermore, relaxometry methods are less sensitive to hardware-related effects (i.e. RF coil sensitivity, electronic amplifier gains etc.) that may vary across scanners or even scanning sessions. This makes these methods ideal for comparison of images acquired across different scanning sites or for longitudinal acquisitions (Deoni et al., 2008).

The structural MRI data described within this thesis was acquired through a DESPOT1 sequence (Deoni et al., 2005, Deoni et al., 2003). In order to determine T_1 at each voxel, DESPOT1 acquires a series of SPGR images with a range of flip angles and constant TR. Signal from an SPGR can be calculated given,

(2.3)

$$\frac{SI_{SPGR}}{sin\alpha} = \frac{SI_{SPGR}}{tan\alpha} X\ E_{-1} + M_o(1 - E_{-1})$$

Where SI_{SPGR} is the SPGR signal intensity given flip angle α, M_o is a factor proportional to the equilibrum longitudinal magnetization, and $E_{-1} = exp\left(-\frac{TR}{T_1}\right)$. By plotting $\frac{SI_{SPGR}}{sin\alpha}$ versus $\frac{SI_{SPGR}}{tan\alpha}$ T_1 can be calculated from the slope of the resulting line,

(2.4)

$$T_1 = -\frac{TR}{\ln(slope)}$$

The results of DESPOT1 mapping were then used to produce synthetic IR T_1 weighted images using the following steps. 1.) Signal from non-brain tissue was removed using the brain extraction tool (BET) (Smith, 2002), 2.) intra-session images were non-linearly co-registered using an automated three-dimensional multi-scale approach based on normalized cross-correlation (Collins et al., 1994). 3.) T_1 maps were then calculated in the *ImageJ* (http://rsb.info.nih.gov/ij/) analysis package using plug-ins freely available at www.fmrib.ox.ac.uk/~sdeoni/ (Deoni et al., 2008). This process resulted in the formation of high-resolution structural T_1 weighted "synthetic" IR images, with 1x1x1mm resolution, a 256x256x176 matrix, TR=1800ms, TI=50ms, FA=20'', and FOV=5cm.

2.5 Cortical Surface Reconstruction using Freesurfer Software

In neuroimaging, morphometry methods comprise techniques that investigate the size and shape of the brain and its structures. Surface Based Morphometry (SBM) relies on reconstructions of the cortical surface from MRI images to quantify different structural aspects of brain anatomy. Here, I describe the pre-processing steps used to generate SBM models of the brain and morphometric features calculated using these models.

Volumetric segmentation and reconstruction of tessellated models of the cortical surface from the T_1 weighted structural MRI images described above was performed using the Freesurfer image analysis suite, which is documented and freely available for download online (http://surfer.nmr.mgh.harvard.edu/). The technical details of the

Freesurfer segmentation and reconstruction procedures are described in prior publications (Dale et al., 1999, Dale and Sereno, 1993, Fischl and Dale, 2000, Fischl et al., 2001, Fischl et al., 2002, Fischl et al., 2004a, Fischl et al., 1999a, Fischl et al., 1999b, Fischl et al., 2004b, Han et al., 2006, Jovicich et al., 2006, Ségonne et al., 2004, Reuter et al., 2010, Reuter et al., 2012) and have been demonstrated to show good test-retest reliability across scanner manufacturers and field strengths (Reuter et al., 2012, Han et al., 2006).

Briefly, the Freesurfer processing pipeline includes motion correction and averaging (Reuter et al., 2010) of one or more volumetric T1 weighted MR images, removal of non-brain tissue using a hybrid watershed/surface deformation procedure (Ségonne et al., 2004), automated Talairach transformation, segmentation of the subcortical white matter and deep grey matter volumetric structures (including hippocampus, amygdala, caudate, putamen, ventricles) (Fischl et al., 2004a, Fischl et al., 2002), intensity normalization (Sled et al., 1998), tessellation of the grey-white matter boundary, automated topology correction (Ségonne et al., 2007, Fischl et al., 2001), and surface deformation following intensity gradients to optimally place the grey-white and grey-cerebrospinal fluid borders at the location where the greatest shift in intensity defines the transition to the other tissue class (Dale et al., 1999, Dale and Sereno, 1993, Fischl and Dale, 2000). Once the cortical models are complete, a number of deformable procedures can be performed for further data processing and analysis including surface inflation (Fischl et al., 1999a), registration to a spherical atlas which is based on individual cortical folding patterns to match cortical geometry across subjects (Fischl et al., 1999b), and parcellation of the cerebral cortex into units with respect to gyral and sulcal structure (Desikan et al., 2006, Fischl et al., 2004b).

Within this thesis tessellated models of the cortical surface were used to calculate a variety of morphometric measures of brain anatomy for later analysis. 1) Cortical thickness (CT) is calculated as the closest distance from the grey-white boundary to the grey-CSF boundary at each vertex on the tessellated surface (Fischl and Dale, 2000). CT maps are created using spatial intensity gradients across tissue classes and are therefore not simply reliant on absolute signal intensity. These maps are not restricted to the voxel resolution of the original data thus are capable of detecting submillimeter differences between groups. Freesurfer procedures for the measurement

of CT have been validated against histological analysis (Rosas et al., 2002) and manual measurements (Salat et al., 2004, Kuperberg et al., 2003). 2) Measures of cortical pial and white matter surface areas (SA) are derived using a pycnophylactic interpolation method described in detail by Winkler et al. (2012). 3) Measures of cortical volume are calculated as the product of pial SA and CT. This Freesurfer approach to calculating volume differs from traditional imaging measures of brain volumes such as VBM in which volume is calculated by counting voxels inclusive to segmentations of GM, WM, and CSF as determined by signal intensity.

Additional measures of the cortical surface may be used to describe the topography of the convolutions in the cortical sheet. These include 4) average convexity or concavity (SULC), which indicates the depth/height at each vertex above the average cortical surface, measuring sulcal depth or gyral height respectively. SULC captures large-scale cortical geometric features and is insensitive to noise in the form of small wrinkles in a surface and can be used to quantify the primary folding pattern of the cortical surface. 5) Mean radial curvature (CURV) quantifies folding of the small secondary and tertiary folds in the cortical surface that would not be captured by measures of large-scale geometric features (i.e. SULC measures). 6) Metric distortion (i.e. Jacobian) is calculated as the degree of displacement and convolution of the cortical surface relative to the average template. Unlike SULC and CURV, which measure specific aspects of cortical geometric features (e.g. folding patterns of sulci and gyri), metric distortion estimates the overall degree of folding including geometric distortions otherwise not specified. 7) Further estimates of the degree of cortical gyrification can be achieved through calculation of the local gyrification index (*l*GI). Methods used to calculate *l*GI have been previously validated by Schaer et al. (2008)**.** In brief, *l*GI measures quantify of the proportion of pial surface invaginated within sulcal folds via a ratio of the outer to pial surface area within spherical regions of interest placed across each vertex on the cortical surface.

It is critical to note that all the above measures are susceptible artefacts caused by movement during image acquisition. The effects of these artefacts, such as motion induced blurring, are not trivial and are particularly relevant when studying conditions associated with atypical movement such as ASD. To date, outside of eliminating

motion during acquisition adequate solutions for dealing with these artefacts are limited (Reuter et al. 2015).

2.6 Mass Univariate Magnetic Resonance Imaging Analyses

Several different methodologies can be employed for analysis of MRI data. Often the goal of these methods is the identification and mapping of differences related to a variable(s) of interest across each individual voxel or vertex. These techniques are referred to as mass univariate methods as they involve repeating univariate statistical tests across each voxel or vertex. Applications of multiple regression, more specifically the general linear model (GLM) (Friston et al., 1994a) are among the most popular methods for this type of MRI investigation. Within this section I will introduce the GLM as well as discuss ways of dealing with statistical limitations that result from calculating significance in mass univariate analyses (i.e. the multiple comparison problem).

2.6.1 The General Linear Model

The GLM builds upon simple linear regression methods for identifying associations between predictor variables and responses. An example first order regression model with two predictor variables can be given as,

$$Y_i = \beta_0 + \beta_1 X_{i1} + \beta_2 X_{i2} + \varepsilon_i \tag{2.5}$$

Where Y_i is the response given predictor variables X_{i1} and X_{i2} in the ith sample. The model parameters in this example are β_0, β_1, and β_2, with an error term ε_i. The β parameters may be referred to as partial regression coefficients as they reflect the partial effect of the corresponding predictor variable when all other predictor variables within the model are held constant. Assuming $E\{\varepsilon_i\} = 0$, the regression function (i.e. regression surface or response surface) for this model example is,

$$E\{Y\} = \beta_0 + \beta_1 X_1 + \beta_2 X_2 \tag{2.6}$$

Points on this regression surface correspond to the mean response Y given any combination of X_1 and X_2.

A GLM may be given using the same formula as the example above. However, the variables (e.g. X_1, X_2) need not only represent qualitative predictor variables. For quantitative (i.e. categorical) variables binary indicator variables are used to identify different classes (e.g. male=0, female=1; patient=0, control=1, etc.). Furthermore, if the effects of predictor variables are not additive (i.e. the effect of one variable is dependent on the level of another) an interaction term can be included.

(2.7)

$$Y_i = \beta_0 + \beta_1 X_{i1} + \beta_2 X_{i2} + \beta_3 X_{i1} X_{i2} + \varepsilon_i$$

Here β_3 represents the interaction effect between variables X_1 and X_2 on Y. The GLM may also take into account non-linear effects through the use of polynomials. For example, quadratic or cubic relationships can be investigated using X_i^2 or X_i^3 respectively,

(2.8)

$$Y_i = \beta_0 + \beta_1 X_{i1} + \beta_2 X_{i1}^2 + \beta_3 X_{i2}$$

The GLM encompasses most types of statistical inference including the *t*-test and analysis of variance (ANOVA). An ANOVA can be given in GLM terms when a predictor variable (i.e. independent variable) is categorical. Within an ANOVA this categorical variable is known as a factor and the categories as levels of the factor. Under GLM framework these levels are coded using dummy variables. For example, an ANOVA with a factor comprised of three levels can be given as,

(2.9)

$$Y_i = \beta_0 + \beta_1 X_{i1} + \beta_2 X_{i2}$$

Here, X_1 codes for the first level such that X_1=1 if the observation is within this level or X_1=0 if not. The same applies for the second level, which is coded for by X_2. The third level's mean is predicted by β_0 and therefore is not coded.

Using the framework outlined above the GLM is able to take into account any number and combination of linear, non-linear, and/or interactions terms within a single model. Thus, the GLM offers flexibility to test for a variety of different effects. Some examples include; group comparisons, effects of age or gender, relationships between

age or gender and diagnosis, and correlations with specific behavioral measures or symptom metrics.

In order to perform a particular statistical test using a GLM, data included in the model is first defined as a design matrix where each column corresponds to a qualitative variable or indicator variable. For example, for the following GLM,

$$Y_i = \beta_0 + \beta_1 Age_{i1} + \beta_2 Gender_{i2} + \beta_3 Age_{i1}\, Gender_{i2} + \varepsilon_i \tag{2.10}$$

a corresponding design matrix would be given as,

β_0	Age	Male	Female	Age * Male	Age * Female
1	23	0	1	0	23
1	24	0	1	0	24
1	29	1	0	29	0
1	30	1	0	30	0
…	…	…	…	…	…

Significance of an effect at each voxel or vertex *i* can be tested using a *t* test (Student, 1908) of linear contrasts between conditions. Using the above design matrix as an example, to test for a difference between genders we would use the contrast c = [0 1 -1 0 0], for a main effect of age c = [1 0 0 0 0], or an interaction effect between age and gender c = [0 0 0 1 -1]. The significance of each of these effects at data point *i* is then tested with,

$$t_i = c.b_i/\varepsilon_i \tag{2.11}$$

Where b_i is the corresponding parameter estimates at data point *i*. This *t* statistic and the number of degrees of freedom can then be used to calculate the probability of significance (i.e. *p* value) for an effect at a particular vertex or voxel. Spatial mapping of t_i is referred to as statistical parametric mapping (SPM) and reflects data points that are statistically related to the user defined contrast (Friston et al., 1994a, Worsley et al., 1996).

Within this thesis, GLM analyses of morphometric brain features were conducted using the *SurfStat* toolbox (http://www.math.mcgill.ca/keith/surfstat/) implemented in MATLAB (R2014a; MathWorks).

2.6.2 Correcting for Multiple Comparisons

Mass univariate analyses of brain imaging data apply a large number of independent statistical tests. Therefore, probability theory dictates that a large degree of false positives will be detected in these analyses (type *I* errors). For example, a *p*-value of 0.05 denotes a 5% *type I* error rate. Setting a significance threshold of $p=<0.05$ one could expect up to 5 false positives for every 100 tests. In vertex wise analyses it is common to employ over 200,000 independent statistical tests, which leads to an unacceptably high rate of expected *type I* errors (approximately 10,000). Addressing this so called multiple comparison problem is critical for valid interpretation of voxel or vertex-wise neuroimaging analyses (Bennett, 2010).

Due to the spatial relationships inherent between voxels or vertices within neuroimaging data (caused by biology, signal acquisition, image smoothing etc.) multiple comparison corrections are often performed on clusters of spatially contiguous significant statistical values. This allows for using a *type I* error rate that determines the likelihood that a cluster or 'family' of spatially contiguous significant statistics has arisen by chance, i.e. a Family-Wise Error (FWE) rate. A traditional method of testing against the null hypothesis using FWE is Bonferroni correction. This correction adjusts the tolerable *type I* error rate (α) for an individual test in order to account for the total number of independent tests (n). such that the corrected p value for an individual test is equal to α/n. However, Bonferronni correction is overly conservative (i.e. prone to *type II* errors) for most neuroimaging analyses. This is due to fewer independent observations (i.e. functional or structurally related brain regions) existing compared to the actual number of voxels or vertices. Furthermore, estimation of the number of independent observations in a particular image is hindered by spatial smoothing (i.e. averaging or 'blurring' of the image) which is commonly implemented to increase the signal to noise ratio in image analyses. Therefore, methods have been developed to correct for the multiple comparison problem while taking into account the smooth spatial covariance that results from SPM, one example being random field theory (RFT) (Friston et al., 1994b).

In brief, given a significant cluster of statistical values (i.e. *t* scores) RFT calculates the height threshold for a smoothed statistical map that gives the desired FWE rate (e.g. $p<0.05$). The height threshold is considered to be the individual statistical value necessary within a cluster in order to reject the null hypothesis that all points in the cluster originated from the null distribution. The process of RFT can be explained by three key stages being; 1) the calculation of the number of resolution elements in an image, these elements being analogous to independent observations (Worsley et al., 1992). 2) The calculation of the Euler characteristic (EC), the EC being equivalent to the number of significantly contiguous clusters of vertices or voxels post thresholding (Worsley, 1994). 3) The application of RFT and subsequent thresholding of significant clusters that do not meet the selected FWE rate. This method of correction has been applied to several types of neuroimaging data including non-isotropic images such as cortical surface based reconstructions (Worsley et al., 1999).

2.7 Multivariate Pattern Classification

Mass univariate analyses offer a powerful tool for investigating differences between groups. However, these methods are not suited to make predictions for individual cases regarding group membership or clinical outcome measures, and thus offer limited translational and clinical value. Alternatively, 'machine learning' based pattern recognition methods can be used to generate image-based predictive models that have the potential to be utilized as diagnostic tools and intervention outcome measures.

Within 'machine learning' an algorithm is said to learn from experience *E* with respect to some class of tasks *T* and performance measure *P*. Learning is said to occur when performance in task *T* improves with experience *E* as measured by performance *P* (Mitchell, 1997). For example, a diagnostic model using pattern recognition could seek to learn to make diagnostic predictions (*T*), based on MRI scans of the brains of patients and controls (*E*), with performance (*P*) being measured by diagnostic accuracy. In supervised learning problems examples from a training set of empirical data are mapped to an output. These outputs may be either a continuous variable, in the case of a regression problem, or class label, in the case of a classification problem.

Within this section I will first describe two multivariate pattern classification (MVPC) algorithms implemented in this thesis, namely the Support Vector Machine (SVM) (Vapnik, 1995, Boser et al., 1992) and Gaussian Process Classifier (GPC) (Rasmussen and Williams, 2006, Marquand et al., 2010). While several MVPC algorithms are available, the SVM and GPC where chosen for this thesis as they have previously been shown to have good performance in neuroimaging problems owing to their ability to handle large dimensionality data in a computationally efficient manner when compared to other options (e.g. neural networks, random forests). I will then discuss potential ways for improving MVPC model performance through feature selection and parameter tuning, in addition to model validation and visualization methods.

2.7.1 The Support Vector Machine

The support vector machine (SVM) is among the most popular algorithms used for MVPC of neuroimaging data. SVMs benefit in their ability to train non-linear predictive models in high dimensional spaces that offer good generalization performance and computational efficiency. The SVM attempts to solve a supervised learning problem by optimally placing a boundary known as a hyper-plane (in cases with more than three dimensions) to separate given examples x_i according to class labels $y \in \{+1, -1\}$ (e.g. patients = +1 controls = -1). The SVM is referred to as a maximum margin classifier as it optimizes the placement of the hyper-plane such that the margin between the two classes is maximized (Figure 2.7). I will now briefly describe the SVM. More detailed coverage has been provided by Bishop (2007) and Smola and Schölkopf (1998).

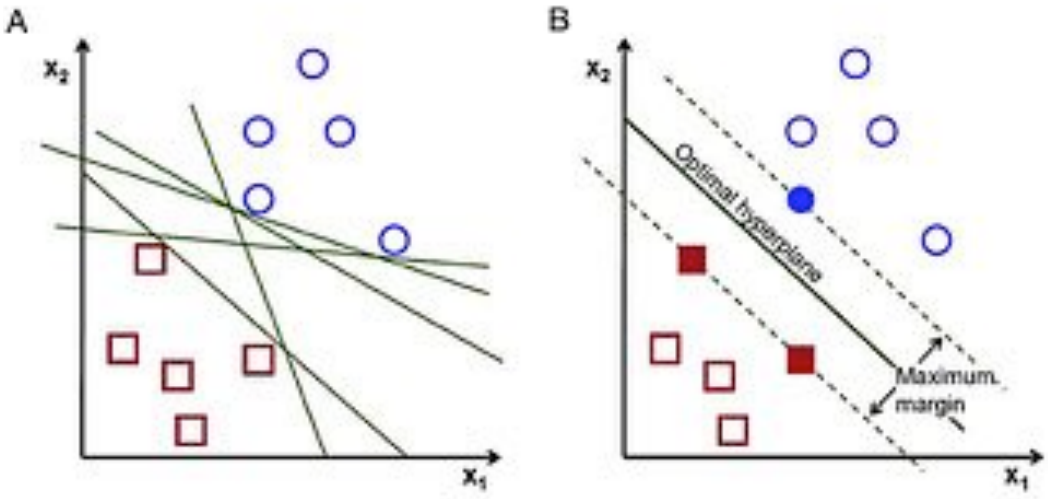

Figure 2.7, The Support Vector Machine (Garcia, 2016): A) In this 2D example the Support Vector Machine (SVM) seeks to separate two classes (red squares and blue circles) using a hyper-plane (green lines). B) The SVM optimizes the hyper-plane by maximizing the margin that separates the two classes. The cases that fall upon this margin (filled squares and circle) are known as the support vectors.

The decision function for a linear SVM can be given as,

(2.12)

$$f(\boldsymbol{x}) = \boldsymbol{w}^T \boldsymbol{x} + b$$

where $\boldsymbol{w}$ is a vector that is orthogonal to the hyper-plane that separates the two classes, $\boldsymbol{x}$ is an example data point and b is a constant offset term that controls the distance of the hyper-plane from the origin. For data points that lie on the hyper-plane $f(\boldsymbol{x})=0$. For other examples the sign of $f(\boldsymbol{x})$ denotes the class $y \in \{+1, -1\}$ of $\boldsymbol{x}$ such that $\boldsymbol{x}_{y+1} = f(\boldsymbol{x}) > 0$ and $\boldsymbol{x}_{y-1} = f(\boldsymbol{x}) < 0$. The SVM aims to maximize the margin between classes by finding, given perfect classification, the vector $\boldsymbol{w}$ with the smallest magnitude $\|\boldsymbol{w}\|$. This vector details the contribution of each data point in a feature set (e.g. vertex or voxel) towards classification and is known as the weight vector.

Within training samples one or more samples may prevent clean separation between classes. This may be due to noise in the inputs (uncertainty in the location of samples) and/or outputs (mislabeling an sample) that cause a sample to be plotted on the "wrong side "of the decision plane. In cases where linear separation between cases is not possible the introduction of 'slack variables' can be used to 'soften' the margin. This can be achieved by introducing a trade off between maximizing the margin and the total number of acceptable miss classifications. This trade off introduces an

optimization problem, which can be viewed from either the primal or dual perspective (Boyd and Vandenberghe, 2004). The soft margin SVM in primal form can be given as,

(2.13)

$$\text{minimize}_{\text{w},b}: \frac{1}{2}\|\mathbf{w}\|^2 + C\sum_{\text{i}=1}^{\text{n}} \xi_i$$

$$\text{subject to:} \quad \begin{matrix} y_i(\mathbf{w}^{\text{T}}\mathbf{x}_i + b) \geq 1 - \xi_i, \\ \xi_i \geq 0, \ i = 1, \dots, n \end{matrix}$$

where we seek to minimize the term $\frac{1}{2}\|\mathbf{w}\|^2$, which is achieved when the margin that separates between classes is maximized. In a hard margin scenario we impose the constraint $y_i(\mathbf{w}^{\text{T}}\mathbf{x}_i + b) \geq 1$, such that the decision function output $f(\mathbf{x}_i) = \mathbf{w}^{\text{T}}\mathbf{x}_i + b$ multiplied by the label t_i (either +1 or -1) must be greater or equal to one, thus no sample can be closer than the margin marked by the $y(\mathbf{x}) = 1$ and $y(\mathbf{x}) = -1$ contour lines. In 2.13 ξ_i are non-negative slack variables, which loosen the constraint on the minimal distance (i.e. 1) that an example may fall from the margin, such that a distance of 1-ξ_i is now acceptable. The trade-off between maximizing the margin and minimizing the number of classifications that violate the margin are controlled by a regularization parameter *C*. As *C* increases, priority is placed on reducing the number of misclassifications over maximizing the margin such that when $C=\infty$ the SVM will have zero tolerance for these violations (i.e. 'hard margin' SVM).

The optimization problem (2.12) can be solved it its duel form using the following Lagrange function,

(2.14)

$$L(\boldsymbol{w}, b, \boldsymbol{\xi}, \boldsymbol{\alpha}, \boldsymbol{\mu}) = \frac{1}{2}\|w\|^2 + C\sum_{i=1}^{n} \xi_i - \sum_{i=1}^{n} \alpha_i\{y_i(\boldsymbol{w}^T\boldsymbol{x}_i + b) - 1 + \xi_i\} - \sum_{i=1}^{n} \mu_i\xi_i$$

where $\alpha_i \geq 0, \mu_i \geq 0$ for $i = 1, \dots, n$ are the Lagrange multipliers (the Lagrangian *L* is a scalar) that the function seeks to minimize with respect to maximizing $\boldsymbol{w}$ and *b*. The solution of (2.14) requires the resulting partial derivatives,

(2.15)

$$\frac{\partial}{\partial \boldsymbol{w}} L(\boldsymbol{w}, b, \boldsymbol{\xi}, \boldsymbol{\alpha}, \boldsymbol{\mu}) = 0,$$

$$\frac{\partial}{\partial b} L(\boldsymbol{w}, b, \boldsymbol{\xi}, \boldsymbol{\alpha}, \boldsymbol{\mu}) = 0.$$

The first of these partial derivatives allows for the optimal weight vector to be expressed as a weighted combination of all examples $\boldsymbol{x}$, with the class label y_i determining the sign and the α_i's determining the magnitude of the contribution of each example to the weight vector, such that

(2.16)

$$\boldsymbol{w} = \sum_{i=1}^{n} \alpha_i y_i \boldsymbol{x}_i$$

The second partial derivative in (2.15) leads to the condition that the sum of the signed weights α_i and y_i equal zero, such that

(2.17)

$$\sum_{i=1}^{n} \alpha_i y_i = 0.$$

Expressions (2.16) and (2.17) allow us to remove the primal variables w and b from the optimization problem outlined in (2.13), giving the dual form of (2.13) as

(2.18)

$$maximize_{\alpha}\colon W(\alpha) = \sum_{i=1}^{n} \alpha_i - \frac{1}{2} \sum_{i=1}^{n} \sum_{j=1}^{n} \alpha_i \alpha_j y_i y_j {x_i}^T x_j$$

$$subject\ to\colon 0 \leq \alpha_i \leq C, \qquad i = 1, \ldots, n$$

$$\sum_{i=1}^{n} \alpha_i\, y_i = 0.$$

The optimization problem (2.13) in dual form (2.18) now seeks to maximize an objective function of the support vector weights α_i. For these optimization problems the constraint that $\boldsymbol{\alpha}_i(y_i f(\boldsymbol{x}_i) - 1 + \xi_i) = 0$ must be satisfied for each example $\boldsymbol{x}_i$ by one of two ways. 1) When for a given example $\boldsymbol{x}_i$, $\alpha_i = 0$ it is given that $y_i f(\mathbf{x}_i) \geq 1 - \xi_i$ and therefore $\boldsymbol{x}_i$ is well classified. 2) When $\alpha_i > 0$ it is given that $y_i f(\mathbf{x}_i) =$

$1 - \xi_i$, therefore $\boldsymbol{x}_i$ is either on the margin ($y_i f(\mathbf{x}_i) = 1$, slack variable $\xi_i = 0$) or within the margin ($y_i f(\mathbf{x}_i) = 1 - \xi_i$, slack variable $\xi_i > 0$) (Bishop, 2007). This highlights the sparse nature of SVM in that all the information relevant to the decision problem (i.e. $\boldsymbol{w}$) is carried by the relatively few examples that fall on or within the margin (i.e. the support vectors).

As training examples $\boldsymbol{x}_i$ and $\boldsymbol{x}_j$ only enter into the optimization problem (2.18) through their inner product it is possible to replace this inner product with a kernel function ($\boldsymbol{K}$). This process, commonly referred to as 'kernel trick', allows mapping into a potentially higher dimensionality space in which a non–linear decision plane can be derived. The simplest form of $\boldsymbol{K}$ is a dot product between the input data and a test case,

(2.19)

$$\boldsymbol{K}(\boldsymbol{x}_i, \boldsymbol{x}) = \boldsymbol{x}_i \cdot \boldsymbol{x}$$

For cases in which classes cannot be separated with a linear decision boundary (even with the aid of a soft margin) the resulting linear kernel $\boldsymbol{K}$ provides a feature space with higher dimensionality in which non-linear separation of the classes may be achievable. It is also possible to transform data from native space using non-linear kernels (e.g. the radial basis function). However, in cases where the number of features is larger than the number of observations non-linear kernels typically offer marginal if any improvement in classification accuracy (Hsu et al., 2003) and are thus not typically applied in neuroimaging problems.

2.7.2 Gaussian Process Classifiers

Pattern classification methods such as the SVM offer power tools to make binary predictions according to class labels. However, in the clinical setting having an estimate of confidence in a prediction is often just as important as the prediction itself. Probability theory offers a coherent way to manage uncertainty and can be introduced into prediction modeling though the application of Bayesian statistics. Bayes' theorem describes the conditional probability of an event given another event is true,

(2.20)

$$p(A|B) = \frac{p(B|A)p(A)}{p(B)}$$

here *A* and *B* are events, *p(B)≠0*. *p(A)* and *p(B)* are the probabilities of event *A* and *B* independent of each other. *p(A|B)* and *p(B|A)* represent conditional probabilities, i.e. the probability of *A* given *B* is true and vice versa (Kendall et al., 1968). Within MVPC the Gaussian process classifier (GPC) (Rasmussen and Williams, 2006) is one Bayesian method that can make probabilistic estimates as to class ownership. This ability gives GPC methods potential clinical benefits over the SVM, which is not a probabilistic prediction device.

According to Rasmussen and Williams (2006), a Gaussian process (GP) can be viewed as an extension of a Gaussian probability distribution. Where as a Gaussian probability distribution describes finite dimensional variables, the GP extends the probability distribution to functions, which are infinite dimensional, under the constraint that any finite number of variables have a multivariate Gaussian distribution. Therefore a GP describes a distribution over functions that can be used for Bayesian inference. There are two complementary and equivalent views of GP inference, the 'weight space' and 'function space' views. I will first introduce the function space view of GP inference and later discuss the weight space view in context of classification. In the view of GP function space a GP prior is placed over a set of interpolating functions *f(x)* the posterior distribution is computed according to Bayes rule. This distribution is then used to explain the relationship between examples (Figure 2.8).

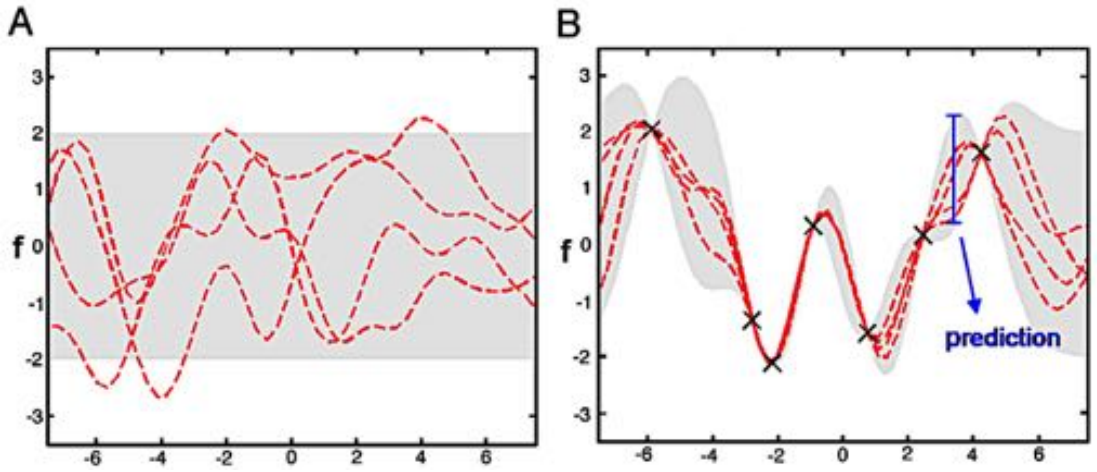

Figure 2.8, The Gaussian Process in a One Dimensional Regression Problem (Marquand et al., 2010, Rasmussen and Williams, 2006): A) Sample functions (dotted lines) selected from a zero-mean Gaussian process prior distribution are shown. B) After the introduction of training cases (black

crosses) sampled functions from the posterior distribution are limited to those that fit the given examples. In both panels the grey shaded area indicates a 95% confidence interval for a prediction at any possible input. One such prediction is shown in blue.

When GP inference is posed as a binary classification problem we wish to predict the class probability for a test example x^*, $p(y = 1|x^*, x_{i...n})$ given a set of training examples $x_{i...n}$ with associated class labels $y \in \{+1, -1\}$. In order to restrict the GP prior over functions *f(x)* (Figure 2.9 A) to give a binary output (i.e. $y \in \{+1, -1\}$), f is 'squashed' point wise through a response function (Figure 2.9 B).

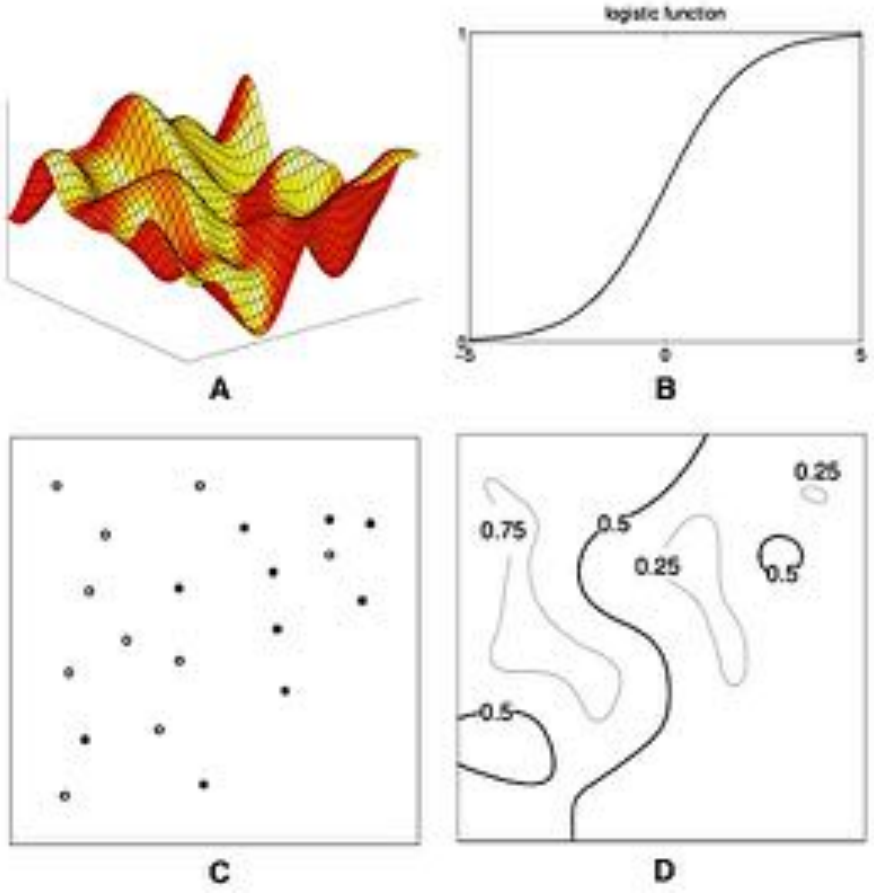

Figure 2.9, The Gaussian Process Classifier (Rasmussen and Williams, 2006): Here the Gaussian process classifier aims to separate examples $x_{i...n}$ sampled from two classes $y \in \{+1, -1\}$. A) A prior GP distribution of *f(x)* is given in a 2-d input space. In order to limit predictions to binary classes a response function is used to squash the GP distribution of *f(x)*. B) Commonly this response function takes the form of a logistic function, $\lambda(z) = (1 + exp(-z))^{-1}$. C) The location of examples $x_{i...n}$ are shown with white dots indicating class +1 and black dots indicating class -1. D) A contour plot depicts predictive probabilities as a function of *x* after the implementation of the response function on the GP priors. Black lines indicate the decision boundary (>0.5 = y_{+1}, <0.5 = y_{-1}).

The theory and implementation of GPC have been previously described by Ebden (2008) and are covered in detail by Rasmussen and Williams (2006). I will now briefly outline the GPC as described by Marquand et al. (2010).

The GPC is an extension of Gaussian process regression (GPR), which in the perspective of the weight space can be seen as a Bayesian extension of linear regression. In linear regression predictions are made by,

(2.21)

$$f(\boldsymbol{x})=\boldsymbol{x}^T\boldsymbol{w}, \qquad y=f(\boldsymbol{x})+\varepsilon$$

where $\boldsymbol{w}$ is a vector of weights, y is a target value, f is a function value, and $\varepsilon \sim N(0,\sigma^2_n)$ is a Gaussian noise term. Given input $\boldsymbol{x}$ the posterior distribution of these weights are computed by Bayes rule,

(2.22)

$$p(\boldsymbol{w}|\boldsymbol{X},\boldsymbol{y},\theta) = \frac{p(w|\theta)p(\boldsymbol{y}|\boldsymbol{X},\boldsymbol{w},\theta)}{p(\boldsymbol{y}|\boldsymbol{X},\theta)}$$

where $\boldsymbol{X}$ is a matrix of input examples $\boldsymbol{x}_{i\ldots n}$ with $\boldsymbol{y}$, in the case of classification, being a vector of corresponding class labels, $\boldsymbol{y} = [y_1 \ldots y_m]T$, and θ being a vector of hyper-parameters. The term $p(\boldsymbol{y}|\boldsymbol{X},\theta)$ is itself a GP and is known as the normalizing constant or marginal likelihood, $p(\boldsymbol{y}|\boldsymbol{X},\theta)=\int p(\boldsymbol{y}|\boldsymbol{X},\boldsymbol{w})p(\boldsymbol{w})d\boldsymbol{w}$. Prediction for a particular test case $\boldsymbol{x}^*$ in data set D comprising of examples $\boldsymbol{x}_i$ and corresponding class labels y_i is performed by averaging all possible values of $\boldsymbol{w}$ and weighting by their posterior probability, $p(f^*|D,\theta,\boldsymbol{x}^*) = \int (f^*|\boldsymbol{w},\boldsymbol{x}^*,\theta)p(\boldsymbol{w}|D,\theta)d\boldsymbol{w}$. Therefore, GP predictions are a weighted average of all possible linear models, under the prior constraints, based on the examples provided by $\boldsymbol{X}$.

In order to determine the posterior distribution, the spatial relationship of each example to all other examples is first described using a covariance function. There are several options for the form of this function (Rasmussen and Williams, 2006), the one used in this thesis being a linear covariance function,

(2.23)

$$\boldsymbol{K} = \frac{1}{l^2}\boldsymbol{X}\boldsymbol{X}^{\boldsymbol{T}} + b$$

here l is a length parameter that controls the scaling of the latent function and b is a bias term that accounts for the offset from zero. To make predictions we make use of

the covariance between training examples and a test case, which are are stored in vector $\boldsymbol{k}^*$. For a regression problem, the posterior predictive distribution can then be calculated as,

(2.24)

$$p(f^*|D,\theta,\boldsymbol{x}^*)\sim N(\mu,\sigma^2)$$
$$\mu = \boldsymbol{k}^{*T}\boldsymbol{C}^{-1}\boldsymbol{y}$$
$$\sigma^2 = k(\boldsymbol{x}^*,\boldsymbol{x}^*) - \boldsymbol{k}^{*T}\boldsymbol{C}^{-1}\boldsymbol{k}^*$$

where $C = K + \sigma_n^2$. For regression problems this posterior predictive distribution is Gaussian. From this distribution we are interested in making a prediction of y^* given $\boldsymbol{y}$. This prediction can be viewed as analogous to the point predictions given by the SVM. However, here in GPR each prediction is accompanied by some degree of estimated variance,

(2.25)

$$var(y_*) = \boldsymbol{K}_{**} - \boldsymbol{K}_*\boldsymbol{K}^{-1}\boldsymbol{K}_*^T$$

The degree of this variance translates to the confidence in the prediction.

In the GPC problem a sigmoidal response function is used to constrain continuous regression predictions to a particular set of target classes. Effectively the response function is used to map the unconstrained latent function provided by GPR to a particular class label. Several response functions can be used to this purpose, here the cumulative Gaussian density or probit likelihood was used,

(2.26)

$$\Phi(x) = \frac{1}{2}erf\left(\frac{x}{\sqrt{2}}\right)+\frac{1}{2}$$

For binary classification the likelihood for a single data point can be given as $p(y_i|f_i) = \Phi(y_i, f_i)$, which enables the posterior distribution over the latent function to be written as:

(2.27)

$$p(\boldsymbol{f}|D,\theta) = \frac{N(\boldsymbol{f}|0,\boldsymbol{K})}{p(D|\theta)}\prod_{i=1}^{m}\Phi(y_i,f_i)$$

where $\boldsymbol{K}$ is the covariance function (2.23). Latent function values for training points are stored by $\boldsymbol{f}=[f_1,\ldots f_m]^T$. $N(\boldsymbol{f}|\boldsymbol{0},\boldsymbol{K})$ describes the prior over the latent function. The likelihood over training samples is factorized, as the class labels are independent given the latent function.

For GP classification; exact inference of the posterior distribution is analytically intractable and is therefore approximated using a Gaussian, $q(\boldsymbol{f}|D,\theta)=N(\boldsymbol{f}|\boldsymbol{m},\Sigma)$, which allows for calculation of the approximate posterior for a test case $q(f^*|D,\theta,\boldsymbol{x}^*)=N(f^*|\mu^*,\sigma^*)$. Several approximation methods are available for this purpose. Here we employed an expectation propagation algorithm (Rasmussen and Williams, 2006), as it has been shown to have favorable results compared to other approximation methods (Kuss and Rasmussen, 2005, Nickisch and Rasmussen, 2008). These GPC based predictions are derived from integrating over the entire distribution for the latent function at a point for test case $\boldsymbol{x}^*$ and therefore differ from the point based predictions provided by the SVM. See Nickisch and Rasmussen (2008) for further details.

In contrast to the SVM which seeks to optimize a margin between classes, 'training' of a GP models refers to finding the best functional form and hyper-parameters for the covariance function. Within this thesis this was achieved through maximizing the logarithm of the marginal likelihood. For GP regression problems this can be computed as,

(2.28)

$$Inp(\boldsymbol{y}|\boldsymbol{X},\theta)=\frac{1}{2}\boldsymbol{y}^T\boldsymbol{C}_\theta^{-1}\boldsymbol{y}-\frac{1}{2}\ln|\boldsymbol{C}_\theta|-\frac{n}{2}ln2\pi$$

where $\boldsymbol{C}_\theta$ is the evaluation of $\boldsymbol{C}$ given hyper-parameters θ. For classification the marginal likelihood is again approximated using EP. Here (2.28) allows the user to select the hyper-parameters among competing models for which the marginal likelihood is optimal. The marginal likelihood calculates the total probability of the data given the model hyper-parameter and represents a trade off between optimal fit and model complexity and thus provides a buffer against over fitting.

2.7.3 Model Performance and Validation for Multivariate Pattern Classification

In supervised classification problems MVPC models learn to classify a group of training examples based on known class labels. These trained models are then applied to independent test examples for which class predictions are made. In order to accurately assess a model's predictive performance it is important that test cases are not used in the training of a model. Ideally model performance is evaluated on completely independent test data. However, independent data is often not available for a variety of reasons. In neuroimaging this is commonly due to the expense of scanning individual subjects or challenges in recruiting large number of patients from a particular disease cohort.

When independent test data is not available cross validation schemes may be used in order to estimate model performance. In *k*-fold cross validation, *k* number of cases are left out of model training, predictions are then made for the left out cases which act as the test data. The cross validation loop is then repeated *n* number of times such that all cases in turn are left out from the training phase and are used as test cases for the model. When k=1 this scheme is known as leave one out (loo) cross validation. By comparing the predictive class labels returned by either independent validation or cross validation to the known labels it is possible to estimate a MVPC model's accuracy. Leave one out cross validation is an effective validation method for minimizing testing bias as this framework allows almost the entire training sample to be used to establish the model for each testing case. However, given loo methods test only a single case each fold this minimization of testing bias comes at the cost of increased variance in performance estimates. Due to the relatively small numbers of training samples within this thesis, loo cross validation was used throughout with the knowledge that this may increase variance in our model performance estimates.

Model accuracy is defined as the percentage of test cases that are correctly classified. In addition to accuracy, models can be assessed by their sensitivity and specificity,

(2.29)

$$sensitivity = TP/(TP+FN)$$
$$specificity = TN/(TN+FP)$$

here *TP* represents the number of true positive cases (e.g. patients classified as patients) and *TN* represents the number of true negatives (e.g. controls classified as controls). Conversely *FP* represents the number false positive cases (e.g. controls classified as patients) and *FN* represents the number of false negative cases (e.g. patients classified as controls). For some instances in the clinical setting a model's sensitivity to catch a potential positive case may be valued over the possibility of making a false positive diagnosis. In other situations a model's specificity for making an accurate diagnosis may be viewed as more important.

Estimates of a model's accuracy (or sensitivity and specificity) in themselves are not sufficient to tell if a model consistently performs above chance level. In order to test a MVPC model's significance permutation testing can be performed. Here class labels are randomly permuted prior to model training and testing. This permutation is then repeated n number of time. Typically, n equals some order of thousands of permutation folds (e.g. n=1000, 10000, etc.). Across all folds the number of instances that the permuted model accuracy exceeds the original estimated accuracy is counted and then divided by the total number of permutations to give a p value for the classification model. As is convention model's with a p-value of <0.05 are seen as statistically significant.

2.7.4 Feature Extraction and Selection

In MVPC the selection of data that is informative of the class labels often has more impact on model performance than the selection of one particular MVPC algorithm over another (e.g. SVM, GPC, etc.). In pattern classification (or regression) a particular characteristic of the data used to train a classification model is known as a feature or collectively as a feature set. Feature extraction is the process of extracting (i.e. calculating) a particular feature from a data set. For example, in this thesis feature extraction is the process of calculating surfaced based cortical measures from structural MRI data resulting in a vertex based feature set.

Feature sets based on MRI data often contain several thousand features per example. Therefore, in order to increase the amplitude of signal with regards to the class label it

is often desired, although not necessary, to remove uninformative features. Broadly speaking feature selection can be performed in two ways, 1) through prior knowledge and expertise (e.g. selection of features from a region of interest known to be involved in a condition) or 2) through an automated feature selection algorithm (Mwangi et al., 2014). Within parts of this thesis automated feature selection is performed through the application of a GLM to identify brain regions associated with a mean difference between classes. Data from vertices comprising these brain regions were then used for subsequent model training and testing.

It is important to note that automated feature selection introduces a strong possibility of over fitting a predictive model to the training set. Thus, it is important that the parameters used to implement automated feature selection are not selected arbitrarily but are tuned using a nested cross validation procedure (Figure 2.10). This avoids bias if the features are selected only using the training data.

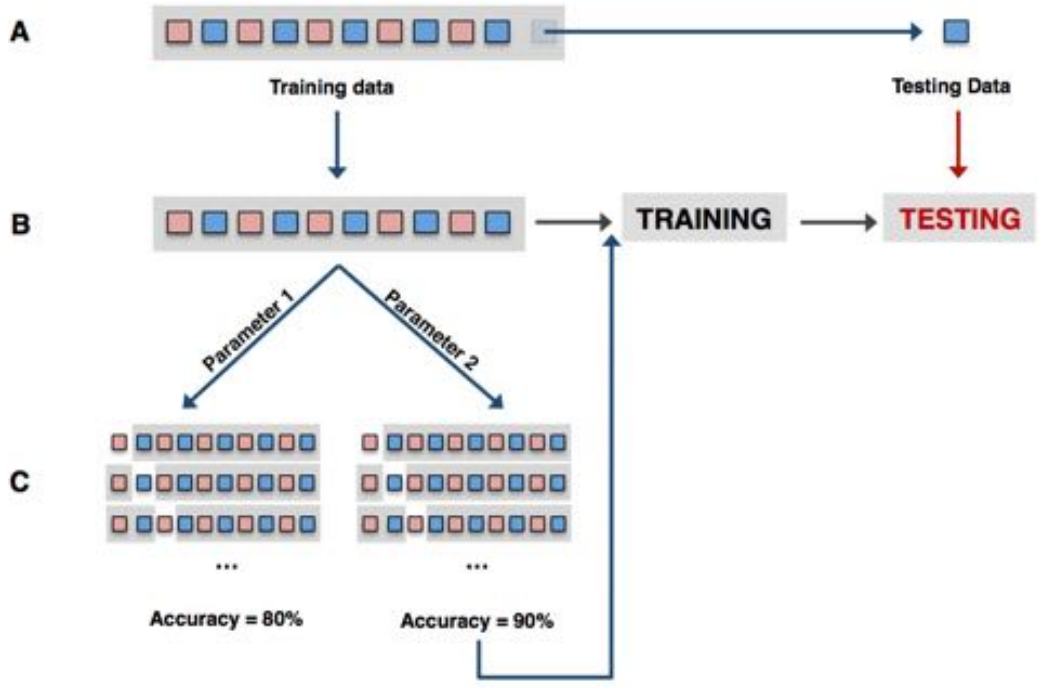

Figure 2.10 Nested Parameter Tuning via Cross Validation: This model depicts one fold of leave one out cross validation with a nested leave one out cross validation loop to tune model parameter values. A) Leave one out validation begins by excluding one case that will act as testing data (blue square) from the training set (red and blue squares in shaded box). B) From the training data set nested cross validation begins by C) performing leave one out cross validation for each parameter value to be tuned. The parameter value that returns the highest model accuracy (here parameter value 2) is then used to train and test the actual model. This nested scheme is then repeated across all cross validation folds.

Many ways of performing feature selection are available including both univariate (e.g. GLM) and multivariate approaches. When using a GLM to perform feature selection the uncorrected *p*-value threshold used to identify regions of interest represents one parameter that is tuned. Thus, for each cross validation fold a range of *p*-value thresholds are tested via nested cross validation. The *p*-value that returns the highest model accuracy is then used in training of the model for that cross validation fold. For this thesis, a GLM feature selection approach was used however such univariate approaches have the limitation of not taking into account relationships between data points. Thus, potentially informative data points may not be selected as they are tested for significance in isolation. Several other multivariate feature selection methods (e.g. recursive feature elimination, lasso) which may provide better results are available (for review see Mwangi et al. (2014)). However, due to time constraints in was beyond the scope of this project to extensively test all these methods.

2.7.5 Model Visualization

The spatial maps of MVPC models are inherently different than those provided by mass univariate methods such as the GLM. The GLM can be viewed as a forward model as it takes a known variable (e.g. class label) and highlights aspects of the data (e.g. brain regions) associated with the variable. This differs from backward models such as MVPCs that extract information from the data as it relates to a variable (Haufe et al., 2014).

Commonly MVPC models are visualized through spatial mapping of the model's weight vector. However, interpretation of these so call "discriminative maps" is made difficult by the fact that you cannot infer that values within $\boldsymbol{w}$ are directly related to the signal of interest (e.g. class label). For example, large weights may be associated with noise and small values the signal of interest. Despite limitations on interpretability several studies still report multivariate discriminative maps along with MVPC models. Thresholding discriminative maps based on a percentage of the maximum weight value has been proposed as one way of reducing noise and clarifying interpretation (Mourão-Miranda et al., 2005, Mourao-Miranda et al., 2006).

Other multivariate mapping methods have recently been proposed to calculate forward maps more in line with those generate by the GLM (Haufe et al., 2014).

An alternative mapping method, known as 'predictive mapping' involves taking the dot product of each individual example ($\boldsymbol{x}_i$) with the corresponding weight vector ($\boldsymbol{w}$), so that $\mathbf{m} = (\boldsymbol{x}_i) \cdot \boldsymbol{w}$ (Marquand et al., 2014). Predictive mapping has two advantages: 1) it shows the total contribution to the prediction for each test point, i.e. the weights derived from the training data *and* from the test data point, and therefore 2) it can be used to determine the spatial distribution of informative regions for cases that were not learned as part of the primary decision problem. In other words, predictive mapping allows us to infer which aspects within a group of test cases underlie predictions derived from the classifier.

2.8 References

BENNETT, C. M., BAIRD, A.A., MILLER, M.B., WOLDROD, G.L. 2010. Neural correlates of interspecies perspective taking in the post-mortem Atlantic salmon: an argument for proper multiple comparisons correction. *Journal of Serendipitous Unxepected Results,* 1**,** 1-5.

BISHOP, C. M. 2007. *Pattern Recognition and Machine Learning,* New York, Springer

BLOCH, F. 1946. Nuclear induction. *Physical review,* 70**,** 460.

BOSER, B. E., GUYON, I. M. & VAPNIK, V. N. A training algorithm for optimal margin classifiers. Proceedings of the fifth annual workshop on Computational learning theory, 1992. ACM, 144-152.

BOYD, S. & VANDENBERGHE, L. 2004. *Convex optimization*, Cambridge university press.

BREGER, R. K., WEHRLI, F. W., CHARLES, H. C., MACFALL, J. R. & HAUGHTON, V. M. 1986. Reproducibility of relaxation and spin‐density parameters in phantoms and the human brain measured by MR imaging at 1.5 T. *Magnetic resonance in medicine,* 3**,** 649-662.

COLLINS, D. L., NEELIN, P., PETERS, T. M. & EVANS, A. C. 1994. Automatic 3D intersubject registration of MR volumetric data in standardized Talairach space. *Journal of computer assisted tomography,* 18**,** 192-205.

DALE, A. M., FISCHL, B. & SERENO, M. I. 1999. Cortical surface-based analysis: I. Segmentation and surface reconstruction. *Neuroimage,* 9**,** 179-194.

DALE, A. M. & SERENO, M. I. 1993. Improved localizadon of cortical activity by combining EEG and MEG with MRI cortical surface reconstruction: a linear approach. *Journal of cognitive neuroscience,* 5**,** 162-176.

DEONI, S. C., PETERS, T. M. & RUTT, B. K. 2005. High‐resolution T1 and T2 mapping of the brain in a clinically acceptable time with DESPOT1 and DESPOT2. *Magnetic resonance in medicine,* 53**,** 237-241.

DEONI, S. C., RUTT, B. K. & PETERS, T. M. 2003. Rapid combined T1 and T2 mapping using gradient recalled acquisition in the steady state. *Magnetic Resonance in Medicine,* 49**,** 515-526.

DEONI, S. C., WILLIAMS, S. C., JEZZARD, P., SUCKLING, J., MURPHY, D. G. & JONES, D. K. 2008. Standardized structural magnetic resonance imaging in multicentre studies using quantitative T1 and T2 imaging at 1.5 T. *Neuroimage,* 40**,** 662-671.

DESIKAN, R. S., SÉGONNE, F., FISCHL, B., QUINN, B. T., DICKERSON, B. C., BLACKER, D., BUCKNER, R. L., DALE, A. M., MAGUIRE, R. P. & HYMAN, B. T. 2006. An automated labeling system for subdividing the human cerebral cortex on MRI scans into gyral based regions of interest. *Neuroimage,* 31**,** 968-980.

EBDEN, M. 2008. Gaussian processes for regression: A quick introduction. *The Website of Robotics Research Group in Department on Engineering Science, University of Oxford*.

FISCHL, B. & DALE, A. M. 2000. Measuring the thickness of the human cerebral cortex from magnetic resonance images. *Proceedings of the National Academy of Sciences,* 97**,** 11050-11055.

FISCHL, B., LIU, A. & DALE, A. M. 2001. Automated manifold surgery: constructing geometrically accurate and topologically correct models of

the human cerebral cortex. *Medical Imaging, IEEE Transactions on,* 20**,** 70-80.
FISCHL, B., SALAT, D. H., BUSA, E., ALBERT, M., DIETERICH, M., HASELGROVE, C., VAN DER KOUWE, A., KILLIANY, R., KENNEDY, D. & KLAVENESS, S. 2002. Whole brain segmentation: automated labeling of neuroanatomical structures in the human brain. *Neuron,* 33**,** 341-355.
FISCHL, B., SALAT, D. H., VAN DER KOUWE, A. J. W., MAKRIS, N., SÉGONNE, F., QUINN, B. T. & DALE, A. M. 2004a. Sequence-independent segmentation of magnetic resonance images. *Neuroimage,* 23**,** 69-84.
FISCHL, B., SERENO, M. I. & DALE, A. M. 1999a. Cortical surface-based analysis: II: Inflation, flattening, and a surface-based coordinate system. *Neuroimage,* 9**,** 195-207.
FISCHL, B., SERENO, M. I., TOOTELL, R. B. H. & DALE, A. M. 1999b. High-resolution intersubject averaging and a coordinate system for the cortical surface. *Human brain mapping,* 8**,** 272-284.
FISCHL, B., VAN DER KOUWE, A., DESTRIEUX, C., HALGREN, E., SÉGONNE, F., SALAT, D. H., BUSA, E., SEIDMAN, L. J., GOLDSTEIN, J. & KENNEDY, D. 2004b. Automatically parcellating the human cerebral cortex. *Cerebral cortex,* 14**,** 11-22.
FRISTON, K. J., HOLMES, A. P., WORSLEY, K. J., POLINE, J. P., FRITH, C. D. & FRACKOWIAK, R. S. J. 1994a. Statistical parametric maps in functional imaging: a general linear approach. *Human brain mapping,* 2**,** 189-210.
FRISTON, K. J., WORSLEY, K. J., FRACKOWIAK, R., MAZZIOTTA, J. C. & EVANS, A. C. 1994b. Assessing the significance of focal activations using their spatial extent. *Human brain mapping,* 1**,** 210-220.
GARCIA, F. I. 2016. *Introduction to Support Vector Machines* [Online]. Available: http://docs.opencv.org/2.4/doc/tutorials/ml/introduction_to_svm/introduction_to_svm.html [Accessed 21 September 2016].
HAN, X., JOVICICH, J., SALAT, D., VAN DER KOUWE, A., QUINN, B., CZANNER, S., BUSA, E., PACHECO, J., ALBERT, M. & KILLIANY, R. 2006. Reliability of MRI-derived measurements of human cerebral cortical thickness: the effects of field strength, scanner upgrade and manufacturer. *Neuroimage,* 32**,** 180-194.
HAUFE, S., MEINECKE, F., GÖRGEN, K., DÄHNE, S., HAYNES, J.-D., BLANKERTZ, B. & BIESSMAN, F. 2014. On the interpretation of weight vectors of linear models in multivariate neuroimaging. *NeuroImage,* 87**,** 96-110.
HSU, C.-W., CHANG, C.-C. & LIN, C.-J. 2003. A practical guide to support vector classification.
JOHNSON, G., ORMEROD, I., BARNES, D., TOFTS, P. & MACMANUS, D. 1987. Accuracy and precision in the measurement of relaxation times from nuclear magnetic resonance images. *The British journal of radiology,* 60**,** 143-153.
JOVICICH, J., CZANNER, S., GREVE, D., HALEY, E., VAN DER KOUWE, A., GOLLUB, R., KENNEDY, D., SCHMITT, F., BROWN, G. & MACFALL, J. 2006. Reliability in multi-site structural MRI studies: effects of gradient non-linearity correction on phantom and human data. *Neuroimage,* 30**,** 436-443.
KENDALL, M. G., STUART, A. & ORD, J. 1968. *The advanced theory of statistics*, London.

KJÆR, L., THOMSEN, C., HENRIKSEN, O., RING, P., STUBGAARD, M. & PEDERSEN, E. 1987. Evaluation of relaxation time measurements by magnetic resonance imaging: a phantom study. *Acta Radiologica,* 28**,** 345-351.
KUPERBERG, G. R., BROOME, M. R., MCGUIRE, P. K., DAVID, A. S., EDDY, M., OZAWA, F., GOFF, D., WEST, W. C., WILLIAMS, S. C. R. & VAN DER KOUWE, A. J. W. 2003. Regionally localized thinning of the cerebral cortex in schizophrenia. *Archives of general psychiatry,* 60**,** 878-888.
KUSS, M. & RASMUSSEN, C. E. 2005. Assessing approximate inference for binary Gaussian process classification. *Journal of Machine Learning Research,* 6**,** 1679-1704.
LAUTERBUR, P. C. 1973. Image formation by induced local interactions: examples employing nuclear magnetic resonance.
MANSFIELD, P. 1977. Multi-planar image formation using NMR spin echoes. *Journal of Physics C: Solid State Physics,* 10**,** L55.
MARQUAND, A., HOWARD, M., BRAMMER, M., CHU, C., COEN, S. & MOURÃO-MIRANDA, J. 2010. Quantitative prediction of subjective pain intensity from whole-brain fMRI data using Gaussian processes. *NeuroImage,* 49**,** 2178-2189.
MARQUAND, A. F., BRAMMER, M., WILLIAMS, S. C. & DOYLE, O. M. 2014. Bayesian multi-task learning for decoding multi-subject neuroimaging data. *NeuroImage,* 92**,** 298-311.
MITCHELL, T. M. 1997. Machine learning. 1997. *Burr Ridge, IL: McGraw Hill,* 45**,** 37.
MOURÃO-MIRANDA, J., BOKDE, A. L. W., BORN, C., HAMPEL, H. & STETTER, M. 2005. Classifying brain states and determining the discriminating activation patterns: Support Vector Machine on functional MRI data. *NeuroImage,* 28**,** 980-995.
MOURAO-MIRANDA, J., REYNAUD, E., MCGLONE, F., CALVERT, G. & BRAMMER, M. 2006. The impact of temporal compression and space selection on SVM analysis of single-subject and multi-subject fMRI data. *NeuroImage,* 33**,** 1055-1065.
MWANGI, B., TIAN, T. S. & SOARES, J. C. 2014. A review of feature reduction techniques in neuroimaging. *Neuroinformatics,* 12**,** 229-244.
NICKISCH, H. & RASMUSSEN, C. E. 2008. Approximations for binary Gaussian process classification. *Journal of Machine Learning Research,* 9**,** 2035-2078.
PURCELL, E. M., TORREY, H. & POUND, R. V. 1946. Resonance absorption by nuclear magnetic moments in a solid. *Physical review,* 69**,** 37.
RASMUSSEN, C. E. & WILLIAMS, C. K. I. 2006. *Gaussian processes for machine learning*, MIT press Cambridge, MA.
REUTER, M., ROSAS, H. D. & FISCHL, B. 2010. Highly accurate inverse consistent registration: a robust approach. *Neuroimage,* 53**,** 1181-1196.
REUTER, M., SCHMANSKY, N. J., ROSAS, H. D. & FISCHL, B. 2012. Within-subject template estimation for unbiased longitudinal image analysis. *Neuroimage,* 61**,** 1402-1418.
REUTER, M., TISDALL, M.D., QURESHI A, BUCKNER RL, VAN DER KOUWE AJW, FISCHL B. 2015 Head Motion during MRI Acquisition Reduces Gray Matter Volume and Thickness Estimates. *NeuroImage*, 107, 107-115.

SALAT, D. H., BUCKNER, R. L., SNYDER, A. Z., GREVE, D. N., DESIKAN, R. S. R., BUSA, E., MORRIS, J. C., DALE, A. M. & FISCHL, B. 2004. Thinning of the cerebral cortex in aging. *Cerebral cortex,* 14**,** 721-730.

SCHAER, M., CUADRA, M. B., TAMARIT, L., LAZEYRAS, F., ELIEZ, S. & THIRAN, J. 2008. A surface-based approach to quantify local cortical gyrification. *Medical Imaging, IEEE Transactions on,* 27**,** 161-170.

SÉGONNE, F., DALE, A., BUSA, E., GLESSNER, M., SALAT, D., HAHN, H. & FISCHL, B. 2004. A hybrid approach to the skull stripping problem in MRI. *Neuroimage,* 22**,** 1060-1075.

SÉGONNE, F., PACHECO, J. & FISCHL, B. 2007. Geometrically accurate topology-correction of cortical surfaces using nonseparating loops. *Medical Imaging, IEEE Transactions on,* 26**,** 518-529.

SLED, J., ZIJDENBOS, A. & EVANS, A. 1998. A nonparametric method for automatic correction of intensity nonuniformity in MRI data. *IEEE Trans Med Imaging,* 17**,** 87 - 97.

SMITH, S. M. 2002. Fast robust automated brain extraction. *Human brain mapping,* 17**,** 143-155.

SMOLA, A. J. & SCHÖLKOPF, B. 1998. *Learning with kernels*, Citeseer.

SPRAWLS, P. 1987. *Physical principles of medical imaging*, Aspen Publishers.

STUDENT 1908. The probable error of a mean. *Biometrika***,** 1-25.

VAPNIK, V. 1995. *The Nature of Statistical Learning Theory,* New York, Springer-Verlag.

WINKLER, A. M., SABUNCU, M. R., YEO, B., FISCHL, B., GREVE, D. N., KOCHUNOV, P., NICHOLS, T. E., BLANGERO, J. & GLAHN, D. C. 2012. Measuring and comparing brain cortical surface area and other areal quantities. *NeuroImage,* 61**,** 1428-1443.

WORSLEY, K., ANDERMANN, M., KOULIS, T., MACDONALD, D. & EVANS, A. 1999. Detecting changes in nonisotropic images. *Human brain mapping,* 8**,** 98-101.

WORSLEY, K. J. 1994. Local maxima and the expected Euler characteristic of excursion sets of χ 2, F and t fields. *Advances in Applied Probability***,** 13-42.

WORSLEY, K. J., EVANS, A. C., MARRETT, S. & NEELIN, P. 1992. A three-dimensional statistical analysis for CBF activation studies in human brain. *Journal of Cerebral Blood Flow & Metabolism,* 12**,** 900-918.

WORSLEY, K. J., MARRETT, S., NEELIN, P., VANDAL, A. C., FRISTON, K. J. & EVANS, A. C. 1996. A unified statistical approach for determining significant signals in images of cerebral activation. *Human brain mapping,* 4**,** 58-73.

Chapter 3: Grey to White Matter Percent Contrast as an in vivo Neuroimaging Feature in Autism Spectrum Disorder

Autism spectrum disorder (ASD) is a condition that manifests during early development that is accompanied by differences in brain anatomy and connectivity (Lange et al., 2015, Ecker et al., 2015, Amaral et al., 2008). Several prior magnetic resonance imaging (MRI) studies of ASD have reported atypical measures of cortical anatomy such as folding, thickness, and surface area (Nordahl et al., 2007, Hyde et al., 2010, Ecker et al., 2013, Schaer et al., 2013). These *in vivo* findings are supported by postmortem reports of atypical cortical structure such as increased numbers of neuron cells, cortical minicolumns and instances of folding abnormalities in ASD (Casanova et al., 2006, Courchesne et al., 2011, Kemper, 1988).

This chapter details a novel application of measures of tissue contrast in an attempt to quantify a specific aspect of neuropathology in ASD, namely poor definition of the grey-white matter boundary (Avino and Hutsler, 2010). This study was recently published in *Cerebral Cortex* (Andrews et al., 2017) and is included in its final published format in the pages that follow. Supplementary materials for this chapter can be found in Appendix II.

Cerebral Cortex, February 2017;27: 877–887

doi: 10.1093/cercor/bhw404
Advance Access Publication Date: 5 January 2017
Original Article

ORIGINAL ARTICLE

In Vivo Evidence of Reduced Integrity of the Gray–White Matter Boundary in Autism Spectrum Disorder

Derek Sayre Andrews[1], Thomas A. Avino[2], Maria Gudbrandsen[1], Eileen Daly[1], Andre Marquand[3,4], Clodagh M. Murphy[1,5], Meng-Chuan Lai[6,7,8], Michael V. Lombardo[6,9], Amber N.V. Ruigrok[6], Steven C. Williams[4], Edward T. Bullmore[10], The MRC AIMS Consortium[11], John Suckling[12], Simon Baron-Cohen[6], Michael C. Craig[1,5], Declan G.M. Murphy[1,5,†] and Christine Ecker[1,12,†]

[1]Department of Forensic and Neurodevelopmental Sciences, Sackler Institute for Translational Neurodevelopment, Institute of Psychiatry, Psychology and Neuroscience, King's College London, London SE5 8AF, UK, [2]Department of Psychiatry and Behavioral Sciences, M.I.N.D. Institute, University of California Davis, Sacramento, CA, USA, [3]Donders Institute for Brain, Cognition and Behaviour, Radboud University, Nijmegen, The Netherlands, [4]Centre for Neuroimaging Sciences, Institute of Psychiatry, Psychology and Neuroscience, King's College, London, UK, [5]National Autism Unit, Bethlem Royal Hospital, South London and Maudsley NHS Foundation Trust, London, UK, [6]Autism Research Centre, Department of Psychiatry, University of Cambridge, Cambridge, UK, [7]Child and Youth Mental Health Collaborative at the Centre for Addiction and Mental Health and The Hospital for Sick Children, Department of Psychiatry, University of Toronto, Toronto, Canada, [8]Department of Psychiatry, National Taiwan University Hospital and College of Medicine, Taipei, Taiwan, [9]Department of Psychology & Center for Applied Neuroscience, University of Cyprus, Nicosia, Cyprus, [10]Brain Mapping Unit, Department of Psychiatry, University of Cambridge, Cambridge, UK, [11]The Medical Research Council Autism Imaging Multicentre Study Consortium (MRC AIMS Consortium) is a UK collaboration between the Institute of Psychiatry, Psychology and Neuroscience at King's College, London, the Autism Research Centre, University of Cambridge, and the Autism Research Group, University of Oxford. The Consortium members in alphabetical order are as follows: Anthony J. Bailey (Oxford), Simon Baron-Cohen (Cambridge), Patrick F. Bolton (IoP), Edward T. Bullmore (Cambridge), Sarah Carrington (Oxford), Marco Catani (IoPPN), Bhismadev Chakrabarti (Cambridge), Michael C. Craig (IoPPN), Eileen M. Daly (IoPPN), Sean C.L. Deoni (IoPPN), Christine Ecker (IoPPN), Francesca Happé (IoPPN), Julian Henty (Cambridge), Peter Jezzard (Oxford), Patrick Johnston (IoPPN), Derek K. Jones (IoPPN), Meng-Chuan Lai (Cambridge), Michael V. Lombardo (Cambridge), Anya Madden (IoPPN), Diane Mullins (IoPPN), Clodagh M. Murphy (IoPPN), Declan G.M. Murphy (IoPPN), Greg Pasco (Cambridge), Amber N.V. Ruigrok (Cambridge), Susan A. Sadek (Cambridge), Debbie Spain (IoPPN), Rose Stewart (Oxford), John Suckling (Cambridge), Sally J. Wheelwright (Cambridge), Steven C. Williams (IoPPN), and C. Ellie Wilson (IoPPN) and [12]Department of Child and Adolescent Psychiatry, Psychosomatics and Psychotherapy, Universitätsklinikum Frankfurt am Main, Goethe-University Frankfurt am Main, Frankfurt, Germany

Address correspondence to Derek Sayre Andrews, Department of Forensic and Neurodevelopmental Science, Institute of Psychiatry, Psychology & Neuroscience, King's College London, PO Box 50, 16 De Crespigny Park, Denmark Hill, London SE5 8AF, UK. Email: Derek.Andrews@KCL.ac.uk

†Declan G.M. Murphy and Christine Ecker contributed equally to the manuscript.

Abstract

Atypical cortical organization and reduced integrity of the gray–white matter boundary have been reported by postmortem studies in individuals with autism spectrum disorder (ASD). However, there are no in vivo studies that examine these particular features of cortical organization in ASD. Hence, we used structural magnetic resonance imaging to examine differences in tissue contrast between gray and white matter in 98 adults with ASD and 98 typically developing controls, to test the hypothesis that individuals with ASD have significantly reduced tissue contrast. More specifically, we examined contrast as a percentage between gray and white matter tissue signal intensities (GWPC) sampled at the gray–white matter boundary, and across different cortical layers. We found that individuals with ASD had significantly reduced GWPC in several clusters throughout the cortex (cluster, $P < 0.05$). As expected, these reductions were greatest when tissue intensities were sampled close to gray–white matter interface, which indicates a less distinct gray–white matter boundary in ASD. Our in vivo findings of reduced GWPC in ASD are therefore consistent with prior postmortem findings of a less well-defined gray–white matter boundary in ASD. Taken together, these results indicate that GWPC might be utilized as an in vivo proxy measure of atypical cortical microstructural organization in future studies.

Key words: ASD, FreeSurfer, imaging, lamination, MRI

Introduction

Autism spectrum disorder (ASD) is a lifelong neurodevelopmental condition characterized by impaired social communication, deficits in social reciprocity, and repetitive and stereotypic behaviors and interests (Wing 1997). These core symptoms typically manifest from early childhood, and are accompanied by developmental differences in brain anatomy and connectivity (for review, see Amaral et al. 2008; Ecker et al. 2015; Lange et al. 2015). For example, prior studies of ASD reported atypical measures of cortical anatomy such as folding, thickness, and surface area (Nordahl et al. 2007; Hyde et al. 2010; Schaer et al. 2013; Ecker et al. 2013a) as well as intra-cortical connectivity (Ecker et al. 2013b). However, the causes of these cortical abnormalities in people with ASD are unknown.

There is some evidence to suggest that the cortical differences accompanying ASD may result from atypical neuronal proliferation, migration, and maturation (Persico et al. 2014). For example, some genetic variants associated with ASD encode for genes that regulate these neurodevelopmental processes (Huguet et al. 2013). It has been suggested that these variations may explain postmortem findings such as irregular cortical lamination, the presence of super-numerous neurons in some layers of the cortex, and poor differentiation of the gray-white matter boundary (for review, see Casanova 2014). For example, histological samples from the superior temporal gyrus (approximate Brodmann area [BA] 21), dorsolateral frontal lobe (BA9) and dorsal parietal lobe (BA7) have shown the gray-white matter boundary to be less distinct in ASD as compared with typically developing (TD) controls (Avino and Hutsler 2010). Thus, there is increasing postmortem evidence for abnormal cell patterning within the gray-white matter boundary in ASD. However, to date no study has investigated differences in the integrity of the gray-white matter boundary in ASD in vivo across the whole brain.

Current in vivo neuroimaging methods for investigating cortical abnormalities in ASD focus on morphometric features such as cortical thickness (CT), that is, the closest distance from the gray-white matter boundary to the gray-cerebral spinal fluid (CSF) boundary (Fischl and Dale 2000). Differences in CT have been reported in children, adolescents, and adults with ASD, and include regional increases and decreases that may mediate some of the behavioral deficits typically observed in the disorder (Hardan et al. 2006; Hyde et al. 2010; Ecker et al. 2013b). However, measures of CT rely on the accurate delineation of gray and white matter and therefore may be confounded by intrinsic histological abnormalities at the gray-white matter boundary in ASD (Avino and Hutsler 2010).

Hence, we investigated between-group differences related to cortical lamination in both adult males and females with ASD, and matched TD controls, using a whole brain quantitative approach that estimated integrity of the gray-white matter boundary. Namely we examined the percent contrast of gray-to-white matter signal intensities (GWPC), sampled across different cortical layers in a continuous fashion. Here, the GWPC calculation we employed in the current manuscript is comparable to the gray-white contrast ratio as originally reported by Salat et al. (2009). We hypothesized the gray-white matter boundary to be less defined and therefore GWPC to differ significantly in individuals with ASD.

Materials and Methods

Participants

Overall, 98 right-handed adults with ASD (49 males and 49 females) and 98 age, sex, and IQ matched TD controls (51 males and 47 females) aged 18–42 years were recruited by advertisement and assessed at the Institute of Psychiatry, Psychology and Neuroscience (IoPPN), London, and the Autism Research Centre, Cambridge. Approximately equal ratios of cases to controls, and males to females, were recruited within sites (Table 1). Exclusion criteria included a history of major psychiatric disorder (e.g. psychosis), head injury, genetic disorder associated with autism (e.g. fragile-X syndrome, tuberous sclerosis), or any other medical condition affecting brain function (e.g. epilepsy), or any participants taking antipsychotic medication, mood stabilizers or benzodiazepines.

ASD diagnosis was made by a consultant psychiatrist using ICD-10 research diagnostic criteria and confirmed using the ADI-R (Lord et al. 1994). ADI-Rs were completed for 94 individuals with ASD (49 males and 45 females). Ninety-three (49 males and 44 females) reached algorithm cut-offs for autism in all domains of the ADI-R (social, communication, and restricted/stereotyped), although failure to reach cut-off in one domain by one point was permitted. The ADI-R rather than ADOS (Lord et al. 2000) was employed as inclusion criteria to ensure that all participants

Table 1 Participant demographics

	ASD (*n* = 98 [49♂, 49♀])	Control (*n* = 98 [51♂, 47♀])
London	*n* = 45 (24♂, 21♀)	*n* = 44 (25♂, 19♀)
Cambridge	*n* = 53 (25♂, 28♀)	*n* = 54 (26♂, 28♀)
Age, years	26 ± 7 (18–48)	27 ± 6 (18–50)
Full-scale IQ, WASI	113 ± 12 (84–136)	116 ± 9 (95–137)
ADI-R social[a]	17 ± 5 (10–28)	*
ADI-R communication[a]	13 ± 4 (2–24)	*
ADI-R repetitive behavior[a]	5 ± 2 (1–10)	*
ADOS social + communication[b]	9 ± 5 (0–21)	*

Data expressed as mean ± standard deviation (range). There were no significant between-groups differences in age or IQ; $P > 0.05$ (2-tailed). All participants were diagnosed using ICD-10 criteria.

[a]The Autism Diagnostic Interview–Revised (ADI-R) was used to confirm ASD diagnosis. ADI-R scores were unavailable for 4 participants. Each of these cases matched.

[b]The Autism Diagnostic Observation Schedule (ADOS) cut-offs for "autism spectrum", for all other participants the ADOS was not used as diagnostic criteria.

*TD controls did not undergo ADI-R or ADOS assessments.

with ASD met the criteria for childhood autism. We were unable to complete ADI-Rs for 4 females with ASD as their parents/caregivers were not available. However, all 4 reached algorithm cut-offs for "autism spectrum" on the ADOS (communication, social) diagnostic algorithm. In all other participants, ADOS scores were used to measure current symptoms and not as inclusion criterion. One ASD female scored one point below cut-off for autism on the communication and repetitive behavior domains of the ADI-R but met ICD-10 criteria for ASD and scored above cut-off for "autism" on the ADOS. Overall intellectual ability was assessed using the Wechsler Abbreviated Scale of Intelligence (WASI; Wechsler 1999). All participants had a full-scale IQ greater than 80 and gave informed written consent in accordance with ethics approval by the National Research Ethics Committee, Suffolk, UK.

Structural MRI Data Acquisition

Scanning was performed at the IoPPN, London, and Addenbrooke's Hospital, Cambridge, using a 3 T GE Signa System (General Electric). A specialized acquisition protocol using quantitative T1 mapping was used to ensure standardization of structural magnetic resonance imaging (MRI) scans across scanner platforms. This protocol has previously been validated and extensively described elsewhere (Deoni et al. 2008; Ecker et al. 2012), resulting in high-resolution structural T1-weighted inversion-recovery images, with 1 × 1 × 1 mm resolution, a 256 × 256 × 176 matrix, TR = 1800 ms, TI = 50 ms, FA = 20°, and FOV = 5 cm.

Cortical Reconstruction Using FreeSurfer

Previous histological studies have largely relied upon manual identification to define the boundary between gray and white matter. For example, Avino and Hutsler (2010) used a sigmoid function to quantify the distinctiveness of the transition between gray and white matter in Nissl-stained histological images. In the current study, however, we employed an automated analytical pipeline using FreeSurfer v5.3.0 software (http://surfer.nmr.mgh.harvard.edu/) to identify the gray–white matter boundary by deriving models of the cortical surface for each T1-weighted image. These well validated and fully automated procedures have been detailed elsewhere (Dale et al. 1999; Fischl et al. 1999; Fischl and Dale 2000; Ségonne et al. 2004; Jovicich et al. 2006). In brief, a single-filled white-matter volume was generated for each hemisphere after intensity normalization, extra-cerebral tissue was cropped, and image segmentation performed using a connected components algorithm. A triangular tessellated surface was then generated for each white matter volume. Deformation of this tessellated white matter surface resulted in a cortical mesh for the surfaces that define the boundary between gray and white matter (i.e. white matter surface), and gray matter and CSF (i.e. pial surface). This surface deformation is the result of the minimization of an energy functional that utilizes intensity gradients in order to place these surfaces where the greatest shift in intensity defines the transition between tissue classes (Dale et al. 1999, Supplementary Material). The use of intensity gradients across tissue classes assures that boundary placement is not reliant solely on absolute signal intensity and allows for subvoxel resolution in the placement of these boundary surfaces (Dale and Sereno 1993; Dale et al. 1999; Fischl and Dale 2000). These automated methods have previously been validated against histological analyses and have shown a high degree of accuracy in placing the gray–white matter boundary (Rosas et al. 2002). The resulting surface models were visually inspected for reconstruction errors. Participant's surface reconstructions with visible inaccuracies were excluded and are not described in this study. Dropout rates due to surface reconstruction errors were equal between groups and represented <10% of the total sample.

Gray-to-White Matter Percent Contrast (GWPC) and Gray-Matter Signal Intensity Measures

Gray-matter tissue intensities (GMI) were sampled continuously across different cortical layers from the gray–white matter boundary (i.e. white matter surface) to the pial surface. These signal intensities were sampled at different percentile fractions of the total orthogonal distance projected from the white matter to pial surfaces (i.e. projection fractions). Starting at the white matter surface, sampling continued at projection fraction intervals of 10% up to 60% of the distance from the white matter to the pial surface, thus yielding a set of 6 GMI measures (i.e. from 10% to 60%; Fig. 1). The outer 40% (i.e. 70–100%) of the cortical sheet was not sampled in order to assure that sampling was performed within the cortical gray matter, and not confounded by voxels composed of CSF. White matter signal intensity (WMI) was measured at 1.0 mm into the white matter from the white matter surface (Fig. 1). Previously reported measures of tissue contrast have used a ratio calculation (i.e. GMI/WMI; Salat et al. 2009), where larger values indicate a reduced contrast. Here, however, we utilized the formula provided by FreeSurfer to calculate tissue contrast as the percentage of GMI at projection fraction (j) to WMI at each cerebral vertex (i),

$$GWPC_{ij} = 100 \times \frac{(WMI_{i\,1\,mm} - GMI_{ij})}{0.5 \times (WMI_{i\,1\,mm} + GMI_{ij})}$$

Thus, by definition, a decrease in GWPC is commensurate with a decrease in contrast between the GMI measured at projection fraction *i*, and the WMI measured at 1.0 mm subjacent to the white matter surface. We also examined the tissue contrast when sampling GMI at the gray–white matter boundary (i.e. at the white matter surface, projection fraction = 0%). The resulting GWPC, GMI, and WMI measures were subsequently smoothed using a 10-mm full-width at half-maximum (FWHM) surface-based

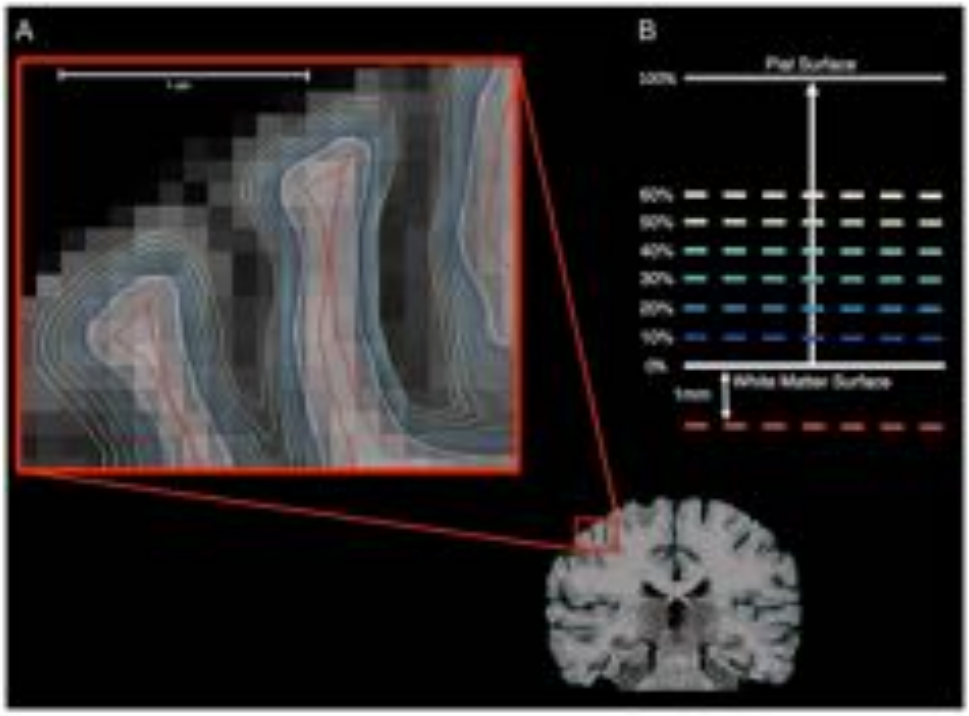

Figure 1. Gray and white matter signal intensity sampling procedure. (A) Gray and white matter signal intensity sampling points are shown for one 2D coronal slice. (B) WMn (red line) were sampled at an absolute distance of 1 mm subjacent to the white matter surface (i.e. gray–white matter boundary). GMI signals (blue to yellow lines) were measured at projection fractions representing a percentage of the total orthogonal distance from the white matter surface to the outer pial surface starting at the white matter surface up to 60% into the cortical sheet at 10% intervals.

Gaussian kernel prior to statistical analyses. We also examine between-group comparisons using a 5-mm FWHM smoothing kernel, which are shown in Supplementary Figure 3 and Table 3.

Statistical Analyses

Vertex-wise statistical analysis of GWPC, GMI, and WMI measures (Y) were estimated by the regression of a general linear model (GLM) with 1) diagnostic group, sex, and acquisition site as categorical fixed-effects factors, 2) a group by sex interaction term, and 3) age and full-scale IQ as continuous covariates:

$$Y_i = \beta_0 + \beta_1 \text{Group} + \beta_2 \text{Sex} + \beta_3 [\text{Group} \times \text{Sex}] + \beta_4 \text{Site} + \beta_5 \text{Age} + \beta_6 \text{FSIQ} + \varepsilon_i$$

where ε_i is the residual error at vertex i. Between-group differences were estimated from the corresponding coefficient β_n normalized by the corresponding standard error. Our model was selected a priori in order to be comparable to previously published research findings based on our sample (Zilles et al. 2013b). Corrections for multiple comparisons across the whole brain were performed using "random field theory" (RFT)-based cluster analysis for non-isotropic images using a cluster-based significance threshold of $P < 0.05$ (2-tailed; Worsley et al. 1999). Initially, we investigated between-group differences in GWPC at different gray-matter projection fractions. Subsequently, we also investigated between-group differences in gray and white matter tissue intensities, which allowed us to determine whether the between-group differences in GWPC were driven by differences within the cortical gray or white matter. Last, between-group differences in CT were examined using the same GLM as described above in order to determine how differences in GWPC might affect variability in CT in ASD.

Results

Participant Demographics and Global Brain Measures

There were no significant differences between individuals (males and females) with ASD and TD controls in age ($t(194) = -0.53$, $P = 0.598$), full-scale IQ ($t(194) = -1.72$, $P = 0.086$), or total GM volume ($t(194) = -0.30$, $P = 0.839$). There were also no significant differences between males and females in age ($t(194) = -0.93$, $P = 0.356$) or full-scale IQ ($t(194) = -1.87$, $P = 0.063$). As expected, total gray matter volume in males was significantly larger than in females ($t(194) = 9.11$, $P < 0.001$). However, there were no significant differences in any of these measures between males with ASD and male controls, or females with ASD and female controls ($P < 0.05$, 2-tailed).

Between-Group Difference in GWPC Across the Cortex

We initially examined vertex-wise between-group differences in GWPC at different projection fractions into the cortical sheet. At all sampling depths, we found that individuals with ASD had a significantly decreased GWPC in several clusters across the cortex, which is consistent with a reduced tissue contrast between gray and white matter (Fig. 2). In accordance with our hypothesis, the reductions in GWPC were most extensive when GMI was sampled at gray–white matter boundary (i.e. the white matter surface, projection fraction = 0%), and gradually decreased in both statistical effect and spatial extent with increasing projection fractions into cortex and away from the gray–white matter boundary. Regions where ASD individuals had reduced GWPC as compared with TD controls included the 1) bilateral posterior cingulate (BA 23/30), medial frontal (BA10) fusiform/entorhinal (BA 34/37) and the inferior and superior

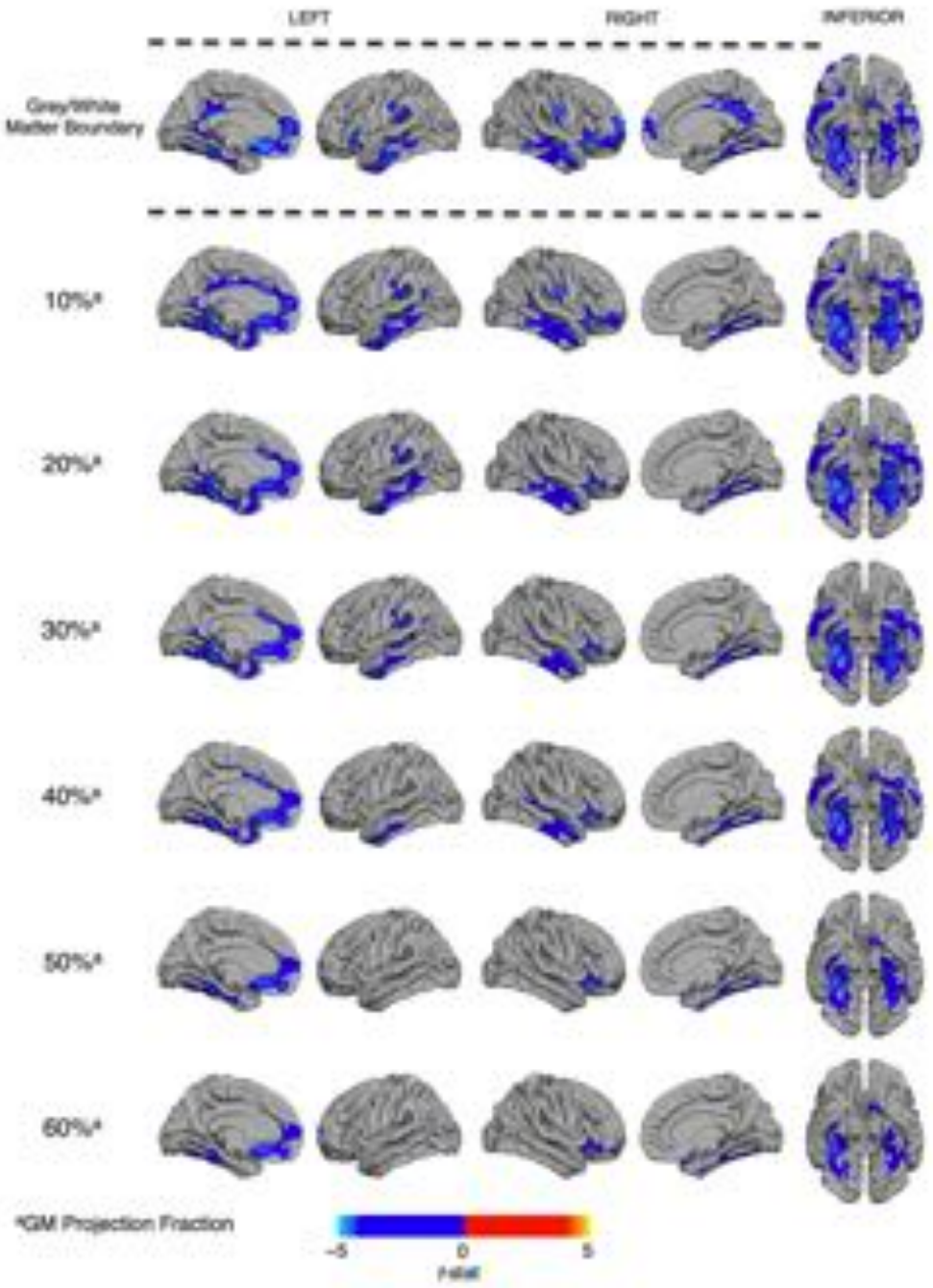

Figure 3. Regions of decreased gray-to-white matter signal intensity percent contrast (GWPC) in ASD. Individuals with ASD showed significantly decreased GWPC ($t(47, P < 0.05)$, indicating less definition between gray and white matter, in several regions highlighted in blue including 1) the posterior cingulate cortex, 2) fronto-temporal and fronto-parietal regions, as well as 3) the bilateral fusiform and extrastriate cortex. The spatial and statistical extent of these differences was greatest when tissue intensities were sampled at the gray-white matter boundary and decreased along with increasing projection fractions (superscript a) into the cortical sheet. See Table 2 for statistical details.

temporal cortices (BA39/21/22); 2) left orbitofrontal cortex (BA11/35) and tempero-parietal junction (BA39/40); and (3) right dorsolateral prefrontal cortex (BA11/45). Statistical details for all clusters are listed in Table 2. There were no brain regions where individuals with ASD had a significantly increased GWPC relative to controls. The pattern of reduced GWPC among individuals with ASD remained significant when total brain volume or mean CT were included as covariates. Furthermore, there was minimal spatial overlap between the pattern of differences in GWPC and CT (see Supplementary Fig. 1 and Table 1).

Between-Group Differences in Gray and White Matter Tissue Intensities

To identify whether the observed differences in GWPC were driven by differences in gray or white matter, or a combination of both, we subsequently examined between group differences in

Table 2 Clusters of significant reductions in gray white matter percent contrast and increases in gray matter intensity in ASD

Measure	Cluster	Region labels	Hemisphere	BA (max)	Vertices	Talairach			t_{max}	$p_{cluster}$
						x	y	z		
GWPC	1	Superior temporal gyrus, insula, lateral orbital frontal cortex, pars orbitalis, pars triangularis, postcentral gyrus, precentral gyrus, rostral middle frontal gyrus, superior frontal gyrus	L	21	10 204	47	−4	−14	−5.95	4.38×10^{-4}
	2	Posterior cingulate cortex, isthmus-cingulate cortex, lingual gyrus, precuneus cortex	R	31	5760	7	−50	39	−5.77	2.05×10^{-4}
	3	Middle temporal gyrus, banks superior temporal sulcus, inferior temporal gyrus, superior temporal gyrus	R	21	4994	54	−11	−18	−5.87	4.48×10^{-4}
	4	Middle temporal gyrus, banks superior temporal sulcus, inferior temporal gyrus, superior temporal gyrus	L	21	4837	−53	−10	−3	−5.59	1.46×10^{-4}
	5	Insula, lateral orbital frontal cortex, pars opercularis, postcentral gyrus, precentral gyrus	L	13	4168	−27	24	−1	−5.64	1.48×10^{-4}
	6	Parahippocampal gyrus, fusiform gyrus, lingual gyrus	R	19	4055	25	−53	−2	−5.34	7.63×10^{-4}
	7	Medial orbital frontal cortex, rostral anterior cingulate cortex, superior frontal gyrus	L	11	3520	−8	35	−14	−6.13	2.14×10^{-4}
	8	Fusiform gyrus, lingual gyrus, parahippocampal gyrus	L	37	3443	−36	−43	−8	−5.26	6.62×10^{-4}
	9	Posterior cingulate cortex, isthmus-cingulate cortex, lingual gyrus, precuneus cortex	L	23	3432	−8	−56	16	−5.33	5.90×10^{-4}
	10	Supramarginal gyrus	L	40	3466	−56	−32	27	−5.15	5.36×10^{-4}
GMI	1	Superior temporal gyrus, banks superior temporal sulcus, fusiform gyrus, inferior parietal cortex, inferior temporal gyrus, insula, isthmus-cingulate cortex, lateral orbital frontal cortex, lingual gyrus, middle temporal gyrus, parahippocampal gyrus, pars triangularis, supramarginal gyrus, temporal pole	R	38	17 958	35	5	−10	4.02	1.69×10^{-4}
	2	Superior temporal gyrus, banks superior temporal sulcus, inferior parietal cortex, inferior temporal gyrus, middle temporal gyrus	L	21	10 279	−51	−26	−2	3.31	2.86×10^{-4}
	3	Fusiform gyrus, inferior temporal gyrus, isthmus-cingulate cortex, lingual gyrus, precuneus cortex	L	37	4295	−44	−40	−14	3.27	2.70×10^{-4}

Notes: Clusters of significant reductions in GWPC and increases in gray matter intensity (GMI) in ASD. BA, left (L), right (R). 'Vertices' indicates the number of vertices within the cluster. t_{max} represents the maximum t-statistic within the cluster located at the x y z Talairach coordinates listed. $p_{cluster}$ is the cluster corrected P value.

both GMI and WMI. Individuals with ASD had significantly increased GMI across all 6 different GMI sampling depths relative to controls in regions where we also observed decreases in GWPC (Fig. 3). These included 1) the bilateral anterior temporal lobes (BA38/30) and the left middle temporal gyrus (BA21), 2) the right temporo-parietal junction (BA39/40), and 3) the bilateral fusiform and entorhinal cortex (BA36). Statistical details for these clusters are listed in Table 1. We did not observe any significant between-group differences in GMI at the gray-white matter boundary (i.e. the white matter surface), or in WMI at 1.0 mm within the white matter (Fig. 3). There were no brain regions where individuals with ASD had significantly decreased GMI relative to controls. Hence, GWPC reductions in ASD were driven predominantly by increased (i.e. brighter) tissue intensities within the cortical gray matter.

Main Effects of Sex and Group by Sex Interactions

Last, we investigated whether biological sex significantly modulates differences in GWPC in ASD by examining group-by-sex interactions. Overall, regardless of diagnosis, males had a significantly greater GWPC than females (Supplementary Fig. 2). This occurred across all sampling depths, and was predominantly in fronto-parietal regions of the left hemisphere, and in bilateral inferior temporal regions (see Supplementary Table 2 for statistical details of these clusters). However, there were no brain regions where we observed significant group by sex interactions for GWPC. Thus, while males tended to have a significant increase in contrast between gray and white matter tissue intensities the reductions in GWPC that we observed in the brain in individuals with ASD were not explained by biological sex.

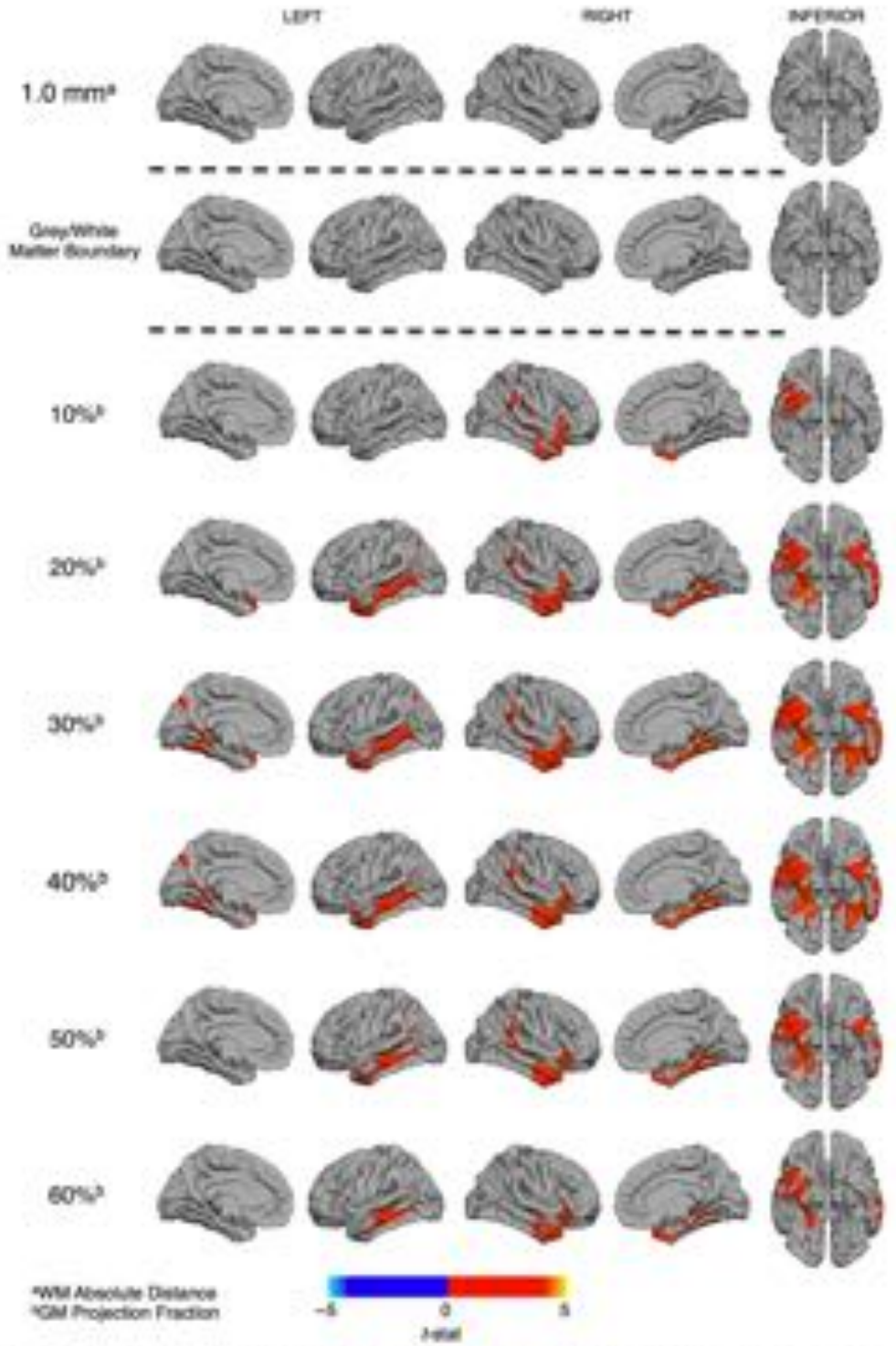

Figure 3. Regional differences in gray (GM) and white matter (WM) signal intensities in ASD. Individuals with ASD showed no significant differences in WM (t_{47}, $P < 0.5$) measured at 1 mm subjacent to the gray–white matter boundary (superscript a) nor tissue intensities measured at the boundary. Significantly increased GM (t_{47}, $P < 0.5$) was observed across all projection fractions (superscript b) within the cortical sheet in ASD participants. The anatomical and spatial extent of these increases in GM were most evident at the 50% projection fraction and incorporated 1) the bilateral anterior temporal lobes and the left middle temporal gyrus, 2) the right temporo-parietal junction, and 3) the bilateral fusiform and entorhinal cortex. See Table 3 for statistical details.

Discussion

Our aim was to determine if previous postmortem reports of poor definition of the gray–white matter boundary in ASD could be detected using a whole brain in vivo MRI approach. As hypothesized, we determined that individuals with ASD had a significantly less well-defined tissue contrast (i.e. GWPC) between gray and white matter at (and around) the gray–white matter boundary. The affected brain regions included the superior temporal gyrus (BA21), the dorsolateral frontal lobe

(BA9), and the dorsal parietal lobe (BA7) where histological abnormalities in the transition from gray-to-white matter have also been reported (Avino and Hutsler 2010). The concordance between the regional pattern and direction of the GWPC differences in our sample with previous histological investigations in postmortem brain tissue supports the biological plausibility of our results. Thus, our findings agree with previous postmortem histological studies and indicate that tissue contrasts across the gray-white matter interface may serve as a potential in vivo proxy measure for atypical organization of the cortical sheet in ASD.

Prior postmortem studies reported abnormalities in the cortical microstructure of individuals with ASD. For example, the boundary between cortical layer VI and underlying white matter has been shown to be significantly less well defined due to increased dispersion of neuronal cells across this interface (Avino and Hutsler 2010). It has been suggested that this may be caused by the presence of supernumerary neurons beneath the cortical plate that arise from disrupted migratory processes or improper resolution of the cortical subplate (Chun and Shatz 1989; Kemper 2010; Hutsler and Avino 2013). The cortical subplate is a transient neurodevelopmental zone that is instrumental in establishing early proper cortical connectivity. Specifically, subplate neurons pioneer the corticothalamic axon pathway, serve as a "signpost" for cortical afferents, drive endogenous oscillatory activity in the cortex, and act as a transient synaptic hub for thalamocortical axons before they directly innervate the cortical plate (Shatz and Luskin, 1986; Ghosh et al., 1990; McConnell et al. 1994; Luhmann et al., 2009). The maximal volume of the subplate is reached around 30 gestational weeks in the human coinciding with the growth of long range cortico-cortico projections (Wang et al. 2016). After their early neurodevelopmental role is complete, a large number of these subplate neurons undergo apoptosis. However, a small percentage of these neurons persist and retain their connections with the overlying cortical plate acting as modulators of cortical afferents (Chun and Shatz 1989; Dupont et al. 2006; Kostović et al. 2011).

Therefore, perturbations to early subplate development may disrupt the establishment of structural and functional brain connectivity, which is abnormal in individuals with ASD (Belmonte et al. 2004; Just et al. 2004; Courchesne and Pierce 2005; Balardin et al. 2015). In addition, the abnormal persistence of these neurons after the large wave of programmed cell death could cause disruptions to cortical communication through their modulatory role of the overlying cortex. In this way, the abnormal persistence of subplate neurons into adulthood has been demonstrated in schizophrenia and seizure disorder and is hypothesized to contribute to the pathophysiology of these conditions (Eastwood and Harrison, 2003, 2005; Andrews et al. 2006; Hildebrandt et al., 2009; Kostović et al. 2011; Yang et al., 2011). Furthermore, a recent genetic study reported a set of subplate-specific genes that are associated with ASD (Gleason-Svabedissen et al. 2013). Thus, there is converging evidence to suggest that neurons of the cortical subplate contribute to the aberrant neuropathology of ASD and that atypical laminar organization, particularly around the gray-white matter boundary, may be a defining characteristic of the condition. However, this has never previously been examined in vivo.

Thus, in this in vivo study, we sought to examine differences in cortical lamination and gray-white matter boundary integrity in ASD. To achieve this, we measured contrasts between gray and white matter tissue intensities (GWPC; Salat 2009). These MRI measures were taken at the interface of gray and white matter and across cortical layers at 6 different depths into the cortical sheet from the gray-white matter boundary (i.e. white matter surface). In our ASD cases, many regions with reduced GWPC also showed significantly increased GM but no differences in WM as compared with TD controls. This suggests (in agreement with prior in vivo work by our group; Ecker et al. 2016) that ASD may be primarily associated with disruptions to cortical gray matter as opposed to white matter. This increased GM in ASD may result from atypical myelination (Sowell et al. 2004) and/or atypical cytoarchitectural organization such as greater numbers of more densely packed cortical minicolumns (Casanova et al. 2006) and reductions in gray level amplitude in these structures (Casanova et al. 2002).

The regional specificity of our findings of decreased tissue contrast may be related to the differential expansion of the subplate between cortical areas. Evolutionarily, the size and complexity of the subplate is most prominent in humans as it accommodates the increased connectivity with cortical and subcortical areas relative to non-human primates and rodents (Kostović and Rakić, 1990; Judas et al., 2013). Within humans, the subplate zone is larger in cortical association areas as a consequence of the increased number of axons invading these regions. These incoming axons displace subplate neurons deeper into the white matter, which occurs to a greater degree in these association areas (Duque et al. 2016). Atypicalities at the gray-white matter interface may therefore impact on MRI intensity values, and may explain the regional specificity observed in our pattern of results. Moreover, the regional pattern of GWPC seems to be linked to the functional deficits that are characteristic for ASD. For example, we observed deficits in GWPC in several regions mediating social processing and wider socio-cognitive functioning, including the insula, fusiform gyrus, cingulate cortex, middle temporal gyrus, superior temporal sulcus, and prefrontal cortical regions (see Just et al. 2012 for review). Thus, while future studies are required to establish the functional relevance of our results directly, it is likely that atypical GWPC contributes to the cluster of clinical symptoms typically observed in ASD.

Findings from this and other studies detailing poor delineation of the gray-white boundary in ASD may be taken by some to call into question the accuracy of in vivo MRI measures such as CT that rely on the placement of a discrete boundary between gray and white matter. However, the spatially distributed patterns of group differences in CT we detected did not significantly overlap with the pattern of differences in GWPC (see Supplementary Fig. 1). Also, including individual's global mean CT as a covariate did not significantly alter the pattern of differences in GWPC. Therefore, while we were able to detect subtle differences in tissue contrast in ASD, at the level of spatial resolution neuroimaging techniques currently offer, these do not appear to be large enough to significantly affect estimates of CT within our sample of adults with ASD. This finding is also in agreement with a recent twin study showing that while both GWPC and CT are highly heritable, they have little shared genetic variance (Panizzon et al. 2012). Taken together, these findings suggest that GWPC characterizes additional cortical structural properties that are distinct to CT. Nevertheless, inter-individual differences in the ability to delineate the gray-white matter boundary should be considered in the future when interpreting neuroanatomical features that are based on clearly delineating gray and white matter.

Our study is not without limitations. For instance, we examined neuroanatomical differences associated with ASD in adulthood. This, and the cross-sectional nature of our study,

inherently limits our ability to draw conclusions on the etiological and neurodevelopmental basis of the atypical neural structure we observed. However, within our sample, all but 4 females with ASD met ADI-R criteria for childhood autism. It is therefore likely that the observed pattern of neocortical differences in GWPC may have evolved as a consequence of meeting ASD criteria during early childhood and is therefore causally related to the condition. Further longitudinal studies will, however, be required to disentangle GWPC differences associated with primary neuropathology from atypical neurodevelopmental trajectories or secondary compensatory mechanisms. Recent work has quantified the volume of transient neurodevelopmental zones in the postmortem human fetal brain using MRI as they relate to major neurogenic events (Vasung et al. 2010). Such information provides a reference for studying early prenatal deviations from TD brain growth and could be used in the future to inform in vivo imaging. We are further limited by the current resolution of structural MRI images (1 mm isotropic voxels). At this resolution, it is not possible for us to distinguish between different aspects of cortical cytoarchitecture or accurately delineate particular layers of the cortical sheet as defined by histological staining. Rather, our sampling approach was based on the geometric criteria of projection fraction percentages into the cortical sheet from the white matter surface (Salat et al. 2009). Furthermore, additional research will be required to elucidate the functional relationship between deficits in GWPC and autistic symptoms and traits.

Taken together, our findings suggest that measures of GWPC sampled across cortical layers may serve as an in vivo proxy measure for irregular microstructural organization of the cortex in ASD (and other disorders). Such novel in vivo measures that are indicative of atypical cortical organization might in the future be used to stratify the condition, and/or to examine the neuropathology of ASD in particular genetic subgroups known to be linked to specific neurodevelopmental deficits.

Supplementary Material

Supplementary material are available at *Cerebral Cortex* online.

Funding

The study represents independent research partly funded by the National Institute for Health Research (NIHR) Biomedical Research Centre at South London and Maudsley NHS Foundation Trust and King's College London. The views expressed are those of the authors and not necessarily those of the NHS, the NIHR or the Department of Health. This work was also supported by funding from the Medical Research Council UK [grant number G0400061], the Innovative Medicines Initiative Joint Undertaking [grant number 115300], which includes financial contributions from the EU Seventh Framework Programme (FP7/2007-2013) from the European Federation of Pharmaceutical Industries and Associations companies in kind, and from Autism Speaks.

Notes

We would like to thank all of our participants and their family members for partaking in this study. The Autism Imaging Multicentre Study Consortium, members in alphabetical order are as follows: Anthony J. Bailey (Oxford), Simon Baron-Cohen (Cambridge), Patrick F. Bolton (IoP), Edward T. Bullmore (Cambridge), Sarah Carrington (Oxford), Marco Catani (IoPPN), Bhismadev Chakrabarti (Cambridge), Michael C. Craig (IoPPN), Eileen M. Daly (IoPPN), Sean C.L. Deoni (IoPPN), Christine Ecker (IoPPN), Francesca Happé (IoPPN), Julian Henty (Cambridge), Peter Jezzard (Oxford), Patrick Johnston (IoPPN), Derek K. Jones (IoPPN), Meng-Chuan Lai (Cambridge), Michael V. Lombardo (Cambridge), Anya Madden (IoPPN), Diane Mullins (IoPPN), Codagh M. Murphy (IoPPN), Declan G.M. Murphy (IoPPN), Greg Pasco (Cambridge), Amber N.V. Ruigrok (Cambridge), Susan A. Sadek (Cambridge), Debbie Spain (IoPPN), Rose Stewart (Oxford), John Suckling (Cambridge), Sally J. Wheelwright (Cambridge), Steven C. Williams (IoPPN), and C. Ellie Wilson (IoPPN). The EU-AIMS Consortium. Furthermore, we would like to thank the National Institute for Health Research Biomedical Research Centre for Mental Health, the Dr Mortimer and Theresa Sackler Foundation, and the German Research Foundation (DFG). *Conflict of Interest*: Professor Edward Bullmore is employed half-time by GlaxoSmithKline and holds GSK shares. Dr Meng-Chuan Lai receives financial support from the O'Brien Scholars Program within the Child and Youth Mental Health Collaborative at the Centre for Addiction and Mental Health and The Hospital for Sick Children, Toronto. None of the remaining authors have declared any conflict of interest or financial interests, which may arise from being named as an author on the manuscript.

References

Amaral DG, Schumann CM, Nordahl CW. 2008. Neuroanatomy of autism. Trends Neurosci. 31:137–145.

Andrews M, Andre V, Nguyen S, Salamon N, Cepeda C, Levine MS, Leite JP, Neder L, Vinters HV, Mathern GW. 2005. Human cortical dysplasia and epilepsy: an ontogenetic hypothesis based on volumetric MRI and NeuN neuronal density and size measurements. Cereb cortex. 15:194–210.

Avino TA, Hutsler JJ. 2010. Abnormal cell patterning at the cortical gray-white matter boundary in autism spectrum disorders. Brain Res. 1360:138–146.

Balardin JB, Comfort WE, Daly E, Murphy C, Andrews D, Murphy DG, Ecker C, MRC AIMS Consortium, Sato J. 2015. Decreased centrality of cortical volume covariance networks in autism spectrum disorders. J Psychiatr Res. 69:142–149.

Belmonte MK, Allen G, Beckel-Mitchener A, Boulanger LM, Carper RA, Webb SJ. 2004. Autism and abnormal development of brain connectivity. J Neurosci. 24:9228–9231.

Casanova MF. 2004. Autism as a sequence: from heterochronic germinal cell divisions to abnormalities of cell migration and cortical dysplasias. Med Hypotheses. 63:30–38.

Casanova MF, Buxhoeveden DP, Switala AE, Roy E. 2002. Neuronal density and architecture (gray level index) in the brains of autistic patients. J Child Neurol. 17:515–521.

Casanova MF, van Kooten IA, Switala AE, van Engeland H, Heinsen H, Steinbusch HW, Hof PR, Trippe J, Stone J, Schmitz C. 2006. Minicolumnar abnormalities in autism. Acta Neuropathol. 112:287–303.

Chun JM, Shatz CJ. 1989. Interstitial cells of the adult neocortical white matter are the remnant of the early generated subplate neuron population. J Comp Neurol. 282:555–569.

Courchesne E, Pierce K. 2005. Why the frontal cortex in autism might be talking only to itself: local over-connectivity but long-distance disconnection. Curr Opin Neurobiol. 15:225–230.

Dale AM, Fischl B, Sereno MI. 1999. Cortical surface-based analysis. I. Segmentation and surface reconstruction. Neuroimage. 9:179–194.

Dale AM, Sereno M. 1993. Improved localization of cortical activity by combining EEG and MEG with MRI cortical surface reconstruction: a linear approach. J Cogn Neurosci. 5:162–176.
Deoni SC, Williams SC, Jezzard P, Suckling J, Murphy DG, Jones DK. 2008. Standardized structural magnetic resonance imaging in multicentre studies using quantitative T1 and T2 imaging at 1.5 T. NeuroImage. 40:662–671.
Dupont E, Hanganu IL, Kilb W, Hirsch S, Luhmann HJ. 2006. Rapid developmental switch in the mechanisms driving early cortical columnar networks. Nature. 439:79–83.
Duque A, Krsnik Z, Kostović I, Rakic P. 2016. Secondary expansion of the transient subplate zone in the developing cerebrum of human and nonhuman primates. Proc Natl Acad Sci. 113:9892–9897.
Eastwood SL, Harrison PJ. 2003. Interstitial white matter neurons express less reelin and are abnormally distributed in schizophrenia: towards an integration of molecular and morphologic aspects of the neurodevelopmental hypothesis. Mol Psychiatry. 8 (9):821–831.
Eastwood SL, Harrison PJ. 2005. Interstitial white matter neuron density in the dorsolateral prefrontal cortex and parahippocampal gyrus in schizophrenia. Schizophr Res. 79 (2): 181–188.
Ecker C, Andrews D, Dell'Acqua F, Daly E, Murphy C, Catani M, de Schotten MT, Baron-Cohen S, Lai M, Lombardo M. 2016. Relationship between cortical gyrification, white matter connectivity, and autism spectrum disorder. Cereb Cortex. 26: 225–230.
Ecker C, Bookheimer SY, Murphy DGM. 2015. Neuroimaging in autism spectrum disorder: brain structure and function across the lifespan. Lancet Neurol. 14:1121–1134.
Ecker C, Ginestet C, Feng Y, Johnston P, Lombardo MV, Lai M-C, Suckling J, Palaniyappan L, Daly E, Murphy CM. 2013b. Brain surface anatomy in adults with autism: the relationship between surface area, cortical thickness, and autistic symptoms. JAMA Psychiatry. 70:59–70.
Ecker C, Ronan L, Feng Y, Daly E, Murphy C, Ginestet CE, Brammer M, Fletcher PC, Bullmore ET, Suckling J. 2013a. Intrinsic gray-matter connectivity of the brain in adults with autism spectrum disorder. Proc Natl Acad Sci. 110:13222–13227.
Ecker C, Suckling J, Deoni SC, Lombardo MV, Bullmore ET, Baron-Cohen S, Catani M, Jezzard P, Barnes A, Bailey AJ, Williams SC, Murphy DGM, Consortium MA. 2012. Brain anatomy and its relationship to behavior in adults with autism spectrum disorder. Arch Gen Psychiatry. 69:195–209.
Fischl B, Dale AM. 2000. Measuring the thickness of the human cerebral cortex from magnetic resonance images. Proc Natl Acad Sci. 97:11050–11055.
Fischl B, Sereno MI, Dale AM. 1999. Cortical surface-based analysis. II: inflation, flattening, and a surface-based coordinate system. NeuroImage. 9:195–207.
Ghosh A, Antonini A, McConnell S, Shatz C. 1990. Requirement for subplate neurons in the formation of thalamocortical connections. Nature. 179–182.
Hardan A, Muddasani S, Vemulapalli M, Keshavan M, Minshew N. 2006. An MRI study of increased cortical thickness in autism. Am J Psychiatry. 163:1290–1292.
Hildebrandt M, Pieper T, Winkler P, Kolodziejczyk D, Holthausen H, Blumcke I. 2005. Neuropathological spectrum of cortical dysplasia in children with severe focal epilepsies. Acta Neuropathol. 110 (1):1–11.
Hoerder-Suabedissen A, Oeschger FM, Krishnan ML, Belgard TG, Wang WZ, Lee S, Webber C, Petretto E, Edwards AD, Molnár Z. 2013. Expression profiling of mouse subplate reveals a dynamic gene network and disease association with autism and schizophrenia. Proc Natl Acad Sci. 110:3555–3560.
Huguet G, Ey E, Bourgeron T. 2013. The genetic landscapes of autism spectrum disorders. Annu Rev Genomics Hum Genet. 14:191–213.
Hutsler JJ, Avino T. 2015. The relevance of subplate modifications to connectivity in the cerebral cortex of individuals with autism spectrum disorders. In: Recent advances on the modular organization of the cortex. New York: Springer. p. 201–224.
Hyde KL, Samson F, Evans AC, Mottron L. 2010. Neuroanatomical differences in brain areas implicated in perceptual and other core features of autism revealed by cortical thickness analysis and voxel-based morphometry. Hum Brain Mapp. 31:556–566.
Jovicich J, Czanner S, Greve D, Haley E, van der Kouwe A, Gollub R, Kennedy D, Schmitt F, Brown G, MacFall J. 2006. Reliability in multi-site structural MRI studies: effects of gradient non-linearity correction on phantom and human data. NeuroImage. 30:436–443.
Judas M, Sedmak G, Kostović I. 2013. The significance of the subplate for evolution and developmental plasticity of the human brain. Front Hum Neurosci. 7:423.
Just MA, Keller TA, Malave VL, Kana RK, Varma S. 2012. Autism as a neural systems disorder: a theory of frontal-posterior underconnectivity. Neurosci Biobehav Rev. 36:1292–1313.
Kemper TL. 2010. The neurochemical basis of autism. New York: Springer. p. 69–82.
Kostović I, Rakic P. 1990. Developmental history of the transient subplate zone in the visual and somatosensory cortex of the macaque monkey and human brain. J Comp Neurol. 297 (3): 441–470.
Kostović I, Judaš M, Sedmak G. 2011. Developmental history of the subplate zone, subplate neurons and interstitial white matter neurons: relevance for schizophrenia. Int J Dev Neurosci. 29:193–205.
Lange N, Travers BG, Bigler ED, Prigge MB, Froehlich AL, Nielsen JA, Cariello AN, Zielinski BA, Anderson JS, Fletcher PT, Alexander AA. 2015. Longitudinal volumetric brain changes in autism spectrum disorder ages 6–35 years. Autism Res. 8:82–93.
Lord C, Risi S, Lambrecht L, Cook EH Jr, Leventhal BL, DiLavore PC, Pickles A, Rutter M. 2000. The Autism Diagnostic Observation Schedule—Generic: a standard measure of social and communication deficits associated with the spectrum of autism. J Autism Dev Disord. 30:205–223.
Lord C, Rutter M, Couteur A. 1994. Autism Diagnostic Interview-Revised: a revised version of a diagnostic interview for caregivers of individuals with possible pervasive developmental disorders. J Autism Dev Disord. 24:659–685.
Luhmann HJ, Kilb W, Hanganu-Opatz IL. 2009. Subplate cells: amplifiers of neuronal activity in the developing cerebral cortex. Front Neuroanat.
McConnell SK, Ghosh A, Shatz CJ. 1994. Subplate pioneers and the formation of descending connections from cerebral cortex. J Neurosci. 14:1892–1907.
Nordahl CW, Dierker D, Mostafavi I, Schumann CM, Rivera SM, Amaral DG, Van Essen DC. 2007. Cortical folding abnormalities in autism revealed by surface-based morphometry. J Neurosci. 27:11725–11735.
Panizzon MS, Fennema-Notestine C, Kubarych TS, Chen C-H, Eyler LT, Fischl B, Franz CE, Grant MD, Hamza S, Jak A. 2012. Genetic and environmental influences of white and gray matter signal contrast: a new phenotype for imaging genetics? NeuroImage. 60:1686–1695.

Pinto D, Delaby E, Merico D, Barbosa M, Merikangas A, Klei L, 2014. Convergence of genes and cellular pathways dysregulated in autism spectrum disorders. Am J Hum Genet. 94:677–694.

Rosas H, Liu A, Hersch S, Glessner M, Ferrante R, Salat D, Van Der Kouwe A, Jenkins B, Dale A, Fischl B. 2002. Regional and progressive thinning of the cortical ribbon in Huntington's disease. Neurology. 58:695–701.

Salat DH, Lee SY, Van Der Kouwe A, Greve DN, Fischl B, Rosas HD. 2009. Age-associated alterations in cortical gray and white matter signal intensity and gray to white matter contrast. Neuroimage. 48:21–28.

Schaer M, Ottet M-C, Scariati E, Dukes D, Franchini M, Eliez S, Glaser B. 2013. Decreased frontal gyrification correlates with altered connectivity in children with autism. Front Hum Neurosci. 7:750–179.

Ségonne F, Dale A, Busa E, Glessner M, Salat D, Hahn H, Fischl B. 2004. A hybrid approach to the skull stripping problem in MRI. Neuroimage. 22:1060–1075.

Shatz CJ, Luskin MB. 1986. The relationship between the geniculocortical afferents and their cortical target cells during development of the cat's primary visual cortex. J Neurosci. 6:3655–3668.

Sowell ER, Thompson PM, Leonard CM, Welcome SE, Kan E, Toga AW. 2004. Longitudinal mapping of cortical thickness and brain growth in normal children. J Neurosci. 24:8223–8231.

Vasung L, Lepage C, Radoš M, Fischi-Gómez E, Kanarska S, Huppi P. 2016. Quantitative and qualitative analysis of transient fetal compartments during prenatal human brain development. Front Neuroanat. 10:11.

Wechsler D. 1999. Wechsler abbreviated scale of intelligence. San Antonio (TX): Psychological Corporation.

Wing L. 1997. The autistic spectrum. Lancet. 350:1761–1766.

Worsley K, Andermann M, Koulis T, MacDonald D, Evans A. 1999. Detecting changes in nonisotropic images. Hum Brain Mapp. 8:98–101.

Yang Y, Tung S, Rothwell A, Tiemeier S, Weickert CS. 2011. Increased interstitial white matter neuron density in the dorsolateral prefrontal cortex of people with schizophrenia. Biol Psychiatry. 69:71–70.

Chapter 4: Clinical Testing of Multivariate Pattern Classification Models for Autism Spectrum Disorder

4.1 Introduction

Until recently, the majority of neuroimaging studies in mental health research have used so called mass-univariate methods which examine mean differences in brain measures between groups of individuals. However, these methods are not suited to make predictions for individual cases on the basis of patterns within the data (e.g. to predict group membership or clinical outcome), and thus offer limited translational value for clinical applications. Increasingly, "machine learning" methods such as multivariate pattern classification (MVPC) have been applied to clinical neuroimaging data to discriminate cases from controls. In brief, MVPC algorithms such as the Support Vector Machine (SVM) (Vapnik, 1995) or Gaussian Process Classifier (GPC) (Rasmussen and Williams, 2006) differentiate between two or more classes in the following way: 1) During a 'training phase' the model is initially established using well-defined samples to determine a mathematical criterion of a decision function that best distinguishes between the groups (e.g. ASD and controls). 2) During the 'testing phase', the decision function is applied to predict the class or label of a new test example (e.g. an unseen data point).

Several proof-of-concept studies having shown promise in classifying patients from controls across several psychiatric and neurodevelopmental conditions (Wolfers et al., 2015, Arbabshirani et al., 2016). Within autism spectrum disorder (ASD), volumetric (Ecker et al., 2010b), morphological (Jiao et al., 2010, Ecker et al., 2010a), diffusion (Ingalhalikar et al., 2011, Ingalhalikar et al., 2010), and functional (Just et al., 2014) MRI brain measures have all been applied to discriminate individuals with ASD from typically developing (TD) controls at accuracies significantly above chance within the research setting (for review see Chapter 1.4.1). However, MVPC model performance (e.g. overall classification accuracy) is most often estimated using cross-validation methods within the same sample. To date, only two studies have evaluated ASD classification models on independent data sets acquired in the 'research setting' (Sabuncu and Konukoglu, 2014, Shen et al., 2017). These studies have reported modest overall accuracy in identifying individuals with ASD (59-72%) when

compared to the literature as a whole, which includes reports of several model performances ranging from 80 to upwards of 100% accuracy.

To date no studies have tested classification models for ASD trained in the research environment on independent samples that are representative of the broader clinical population. This is important because several differences exist between research and clinical ASD cohorts. For example, individuals with ASD recruited within the research environment will generally be excluded if they have comorbid conditions, are taking certain medications, or fail to reach cut-offs on behavioural metrics such as the autism diagnostic interview (ADI) and/or autism diagnostic observation schedule (ADOS). In addition, low functioning ASD cases are often not included in imaging research. As such, many individuals who would qualify for a clinical ASD diagnosis would not meet inclusion criteria for research. As a result, the clinical phenotype between individuals with ASD in research and clinical samples is likely to differ to some degree.

Furthermore, proof of concept classification studies report model performance when distinguishing individuals with ASD from typically developing (TD) controls. However, individuals in clinical populations who do not qualify for an ASD diagnosis usually would not be considered TD. Rather individuals who are referred for specialist ASD diagnostic services and found not to have the condition often qualify for a diagnosis of a different but related disorder (e.g. obsessive-compulsive disorder, social anxiety disorder, learning disability etc.) or have a subclinical behavioral presentation that would exclude them from qualifying as a TD control. Taking the above into account, training sets on which classification models are established are not necessarily exchangeable with the testing population of interest (i.e. clinical population).

Thus, this study sought to (1) establish discriminative models for ASD within a research sample of TD controls and ASD adults, and then (2) test the efficacy of these models to identify ASD in an independent sample of individuals who had been referred to a specialist clinical service for ASD diagnosis. Two types of classification algorithms, i.e. the SVM and GPC were examined separately. The SVM and GPC were selected as they have both been successfully applied previously to neuroimaging

based classification problems (Ecker et al. 2010A, Ecker et al. 2010B, Marquand 2010). These methods were applied to several different morphometric measures including volumetric as well as geometric features, which have previously been shown to be atypical in individuals with ASD (Ecker et al., 2010a, Sabuncu and Konukoglu, 2014, Jiao et al., 2010, Andrews et al., 2017). Based on previous reports we hypothesize that measures of cortical morphometry will be able to significantly discriminate ASD individuals from controls at accuracies above chance level within the research setting. However, given the inherent differences between our research training and clinical testing samples and previous findings of classification models showing reduced performance in the range of 10-15% when applied to independent testing sets (Sabuncu and Konukoglu, 2014), we expected a reduction in overall accuracy when predicting ASD diagnosis within the clinical sample.

4.2 Methods

4.2.1 Research Group Participant Demographics

The research cohort included structural MRI data obtained in 27 male right-handed adults with ASD (Ages 18-38, 25±6.3yrs) and 27 matched TD developing controls (Ages 18-42, 28±6.1yrs), that were recruited by advertisement and assessed at the Institute of Psychiatry, Psychology and Neuroscience, London UK. Exclusion criteria included a history of major psychiatric disorder (e.g., psychosis), head injury, genetic disorder associated with autism (e.g., fragile-X syndrome, tuberous sclerosis), or any other medical condition affecting brain function (e.g., epilepsy). We excluded participants on antipsychotic medication, mood stabilizers, or benzodiazepines.

All participants with ASD within the training set were diagnosed according to ICD-10 research criteria. Diagnoses were confirmed using the Autism Diagnostic Interview (ADI-R; (Lord et al., 1994). All cases reached the diagnostic algorithm cutoffs for adults in the three domains of the ADI-R, although failure to reach cutoff in one domain by one point was permitted. Current symptoms were assessed using the Autism Diagnostic Observation Schedule (Lord et al., 2000) but were not used as inclusion criteria. Overall, intellectual ability was assessed using the *Wechsler Abbreviated Scale of Intelligence* (WASI) (Wechsler, 1999). All participants had a full-scale IQ score greater than 75. Group differences in age and full scale IQ were

assessed using a two-tailed independent samples *t*-test. All participants gave informed written consent in accordance with ethics approval by the National Research Ethics Committee, Suffolk, United Kingdom.

Table 4.1. Participant Demographics (Research Sample)

	ASD (*n*=27♂),	TD Controls (*n*=27♂)
Age, years	25 ± 6.3 (18-38)	28 ± 6.1 (18-42)
Full-scale IQ, WASI	106 ± 13.0 (83 - 133)	110 ± 14.0 (77 - 130)
ADI-R social	17 ± 5.8 (9 - 28)	*
ADI-R communication	12 ± 12.4 (8 - 24)	*
ADI-R repetitive behavior	4 ± 1.7 (1 - 8)	*
ADOS social + communication	11 ± 3.6 (7 - 21)	*

***Note*: Values given as Mean ± (Range), TD controls did not undergo ADI or ADOS assessment.**

There were no significant differences between individuals with ASD and TD controls within the training set in terms of age (t=1.703, p=0.095), full-scale IQ (t=.946, p=0.348), or total GM volume (t=.399 , p=0.691).

4.2.2 Clinical Group Demographics

In addition to the participants described above, 62 right handed male individuals who had received referrals for a specialist ASD assessment were recruited from the Autism Assessment and Behavioral Genetics Service at the Bethlem Royal Hospital, South London and Maudsley NHS Foundation Trust. All individuals within this sample were diagnosed according to ICD-10 research criteria. Of the 62 individuals, 14 did not receive an ASD diagnosis, 17 met ICD-10 criteria for ASD but not ADI-R or ADOS cutoffs (i.e. 'clinical' diagnosis for ASD), and 31 met ICD-10 and ADI-R and/or ADOS cutoffs for the condition (i.e. obtained a 'research' diagnosis of ASD). Individuals within this sample were representative of patients assessed in the clinical setting who often present with comorbid conditions. High rates of obsessive compulsive disorder (OCD), attention deficit disorder (ADD), phobias, depression, general and social anxiety disorders were observed across each subgroup within the clinical sample (Figure 4.2).

Table 4.2. Participant Demographics (Clinical Sample)

	No ASD (*n*=14)	Clinical ASD (*n*=17)	Research ASD (*n*=31)
Age, years	34 ± 9.19 (20-45)	27 ± 5.67 (19-36)	29 ± 7.65 (18-44)

Full-scale IQ, WASI	120 ± 12.4 (96 - 136)	115 ± 16.1 (85 - 141)	111 ± 15.2 (83 - 136)
ADI-R social [a]	5 ± 5.3 (0 - 16)	7 ± 3.5 (2 - 13)	13 ± 6.9 (1 - 27)
ADI-R communication [a]	5 ± 3.8 (0 - 11)	6 ± 3.2 (2 - 12)	10 ± 4.6 (2 - 21)
ADI-R repetitive behavior [a]	2 ± 1.5 (0 - 5)	2 ± 1.4 (0 - 4)	4 ± 2.2 (0 - 8)
ADOS social + communication [b]	6 ± 2.4 (3 - 9)	7 ± 2.7 (2 - 12)	12 ± 3.25 (7 - 21)
Percentage with Comorbid Condition	69% (9/13)	71% (12/17)	58% (18/31)

***Note*: Values given as Mean ± (Range). Of the full sample 48 individuals completed ADI-R and 55 completed ADOS. Among the three subgroups ADI-R and ADOS completion numbers were as follows; No ASD ADI-R *n* = 9, ADOS *n*=7; Clinical ASD, ADI-R *n*= 14, ADOS *n*=12; Research ASD, ADI-R *n*=23, ADOS *n*=30.**

Within the clinical sample; individuals who did not receive an ASD diagnosis were significantly older than those with a clinical diagnosis of ASD (t=2.574, p=0.015) but not those with a research diagnosis of ASD (t=1.865, p=0.015). No significant difference in full scale IQ was observed between individuals with no ASD diagnosis and those with a clinical (t=1.017, p=0.318) or research diagnosis of ASD (t=1.930, p=0.060). Furthermore, individuals with clinical and research diagnoses did not significantly differ (p<0.05) in terms of age or FSIQ.

In terms of ASD symptom severity as measured by the ADI-R and ADOS, individuals who received a clinical referral but did not meet ICD-10 criteria for an ASD diagnosis did not show a significant difference in any of the ADI-R subdomains or combined ADOS social and communication scores from individuals who met criteria for a clinical ASD diagnosis but did not reach ADI-R and ADOS cutoffs for a research diagnosis (p<0.05). Those with a research diagnosis showed statistically significant increases across all these measures compared to both the no ASD and clinical ASD groups (p<0.05).

4.2.3 MRI Data Acquisition:

All MRI scanning was conducted at the Institute of Psychiatry, Psychology and Neuroscience, King's College London, UK, using a 3T GE Signa System (General-Electric). A quantitative T_1-mapping sequence (see Chapter 2.4; Deoni et al., 2008) was used to derive synthetic high-resolution structural T_1-weighted inversion-recovery images, with 1 × 1 × 1 mm resolution, a 256 × 256 × 176 matrix, repetition time = 1,800 ms, inversion time = 50 ms, flip angle = 20°, and field-of-view = 25 cm.

4.2.4 Cortical Surface Reconstruction

The FreeSurfer software package (http://freesurfer.net/ ,v5.3.0) was used to derive models of the cortical surface for each T_1-weighted image (see Chapter 2.5). In brief, a single filled white-matter volume was generated for each hemisphere after intensity normalization, the removal of extra cerebral tissue, and image segmentation using a connected components algorithm. A triangular surface tessellation was then generated for each white-matter volume by fitting a deformable template, resulting in a cortical mesh for the white and grey/pial (i.e., outer) surfaces with ~ 150,000 vertices (i.e., points) per hemisphere. Prior to surface reconstruction a radiologist screened scans to exclude participants with clinically significant abnormalities or excessive motion artifacts. A secondary quality check was then performed to identify cortical surface reconstructions of insufficient quality (i.e. with visible reconstruction errors), which were excluded from the analysis and are not described here. Overall the drop out within the training set was equal between groups and was <10% of the total available sample. In order to avoid the introduction a subjective bias no further manual edits were performed.

Each individual's surface reconstructions were used to calculate vertex-wise measures of cortical morphometry, which included *i*) point-wise estimates of cortical volume (VOL), *ii*) cortical thickness (CT), *iii*) pial surface area (SA), *iv*) the local gyrification index (*l*GI), *v*) average convexity/concavity (SULC, i.e. sulcal depth), and *vi*) percent contrast of grey-white matter signal intensity (GWPC), where grey matter intensity was sampled at the grey-white matter boundary (i.e. 0% projection fraction) and contrasted with white matter intensity sampled at 1mm subjacent to the grey-white matter boundary. Further details on the calculation of these measures are provided in Chapter 2.5 (for CT, SA, *l*GI, and SULC) and the methods section of Chapter 3 (for GWPC). Prior to further statistical analyses, each morphometric feature (excluding *l*GI) was smoothed using a 15mm FWHM surface based Gaussian kernel. As *l*GI utilizes cortical SA measures sampled from a 15mm diameter spherical ROI, and is hence an inherently smooth feature, no additional smoothing was applied to measures of *l*GI.

4.2.5 Pattern Classification

Classification of individuals with ASD and TD controls was performed using two

pattern classification algorithms, the support vector machine (SVM) (Vapnik, 1995) and Gaussian process classification (GPC) (Rasmussen and Williams, 2006, Marquand et al., 2010). Whole brain vertex-wise measures of the six morphometric features described above were each used independently of each other as feature sets for classification. Details of SVM and GPC methods are provided in Chapter 2.7. In brief, SVMs operate by identifying a decision boundary (linear or non-linear) known as a hyperplane. The hyperplane separates the experimental classes with a maximum margin. Test cases are then classified as cases or controls depending on which side of the hyperplane they are projected to (Boser et al., 1992). GPC is a Bayesian classification method, which provides probabilistic predictions of class ownership. These predictive class probabilities make GPCs particularly well suited for clinical contexts where the probability of an individual having a particular condition (i.e. psychiatric disorder) is of primary interest. In brief, GPCs can be understood as a distribution over functions, with GP inference consisting of applications of Bayes' rule to find the posterior function distribution that best approximates the training data.

The performance of each SVM and GPC model within the research sample was assessed via leave one out cross validation (LOO-CV). Within each LOO-CV fold, data from all but one individual was used to train the classifier. The resulting pattern recognition model was then tested on the individual who was excluded from the training phase. This process was repeated S times (were S is the total number of subjects). Classification accuracy was then defined as the percentage of subjects correctly assigned to the ASD or control group. For each classification model prediction sensitivity (SE) and specificity (SP) were also calculated (see Chapter 2.7.3). Model significance was then assessed via n=1000 permutations of the class labels to derive a null distribution of model accuracies by which to test significance against.

Following the training phase, the established models that showed the highest overall accuracies within the research training sample were used to predict the class membership of individuals within the independent clinical sample. This sample contained both ASD positive (clinical or research criteria) and ASD negative cases, which for purposes of classification were labeled as analogous to TD controls in the training sample. Within the clinical sample, in addition to overall classification

accuracy, prediction accuracy within the ASD negative, clinical and research ASD subgroups was calculated.

4.2.6 Classification Using Feature Selection

In addition to the models above we retrained each classifier using a general linear model (GLM) based feature selection technique (see Chapter 2.7.4). This method sought to limit vertices used to train models to only those that had a significant mean difference between groups, and thus increase the amplitude of signal in the data with regards to the class labels (i.e. ASD/TD). For each cortical feature the main effect of group was identified by a regression of a GLM using only the training data. Here, we used diagnostic group as a categorical fixed-effects factor and age and full-scale IQ as continuous covariates:

$$Y_i = \beta_0 + \beta_1 Group + \beta_2 Age + \beta_3 FSIQ + \varepsilon_i \quad (3.6)$$

where ε_i is the residual error at vertex i. A nested LOO-CV procedure was then applied to select the p-value used to threshold the vertex-wise statistical maps, such that only vertices with a statistically significant effect of group (β_1) that exceeded this threshold were included as input features for classification.

This nested LOO-CV procedure followed the following steps. *i*) For each LOO-CV fold across the research sample (S) one individual was left out to act as a test case, with the remaining individuals (S-*1)* acting as training data for that fold. *ii*) Within each of these LOO-CV folds a second nested LOO-CV loop was performed within the training data (i.e. S-1) for that particular fold. *iii*) For each of these nested LOO-CV folds another individual was left out and acted as a test case within the nested fold. *iv*) Using only the remaining training data within the nested fold, the above GLM was fit and the statistical maps for the main effect of group (β_1) thresholded separately for a range of p-values (p> 0.4, 0.3, 0.2, 0.1, 0.05, 0.01, 0.001). *v*) Within the same nested training group, classification models were trained for each p-value using only vertices where the effect of group (β_1) exceeded the significance threshold. *vi*) Model accuracy was estimated for each of these classifiers using LOO-CV within the nested loop. *vii*) The p-value threshold that yielded the highest classification accuracy within the nested LOO-CV loop was then selected and applied to the initial left out training

sample (*S*-1). *viii*) Thus, only vertices that showed a main effect of group that exceeded the *p*-value selected through nested LOO-CV to provide the highest overall accuracy were used to train the classifier within the initial training sample (*S*-1) to make a prediction on the initial left out test case.

To apply this procedure within the independent clinical validation data set *i*) the *p*-value threshold that yielded the highest estimated CV accuracy on average across all LOO folds in the research training set was selected. *ii*) This *p*-value threshold was then applied to statistical maps of the main effect of group across the entire research training set. *ii*) Vertices exceeding this statistical threshold were then used to retrain classifiers on the entire research training set. *iv*) These established models were then used to make predictions within the independent clinical data set.

4.3 Results

4.3.1 Classification of ASD and TD individuals in the research sample

Using whole brain vertex wise morphometric measures SVM was not able to classify individuals with ASD from TD controls within the research sample at accuracies above what would be expected statistically by chance (VOL 50% Accuracy [48/52% SE/SP], p=0.56; CT 50% [48/52%], p=0.53; SA 54% [52/56%], p=0.11; *l*GI 41% [37/44%], p=0.88; SULC 56% [56/56%], p=0.44; GWPC 50% [48/52%], p=0.48), Figure 4.1.

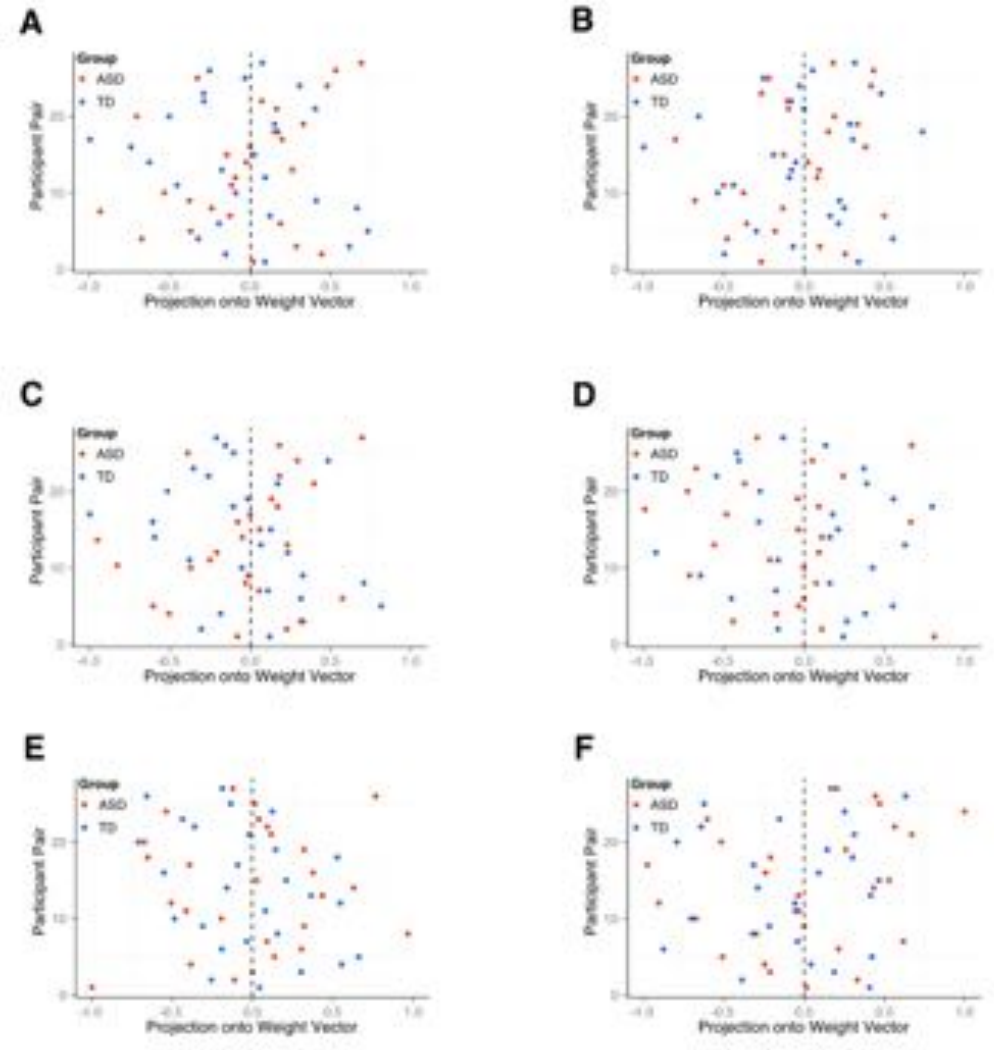

Figure 4.1: Support Vector Machine Predictions Within the Training Set: Class predictions for individuals within the training set derived by leave one out cross validation are shown in scatter plots for each cortical feature. A = cortical volume, B = cortical thickness, C = surface area, D = local gyrification index, E = sulcal depth, D= grey-white matter percent contrast. 'Projection onto Weight Vector' represents unthresholed SVM predictions, normalized between -1 (TD) and 1 (ASD) for visualization.

Similar model performance was achieved using GPC (VOL 52% [52/52%], p=0.41; CT 50% [48/52%], p=0.46; SA 57% [59/56%], p=0.13; *l*GI 41% [33/48%], p=0.81; SULC 52% [48/56%], p=0.33; GWPC 52% [52/52%], p=0.44), Figure 4.2.

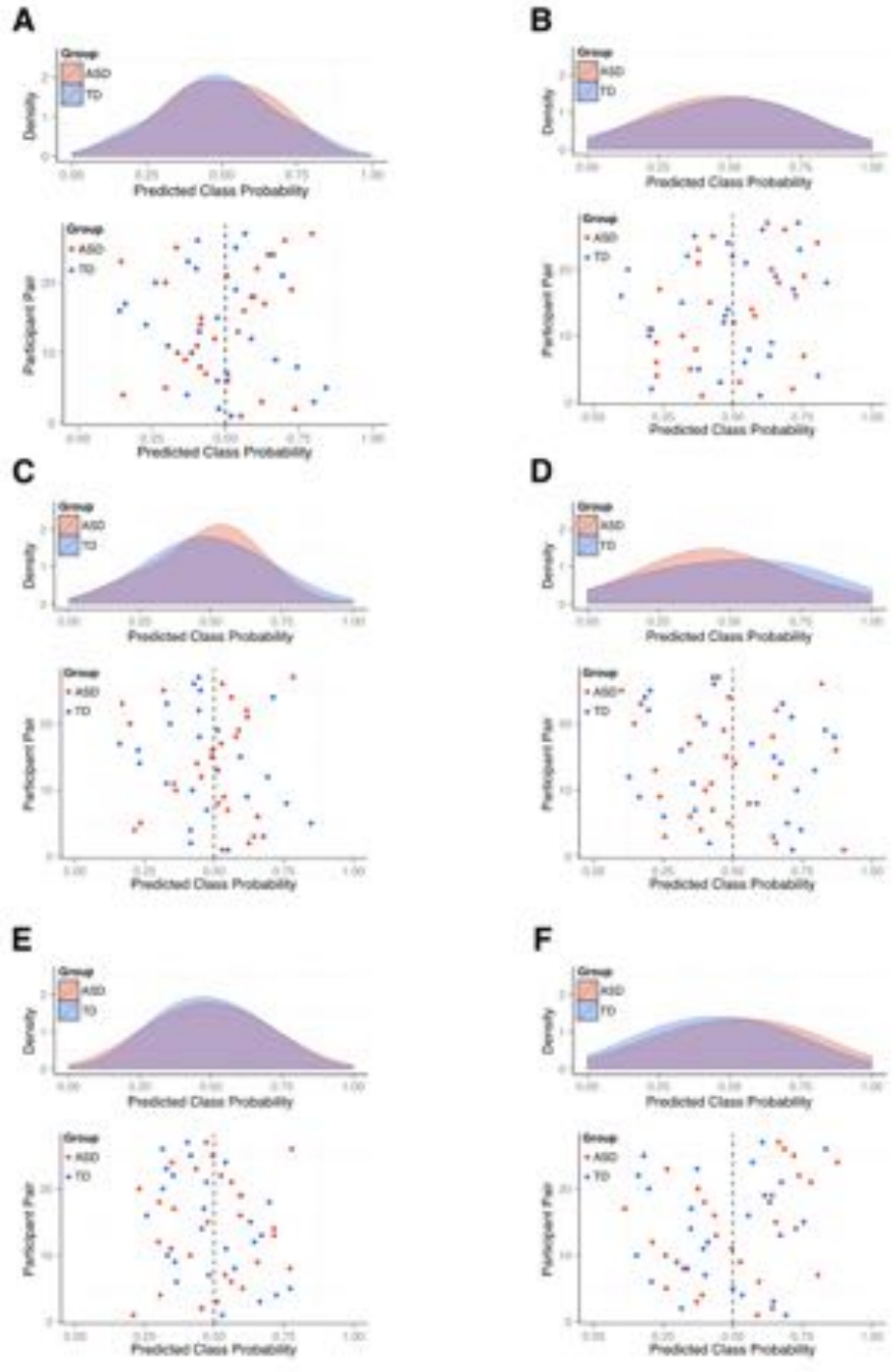

Figure 4.5: Gaussian Process Classification Predictions within the Training Set: Predictive class probabilities for individuals within the training set derived by leave one out cross validation are shown in density and scatter plots for each cortical feature. Predicted class probability >0.5=ASD, <0.5=TD. A = cortical volume, B = cortical thickness, C = surface area, D = local gyrification index, E = sulcal depth, D= grey-white matter percent contrast

When limiting the feature set to include only vertices that showed a significant group difference according to a traditional GLM both SVM (VOL 44% [37/52%]; CT 52% [52/52%]; SA 50% [56/44%]; *l*GI 41% [37/44%]; SULC 61% [67/56%] p=0.345; GWPC 48% [52/44%]; Figure 4.3) and GPC (VOL 50% [48/52%]; CT 54%

[48/59%]; SA 50% [56/44%]; *l*GI 43% [37/48%]; SULC 61% [59/63%], p=0.074; GWPC 56% [56/56%], p=0.197) Figure 4.4) overall classification accuracies remained modest.

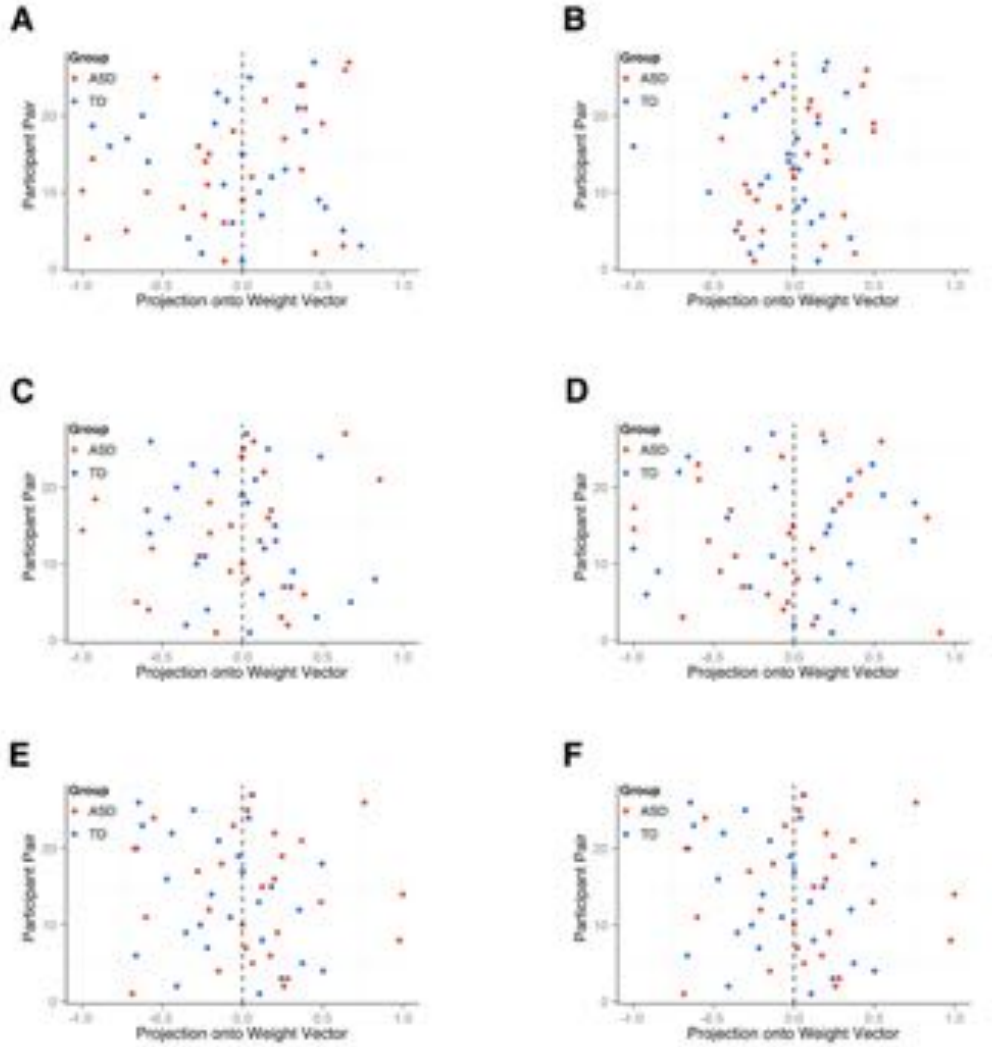

Figure 4.3: Support Vector Machine Predictions within the Training Set using GLM based Feature Selection: Class predictions for individuals within the training set derived by leave one out cross validation are shown in scatter plots for each cortical feature. A = cortical volume, B = cortical thickness, C = surface area, D = local gyrification index, E = sulcal depth, D= grey-white matter percent contrast. 'Projection onto Weight Vector' represents unthresholed SVM predictions, normalized between -1 (TD) and 1 (ASD) for visualization.

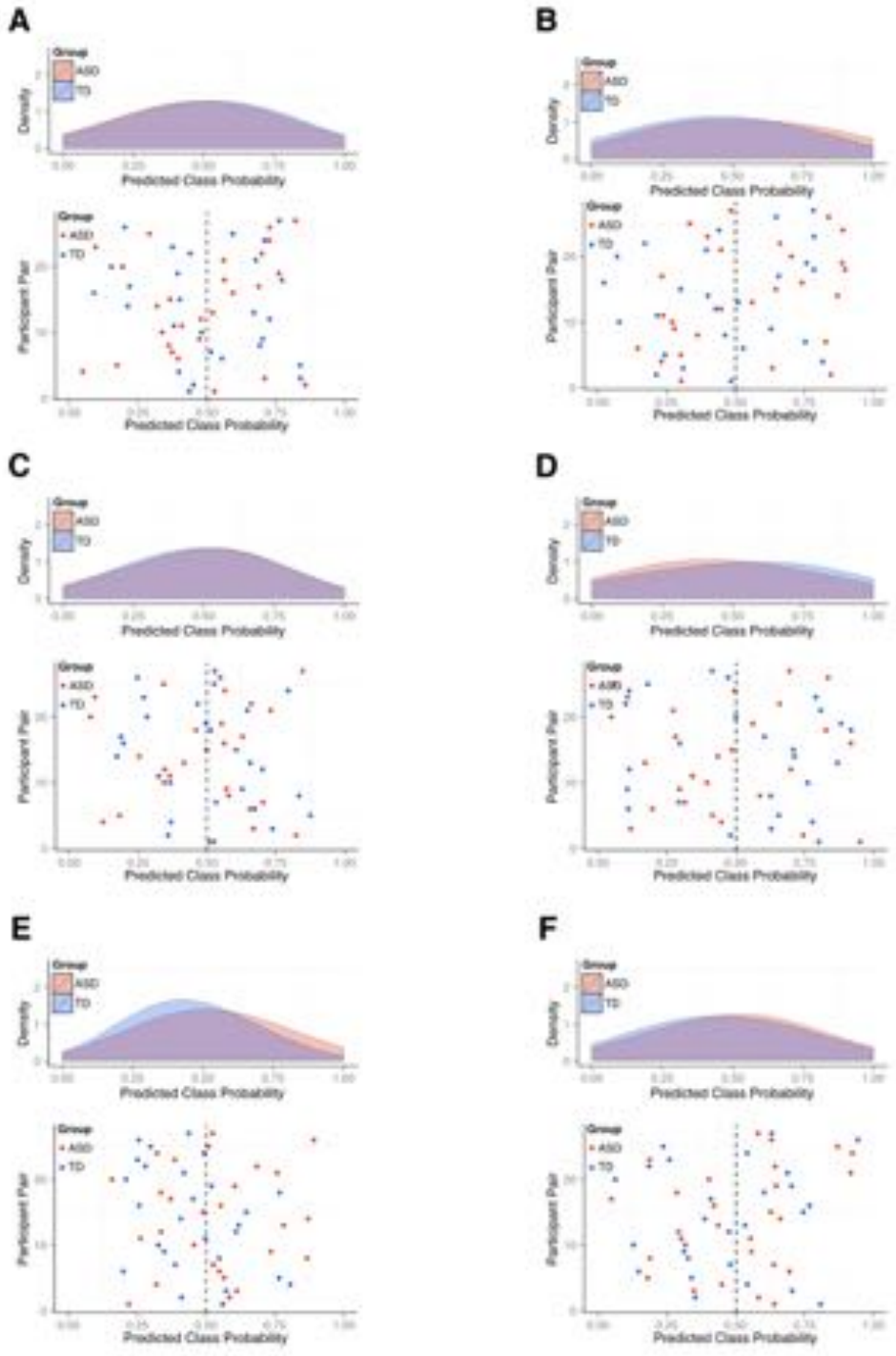

Figure 4.4: Gaussian Process Classification Predictions within the Training Set using GLM based Feature Selection: Predictive class probabilities for individuals within the training set derived by leave one out cross validation are shown in density and scatter plots for each cortical feature. Predicted class probability >0.5=ASD, <0.5=TD. A = cortical volume, B = cortical thickness, C = surface area, D = local gyrification index, E = sulcal depth, D= grey-white matter percent contrast

4.3.2 Predicting ASD Diagnosis within Clinical Sample

The best performing classification models within the research training sample showed relatively modest overall classification accuracy (61%). While this is in line with a previous reports in large ASD cohorts using measures of CT (Sabuncu and Konukoglu, 2014), given the relatively small size of our training sample we were not able to show these results were statistically significant relative to chance. Thus, interpretation these classifiers ability to make predictions within the clinical testing set is made difficult as it is uncertain if this predictive value is reflective of biological differences between the groups. However, as an exploratory step we applied the best performing models (>55% overall accuracy) to make class predictions within the clinical sample.

Across all SVM models, those trained on SULC measures with (61%, p=0.345) and without feature selection (56%, p=0.44) showed the highest classification accuracies within the research training sample. When these models were applied to the clinical sample they showed overall classification accuracies below chance levels with (39%) and without feature selection (39%), Table 4.5. These classifiers performed equally at or below chance level across all patient subgroups including those with no ASD diagnosis, a clinical, or a research diagnosis of ASD, Figure 4.3.

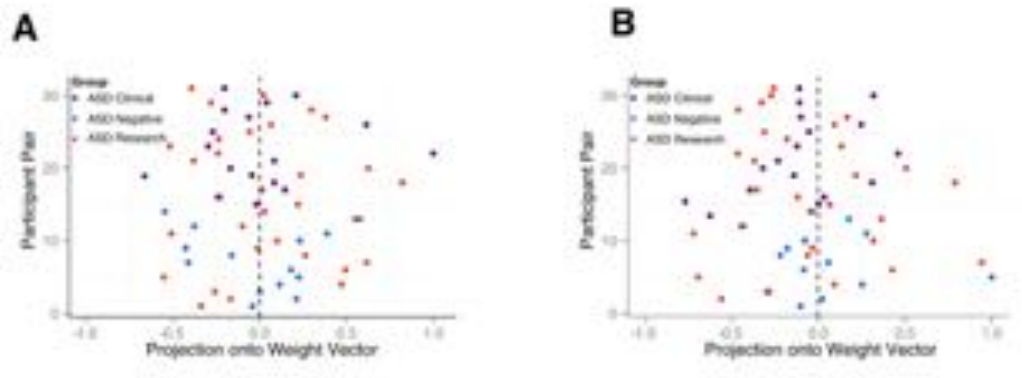

Figure 4.5: Support Vector Machine Predictions within the Testing Set: Class predictions for individuals within the testing set are shown in scatter plots for SVM classifiers trained on vertex wise measures of sulcal depth both with (A) and without (B) GLM based feature selection. 'Projection onto Weight Vector' represents unthresholed SVM predictions, normalized between -1 (TD) and 1 (ASD) for visualization.

Table 4.3 Classification Accuracies within Subgroups of the Clinical Sample

		Classification Accuracy		
Classifier	Overall	No ASD	Clinical ASD	Research ASD
SVM SULC	24/62 (39%)	7/14 (50%)	6/17 (35%)	11/31 (35%)
SVM SULC*	24/62 (39%)	6/14 (43%)	6/17 (35%)	12/31 (39%)
GPC SA	25/62 (40%)	4/14 (29%)	11/17 (65%)	10/31 (32%)
GPC SULC*	26/62 (42%)	7/14 (50%)	6/17 (35%)	13/31 (42%)
GPC GWPC*	50/62 (81%)	12/14 (86%)	15/17 (88%)	23/31 (74%)

Note: **Classification accuracies for models applied to the clinical sample are given as number of correctly labeled / total number of individuals overall and for each subgroup. SVM=Support Vector Machine, GPC=Gaussian Process Classifier, SULC=Sulcal Depth, SA=Surface Area, GWPC=grey:white matter percent contrast. *Classifier used general linear model based feature selection.**

Among GPC models trained within the research sample without GLM based feature selection, measures of SA were found to return the highest overall classification accuracy (57%, p=0.13), but showed below chance levels when applied to the clinical sample (40%), Figure 4.6. Two additional GPC models trained using feature selection on measures of SULC (61%, p=0.074) and GWPC (56%, p=0.197) showed overall classification accuracies above 55% within the research sample. When applied to the clinical sample the model based on measures of SULC showed overall accuracies bellow chance levels (42%), Figure 4.6. Accuracies for these models within the clinical subgroups are given in Table 4.3.

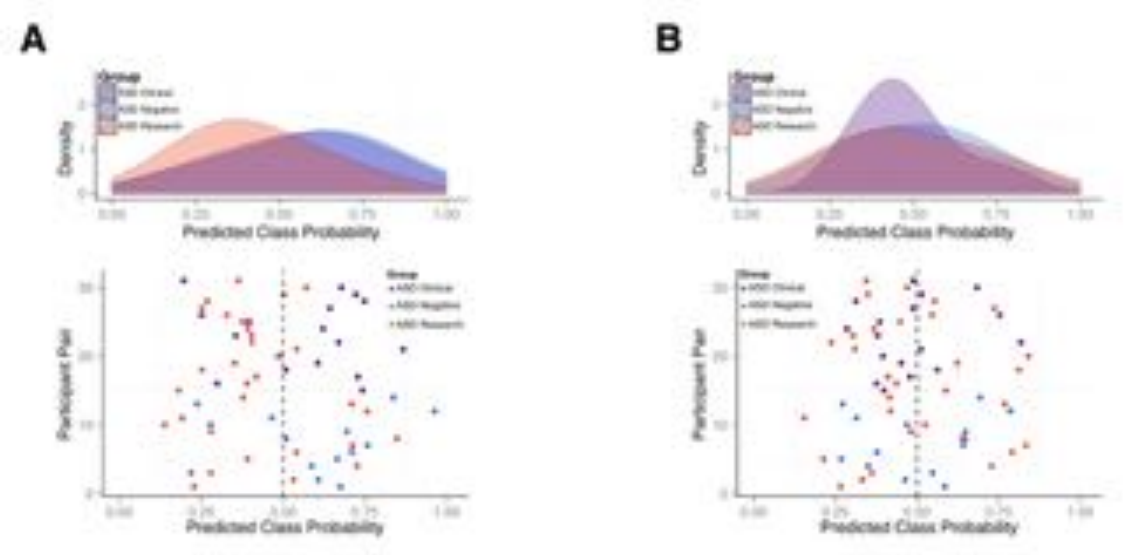

Figure 4.6: Gaussian Process Classification Predictions within the Testing Set: Predictive class probabilities for individuals within the test set are shown in density and scatter plots for the GPC trained on measures of (A) surface area and (B) sulcal depth when using GLM based feature selection (B).

However, the GPC trained on GWPC measures that were restricted to vertices that showed a significant effect of group (p value threshold of 0.05) within the training set showed a high overall accuracy (81%) within the clinical set, across all clinical subgroups (Table 4.3). However, we were unable to show this model performed above chance at a statistically significant level within the training set (57%, p=0.25).

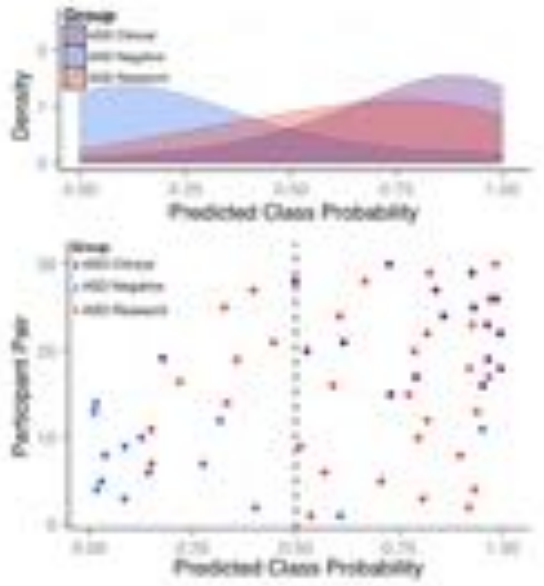

Figure 4.7: Gaussian Process Classification Predictions within the Testing Set using measures of Tissue Contrast and GLM based Feature Selection: Predicted class probabilities for individuals within the test set are shown in density and scatter plots for measures of grey-white matter percent contrast using GLM based feature selection

4.4 Discussion

The first aim of this study was to establish predictive models for ASD based on different morphometric cortical features within a training set of TD controls and individuals with ASD acquired in a research setting. Secondly, this study aimed to test the ability of these classifiers to predict ASD within an independent sample of individuals who had been referred for a clinical ASD diagnostic assessment, thus representing a 'real-world' clinical setting. While previous reports suggest that measures of cortical structure can be used to classify ASD individuals (Ecker et al., 2010a, Wee et al., 2014, Jiao et al., 2010, Hazlett et al., 2017, Sabuncu and Konukoglu, 2014), the current study was not able to replicate these findings in our research training sample. As an exploratory step, we applied the best performing classifiers within the research sample to make predictions as to ASD diagnosis within an independent clinical sample. In this context, one model showed the ability to discriminate individuals with and without ASD diagnoses at high overall accuracy

(81%). However, given this model's performance in the research setting this result must be considered as preliminary and suggestive only.

While a number of classifiers for ASD have been proposed and reported to show significant classification accuracies when discriminating individuals with ASD from TD controls within research settings, we were not able to replicate these results within our sample. A likely key contributor to this is the highly heterogeneous nature of the ASD phenotype. Within a heterogeneous cohort such as the ASD population, maximal classification accuracy based on measures of brain structure is likely to be rather modest. For example, classification studies reporting validation on independent ASD research samples have reported accuracies in the range of 59-72% (Sabuncu and Konukoglu, 2014, Shen et al., 2017). Whilst some of the accuracies we report here are in this range, we were not able to establish the statistical significance of these classifiers due to the small size of our research sample.

When classifiers are trained on relatively small samples (i.e. $n<100$) drawn from a heterogeneous population (e.g. ASD) a high degree of variance in model performance is to be expected. Furthermore, cross validation methods that test a small number of cases for at each fold (i.e. $n=1$) may also increase variance in estimates of model performance. Such variance has been shown across classification studies in heterogeneous psychiatric and neurodevelopmental conditions along with a trend towards decreasing model performance with increasing training sample sizes (Wolfers et al., 2015) (Figure 4.8). Thus, the development of approaches that directly address phenotypic heterogeneity within ASD will be of critical importance for the successful delivery of classification methods that have translational value in clinical settings. Methods that seek to parse heterogeneity based on one particular source of variance (e.g. biological sex) could be of particular benefit and are a major theme in the chapters that follow in this thesis.

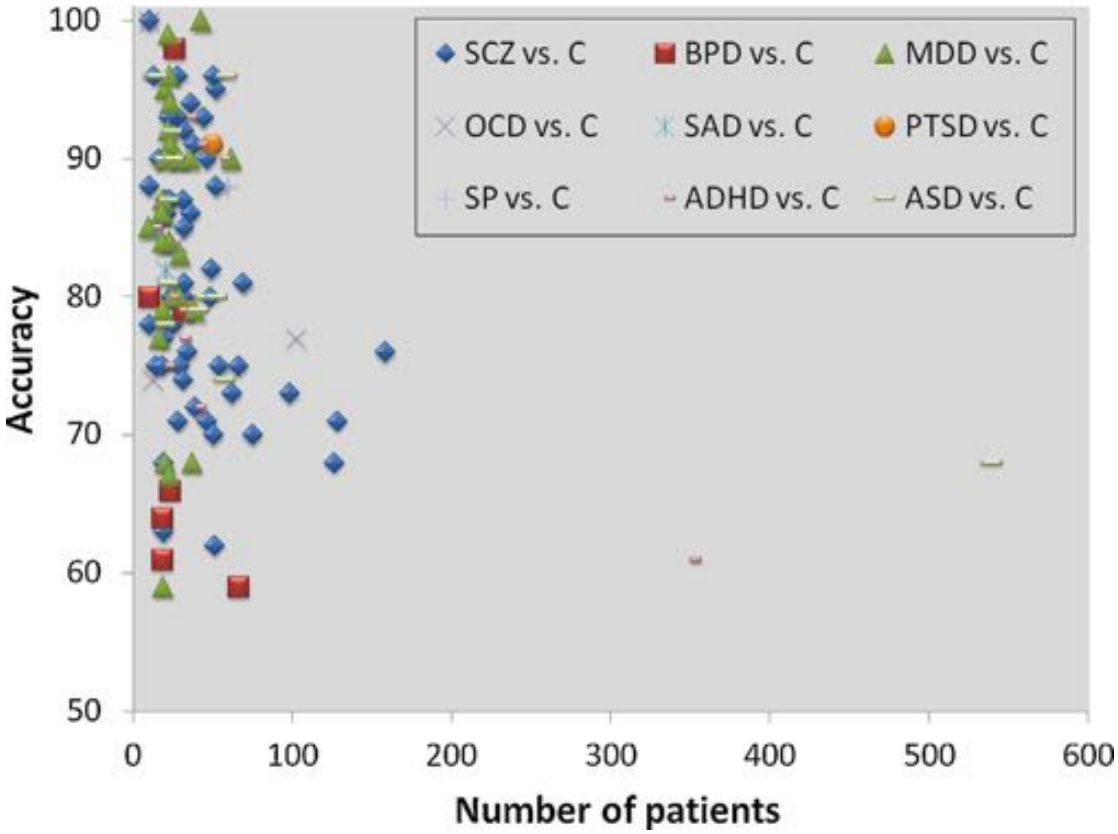

Figure 4.8 Accuracy as a Function of Number of Included Patients in the Classification of Psychiatric and Neurodevelopmental Conditions (Wolfers et al., 2015): This figure shows a plot of classification accuracies for studies based on brain imaging data as a function of the number of patients included in those studies across a variety of heterogeneous psychiatric and neurodevelopmental conditions, including ASD. Two trends are of note, *i*) A high degree of variance in accuracies of studies including less than 100 patients can be observed. *ii*) Classifier performance is also seen to decrease with increasing numbers of patients within each study, which likely is attributable to increased sample heterogeneity. SCZ = schizophrenia; BPD = bipolar disorder; MDD = major depressive disorder; OCD = obsessive compulsive disorder; SAD = social anxiety disorder; PTSD = post-traumatic stress disorder; SP = specific phobia; ADHD = attention-deficit/hyperactivity disorder; ASD = Autism spectrum disorder; C = controls.

When comparing the current results to previous ASD classification studies in small research samples that have reported good model performance (e.g. 70-100% accuracy) it is important to carefully note if and how feature selection has been applied. Broadly speaking, feature selection incorporates a variety of methods used to identify and include only features (e.g. MRI data points) that are informative to the classification problem at hand (Cuingnet et al., 2011, Chu et al., 2012, Mwangi et al., 2014). While feature selection offers a valid way to increase signal within data to allow for better classification between groups, it also introduces the possibility of over fitting one's model to the training set. To avoid over fitting it is essential to perform feature selection in a non-biased fashion such as through a nested LOO-CV framework like was conducted in the current study or to ensure so called 'expert

based' feature selection (e.g. ROI selection) is fixed a-priori. Ultimately, the gold standard test for over fitting is the application of a trained classifier to a completely independent test set. Thus, while previous studies reporting exceptional model performance through applications of feature selection in ASD are valuable for their ability to identify features that can distinguish cases from controls within individual research samples, testing of these models on independent research or clinical samples is required in order to establish their translational ability.

Whilst our trained classifiers did not statistically exceed chance, as an exploratory step we applied our best performing models to predict ASD diagnoses within our independent clinical sample. This is based on the rationale that these classifiers may still have learned useful discriminating information, despite not exceeded chance owing to the small size of the training set. We found the majority of these models showed decreased overall classification performance within the clinical testing set. This result was expected based on previous reports that overall classification accuracy decreases when models are applied to independent samples (Sabuncu and Konukoglu, 2014) and was likely further enhanced by the clinical nature of our testing sample, which introduces differences in both class frequencies (Hahn et al., 2013) and the clinical ASD phenotype between the research and clinical samples.

One noteable exception to the above results was the GPC trained on measures of grey-white matter percent contrast (GWPC) taken at the grey-white matter boundary (Andrews et al. 2017) which showed high overall accuracy within the clinical sample (81%) and across all diagnostic sub-categories (74-88%). This is potentially of interest as this feature was designed with intent to investigate a particular aspect of ASD neuropathology, namely poor definition of the grey-white matter boundary (Avino and Hutsler, 2010) and thus may have increased sensitivity to detect the condition compared too more general measures of cortical morphology. However, interpretation of this finding is limited in light of our inability to show this model performed significantly above chance level within the research sample, or within the clinical sample via LOO-CV. The possibliity of this result being attributed to chance is further increased given the relatively large number of models trained within this study (n=24). If this model was found to identify individuals with ASD in a statistically significant fashion, correction for multiple comparisions would be

critically important before the results could be confidently attributed to a informative biological pattern in the data.

It is important to note that if the above limitations can be addressed and an efficacious imaging biomarker for ASD is developed, the current high cost of MRI scanning makes the use of imaging as a population screening tool for ASD implausible at this time. However, MRI based screenings may still be able to offer benefits to populations at high risk for the condition. For example, within the current study ASD prevalence was found to be 77% among the sample of individuals referred for a clinical ASD assessment. This is important due to the fact that models trained on artificially balanced groups will suffer from high rates of false positives (type I errors) when applied to a general population with prevalence rates in the low single digits, regardless of initial model performance (i.e. high SE and SP). Accordingly, once a classification model has been established it is important to take into account any differences in class frequencies that may exist between training and test groups (Hahn et al., 2013). Taking the above factors into account, if an imaging based biomarker is to be successfully implemented targeting screening within appropriate high-risk populations with elevated ASD prevalence will be as equally as important as the identification of the biomarker in the first place.

4.5 Conclusions

Autism spectrum disorder (ASD) is a highly heterogeneous condition that poses several hurdles in the development of a MRI based biomarker for the condition. While a large body of evidence suggests that ASD is accompanied by changes in brain structure, the current study was not able to replicate previously reported findings that measures of cortical morphometry can identify individuals with ASD with significant accuracy in the research setting. Accordingly, we were not able to test the hypothesis that models trained within the research setting translate to clinical samples. Future classification studies would benefit by recruiting large scale ASD clinical samples that allow for the development of methodologies that directly address issues of heterogeneity in the condition though biological subtyping. This along with the identification of imaging features with increased sensitivity to detect ASD phenotypes should improve upon maximal classification accuracies within the condition.

References

ANDREWS, D. S., AVINO, T. A., GUDBRANDSEN, M., DALY, E., MARQUAND, A., MURPHY, C. M., LAI, M.-C., LOMBARDO, M. V., RUIGROK, A. N. & WILLIAMS, S. C. 2017. In Vivo Evidence of Reduced Integrity of the Gray–White Matter Boundary in Autism Spectrum Disorder. *Cerebral Cortex*.

ARBABSHIRANI, M. R., PLIS, S., SUI, J. & CALHOUN, V. D. 2016. Single subject prediction of brain disorders in neuroimaging: Promises and pitfalls. *NeuroImage*.

AVINO, T. A. & HUTSLER, J. J. 2010. Abnormal cell patterning at the cortical gray–white matter boundary in autism spectrum disorders. *Brain Research,* 1360**,** 138-146.

BOSER, B. E., GUYON, I. M. & VAPNIK, V. N. A training algorithm for optimal margin classifiers. Proceedings of the fifth annual workshop on Computational learning theory, 1992. ACM, 144-152.

CHU, C., HSU, A.-L., CHOU, K.-H., BANDETTINI, P., LIN, C. & INITIATIVE, A. S. D. N. 2012. Does feature selection improve classification accuracy? Impact of sample size and feature selection on classification using anatomical magnetic resonance images. *Neuroimage,* 60**,** 59-70.

CUINGNET, R., GERARDIN, E., TESSIERAS, J., AUZIAS, G., LEHÉRICY, S., HABERT, M.-O., CHUPIN, M., BENALI, H. & COLLIOT, O. 2011. Automatic classification of patients with Alzheimer's disease from structural MRI: A comparison of ten methods using the ADNI database. *NeuroImage,* 56**,** 766-781.

DEONI, S. C., WILLIAMS, S. C., JEZZARD, P., SUCKLING, J., MURPHY, D. G. & JONES, D. K. 2008. Standardized structural magnetic resonance imaging in multicentre studies using quantitative T1 and T2 imaging at 1.5 T. *Neuroimage,* 40**,** 662-671.

ECKER, C., MARQUAND, A., MOURÃO-MIRANDA, J., JOHNSTON, P., DALY, E. M., BRAMMER, M. J., MALTEZOS, S., MURPHY, C. M., ROBERTSON, D. & WILLIAMS, S. C. 2010a. Describing the brain in autism in five dimensions—magnetic resonance imaging-assisted diagnosis of autism spectrum disorder using a multiparameter classification approach. *The Journal of Neuroscience,* 30**,** 10612-10623.

ECKER, C., ROCHA-REGO, V., JOHNSTON, P., MOURAO-MIRANDA, J., MARQUAND, A., DALY, E. M., BRAMMER, M. J., MURPHY, C. & MURPHY, D. G. 2010b. Investigating the predictive value of whole-brain structural MR scans in autism: A pattern classification approach. *NeuroImage,* 49**,** 44-56.

HAHN, T., MARQUAND, A. F., PLICHTA, M. M., EHLIS, A. C., SCHECKLMANN, M. W., DRESLER, T., JARCZOK, T. A., EIRICH, E., LEONHARD, C. & REIF, A. 2013. A novel approach to probabilistic biomarker‐based classification using functional near‐infrared spectroscopy. *Human brain mapping,* 34**,** 1102-1114.

HAZLETT, H. C., GU, H., MUNSELL, B. C., KIM, S. H., STYNER, M., WOLFF, J. J., ELISON, J. T., SWANSON, M. R., ZHU, H. & BOTTERON, K. N. 2017. Early brain development in infants at high risk for autism spectrum disorder. *Nature,* 542**,** 348-351.

INGALHALIKAR, M., KANTERAKIS, S., GUR, R., ROBERTS, T. P. & VERMA, R. 2010. DTI based diagnostic prediction of a disease via pattern classification.

Medical Image Computing and Computer-Assisted Intervention–MICCAI 2010. Springer.
INGALHALIKAR, M., PARKER, D., BLOY, L., ROBERTS, T. P. L. & VERMA, R. 2011. Diffusion based abnormality markers of pathology: Toward learned diagnostic prediction of ASD. *NeuroImage,* 57**,** 918-927.
JIAO, Y., CHEN, R., KE, X., CHU, K., LU, Z. & HERSKOVITS, E. H. 2010. Predictive models of autism spectrum disorder based on brain regional cortical thickness. *Neuroimage,* 50**,** 589-599.
JUST, M. A., CHERKASSKY, V. L., BUCHWEITZ, A., KELLER, T. A. & MITCHELL, T. M. 2014. Identifying autism from neural representations of social interactions: Neurocognitive markers of autism. *PloS one,* 9**,** e113879.
LORD, C., RISI, S., LAMBRECHT, L., COOK JR, E. H., LEVENTHAL, B. L., DILAVORE, P. C., PICKLES, A. & RUTTER, M. 2000. The Autism Diagnostic Observation Schedule—Generic: A standard measure of social and communication deficits associated with the spectrum of autism. *Journal of autism and developmental disorders,* 30**,** 205-223.
LORD, C., RUTTER, M. & COUTEUR, A. 1994. Autism Diagnostic Interview-Revised: a revised version of a diagnostic interview for caregivers of individuals with possible pervasive developmental disorders. *Journal of autism and developmental disorders,* 24**,** 659-685.
MARQUAND, A., HOWARD, M., BRAMMER, M., CHU, C., COEN, S. & MOURÃO-MIRANDA, J. 2010. Quantitative prediction of subjective pain intensity from whole-brain fMRI data using Gaussian processes. *NeuroImage,* 49**,** 2178-2189.
MWANGI, B., TIAN, T. S. & SOARES, J. C. 2014. A review of feature reduction techniques in neuroimaging. *Neuroinformatics,* 12**,** 229-244.
RASMUSSEN, C. E. & WILLIAMS, C. K. I. 2006. *Gaussian processes for machine learning*, MIT press Cambridge, MA.
SABUNCU, M. R. & KONUKOGLU, E. 2014. Clinical Prediction from Structural Brain MRI Scans: A Large-Scale Empirical Study. *Neuroinformatics***,** 1-16.
SHEN, M. D., KIM, S. H., MCKINSTRY, R. C., GU, H., HAZLETT, H. C., NORDAHL, C. W., EMERSON, R. E., SHAW, D., ELISON, J. T., SWANSON, M. R., FONOV, V. S., GERIG, G., DAGER, S. R., BOTTERON, K. N., PATERSON, S., SCHULTZ, R. T., EVANS, A. C., ESTES, A. M., ZWAIGENBAUM, L., STYNER, M. A., AMARAL, D. G. & PIVEN, J. 2017. Increased Extra-axial Cerebrospinal Fluid in High-Risk Infants who Later Develop Autism. *Biological Psychiatry*.
VAPNIK, V. 1995. *The Nature of Statistical Learning Theory,* New York, Springer-Verlag.
WECHSLER, D. 1999. *Wechsler abbreviated scale of intelligence*, Psychological Corporation.
WEE, C. Y., WANG, L., SHI, F., YAP, P. T. & SHEN, D. 2014. Diagnosis of autism spectrum disorders using regional and interregional morphological features. *Human brain mapping,* 35**,** 3414-3430.
WOLFERS, T., BUITELAAR, J. K., BECKMANN, C. F., FRANKE, B. & MARQUAND, A. F. 2015. From estimating activation locality to predicting disorder: A review of pattern recognition for neuroimaging-based psychiatric diagnostics. *Neuroscience & Biobehavioral Reviews,* 57**,** 328-349.

Chapter 5: Association Between the Probability of Autism Spectrum Disorder and Normative Sex-Related Phenotypic Diversity in Brain Structure

Male preponderance is an understudied hallmark of autism spectrum disorder (ASD) and many other neurodevelopmental and psychiatric conditions. While some degree of this male preponderance is likely attributable to sex differences in the ASD phenotype and male biased diagnostic tools, it has been purposed that variance in biology attributable to normative sex differences may modulate ASD risk (Werling, 2016).

The following chapter details a study providing an initial 'proof of concept' for a novel use of multivariate pattern recognition to characterize normative phenotypic diversity associated with biological sex, and how this aspect of neuro-diversity is associated with probability for ASD. This study was recently published in *JAMA Psychiatry* (Ecker, et al 2017) and is included in its final published format in the pages that follow. Contributions to this publication by the current author included significant input on the study concept and design, data analysis and interpretation, and drafting of the manuscript. Supplementary materials for this chapter can be found in Appendix III.

JAMA Psychiatry | Original Investigation

Association Between the Probability of Autism Spectrum Disorder and Normative Sex-Related Phenotypic Diversity in Brain Structure

Christine Ecker, PhD; Derek S. Andrews, MSc; Christina M. Gudbrandsen, MSc; Andre F. Marquand, PhD; Cedric E. Ginestet, PhD; Eileen M. Daly, PhD; Clodagh M. Murphy, PhD; Meng-Chuan Lai, PhD; Michael V. Lombardo, PhD; Amber N. V. Ruigrok, PhD; Edward T. Bullmore, PhD, FRCPsych; John Suckling, PhD; Steven C. R. Williams, PhD; Simon Baron-Cohen, PhD; Michael C. Craig, PhD; Declan G. M. Murphy, FRCPsych; for the Medical Research Council Autism Imaging Multicentre Study (MRC AIMS) Consortium

Editorial page 318

Supplemental content

IMPORTANCE Autism spectrum disorder (ASD) is 2 to 5 times more common in male individuals than in female individuals. While the male preponderant prevalence of ASD might partially be explained by sex differences in clinical symptoms, etiological models suggest that the biological male phenotype carries a higher intrinsic risk for ASD than the female phenotype. To our knowledge, this hypothesis has never been tested directly, and the neurobiological mechanisms that modulate ASD risk in male individuals and female individuals remain elusive.

OBJECTIVES To examine the probability of ASD as a function of normative sex-related phenotypic diversity in brain structure and to identify the patterns of sex-related neuroanatomical variability associated with low or high probability of ASD.

DESIGN, SETTING, AND PARTICIPANTS This study examined a cross-sectional sample of 98 right-handed, high-functioning adults with ASD and 98 matched neurotypical control individuals aged 18 to 42 years. A multivariate probabilistic classification approach was used to develop a predictive model of biological sex based on cortical thickness measures assessed via magnetic resonance imaging in neurotypical controls. This normative model was subsequently applied to individuals with ASD. The study dates were June 2005 to October 2009, and this analysis was conducted between June 2015 and July 2016.

MAIN OUTCOMES AND MEASURES Sample and population ASD probability estimates as a function of normative sex-related diversity in brain structure, as well as neuroanatomical patterns associated with low or high ASD probability in male individuals and female individuals.

RESULTS Among the 98 individuals with ASD, 49 were male and 49 female, with a mean (SD) age of 26.88 (7.18) years. Among the 98 controls, 51 were male and 47 female, with a mean (SD) age of 27.39 (6.44) years. The sample probability of ASD increased significantly with predictive probabilities for the male neuroanatomical brain phenotype. For example, biological female individuals with a more male-typic pattern of brain anatomy were significantly (ie, 3 times) more likely to have ASD than biological female individuals with a characteristically female brain phenotype ($P = .72$ vs $.24$, respectively; $\chi^2_1 = 20.26$; $P < .001$; difference in P values, 0.48; 95% CI, 0.29-0.68). This finding translates to an estimated variability in population prevalence from 0.2% to 1.3%, respectively. Moreover, the patterns of neuroanatomical variability carrying low or high ASD probability were sex specific (eg, in inferior temporal regions, where ASD has different neurobiological underpinnings in male individuals and female individuals).

CONCLUSIONS AND RELEVANCE These findings highlight the need for considering normative sex-related phenotypic diversity when determining an individual's risk for ASD and provide important novel insights into the neurobiological mechanisms mediating sex differences in ASD prevalence.

JAMA Psychiatry. 2017;74(6):329-338. doi:10.1001/jamapsychiatry.2016.3990
Published online February 8, 2017.

Author Affiliations: Author affiliations are listed at the end of this article.

Group Information: The Medical Research Council Autism Imaging Multicentre Study (MRC AIMS) Consortium members are listed at the end of this article.

Corresponding Author: Christine Ecker, PhD, Department of Child and Adolescent Psychiatry, Psychosomatics, and Psychotherapy, Goethe University, Deutschordenstrasse 50, 60528 Frankfurt am Main, Germany (christine.ecker@kgu.de).

Autism spectrum disorder (ASD) is a complex neurodevelopmental condition that is 2 to 5 times more common in male individuals than in female individuals.[1,2] While the male preponderant prevalence of ASD might partially be explained by sex differences in clinical symptoms,[3,4] etiological models suggest that the biological male phenotype itself (ie, in general) carries a higher risk for ASD than the female phenotype.[5] However, despite the growing number of studies examining sex differences in the brain in ASD (eg, those by Lai et al[6] and by Schaer et al[7]), this hypothesis has never been tested directly, to our knowledge, and the neurobiological mechanisms that underpin the male preponderant prevalence of ASD remain elusive.[8]

This study examined the probability of ASD as a function of normative sex-related phenotypic diversity in brain structure. To do so, we initially developed a predictive model of biological sex based on multivariate differences in brain structure in a sample of typically developing (TD) male and female control individuals. This normative model was subsequently applied to male individuals and female individuals with ASD. Unlike recent studies examining sexual dimorphism of the brain (reviewed by Ingalhalikar et al[9]), we used a probabilistic pattern classification approach,[10] which allowed us to accommodate inter-individual phenotypic diversity within and across the binary categories dictated by biological sex.[11] As a result, we were able (1) to examine the probability of ASD along a normative phenotypic axis ranging from the characteristic female to male brain phenotype and (2) to identify the patterns of sex-related neuroanatomical variability associated with low or high probability of ASD.

We based our analysis on measures of cortical thickness (CT) because these measurements have previously been shown to be highly variable between neurotypical male individuals and female individuals[10,11] and tend to be significantly altered in individuals with ASD (eg, as shown by Ecker et al[12] and by Wallace et al[13]). Moreover, measures of CT are less sensitive to global confounders associated with biological sex (eg, differences in total brain volume) than other morphometric features (eg, surface area).[10,14] Last, we investigated whether the cortical underpinnings of ASD are significantly modulated by biological sex and whether ASD has common or distinct neuroanatomical underpinnings in male individuals and female individuals.

Key Points

Question Does the neuroanatomical male brain phenotype carry a higher intrinsic risk for autism spectrum disorder than the female neurophenotype, which could explain the male preponderant prevalence of autism spectrum disorder?

Findings In this case-control study of 98 adults with autism spectrum disorder and 98 matched neurotypical control individuals, the neurobiological male phenotype was associated with a higher risk for autism spectrum disorder than the female phenotype across the binary categories dictated by biological sex.

Meaning In addition to genetic and environmental factors, normative sex-related phenotypic diversity should be considered when determining an individual's risk for autism spectrum disorder.

Methods

Participants

Ninety-eight right-handed adults with ASD (49 male and 49 female; mean [SD] age, 26.88 [7.18] years) and 98 matched neurotypical controls (51 male and 47 female; mean [SD] age, 27.39 [6.44] years) aged 18 to 42 years were recruited locally by advertisement and assessed at the Institute of Psychiatry, Psychology and Neuroscience (IoPPN), London, England, and the Autism Research Centre, Cambridge, England (**Table**). Approximately equal ratios of cases to controls and male individuals to female individuals were recruited within sites (eTable 1 in the Supplement). Exclusion criteria included a history of major psychiatric disorder (eg, psychosis), head injury, ASD-associated genetic disorders (eg, fragile X syndrome and tuberous sclerosis), or any other medical condition affecting brain function (eg, epilepsy). We also excluded individuals taking antipsychotic medication, mood stabilizers, or benzodiazepines.

All participants with ASD were diagnosed according to the *International Statistical Classification of Diseases, Tenth Revision* research criteria. The clinical diagnosis was confirmed using the Autism Diagnostic Interview–Revised (ADI-R)[15] or the Autism Diagnostic Observation Schedule (ADOS).[16] All participants diagnosed with the ADI-R reached algorithm cutoffs in the 3 domains of (1) communication (cutoff of 8), (2) reciprocal social interaction (cutoff of 10), and (3) repetitive behaviors and stereotyped patterns of interest (cutoff of 3), although failure to reach the cutoff in the repetitive domain by maximally 2 points was permitted. Because reliable informants were unavailable, we were unable to obtain ADI-R diagnostic data from 5 female individuals with ASD and confirmed diagnostic status using ADOS cutoffs. In all other participants, the ADOS scores were used to assess the severity of current symptoms. One female individual with ASD fell short by 1 point on the ADI-R communication and repetitive behavior domains but met ADOS criteria. All participants had a full-scale IQ greater than 70 assessed using the Wechsler Abbreviated Scale of Intelligence.[17] Participants gave informed written consent in accord with ethics approval by the National Research Ethics Committee, Suffolk, England. The study dates were June 2005 to October 2009, and this analysis was conducted between June 2015 and July 2016.

Magnetic Resonance Imaging Data Acquisition

Imaging took place at the IoPPN and the Addenbrooke's Hospital, Cambridge, using a 3-T system (Signa; GE Medical Systems). A specialized acquisition protocol using quantitative, T1-weighted mapping was used to ensure standardization of structural magnetic resonance imaging scans across sites,[13,18] which resulted in high-resolution structural T1-weighted inversion recovery images, with 1 × 1 × 1–mm resolution, a 256 × 256 × 176–pixel matrix, repetition time of 1800 milliseconds, inversion time of 50 milliseconds, flip angle of 20°, and field of view of 25 cm.

Cortical Reconstruction Using FreeSurfer

A software program (FreeSurfer, version 5.3.0; http://surfer.nmr.mgh.harvard.edu) was used to derive cortical surface models for each T1-weighted image. These well-validated and fully automated procedures have been extensively described elsewhere.[16,17] All surface models were visually inspected for errors, and scans with visible reconstruction inaccuracies were excluded from the statistical analysis (dropout = 10%). We based our analysis on measures of CT (ie, the closest distance from the gray matter (GM) or white matter boundary to the GM or cerebrospinal fluid boundary at each cerebral vertex).[18] Cortical thickness maps were smoothed with a 15-mm surface-based gaussian kernel.

Gaussian Process Classification

Gaussian process classification (GPC)[19,20] was used for the probabilistic prediction of biological sex based on neuroanatomical variability in CT (details are available in the eMethods in the Supplement). In brief, we initially developed a normative model of biological sex by predicting the binary class labels $y_i \in \{-1, +1\}$ for female and male TD controls, respectively, using CT measures estimated at approximately 320 000 vertices on the cortical surface (Gaussian Processes for Machine Learning Matlab toolbox; http://www.gaussianprocess.org/gpml/code/matlab/doc/). In addition to the overall model accuracy (ie, proportion of biological male individuals or female individuals correctly classified as phenotypic male individuals or female individuals), GPC returned a set of predictive class probabilities indicating the probability of an individual belonging to the male or female category. Class probabilities ranged from 0 to 1 for the characteristic female to male brain phenotype, respectively, so that a class probability of 0.5 represents a binary cutoff separating both classes. Classifier performance was validated by cross-validation and tested for statistical significance via 1000 permutations of class labels. The normative model was subsequently applied to male individuals and female individuals with ASD.

A predictive mapping approach[19] was used to identify (1) the spatially distributed patterns of neuroanatomical variability in CT characteristics for the neurotypical female or male brain phenotype and (2) the set of brain regions associated with low or high probability of ASD. Normative or risk (ie, low or high probability) patterns were derived by quantifying the extent to which the individual's neuroanatomy interacts with the spatial representation of the decision function (ie, the weight vector w separating neurotypical male individuals from female individuals phenotypically (ie, the product of w and CT). The high ASD probability pattern included all male individuals (or female individuals) with a male neuroanatomical phenotype (ie, class probability >0.5). The low ASD probability pattern included all male individuals (or female individuals) with a female neuroanatomical phenotype (ie, class probability <0.5). We also identified these patterns across all individuals along the normative axis of predictive class probabilities. At each vertex, the resulting maps were summarized by the mean value across all individuals within examined groups.

Table. Participant Demographics and Global Brain Measures[a]

Variable	Mean (SD) [Range] ASD (n = 98)	TD Control (n = 98)
Male Individuals (n = 100)		
No.	49	51
Age, y	24.16 (7.20) [18-41]	27.22 (5.58) [18-42]
IQ		
Full-scale WASI	112.61 (12.27) [89-131]	114.67 (10.88) [91-137]
Verbal	110.51 (13.02) [83-137]	110.86 (11.00) [88-137]
Performance	112.00 (11.65) [85-138]	116.74 (10.90) [91-141]
ADI-R		
Social	17.57 (5.56) [10-28]	NA
Communication	13.86 (4.36) [8-24]	NA
Repetitive behavior	4.96 (2.37) [1-10]	NA
ADOS		
Social plus communication	9.43 (4.39) [1-21]	NA
Stereotypic behavior	1.37 (1.27) [0-5][b]	NA
Cortical thickness, mm	2.35 (0.10)	2.33 (0.10)
Volume, L		
Total gray matter	0.76 (0.08)	0.76 (0.07)
Total intracranial	1.58 (0.21)	1.58 (0.17)
Female Individuals (n = 98)		
No.	49	47
Age, y	27.69 (7.37) [18-46]	27.68 (7.31) [18-52]
IQ		
Full-scale WASI	114.88 (12.16) [84-136]	118.38 (7.32) [99-129]
Verbal[c]	116.69 (12.15) [76-144]	117.83 (8.81) [96-135]
Performance[c]	110.56 (14.50) [67-138]	114.38 (8.26) [96-128]
ADI-R		
Social	16.32 (4.24) [10-26]	NA
Communication	12.43 (3.96) [3-22]	NA
Repetitive behavior	4.36 (1.88) [1-9]	NA
ADOS		
Social plus communication	7.73 (5.28) [0-19]	NA
Stereotypic behavior	0.75 (0.97) [0-3][b]	NA
Cortical thickness, mm	2.32 (0.11)	2.38 (0.10)
Volume, L		
Total gray matter	0.67 (0.06)	0.68 (0.06)
Total intracranial	1.32 (0.16)	1.32 (0.17)

Abbreviations: ADI-R, Autism Diagnostic Interview–Revised; ADOS, Autism Diagnostic Observation Schedule; ASD, autism spectrum disorder; NA, not applicable; TD, typically developing; WASI, Wechsler Abbreviated Scale of Intelligence.

[a] There were no significant between-group differences in age, full-scale IQ, mean cortical thickness, total gray matter volume, or total intracranial volume (2-tailed $P > .05$). The ADI-R values were based on 49 male individuals and 49 female individuals with ASD. The ADOS values were based on 49 male individuals and 46 female individuals with ASD.

[b] Statistically significant between-male individuals and female individuals based on 2-tailed $P < .05$ ($t_{94} = 3.21$, $P = .03$).

[c] Verbal and performance IQ data were not available for 1 female individual with ASD.

Estimation of ASD Probability

To examine the probability of ASD as a function of normative phenotypic variability in brain structure, we converted the continuous axis of class probabilities into a set of discrete bins (eg, from 0 to 1 in steps of 0.125). Within each bin, the sample probability of ASD was determined as the ratio of individuals with ASD relative to the total number of individuals per bin. Moreover, these data allowed us to estimate the population prevalence of ASD given that an individual exhibits a male or female neuroanatomical phenotype in addition to being biologically male or female (details are available in the eMethods in the Supplement). In brief, using Bayes theorem, we combined our sample prevalence estimates with previously published population prevalence rates of ASD for biological male individuals and female individuals (ie, 1:42 for male individuals and 1:189 for female individuals[28]). In this way, we were able to estimate the population prevalence of ASD ($D = 1$) given a male (or female) neuroanatomical brain phenotype (M) for biological male individuals (or female individuals) (5), that is $P(D = 1 \mid M, 5)$. Confidence intervals were determined using an exact binomial test implemented in a software package (R Project for Statistical Computing; https://www.r-project.org).

Vertexwise Between-Group Comparison of CT

Vertexwise statistical analysis of CT measures was conducted using the SurfStat Matlab toolbox (SurfStat; http://www.math.mcgill.ca/keith/surfstat). For the comparison between male and female controls, parameter estimates were obtained by regression of a general linear model at each vertex i, with biological sex and center as categorical fixed-effects factors and total GM volume as a continuous covariate. To examine whether the neuroanatomy of ASD is significantly modulated by biological sex, we also included a main effect of diagnostic group and biological sex and a group × sex interaction as follows:

$$y_i = \beta_0 + \beta_1 \text{Group} + \beta_2 \text{Sex} + \beta_3 (\text{Group} \times \text{Sex}) + \beta_4 \text{GM}_{\text{Total}} + \beta_5 \text{Center} + \varepsilon_i$$

where y refers to the variable that is predicted by the model (ie, the CT at voxel i) and ε_i is the residual error. Effects were estimated from the coefficients β_{1-5} normalized by the corresponding standard error. Corrections for multiple comparisons were performed using a random field theory–based cluster analysis for nonisotropic images at a cluster threshold of 2-tailed $P < .05$.[30] We also confirmed our findings using a nonparametric clustering approach (2-tailed $P = .05$) using 10 000 permutations of the original data.[29]

Results

Prediction of Biological Sex Based on Normative Variability in CT

Overall, our CT-driven probabilistic classifier predicted biological sex at an accuracy of 71.4% under cross-validation in neurotypical controls, which was significantly higher than would be expected by chance ($P < .001$ obtained via permutation testing). In total, 68.1% (32 of 47) of all biological female individuals were correctly allocated to the category of phenotypic female individuals and 74.5% (38 of 51) of all biological male individuals to the category of phenotypic male individuals (**Figure 1A**, lower panel). Across individuals, class probabilities ranged continuously from 0 to 1 for the characteristic female to male brain phenotype, respectively (Figure 1A, upper panel). Moreover, the patterns of CT variability associated with the phenotypic shift of the brain from a female to male presentation resembled the set of brain regions where female individuals significantly differed from male individuals (eFigure 1 and eFigure 2 in the Supplement). Therefore, while a perfect phenotypic differentiation between biological sexes could not be achieved, we were able to separate male individuals from female individuals in most cases based on multivariate differences in brain structure.

Phenotypic Prediction of Biological Sex for Individuals With ASD

When applying our normative predictive model of biological sex to the independent sample of individuals with ASD, we found that, in female individuals with ASD, predictive class probabilities for the male neuroanatomical brain phenotype were significantly increased relative to female controls ($t_{94} = 6.13$; $P < .001$) (Figure 1B). Overall, 30 of 49 female individuals (79.6%) with ASD were allocated to the category of phenotypic male individuals, which was significantly more frequent than expected based on the typical rate of misclassification for female controls (79.6% [39 of 49] vs 41.9% [15 of 47], respectively; $\chi^2_1 = 20.26$, $P < .001$). No such differences were observed in male individuals with ASD, who were correctly allocated to the male category in 80.6% (46 of 49) of all cases and also did not differ significantly from male controls in predictive class probabilities ($t_{96} = 1.35$, 2-tailed $P > .17$). Therefore, when representing individuals along a single axis of normative sex-related phenotypic diversity in brain structure, female individuals with ASD displayed a CT pattern that resembled more closely the neurotypical male rather than female neurophenotype. This phenotypic shift to female individuals is likely to influence the probability of ASD.

ASD Probability as a Function of Normative Sex-Related Phenotypic Variability in Brain Structure

In female individuals with ASD, the sample probability of ASD increased with increasing predictive probabilities for the male neuroanatomical brain phenotype (eFigure 3A in the Supplement). More specifically, female individuals with class probabilities exceeding the binary sex cutoff of 0.5 (ie, biological female individuals falling into the category of phenotypic male individuals) were significantly (ie, 3 times) more likely to have a diagnosis of ASD than biological female individuals with a class probability lower than 0.5 ($P = .22$ vs $.24$, respectively; $\chi^2_1 = 20.26$; $P < .001$; difference in P values, 0.48; 95% CI, 0.29-0.68). Reciprocally, male individuals with class probabilities lower than 0.5 (ie, biological male individuals falling into the category of phenotypic female individuals) were 1.2 times less likely to have ASD than male individuals allocated to the category of phenotypic male individuals ($P = .41$ vs $.51$, respec-

Figure 1. Gaussian Process Classification of Biological Sex

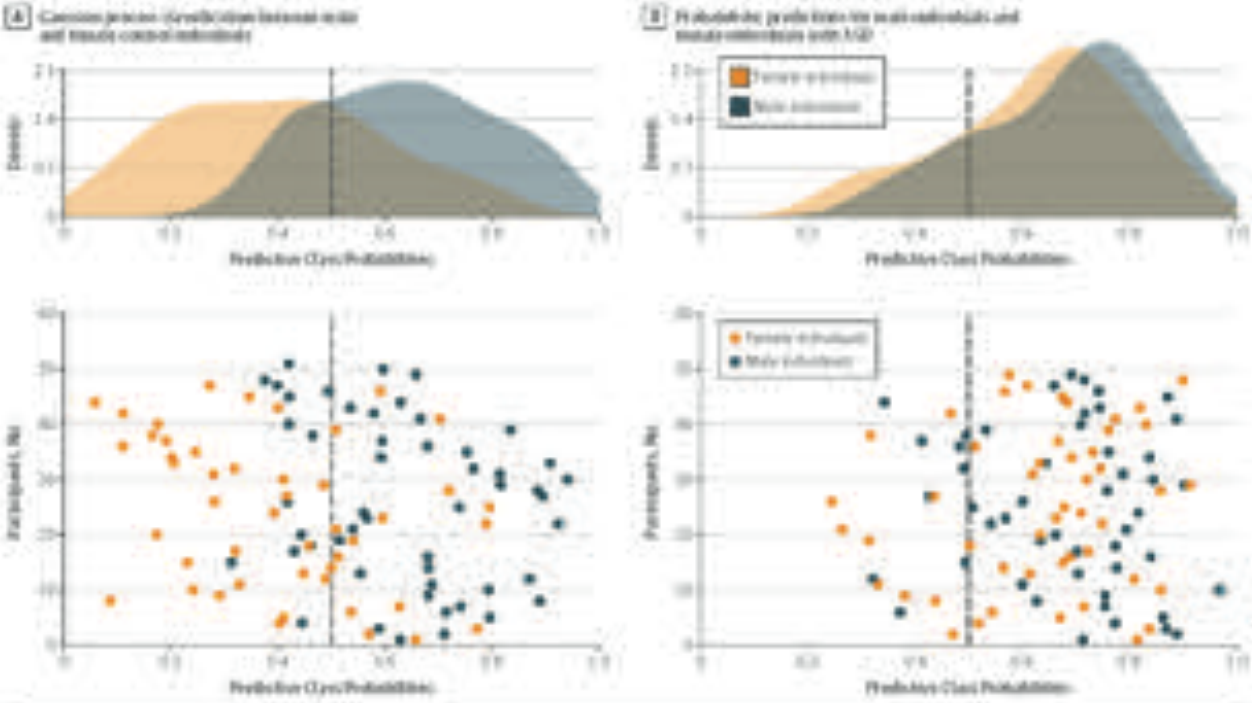

A, Gaussian process classification between male and female typically developing (TD) control individuals based on normative (ie, neurotypical) variability in cortical thickness. The x-axis indicates pseudo-class probabilities. Therefore, a class probability of 0.5 served as a binary cutoff separating male individuals from female individuals. The y-axis indicates the position of each individual on the normative axis of sex-related phenotypic diversity in brain structure (lower panel). The upper panel shows the density (ie, frequency) of male individuals and female individuals along the normative axis of class probabilities. B, Probabilistic pseudo-scores for male individuals and female individuals with autism spectrum disorder (ASD) using the normative model for biological sex. The density functions for male individuals and female individuals with ASD (upper panel) show the phenotypic shift of the brain in female individuals with ASD toward a more male phenotypic presentation. Of 93 female individuals with ASD, 36/51(70%) fell within the category of phenotypic male individuals (lower panel).

tively; $\chi^2_1 = 0.38$; $P > .53$; difference in P values, −0.10; 95% CI, −0.36 to 0.15) (eFigure 3B in the Supplement). If one combines these sample probabilities with previously published prevalence rates of ASD in the general population (eg, 1:42 for male individuals and 1:189 for female individuals[29]), our study shows that biological female individuals with male neuroanatomical features were 6.5 times more likely to have ASD than biological female individuals with a characteristically female neuroanatomy, which translates to an estimated variability in population prevalence between 0.2% to 1.3%, respectively (eTable 2 in the Supplement). Therefore, normative sex-related phenotypic diversity in brain structure significantly affected the probability of ASD in addition to biological sex alone, with male neuroanatomical characteristics carrying a higher intrinsic risk for ASD than female characteristics.

The particular patterns of neuroanatomical variability associated with low or high ASD probability differed between men and women in sign and regional composition (**Figure 2** and eTable 3 and eFigure 4 in the Supplement). For example, CT variability in the left and right inferior temporal lobe differentiated between low or high risk in women but not in men ($t_{max} = 3.78$, cluster $P = 6.39 \times 10^{-6}$ for the left; $t_{max} = 3.42$, cluster $P = 1.00 \times 10^{-3}$ for the right). Therefore, while it is possible to link the probability of ASD to particular patterns of neuroanatomical variability in CT, our findings suggest that these patterns are not specific.

Biological Sex Significantly Modulates the Cortical Anatomy of ASD

Last, using a conventional general linear model, we tested for significant CT differences between men and women with ASD and group × sex interactions. We found that the cortical neuroanatomy of ASD was significantly modulated by biological sex, particularly in the bilateral parahippocampal and entorhinal cortex (Brodmann area [BA] 28/34), the fusiform and lingual gyrus (BA 30/37/19), and the inferior or middle temporal lobe (BA 21/22) (**Figure 3** and eTable 4 and eFigure 5 in the Supplement). In these regions, the degree of cortical abnormality in female individuals significantly exceeded the degree of abnormality observed in male individuals compared with their respective normative populations ($t = 3.29$, cluster $P = 3.5 \times 10^{-6}$ for the left; $t = 3.43$, cluster $P = 5.40 \times 10^{-4}$ for the right) (Figure 3B and C and eFigure 6 in the Supplement). However, female individuals with ASD were not more significantly impaired than male individuals in clinical symptom severity (eTable 5 in the

Figure 2. Neuroanatomical Pathways Associated With Low and High Autism Spectrum Disorder (ASD) Probability

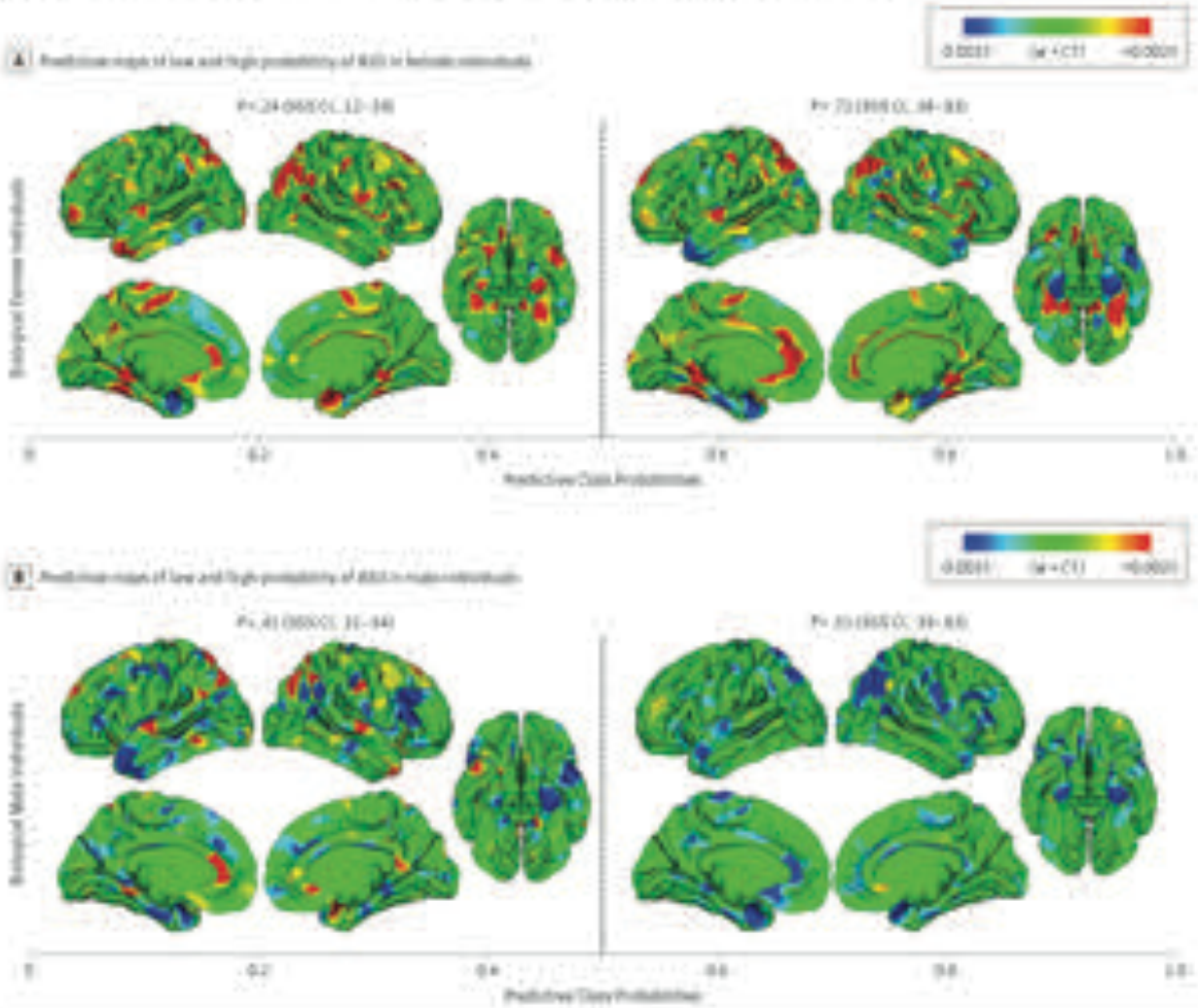

Predictive maps (ie, $w' \times CT$) associated with low and high probability of ASD in female individuals (A) and male individuals (B). Low ASD probability maps were computed across all male individuals (or female individuals) with predictive probabilities lower than 0.5 (ie, biological male individuals or female individuals falling into the category of phenotypic female individuals). High ASD probability maps were computed across all male individuals (or female individuals) with predictive probabilities larger than 0.5 (ie, biological male individuals or female individuals falling into the category of phenotypic male individuals). At each vertex, the color scale thus indicates the product of the weight vector w and cortical thickness (CT), averaged across all individuals within the A probability groups. The probability of ASD was determined as the number of male individuals (or female individuals) with ASD relative to the total number of individuals within predictive probability bins.

Supplement). The clusters with significant group × sex interactions also remained significant when controlling for variability in verbal and performance IQ (eTable 5 and eFigure 7 in the Supplement) and thus do not seem to reflect a simple functional difference in these clinical or neurocognitive measures (further details are available in eFigure 8 and the eAppendix in the Supplement).

Discussion

Our study demonstrates that normative sex-related phenotypic diversity in brain structure affects the prevalence of ASD in addition to biological sex alone, with male neuroanatomical characteristics carrying a higher intrinsic risk for ASD than female characteristics. This increase in risk was predominantly driven by female individuals with ASD, who displayed a pattern of neuroanatomical variability in CT that resembled more closely the neurotypical male rather than female neurophenotype overall. Moreover, our study links low and high risk (ie, probability) of ASD to particular patterns of sex-related neuroanatomical variability, thus providing important novel insights into the neurobiological mechanisms underpinning the male preponderant prevalence of ASD.

An important feature of GPC is that it is possible to summarize the highly complex and multivariate pattern of normative sex-related phenotypic diversity in brain struc-

Figure 3. Signific and Group × Sex Interactions

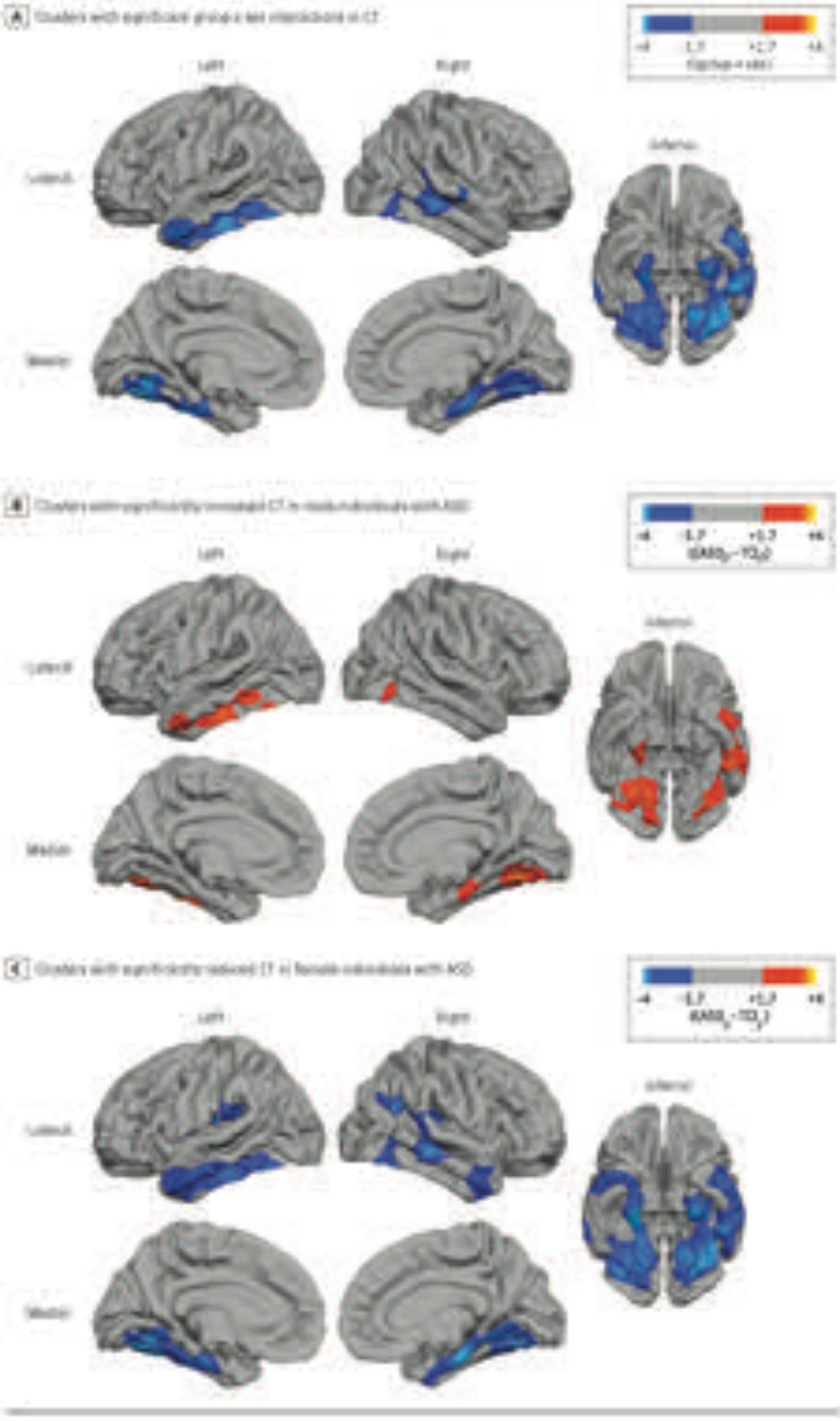

A, Clusters with significant group × sex interactions on cortical thickness (CT) as examined by a conventional general linear model–type approach. In these regions, the difference in CT between female individuals with autism spectrum disorder (ASD) and female control individuals significantly exceeded the difference between male individuals with ASD and male controls (statistical details are available in eTable 4 in the Supplement). The group × sex interactions were driven by reduced CT in female individuals with ASD relative to female controls and increased CT in male individuals with ASD relative to male controls (eFigure 6 in the Supplement). B, Clusters with significantly increased CT in male individuals with ASD relative to male controls (random field theory–based, cluster-corrected $P < .05$). C, Clusters with significantly reduced CT in female individuals with ASD relative to female controls (random field theory–based, cluster-corrected $P < .05$). eFigure 5 in the Supplement shows results of the permutation-based cluster thresholding of the same contrasts. TD indicates typically developing.

ture-to-a single measure (ie, class probability) indicative of the individual's neurophenotypic sex. This ability sets our approach apart from existing studies (eg, those by Ruigrok et al[7] and by Bao and Lai et al[10]) examining sexual dimorphism of the brain based on univariate group differences between male individuals and female individuals, which precludes the inves-

tigation of interindividual phenotypic diversity across the binary categories dictated by biological sex. This study is of importance because it has recently been suggested that, on a phenotypic scale, the brain should be considered a "mosaic" of regions, each of relative maleness or femaleness, resulting in significant interindividual variability both within and between sexes.[15,75] Therefore, the multivariate patterns derived from the classification between neurotypical male and female controls may be interpreted as being representative of such a mosaic, which drives the brain toward a female or male phenotypic end point overall (see also the study by Chekroud et al[76]).

Furthermore, we demonstrated that the normative pattern of sex-related neuroanatomical variability is predictive of ASD probability, particularly in female individuals, and that low and high ASD probability can be linked to regional differences in CT. These patterns not only included many of the brain regions where women typically differ from men in CT[17,21] but also highlighted brain areas that have previously been linked to the core behavioral deficits characteristic of ASD (reviewed by Amaral et al[12] and by Eyler et al[10]). Notably, some of these brain regions (eg, inferior temporal lobes) carried low or high probability of ASD in women but not in men. Herein, we found that the degree of cortical abnormality in female individuals with ASD significantly exceeded the degree of abnormality in male individuals compared with their respective normative population. Yet, female individuals with ASD were not more severely impaired than male individuals on the level of autistic symptoms. Therefore, our finding agrees with previous reports suggesting that (1) biological sex significantly modulates the neurobiological basis of ASD (eg, the studies by Lai et al[8] and by Schaer et al[9]) and (2) female individuals may have a higher threshold (ie, minimum liability sufficient to cause ASD) for reaching affection status than male individuals (reviewed by Werling and Geschwind[77]) and may need to deviate more neurobiologically from their normative population to demonstrate a clinical ASD phenotype.

Limitations

While our approach holds promise for future investigations into the neurobiological mechanisms that underpin risk and resilience for conditions with a sex difference in prevalence, this study has several limitations. First, our study was designed to establish the statistical association between normative sex-related phenotypic diversity and ASD probability. Therefore, future studies are needed to examine the causal mechanisms for this association (eg, as shown by Lai et al[8] and Baron-Cohen et al[78]). Second, because of reasons outlined above, we based our study on measures of CT in a sample of high-functioning adults with ASD. While this scope is sufficient to provide proof of concept, it will be necessary in the future to extend our approach to other neurobiological features that have previously been linked to ASD (eg, cortical surface area and regional volumes[79]) and to replicate our findings in other subgroups on the autism spectrum (eg, different age groups and individuals with learning disabilities). Third, in future research, it will be crucial to further explore the functional relevance of our findings and to examine how normative sex-related phenotypic diversity in brain structure relates to sex differences in general cognitive or behavioral profiles (eg, as shown by Miller and Halpern[80] and by Hyde[81]) and to different clinical ASD phenotypes.[3,82-84]

Conclusions

Our findings suggest that the neurobiological male phenotype carries a higher intrinsic risk for ASD than the female phenotype across the binary categories dictated by biological sex. In addition to genetic and environmental factors, normative sex-related phenotypic diversity should thus be taken into account when determining an individual's probability of ASD. Therefore, our approach to modeling normative sex-related phenotypic diversity may be more widely used in the future to elucidate the neurobiological mechanisms that underpin risk and resilience for mental health disorders.

ARTICLE INFORMATION

Accepted for Publication: November 10, 2016.

Published Online: February 8, 2017. doi:10.1001/jamapsychiatry.2016.3959

Author Affiliations: Department of Child and Adolescent Psychiatry, Psychosomatics, and Psychotherapy, Goethe University Frankfurt am Main, Germany (Ecker); Department of Forensic and Neurodevelopmental Sciences, Sackler Institute for Translational Neurodevelopmental Sciences, Institute of Psychiatry, Psychology and Neuroscience, King's College London, London, England (Ecker, Andrews, Gudbrandsen, Daly, C. M. Murphy, Craig, D. G. M. Murphy); Donders Institute for Brain, Cognition and Behaviour, Radboud University, Nijmegen, the Netherlands (Marquand); Centre for Neuroimaging Sciences, Institute of Psychiatry, Psychology and Neuroscience, King's College London, London, England (Marquand, Williams); Department of Biostatistics and Health Informatics, Institute of Psychiatry, Psychology and Neuroscience, King's College London, London, England (Lukito); Behavioural Genetics Clinic, Adult Autism Service, Behavioural and Developmental Psychiatry Clinical Academic Group, South London and Maudsley Foundation National Health Service Trust, London, England (C. M. Murphy, D. G. M. Murphy); Autism Research Centre, Department of Psychiatry, University of Cambridge, Cambridge, England (Lai, Lombardo, Ruigrok, Baron-Cohen); Child and Youth Mental Health Collaborative at the Centre for Addiction and Mental Health, The Hospital for Sick Children, Department of Psychiatry, University of Toronto, Toronto, Ontario, Canada (Lai); Department of Psychiatry, National Taiwan University Hospital and College of Medicine, Taipei (Lai); Department of Psychology and Centre for Applied Neuroscience, University of Cyprus, Nicosia (Lombardo); Brain Mapping Unit, Department of Psychiatry, University of Cambridge, Cambridge, England (Suckling); National Autism Unit, Bethlem Royal Hospital, South London and Maudsley Foundation National Health Service Trust, London, England (Craig).

Author Contributions: Dr Ecker had full access to all the data in the study and takes responsibility for the integrity of the data and the accuracy of the data analysis. Drs Craig and D. G. M. Murphy contributed equally to this article.

Study concept and design: Ecker, Andrews, Marquand, C. M. Murphy, Lai, Bullmore, Williams, Baron-Cohen, Craig, D. G. M. Murphy.

Acquisition, analysis, or interpretation of data: Ecker, Andrews, Gudbrandsen, Marquand, Ginestet, Daly, C. M. Murphy, Lai, Lombardo, Ruigrok, Suckling, Williams, Craig, D. G. M. Murphy.

Drafting of the manuscript: Ecker, Andrews, Ginestet, Daly, Lai, Lombardo, Suckling, Williams, Craig, D. G. M. Murphy.

Critical revision of the manuscript for important intellectual content: Ecker, Gudbrandsen, Marquand, Ginestet, C. M. Murphy, Lai, Ruigrok, Bullmore, Williams, Baron-Cohen, Craig, D. G. M. Murphy.

Statistical analysis: Ecker, Andrews, Marquand, Greenhut, Daly, Lai, Suckling, D. G. M. Murphy, Obsessions/Funding: Baron-Cohen, D. G. M. Murphy. Administrative, technical, or material support: Goldenfeld, C. M. Murphy, Lombardo, Bolton, Williams, Craig, D. G. M. Murphy. Study supervision: Williams, Baron-Cohen, Craig, D. G. M. Murphy.

Conflict of Interest Disclosures: Dr Bolton reported being employed half-time by GlaxoSmithKline and reported being a stockholder of GlaxoSmithKline shares. No other disclosures were reported.

Funding/Support: This work was supported by the AIMS-2-TRIALS Multicentre Study Consortium, funded by Medical Research Council United Kingdom grant G0800302, and by the European Union Autism Imaging Multicentre Study Consortium, supported by the Innovative Medicines Initiative Joint Undertaking under grant nos. 115300, which includes financial contributions from the European Union Seventh Framework Programme (FP7/2007-2013), the European Federation of Pharmaceutical Industries and Associations companies in kind, and Autism Speaks. Dr Ecker acknowledges support by grants EC488/1-1 and EC488/2-1 from the German Research Foundation under the Heisenberg Programme. Dr Marquand acknowledges support by grant 016.135.006 from the Netherlands Institute for Scientific Research under the Gravitation Programme. Dr Lai acknowledges support from the William Binks Autism Neuroscience Fellowship, Cambridge, England, and the Olitzon Scholars Program within the Child and Youth Mental Health Collaborative at the Centre for Addiction and Mental Health and The Hospital for Sick Children, Toronto, Ontario, Canada. Drs Suckling and Baron-Cohen acknowledge support from the Autism Research Trust.

Role of the Funder/Sponsor: The funding sources had no role in the design and conduct of the study; collection, management, analysis, and interpretation of the data; preparation, review, or approval of the manuscript; and decision to submit the manuscript for publication.

Group Information: The Medical Research Council Autism Imaging Multicentre Study (MRC AIMS) Consortium members were (in alphabetical order) Anthony J. Bailey, FRCPsych (University of Oxford, Oxford, England), Simon Baron-Cohen, PhD (University of Cambridge, Cambridge, England), Patrick F. Bolton, PhD, FRCPsych (Institute of Psychiatry, Psychology and Neuroscience [IoPPN], London, England), Edward T. Bullmore, PhD, FRCP, FRCPsych, FMedSci (University of Cambridge), Sarah Carrington, PhD (University of Oxford), Marco Catani, PhD (IoPPN), Bhismadev Chakrabarti, PhD (University of Cambridge), Michael C. Craig, PhD (IoPPN), Eileen M. Daly, PhD (IoPPN), Susan C. L. Deoni, PhD (IoPPN), Christine Ecker, PhD (IoPPN), Fruzsina Happé, PhD (IoPPN), Julian Henty, PhD (University of Cambridge), Petra Jezzard, PhD (University of Oxford), Patrick Johnston, PhD (IoPPN), Derek K. Jones, PhD (IoPPN), Meng-Chuan Lai, PhD (University of Cambridge), Michael V. Lombardo, PhD (University of Cambridge), Anya Madden, MSc (IoPPN), Diane Mullins, MD (IoPPN), Clodagh M. Murphy, PhD (IoPPN), Declan G. M. Murphy, FRCPsych (IoPPN), Greg Pasco, PhD (University of Cambridge), Antonia Pretzsch, PhD (University of Cambridge), Susan A. Sadek, BSc (IoPPN), Joseph V. Spyridakis, BSc (University of Cambridge), Rose Venuti, MSc (University of Oxford), John Suckling, PhD (University of Cambridge), Sally J. Wheelwright, MSc (University of Cambridge), Steven C. R. Williams, PhD (IoPPN), and E. Ellie Wilson, PhD (IoPPN).

Additional Contributions: We thank the National Institute for Health Research Biomedical Research Centre for Mental Health and The Dr Mortimer and Theresa Sackler Foundation. The MRC AIMS Consortium is a United Kingdom collaboration between the Institute of Psychiatry, Psychology and Neuroscience at King's College London; the Autism Research Centre at the University of Cambridge; and the Autism Research Group at the University of Oxford.

REFERENCES

1. Lai MC, Lombardo MV, Auyeung B, Chakrabarti B, Baron-Cohen S. Sex/gender differences and autism: setting the scene for future research. *J Am Acad Child Adolesc Psychiatry*. 2015;54(1):11-24.

2. Fombonne E. Epidemiology of autistic disorder and other pervasive developmental disorders. *J Clin Psychiatry*. 2005;66(suppl 10):3-8.

3. Szatmari P, Liu XQ, Goldberg J, et al. Sex differences in repetitive stereotyped behaviors in autism: implications for genetic liability. *Am J Med Genet B Neuropsychiatr Genet*. 2012;159B(1):5-12.

4. Dworzynski K, Ronald A, Bolton P, Happé F. How different are girls and boys above and below the diagnostic threshold for autism spectrum disorders? *J Am Acad Child Adolesc Psychiatry*. 2012;51(8):788-797.

5. Werling DM, Geschwind DH. Sex differences in autism spectrum disorders. *Curr Opin Neurol*. 2013;26(2):146-153.

6. Lai MC, Lombardo MV, Suckling J, et al; MRC AIMS Consortium. Biological sex affects the neurobiology of autism. *Brain*. 2013;136(pt 9):2799-2815.

7. Schaer M, Ricebulla J, Padmanabhan A, Supekar K, Menon V. Sex differences in cortical volume and gyrification in autism. *Mol Autism*. 2015;6(1):42.

8. Lai MC, Lerch JP, Floris DL, et al. Imaging sex/gender and autism in the brain: etiological implications. *J Neurosci Res*. 2017;95(1-2):380-397.

9. Ruggeri AN, Sakou Khorshidi G, Lai MC, et al. A meta-analysis of sex differences in human brain structure. *Neurosci Biobehav Rev*. 2014;39:34-50.

10. Rasmussen CE, Williams CKI. *Gaussian Processes for Machine Learning*. Cambridge, MA: MIT Press; 2006.

11. McCarthy MM, Arnold AP. Reframing sexual differentiation of the brain. *Nat Neurosci*. 2011;14(6):677-683.

12. Sowell ER, Peterson BS, Kan E, et al. Sex differences in cortical thickness mapped in 176 healthy individuals between 7 and 87 years of age. *Cereb Cortex*. 2007;17(7):1550-1560.

13. Im K, Lee JM, Lee J, et al. Gender difference analysis of cortical thickness in healthy young adults with surface-based methods. *Neuroimage*. 2006;31(1):31-38.

14. Ecker C, Ginestet C, Feng Y, et al; MRC AIMS Consortium. Brain surface anatomy in adults with autism: the relationship between surface area, cortical thickness, and autistic symptoms. *JAMA Psychiatry*. 2013;70(1):59-70.

15. Wallace GL, Dankner N, Kenworthy L, Giedd JN, Martin A. Age-related temporal and parietal cortical thinning in autism spectrum disorders. *Brain*. 2010;133(pt 12):3745-3754.

16. Lenroot RK, Giedd JN. Sex differences in the adolescent brain. *Brain Cogn*. 2010;72(1):46-55.

17. Lenroot RK, Gogtay N, Greenstein DK, et al. Sexual dimorphism of brain developmental trajectories during childhood and adolescence. *Neuroimage*. 2007;36(4):1065-1073.

18. Geschwind DH, Pakkir P. Control of evolution: judge the brain by its cover. *Neuron*. 2013;80(3):613-617.

19. Zilles K, Palomero-Gallagher N, Amunts K. Development of cortical folding during evolution and ontogeny. *Trends Neurosci*. 2013;36(5):275-284.

20. Lord C, Rutter M, Le Couteur A. Autism Diagnostic Interview-Revised: a revised version of a diagnostic interview for caregivers of individuals with possible pervasive developmental disorders. *J Autism Dev Disord*. 1994;24(5):659-685.

21. Lord C, Rutter M, Goode S, et al. Autism Diagnostic Observation Schedule: a standardized observation of communicative and social behavior. *J Autism Dev Disord*. 1989;19(2):185-212.

22. Wechsler D. *Wechsler Abbreviated Scale of Intelligence (WASI)*. San Antonio, TX: Harcourt Assessment; 1999.

23. Deoni SC, Williams SC, Jezzard P, Suckling J, Murphy DG, Jones DK. Standardized structural magnetic resonance imaging in multicentre studies using quantitative T1 and T2 imaging at 1.5 T. *Neuroimage*. 2008;40(2):662-671.

24. Ecker C, Suckling J, Deoni SC, et al; MRC AIMS Consortium. Brain anatomy and its relationship to behavior in adults with autism spectrum disorder: a multicenter magnetic resonance imaging study. *Arch Gen Psychiatry*. 2012;69(2):195-209.

25. Fischl B, Sereno MI, Dale AM. Cortical surface-based analysis, II: inflation, flattening, and a surface-based coordinate system. *Neuroimage*. 1999;9(2):195-207.

26. Dale AM, Fischl B, Sereno MI. Cortical surface-based analysis, I: segmentation and surface reconstruction. *Neuroimage*. 1999;9(2):179-194.

27. Seiguene F, Dale AM, Busa E, et al. A hybrid approach to the skull stripping problem in MRI. *Neuroimage*. 2004;22(3):1060-1075.

28. Fischl B, Dale AM. Measuring the thickness of the human cerebral cortex from magnetic resonance images. *Proc Natl Acad Sci U S A*. 2000;97(20):11050-11055.

29. Marquand A, Howard JM, Brammer M, Chu C, Coen S, Mourão-Miranda J. Quantitative prediction of subjective pain intensity from whole-brain fMRI data using Gaussian processes. *Neuroimage*. 2010;49(3):2178-2189.

30. Marquand AF, Brammer M, Williams SC, Doyle OM. Bayesian multi-task learning for decoding multi-subject neuroimaging data. *Neuroimage*. 2014;92:298-311.

31. Baio J; Developmental Disabilities Monitoring Network Surveillance Year 2010 Principal Investigators; Centers for Disease Control and Prevention (CDC). Prevalence of autism spectrum

disorder among children aged 8 years: Autism and Developmental Disabilities Monitoring Network, 11 sites, United States, 2010. MMWR Surveill Summ. 2014;63(2):1-21.

32. Worsley KJ, Andermann M, Koulis T, MacDonald D, Evans AC. Detecting changes in nonisotropic images. Hum Brain Mapp. 1999;8(2-3):98-101.

33. Taylor DV Jr, Saggio AP, Severino MI. Smoothing and cluster thresholding for cortical surface-based group analysis of fMRI data. Neuroimage. 2006;33(4):1083-1093.

34. Ecker C, Ronan L, Feng Y, Martinez K, Suckling J, Catani M, Calvo R. Sex differences in neocortical structure and cognitive performance: a surface-based morphometry study. Neuroimage. 2015;104:351-365.

35. Joel D, McCarthy MM. Incorporating sex as a biological variable in neuropsychiatric research: where are we now and where should we be? Neuropsychopharmacology. 2017;42(2):379-385.

36. Chekroud AM, Ward EJ, Rosenberg MD, Holmes AJ. Patterns in the human brain mirror developmental trajectories. Proc Natl Acad Sci U S A. 2016;113(34):E4969. doi:10.1073/pnas.1523888113

37. Amaral DG, Schumann CM, Nordahl CW. Neuroanatomy of autism. Trends Neurosci. 2008;31(3):137-145.

38. Ecker C, Bookheimer SY, Murphy DG. Neuroimaging in autism spectrum disorder: brain structure and function across the lifespan. Lancet Neurol. 2015;14(10):1121-1134.

39. Baron-Cohen S, Ashwin E, Ashwin C, Tavassoli T, Chakrabarti B. Talent in autism: hyper-systemizing, hyper-attention to detail and sensory hypersensitivity. Philos Trans R Soc Lond B Biol Sci. 2009;364(1522):1377-1383.

40. Miller DI, Halpern DF. The new science of cognitive sex differences. Trends Cogn Sci. 2014;18(1):37-45.

41. Hyde JS. Sex and cognition: gender and cognitive functions. Curr Opin Neurobiol. 2016;38:53-56.

42. Wolfe S, Dukette E, Poundja H, Hohlmann M. Sex differences in cognitive processes and their clinical correlations higher than learning-system-type brain disorders. Autism. 2013;5(4):402-418.

43. Mandy W, Chilvers R, Chowdhury U, Salter G, Seigal A, Skuse D. Sex differences in autism spectrum disorder: evidence from a large sample of children and adolescents. J Autism Dev Disord. 2012;42(7):1304-1313.

44. Solomon M, Miller M, Taylor SL, Hinshaw SP, Carter CS. Autism symptoms and internalizing psychopathology in girls and boys with autism spectrum disorders. J Autism Dev Disord. 2012;42(1):48-59.

Chapter 6: Normative Sex-Related Phenotypic Diversity Across Multiple Measures of Brain Anatomy is Associated with Probability for Autism Spectrum Disorder

This chapter represents a critical extension of the study detailed in chapter 5 regarding the association between sex-related phenotypic diversity in measures of cortical thickness (CT) and the probability for autism spectrum disorder (ASD). As has been noted by others (Cahill 2017) it is unknown if and how the previous results detailed in Chapter 5 (Ecker, et al 2017) will extend to other measures of neuro-anatomy. Here, we extended our initial findings to consider multiple aspects of brain anatomy including both volumetric and geometric cortical features in order to (*i*) provide a more comprehensive characterization of normative sex related differences in brain structure, (*ii*) determine how diversity in sex based neurophenotypes are associated with ASD probability, and (*iii*) estimate how much ASD prevalence in the general population might vary as a function of normative sex-related phenotypic diversity.

This study is currently under review with *The American Journal of Psychiatry* and is presented in the pages that follow in its most recent format as of time of writing. Supplementary materials for this chapter are presented in Appendix IV, the current manuscript proof is presented in Appendix V.

Title: Normative Sex-Related Phenotypic Diversity Across Multiple Measures of Brain Anatomy is Associated with Probability for Autism Spectrum Disorder

Authors: Derek S. Andrews[a] MSc, Andre Marquand[b,c] PhD, Cedric E Ginestet[c] PhD, Maria Gudbrandsen[a] MSc, Eileen Daly[a] PhD, Clodagh M. Murphy[a,d] MBBS PhD, Meng-Chuan Lai[f,e,g] MD PhD, Michael V. Lombardo[h,e] PhD, Amber N.V. Ruigrok[e] PhD, the MRC AIMS Consortium[*], Steven C. Williams[c] PhD, Edward T. Bullmore[i], MBBS PhD, John Suckling[i] PhD, Simon Baron-Cohen[f] PhD, Michael C. Craig[a,d] MBBS PhD, Declan G.M. Murphy[a,d**] MBBS MD, & Christine Ecker[j,a**] PhD

Affiliations:

[a] Department of Forensic and Neurodevelopmental Sciences, and the Sackler Institute for Translational Neurodevelopment, Institute of Psychiatry, Psychology and Neuroscience, King's College London, UK

[b] Donders Institute for Brain, Cognition and Behaviour, Radboud University, Nijmegen, Netherlands

[c] Centre for Neuroimaging Sciences, Institute of Psychiatry, Psychology and Neuroscience, King's College, London, UK

[d] National Autism Unit, Bethlem Royal Hospital, South London and Maudsley NHS Foundation Trust, UK

[e] Autism Research Centre, Department of Psychiatry, University of Cambridge, Cambridge, UK

[f] Child and Youth Mental Health Collaborative at the Centre for Addiction and Mental Health and The Hospital for Sick Children, Department of Psychiatry, University of Toronto, Toronto, Canada

[g] Department of Psychiatry, National Taiwan University Hospital and College of Medicine, Taiwan

[h] Department of Psychology & Center for Applied Neuroscience, University of Cyprus, Nicosia, Cyprus

[i] Brain Mapping Unit, Department of Psychiatry, University of Cambridge, UK

[k] Department of Child and Adolescent Psychiatry, Psychosomatics and Psychotherapy, Universitätsklinikum Frankfurt am Main, Goethe-University Frankfurt am Main, Germany

[*] The Medical Research Council Autism Imaging Multicentre Study Consortium (MRC AIMS Consortium) is a UK collaboration between the Institute of Psychiatry, Psychology and Neuroscience at King's College, London, the Autism Research Centre, University of Cambridge, and the Autism Research Group, University of Oxford. The Consortium members in alphabetical order are: Anthony J. Bailey (Oxford), Simon Baron-Cohen (Cambridge), Patrick F. Bolton (IoP), Edward T. Bullmore (Cambridge), Sarah Carrington (Oxford), Marco Catani (IoPPN), Bhismadev Chakrabarti (Cambridge), Michael C. Craig (IoPPN), Eileen M. Daly (IoPPN), Sean C. L. Deoni (IoPPN), Christine Ecker (IoPPN), Francesca Happé (IoPPN), Julian Henty (Cambridge), Peter Jezzard (Oxford), Patrick Johnston (IoPPN), Derek K. Jones (IoPPN), Meng-Chuan Lai (Cambridge), Michael V. Lombardo (Cambridge), Anya Madden (IoPPN), Diane Mullins (IoPPN), Clodagh M. Murphy (IoPPN), Declan G. M. Murphy (IoPPN), Greg Pasco (Cambridge), Amber N. V. Ruigrok (Cambridge), Susan A. Sadek (Cambridge), Debbie Spain (IoPPN), Rose Stewart (Oxford), John Suckling (Cambridge), Sally J. Wheelwright (Cambridge), Steven C. Williams (IoPPN), and C. Ellie Wilson (IoPPN).

[**] These authors contributed equally to the manuscript

6.1 Abstract

Objective: Males are 2 to 5 times more likely to be diagnosed with Autism spectrum disorder (ASD) than females. The reasons for this bias are not fully understood. However, normative diversity in brain structure associated with biological sex is one possible mediator for ASD risk. The authors therefore examined the probability of ASD as a function of sex-related variability in multiple measures of brain anatomy.

Method: 98 adults with ASD (49 males, 49 females) and 98 typically developing controls (51 males, 47 females) underwent structural MRI scanning. Measures of cortical morphometry (i.e. cortical thickness, surface area, the local gyrification index, and sulcal depth) were used to establish normative models of biological sex. These models were subsequently applied to males and females with ASD. Sample probabilities for ASD were calculated across features according to sex-based neuroanatomical phenotypes and extrapolated to estimate ASD risk within the general population.

Results: Across morphometric features, females with ASD displayed a statistically significant neuroanatomical shift towards more male-typical presentations (p<0.001). Moreover, within both biological males and females sample probabilities for ASD increased with predicted probabilities for male-typical brain phenotypes. For biological females, this translated to an estimated variability in population prevalence ranging from 0.01 to 2.6% depending on having either a female- or male-typical neurophenotype.

Conclusions: Male-typical neurophenotypes are associated with higher probability for having an ASD diagnosis than female-typical neurophenotypes across a range of neuroanatomical features. In addition to genetic and environmental factors, normative sex-related phenotypic diversity in brain structure should be considered when investigating risk and resilience for ASD.

6.2 Introduction

Autism spectrum disorder (ASD) is a complex neurodevelopmental condition estimated to be 2-5 times more common in males than females (Lai et al., 2015, Fombonne, 2009). While the preponderance of males with ASD has partially been attributed to sex differences in clinical phenotypes (Szatmari et al., 2012, Bölte et al., 2011, Dworzynski et al., 2012, Mandy et al., 2012, Solomon et al., 2012), etiological models propose that factors inherent to normative sex differences may modulate ASD liability (for review see (Werling, 2016)). However, it remains unknown what "male risk" and/or "female protective" factors may contribute to the male preponderance of ASD, and how these factors may affect the biological underpinnings of the condition.

To identify potential sex-related risk (and protective) factors, we recently examined the probability of ASD as a function of normative sex-related phenotypic diversity in brain structure (Ecker et al., 2017). To do so, we initially developed a multivariate predictive model of biological sex based on differential patterns of brain structure in a sample of typically developing (TD) males and females. This model of normative sex differences was subsequently applied to males and females with ASD, which allowed us to (*i*) examine the probability of ASD along a phenotypic axis, ranging from the characteristic female to male brain phenotype, and (*ii*) identify patterns of sex-related neuroanatomical variability associated with low and high probability of ASD. In this previous study we reported that normative sex-related phenotypic diversity in brain structure significantly affects the risk of ASD in addition to biological sex alone, with male-typical neuroanatomical characteristics carrying a higher intrinsic risk for ASD than female-typical characteristics. This increased risk was predominantly driven by a phenotypic shift of the brain in females with ASD for a male-typical rather than female-typical presentation. Moreover, using a mapping approach that enabled us to estimate patterns of atypically at the level of each individual subject (Marquand et al., 2014), we demonstrated that high and low risk of ASD is associated with particular patterns of neuroanatomical variability that included many of the brain regions where males typically differ from females on average (e.g. (Sowell et al., 2007, Im et al., 2006)). Taken together, these findings highlight the need for considering normative sex-related phenotypic diversity in addition to genetic and environmental factors when estimating an individual's risk for ASD.

However, in this prior 'proof-of-concept' study, our analysis was based exclusively on measures of cortical thickness (CT) as previous neuroimaging studies have shown CT to be highly variable between TD males and females (Sowell et al., 2007, Im et al., 2006), and significantly altered in individuals with ASD (Wallace et al., 2010, Ecker et al., 2013). Thus, as has been raised by others (Cahill, 2017), it is unknown whether or how our initial findings generalize to other morphometric features that have been reported to be atypical in ASD. These include vertex-wise estimates of surface area (SA; (Ecker et al., 2013)), the local gyrification index (*l*GI; (Ecker et al., 2016, Schaer et al., 2013)), and sulcal depth (SULC; (Nordahl et al., 2007)). Here, we extended these findings to consider multiple aspects of brain anatomy including both volumetric and geometric cortical features in order to (*i*) provide a more comprehensive characterization of normative sex related differences in brain structure, (*ii*) determine how diversity in sex based neurophenotypes are associated with ASD probability, and (*iii*) estimate how much ASD prevalence in the general population might vary as a function of normative sex-related phenotypic diversity. We expect that our initial finding of a phenotypic shift of the brain in ASD females towards a more male-typical neurophenotype generalizes to other morphometric features, and for sex differences in cortical morphometry to be associated with population risk for ASD.

6.3 Methods

6.3.1 Participants

98 right-handed adults with ASD (49 males and 49 females) and 98 age and IQ matched TD controls (51 males and 47 females) aged 18-42 years were recruited by advertisement and assessed at the Institute of Psychiatry, Psychology and Neuroscience (IoPPN), London, and the Autism Research Centre, Cambridge. Approximately equal ratios of cases to controls, and males to females, were recruited within sites (Table 6.1). Exclusion criteria included a history of major psychiatric

disorder (e.g. psychosis), head injury, genetic disorder associated with ASD (e.g. fragile-X syndrome, tuberous sclerosis), or any other medical condition affecting brain function (e.g. epilepsy). We also excluded participants on antipsychotic medication, mood stabilizers or benzodiazepines.

Table 6.1. Participant Demographics and Global Brain Measures

	ASD (*n* = 98)	TD Control (*n* = 98)
Male Participants (*n* = 100)	*n* = 49	*n* = 51
Age [years]	26.16 ± 7.2 (18 - 41)	27.22 ± 5.58 (18 - 42)
Full-scale IQ (WASI)	112.61 ± 12.27 (89 - 135)	114.67 ± 10.88 (93 - 137)
Verbal IQ	110.51 ± 13.01 (83 - 137)	109.86 ± 11.03 (88 - 137)
Performance IQ	112.00 ± 13.65 (85 - 138)	116.74 ± 10.90 (93 - 133)
ADI-R Social	17.57 ± 5.50 (10 - 28)	-
ADI-R Communication	13.86 ± 4.16 (8 - 24)	-
ADI-R Repetitive Behavior	4.96 ± 2.37 (1 - 10)	-
ADOS Social + Communication	9.43 ± 4.39 (1 - 21)	-
ADOS Stereotypic Behaviour	1.27 ± 1.27 (0 - 5) *	-
Mean Cortical Thickness [mm]	2.35 ± 0.10	2.33 ± 0.10
Mean Surface Area	0.7680 ± 0.71	0.7683 ± 0.05
Mean local Gyrification Index	3.04 ± 0.12	3.04 ± 0.10
Mean Sulcal Depth	0.0341 ± 0.007	0.0356 ± 0.006
Total Grey Matter Volume [litre]	0.76 ± 0.08	0.76 ± 0.05
Total Intracranial Volume [litre]	1.59 ± 0.21	1.58 ± 0.17
Female Participants (*n* = 96)	*n* = 49	*n* = 47
Age [years]	27.60 ± 7.12 (18 - 48)	27.60 ± 7.31 (19 - 52)
Verbal IQ[a]	116.60 ± 12.15 (76 - 144)	117.83 ± 8.81 (96 - 135)
Performance IQ[a]	110.56 ± 14.50 (67 - 138)	114.38 ± 8.26 (96 - 128)
Full-scale IQ (WASI)	114.88 ± 12.36 (84 - 136)	118.38 ± 7.32 (99 - 129)
ADI-R Social	16.32 ± 4.24 (10 - 26)	-
ADI-R Communication	12.43 ± 3.96 (7 - 22)	-
ADI-R Repetitive Behavior	4.36 ± 1.98 (1 - 9)	-
ADOS Social + Communication	7.71 ± 5.28 (0 - 19)	-
ADOS Stereotypic Behaviour	0.75 ± 0.97 (0 - 3) *	-
Mean Cortical Thickness [mm]	2.32 ± 0.11	2.34 ± 0.10
Mean Surface Area	0.6895 ± 0.05	0.6865 ± 0.06104
Mean local Gyrification Index	2.95 ± 0.09	2.96 ± 0.10
Mean Sulcal Depth	0.0378 ± 0.008	0.0380 ± 0.007
Total Grey Matter Volume [litre]	0.67 ± 0.06	0.68 ± 0.06
Total Intracranial Volume [litre]	1.32 ± 0.18	1.32 ± 0.17

Table 6.1 Participant Demographics and Global Brain Measures: Data expressed as mean ± standard deviation (range). There were no significant between-group differences in age, FSIQ, mean cortical thickness, total grey matter volume, or total intracranial volume ($p<0.05$, two-sided). ADI-R values based on 49 males and 44 females with ASD. ADOS values based on 49 males and 48 females. * statistically significant between males and females based on $p<0.05$, two-sided ($t(95)=2.23$, $p=0.028$). [a] verbal and performance IQ data was not available for one ASD female

All participants with ASD were diagnosed according to International Statistical Classification of Diseases, 10th Revision (ICD-10) research criteria. Clinical diagnoses were confirmed using the Autism Diagnostic Interview Revised (ADI-R; (Lord et al., 1994)(19)) or the Autism Diagnostic Observation Schedule (ADOS; (Lord et al., 2000)). All ADI-R diagnosed participants reached algorithm cut-offs in the three domains of the ADI-R, although failure to reach cut-off in one domain by maximally two points was permitted. Due to reliable informants being unavailable, we were unable to obtain ADI-R diagnostic data from five females with ASD, for whom diagnostic status was confirmed using ADOS-G cut-offs for ASD. In all other participants, ADOS-G scores were used to assess the severity of current symptoms and were not used as an inclusion criterion. One female with ASD fell short one point on the ADI-R communication and repetitive domain but met ADOS-G criteria. Overall intellectual ability was assessed using the Wechsler Abbreviated Scale of Intelligence (Wechsler, 1999)(21). All participants had a full-scale IQ greater than 80 and gave informed written consent in accordance with ethics approval by the National Research Ethics Committee, Suffolk, UK.

6.3.2 Structural MRI Data Acquisition

Scanning took place at the IoPPN, London, and the Addenbrooke's Hospital, Cambridge, using matched 3T GE Signa systems (General-Electric, Milwaukee, USA). A quantitative T_1-mapping sequence was used to ensure standardization of structural MRI scans across scanner platforms (Deoni et al., 2008, Ecker et al., 2012), which resulted in high-resolution structural T_1-weighted inversion-recovery images, with 1x1x1mm resolution, a 256x256x176 matrix, TR=1800ms, TI=50ms, FA=20'', and FOV=25cm.

6.3.3 Cortical Reconstruction using FreeSurfer

FreeSurfer v5.3.0 software (http://surfer.nmr.mgh.harvard.edu/) was used to derive tessellated models of the cortical surface for each T_1-weighted image. These well-validated and fully automated procedures have been extensively described elsewhere (e.g. (Dale et al., 1999, Fischl et al., 1999, Ségonne et al., 2004, Jovicich et al., 2006, Fischl and Dale, 2000)). Resulting surface models were visually inspected for

reconstruction errors. Surface reconstructions with visible inaccuracies were further excluded from the statistical analysis and are not described in this study. Dropout rates were equal across groups and were <10% of the total sample.

From each individual's surface reconstructions four separate vertex based morphometric cortical features were calculated. (*i*) Cortical thickness (CT), i.e. the closest distance between corresponding vertices between the grey-white matter and gray matter-cerebrospinal fluid boundaries (Fischl and Dale, 2000); (*ii*) vertex-wise estimates of pial (i.e. grey matter) surface area (SA) (Winkler et al., 2012). And measures of cortical geometry including (*iii*) the local gyrification index (*l*GI) (Schaer et al., 2008) and (*iv*) sulcal depth (SULC, i.e. average convexity, the depth/height of each vertex above the average cortical surface). Prior to further analysis all features (excluding *l*GI) were smoothed using a 15mm surface-based FWHM Gaussian kernel. As *l*GI utilizes SA values sampled within spherical regions on interest with a 15mm diameter, no additional smothing was performed for this measure.

6.3.4 Gaussian Process Classification

Gaussian Process Classification (GPC) (Rasmussen and Williams, 2006, Marquand et al., 2010) models were employed to discriminate biological sex among TD participants on the basis of each of the four cortical features (i.e. CT, SA, *l*GI, SULC) separately. These classifiers provide a predictive class probability (y_p) for each individual ranging from 0 to 1 for the characteristic female to male brain phenotype, with y_p=0.5 serving as the binary cut-off between classes. The overall classification accuracy of each model was estimated using leave-one-out cross validation and tested for significance by repeating the cross-validation procedure n=1,000 times after randomly permuting the class labels. Subsequently, we applied these four classifiers for biological sex in TD participants to predict the sex of males and females with ASD. The resulting classification accuracies for the ASD cases were tested for statistical significance using permutation testing as outlined above.

To visualize the patterns of brain regions representative of normative sex differences, we present spatial representations of the maximum a-posteriori estimate of each model's weight vector ($\boldsymbol{w}$), which is indicative of the regional contribution to the overall prediction of biological sex (Marquand et al., 2010). For each classifier, $\boldsymbol{w}$ was

derived by training the GPC on all TD individuals. As individuals with ASD were not included in the initial training of the classifiers they do not contribute to $\boldsymbol{w}$, thus we used a "predictive mapping" approach (Marquand et al., 2014) to determine which cortical features are driving sex related differences in ASD among groups of males and females with high and low probability for ASD. Here, groups of high and low ASD probability were determined according to predicted class probabilities, with y_p>0.5 (i.e. male-typical phenotype) representing high and y_p<0.5 (i.e. female-typical phenotype) representing low probability. For each test example i in both male (and female) high (and low) probability groups j, we calculated the element-wise (i.e. Hadamard) product of each individuals data ($\boldsymbol{x}_{ij}$) and the corresponding weights ($\boldsymbol{w}$), so that ($\boldsymbol{x}_{ij}$).*$\boldsymbol{w}$ (Marquand et al., 2014). For each group (i.e. male and female, high and low ASD probability) brain regions contributing the most to the classification were summarized by taking the mean of the ($\boldsymbol{x}_{ij}$).*$\boldsymbol{w}$ values at each vertex.

6.3.5 Estimating ASD Probability

To examine how normative sex based phenotypic diversity in brain structure is associated with probability for ASD we first calculated the mean of each individual's predictive class probabilities across the four classification models. This provided a single class probability for each individual that takes into account normative sex variability across all four cortical features. We then converted the continuous axis of class probabilities into a set of discrete bins (e.g., from 0 to 1 in steps of 0.125). Within each bin, the sample probability of ASD was calculated as the ratio of the number of individuals with ASD relative to the total number of individuals within the bin. Confidence intervals for these sample probabilities were determined using an exact binomial test implemented in R Project for Statistical Computing (https://www.r-project.org). Furthermore, these data allowed us to estimate the population prevalence of ASD given a male- or female-typical neuroanatomical phenotype in addition to being biologically male or female. Details of these methods are provided in the supplementary materials. In brief, using Bayes theorem, we combined our sample prevalence estimates with previously published prevalence rates of ASD for biological male and female individuals in the general population (i.e., 1:42 for male and 1:189 for female individuals; (Baio, 2014)). In this way, we were able to estimate the population prevalence of ASD diagnosis (D = 1) given an

individual's predicted neuroanatomical sex phenotype (M) and biological sex (S), that is $\mathbb{P}(D = 1 \mid M, S)$.

6.3.6 Vertex-wise between-group comparison of cortical measures

Vertex-wise statistical analyses of each cortical feature were conducted using the SurfStat toolbox (www.math.mcgill.ca/keith/surfstat/) for MATLAB (R2014a, The Mathworks, Massachusetts). For the comparisons between TD males and females, parameter estimates were obtained by regression of a GLM at each vertex *i* with biological sex and center as categorical fixed-effects factors, and total grey matter (GM) volume as a continuous covariate. To examine whether the neuroanatomy of ASD is significantly modulated by biological sex, we also included a main effect of diagnostic group and a group-by-sex interaction, i.e.

$$Y_i = \beta_0 + \beta_1\, Group + \beta_2\, Sex + \beta_3\, (Group \times Sex) + \beta_4\, GM_{total} + \beta_5\, Center + \varepsilon_i,$$

where ε_i is the residual error. Additionally, total SA was used as a continuous covariate for analyses of SA. Effects of interest were estimated from the coefficients $\beta_{1\text{-}3}$ normalized by the corresponding standard error. Corrections for multiple comparisons were performed using a 'random field theory' (RFT)-based cluster analysis for non-isotropic images at a cluster-threshold of $p<0.05$ (two-tailed) (Worsley et al., 1999).

6.4 Results

6.4.1 Participant Demographics and Global Brain Measures

There were no significant differences between all individuals with ASD and TD controls in age ($t(194)=-0.53$, $p=0.598$), full-scale IQ ($t(194)=-1.72$, $p=0.086$), mean CT ($t(194)=0.08$, $p=0.936$), mean SA ($t(194)=0.03$, $p=0.976$), mean *l*GI ($t(194)=0.24$, $p=0.810$), mean SULC ($t(194)=0.67$, $p=0.499$), and total GM volume ($t(194) = -0.20$, $p=0.839$). There were also no significant differences between males and females in age ($t(194)=-0.93$, $p=0.356$), full-scale IQ ($t(194)=-1.87$, $p=0.063$), mean CT ($t(194)=0.95$, $p=0.344$), or mean SULC ($t(194)=-2.80$, $p=0.006$) across diagnostic groups. As expected, total grey matter volume was significantly larger in males than in females ($t(194)=9.11$, $p<0.001$). Furthermore, across the entire sample males

showed significantly greater mean SA ($t(194)=9.43$, $p<0.001$) and mean *l*GI ($t(194)=5.56$, $p<0.001$) than females. There were no significant differences in any of these measures between TD and ASD males, or between TD and ASD females ($p<0.05$, 2-tailed).

6.4.2 Prediction of Biological Sex Based on Normative Variability in Cortical Morphometry

Across all four vertex based cortical features GPC was able to separate male from female TD controls at cross validated accuracies significantly above what would be expected by chance (SA 78%, $p<0.001$; CT 71%, $p<0.001$; SULC 74%, $p<0.001$; *l*GI 77%, $p<0.001$). Using each classifiers predictive class probabilities for individuals we were able to represent normative sex based variability in brain phenotypes along a singular phenotypic axis, ranging from the female- to male-typical neurophenotype (Figure 1). For each morphological measure, the GPC model weights ($\boldsymbol{w}$) followed a spatial pattern similar to the distribution of group differences observed between TD males and females as determined via a conventional GLM (Figure 6.1, Supplementary Figure 1, Supplementary Table 1).

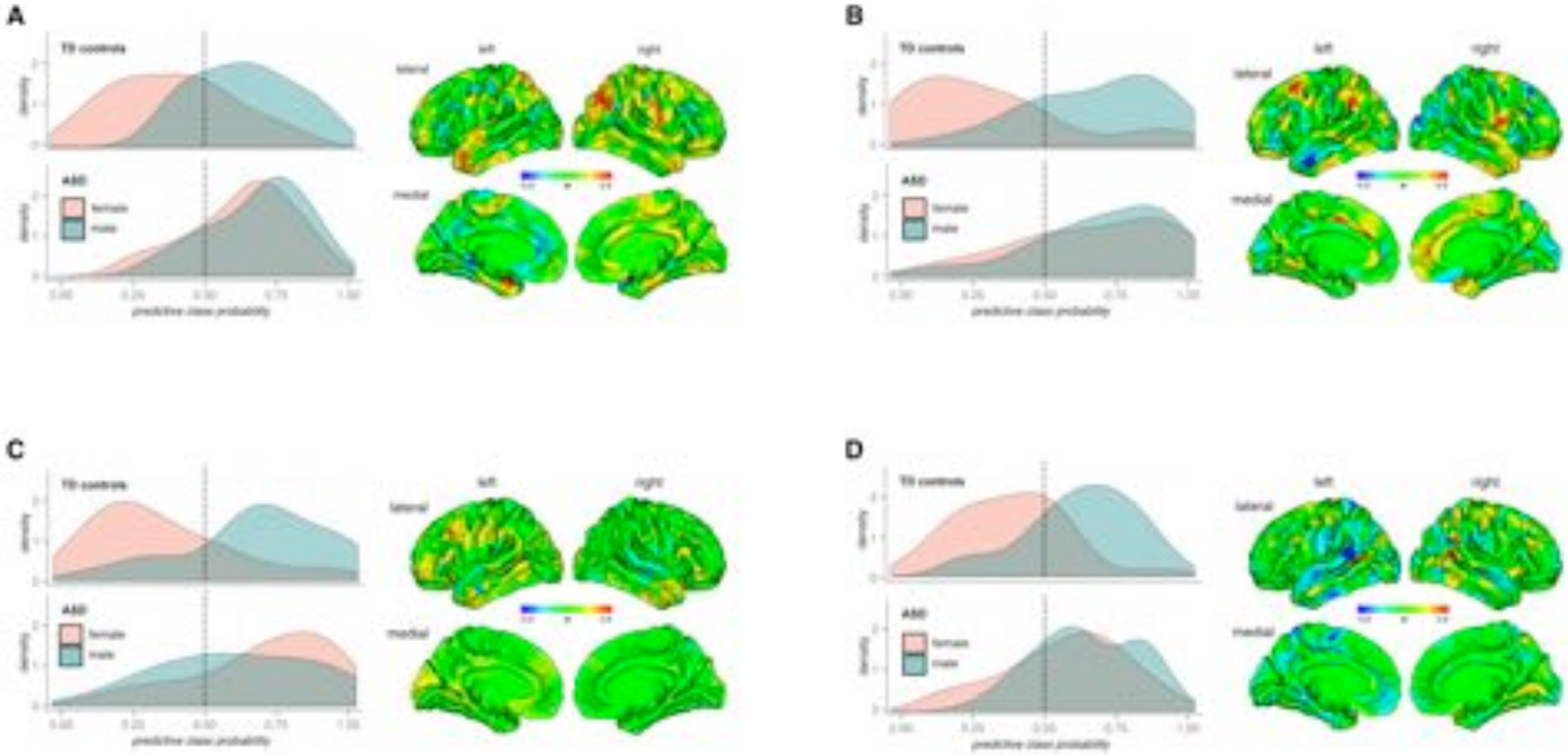

Figure 6.1 Gaussian Process Classification of Biological Sex: The results of Gaussian Process Classification (GPC) according to biological sex categories are shown for each of the fo cortical features investigated: (A) cortical thickness (CT), (B) surface area (SA), (C) the local gyrification index (*l*GI), and (D) sulcal depth (SULC). Each model was able to separate males from females at accuracies significantly above what would be expected by chance (top left). When these models of normative sex differences in cortical morphology whe applied to males and females with ASD, females with ASD were more frequently classified to the male class (bottom left) indicating a male-typic morphological presentation amon females with ASD. Spatial representations of each discriminative model (i.e. weight vectors) are shown (right). These patterns largely corresponded with brain regions that differ between TD males and females as identified using a conventional general linear model (see supplementary Figure 1).

6.4.3 Prediction of Biological Sex Among Individuals with ASD

When predicting biological sex for individuals with ASD we found that females with ASD were more frequently allocated to the male rather than the female class in all four models (SA 71%, p=0.002; CT 80%, p=0.002; SULC 65%, p=0.009; *l*GI 78%, p=0.001). Females with ASD were significantly allocated to the male class more frequently than would be expected based on the typical rates of misclassification for female controls (SA χ^2=26.41, p<0.001; CT χ^2=22.15, p<0.001; SULC χ^2=13.65, p<0.001; *l*GI χ^2=26.01, p<0.001). Furthermore, the mean across the predicted class probabilities for ASD females was significantly increased in females with ASD relative to female controls, indicating a shift towards male-typical morphological patterns in the brain (SA t=6.158, p<0.001; CT t=6.13, p<0.001; SULC t=4.44, p<0.001; *l*GI t=6.85, p<0.001). Across all four models there were no significant differences (p<0.05) between the predicted class probabilities for TD and ASD males, or between males and females with ASD.

6.4.4 ASD Probability as a Function of Normative Sex Variability in Cortical Morphometry

Within our sample we found that the number of individuals with ASD significantly increased along the female to male phenotypic axis (i.e. from female to male) as defined by predicted class probabilities. This effect was predominantly driven by the shift of females with ASD towards a more male-typical neuroanatomical brain phenotype (See Figure 6.2, Supplementary Figure 2). When these sample probabilities were combined with previously reported ASD prevalence rates in the general population among males (1/43, i.e. 2.3%) and females (1/190, i.e. 0.5%) (Baio, 2014), we found that biological females with male-typical brain morphology (0.1% estimated prevalence) were twenty six times more likely to have ASD compared to biological females with female-typical neuroanatomical phenotypes (2.6% estimated prevalence). Biological males with male-typical brain morphometry showed an estimated population prevalence of 2.4% in line with previously reported rates. However, males with female-typical phenotypes showed a reduced prevalence estimate for ASD (1.9%) indicative of a 'female protective effect' in relation to brain anatomy (see Supplementary Table 2).

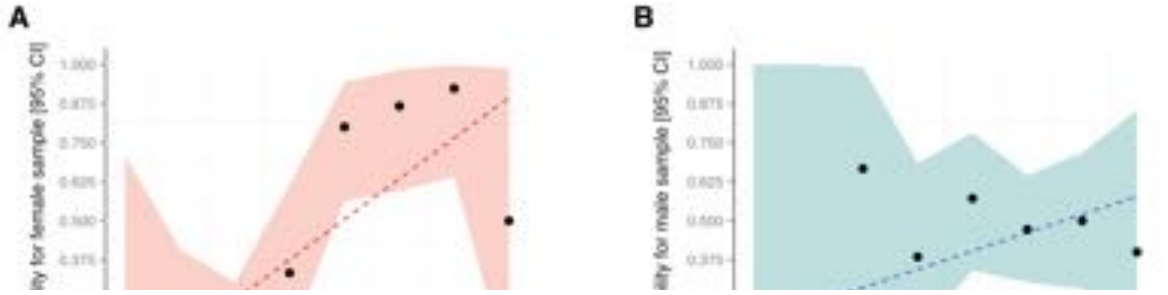

Figure 6.2 Probability for ASD as a Function of Normative Sex-Related Phenotypic Variability in Brain Morphology: Probability estimates for ASD across eight discrete bins along the axis of probabilistic class predictions for biological sex are plotted for (A) biological females and (B) males. Each individual's probabilistic class prediction was calculated as the mean prediction across all four classification models. Probability for ASD was seen to increase along with increasingly male-typic class predictions. This relationship was particularly apparent in females due to the statistically significant shift in females with ASD towards the male-typic neuroanatomical phenotype.

Predictive maps identifying patterns of neuroanatomical variability associated with high and low probability of ASD across sexes are shown in Figure 6.3. While a similar set of brain regions conferred high (and low) probability for ASD in men and women within features, certain brain regions were unique to or differed in sign between particular risk groups and sexes. For example, negative predictive mapping values for CT in the left parahippocampal gyrus and SULC in the superior temporal gyrus were observed across all males and high-probability females, while low probability females showed positive values in these regions. For predictive mapping measures of SA and *l*GI, regions of the inferior and superior temporal gyri appear to show a sex-specific relationship with high probability males showing negative values compared to positive values amongst females and low probability males. This indicates that morphometric measures in particular brain regions that are important for classifying sex differences differ between individuals with high and low risk for ASD and may be sex-specific.

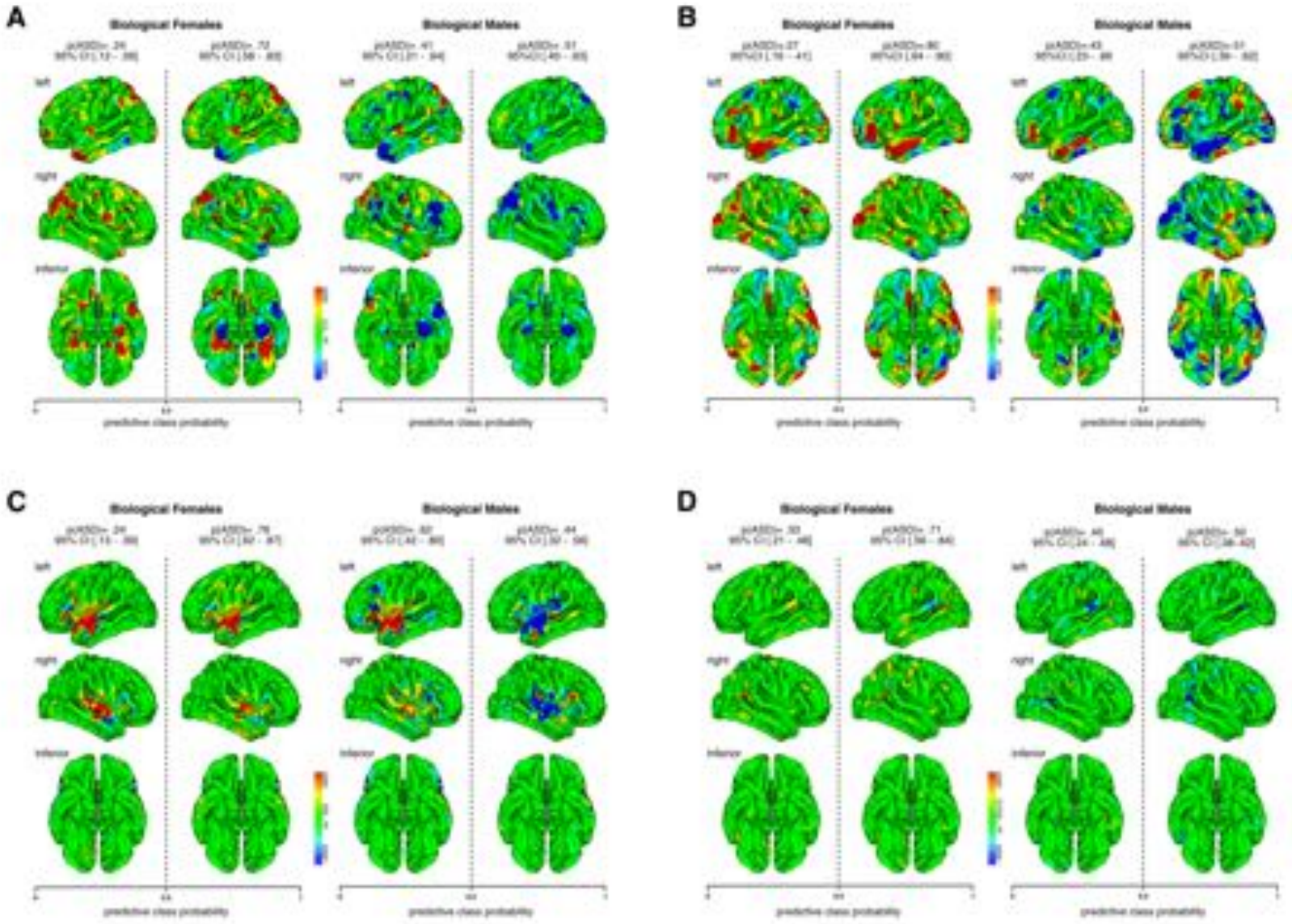

Figure 6.3 Prediction Maps for High and Low ASD Probability Males and Females: Prediction maps highlighting brain regions most relevant to classifying biological sex among high and low risk males and females are shown for each cortical feature, (A) cortical thickness (CT), (B) surface area (SA), (C) local gyrification index (*l*GI), and (D) sulcal depth (SULC). For male and female individuals high and low probability groups were determined according to class probabilities with <0.5 (i.e. female-typic) indicating low and >0.5 (i.e. male-typic) indicating high probability. For each subgroup the product of the decision function for classifying biological sex (w) and each individual's data (x_i) was calculated. Mean values at each vertex were then used to summarize maps within subgroups.

6.4.5 Cortical Morphometry in ASD is Modulated by Biological Sex

Lastly, we used a conventional GLM to test for significant between-group differences and diagnosis-by-group interactions in the four examined morphometric features. Overall, we found that measures of CT, SA, and *l*GI in ASD were significantly modulated by biological sex (Figure 6.4, also Supplementary Figure 3). Such group-by-sex interactions therefore need to be taken into account when interpreting main effects of group. Significant group-by-sex interactions in measures of CT were observed across the temporal lobe, including the fusiform and parahippocampal gyri. Across this cluster the degree of CT abnormality in females with ASD exceeded those of males, despite no differences in measures of ASD symptom severity (9). Additionally, group-by-sex interactions were observed for measures of SA and *l*GI in the medial orbital frontal cortex showing decreases in females with ASD and increases in males with ASD. Statistical details of these clusters are provided in Supplementary Table 3.

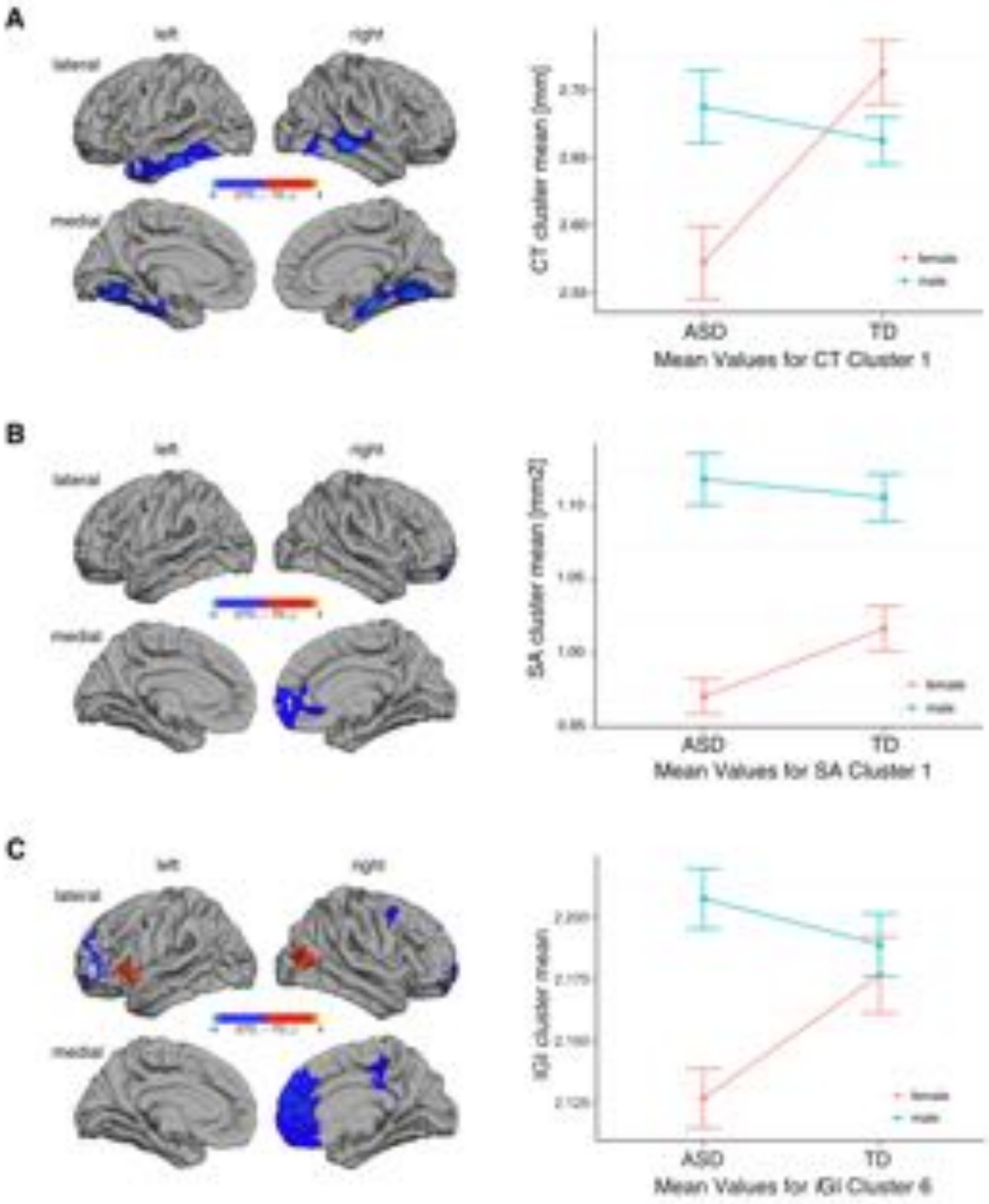

Figure 6.4 Group by Sex Interaction Effects in Cortical Morphometry: Clusters of significant (RFT p<0.5) group x sex interactions in (A) cortical thickness (CT), (B) surface area (SA), and (C) the local gyrification index (*l*GI). No significant group x sex interactions were observed in measures of sulcal depth (SULC). Statistical details of these clusters are provided in Supplementary Table 3.

6.5 Discussion

The present study builds upon a previous 'proof-of-concept' suggesting that probability of ASD increases significantly from a characteristic female to male neuroanatomical brain phenotype (Ecker et al., 2017). In this prior study, which examined measures of cortical thickness (CT) only, the increase in ASD probability was predominantly driven by a phenotypic shift of the brain in females with ASD towards a male-typical neurophenotype (Ecker et al., 2017). In the current study, we show that this phenotypic shift is not restricted to measures of CT, but generalizes to other cortical features including vertex-wise estimates of surface area (SA), the local gyrification index (*l*GI), and sulcal depth (SULC). The findings of the present study therefore not only support our original report in suggesting that male-typical neuroanatomical characteristics carry a higher probability for ASD than female-typical characteristics, but further show this effect to be broadly and consistently related across multiple measures of cortical morphometry.

The extension of our approach to include multiple morphometric features is of crucial importance as there is evidence to suggest that different cortical features are etiologically and phenotypically distinct. For example, it has been shown that measures of CT and SA (*i*) are mediated by different sets of genes (Panizzon et al., 2009), (*ii*) have different developmental trajectories (Ecker et al., 2014), and (*iii*) represent distinct aspects of the cortical architecture (Rakic, 1995). Therefore, the observation that the phenotypic shift of the brain in ASD females is consistent across morphometric features may indicate the existence of a common underlying mechanism, such as atypical cortical neurogenesis and migration (Casanova, 2014), that steers multiple aspects of brain anatomy towards a similar phenotypic endpoint overall. Yet, the neuroanatomical patterns associated with the prediction of biological sex, and the patterns carrying high/low ASD probability in males and females, differed in sign and regional distribution between the cortical features. Thus, while there may be a common etiology for the phenotypic differences in brain anatomy in ASD within the sexes, our findings are consistent with the notion that sex differentiation mechanisms in the brain have region specific effects (for review see (McCarthy, 2017, McCarthy and Konkle, 2005)). Therefore, differences in these neuroanatomical patterns associated with high probability for ASD may be beneficial

in identifying brain regions where sexual differentiation may contribute to male preponderance in ASD.

Moreover, we established that the neuroanatomy of ASD in some regions of the brain is modulated by biological sex by examining sex-by-diagnosis interactions for multiple cortical features. This suggests that in these brain regions (*i*) there are not only quantitative differences in the degree of neuroanatomical abnormality between males and females with ASD and their respective normative population, but also that (*ii*) ASD potentially interacts with sexually-differential neurobiological phenotypes to give rise to qualitative differences in brain anatomy between males and females with the condition. This is also relevant in view of a recent genetic study, suggesting that while ASD risk genes are expressed at similar levels in males and females, the impact of these genes is likely modulated by their interactions with sex-differential processes (e.g. in cortical microglia and/or astrocytes) that may play a critical role in setting males at a greater risk for ASD (Werling et al., 2016). An individual's risk or probability of ASD is therefore not only dependent on genetic load itself, but also on naturally occurring sex-differential biological pathways.

With respect a biological organ as complex as the brain it has been suggested that on a phenotypic level, the brain should be considered a 'mosaic' of regions that differ between degrees of relative maleness or femaleness, or not at all (i.e. unisex), resulting in a potentially infinite variety of brain phenotypes both within and between sexes (McCarthy, 2017, McCarthy and Konkle, 2005). In order to identify an individual's position on such a multi-dimensional 'spectrum' of sex-related phenotypic variability, it is important to develop analytical frameworks that can accommodate inter-individual phenotypic diversity within and across the binary categories dictated by biological sex, such as the probabilistic multivariate pattern classification approach utilized in the present study (see also (Ecker et al., 2017)). In this way we were able to estimate an individual's risk of ASD based on phenotypic, rather than biological sex and in doing so demonstrated that an individual's probability for developing ASD may vary from as much as 0.1 to 2.6% in the general population depending on having a female- or male-typical neuroanatomical

phenotype, in addition to being biologically male or female. Our approach to modeling normative sex-related phenotypic diversity may therefore be extended to various additional phenotypic features in the future, and to contribute to the development of multivariate disease liability models for complex neurobiological phenotypes.

Despite the advantages of the current approach over the original proof-of-concept study, a number of limitations remain. Most importantly, it is crucial to highlight that while we were able to show a statistical association between normative sex-related phenotypic diversity in brain structure and ASD probability, this relationship should not be interpreted as being 'causal'. Future studies will be needed to uncover the genetic and/or neurobiological mechanisms underpinning this relationship (e.g. (Baron-Cohen et al., 2015, Werling et al., 2016, Lai et al., 2017)). Second, due to the limited range of clinical/behavioral measures acquired in the current study, we were unable to determine the functional relevance of our findings. In the future it will be crucial to identify how diversity in normative sex-related morphometric phenotypes relates to sex-differences in general cognitive and/or behavioral profiles (Miller and Halpern, 2014, Hyde, 2016), or to different clinical ASD phenotypes (Szatmari et al., 2012, Bölte et al., 2011, Solomon et al., 2012, Mandy et al., 2012). Last, our study was based on a sample of adults with ASD without learning disability using a cross-sectional study design. The fact that our sample is not representative of the entire ASD population limits the generalizability of our sample probability estimates for ASD to the general population. Furthermore, our population estimations are based on previously reports of male preponderance in ASD being roughly a 4:1 male to female ratio (Baio, 2014), however other studies have shown this ratio may actually to be closer to 2:1 (Werling, 2016). The nature of our sample means further studies will thus be required to (*i*) replicate our findings in other subgroups on the autism spectrum (e.g. in children and adolescents, or individuals with a learning disability), and (*ii*) to identify how stable (or variable) our neuroanatomical indicators of biological sex are across different stages of development.

6.6 Conclusions

Taken together, our findings suggest that the male-typical neurobiological brain phenotype carries a higher probability for ASD than the female-typical phenotype across the binary categories dictated by biological sex, and across a range of neuroanatomical features that include both volumetric as well as geometric measures. In addition to genetic and environmental factors, multiple morphometric features characteristic of normative phenotypic diversity in brain structure should therefore be considered when investigating risk and resilience for ASD.

6.7 References

BAIO, J. 2014. Prevalence of autism spectrum disorder among children aged 8 years - autism and developmental disabilities monitoring network, 11 sites, United States, 2010. *MMWR Surveill Summ,* 63**,** 1-21.

BARON-COHEN, S., AUYEUNG, B., NØRGAARD-PEDERSEN, B., HOUGAARD, D., ABDALLAH, M., MELGAARD, L., COHEN, A., CHAKRABARTI, B., RUTA, L. & LOMBARDO, M. 2015. Elevated fetal steroidogenic activity in autism. *Molecular psychiatry,* 20**,** 369-376.

BÖLTE, S., DUKETIS, E., POUSTKA, F. & HOLTMANN, M. 2011. Sex differences in cognitive domains and their clinical correlates in higher-functioning autism spectrum disorders. *Autism***,** 1362361310391116.

CAHILL, L. 2017. A New Link Between Autism and Masculinity. *Jama psychiatry,* 74**,** 318-318.

CASANOVA, M. F. 2014. Autism as a sequence: from heterochronic germinal cell divisions to abnormalities of cell migration and cortical dysplasias. *Medical hypotheses,* 83**,** 32-38.

DALE, A. M., FISCHL, B. & SERENO, M. I. 1999. Cortical surface-based analysis: I. Segmentation and surface reconstruction. *Neuroimage,* 9**,** 179-194.

DEONI, S. C., WILLIAMS, S. C., JEZZARD, P., SUCKLING, J., MURPHY, D. G. & JONES, D. K. 2008. Standardized structural magnetic resonance imaging in multicentre studies using quantitative T1 and T2 imaging at 1.5 T. *Neuroimage,* 40**,** 662-671.

DWORZYNSKI, K., RONALD, A., BOLTON, P. & HAPPE, F. 2012. How different are girls and boys above and below the diagnostic threshold for autism spectrum disorders? *J Am Acad Child Adolesc Psychiatry,* 51**,** 788 - 97.

ECKER, C., ANDREWS, D., DELL'ACQUA, F., DALY, E., MURPHY, C., CATANI, M., DE SCHOTTEN, M. T., BARON-COHEN, S., LAI, M. & LOMBARDO, M. 2016. Relationship Between Cortical Gyrification, White Matter Connectivity, and Autism Spectrum Disorder. *Cerebral Cortex***,** bhw098.

ECKER, C., ANDREWS, D. S., GUDBRANDSEN, C. M. & ET AL. 2017. Association between the probability of autism spectrum disorder and normative sex-related phenotypic diversity in brain structure. *JAMA Psychiatry*.

ECKER, C., GINESTET, C., FENG, Y., JOHNSTON, P., LOMBARDO, M. V., LAI, M.-C., SUCKLING, J., PALANIYAPPAN, L., DALY, E. & MURPHY, C. M. 2013. Brain Surface Anatomy in Adults With Autism - The Relationship Between Surface Area, Cortical Thickness, and Autistic Symptoms. *JAMA psychiatry,* 70**,** 59-70.

ECKER, C., SHAHIDIANI, A., FENG, Y., DALY, E., MURPHY, C., D'ALMEIDA, V., DEONI, S., WILLIAMS, S. C., GILLAN, N., GUDBRANDSEN, M., WICHERS, R., ANDREWS, D., VAN HEMERT, L. & MURPHY, D. G. M. 2014. The effect of age, diagnosis, and their interaction on vertex-based measures of cortical thickness and surface area in autism spectrum disorder. *Journal of Neural Transmission,* 121**,** 1157-1170.

ECKER, C., SUCKLING, J., DEONI, S. C., LOMBARDO, M. V., BULLMORE, E. T., BARON-COHEN, S., CATANI, M., JEZZARD, P., BARNES, A., BAILEY, A. J., WILLIAMS, S. C., MURPHY, D. G. M. & CONSORTIUM, M. A. 2012. Brain Anatomy and Its Relationship to Behavior in Adults With Autism Spectrum Disorder. *Archives of General Psychiatry,* 69**,** 195-209.

FISCHL, B. & DALE, A. M. 2000. Measuring the thickness of the human cerebral cortex from magnetic resonance images. *Proceedings of the National Academy of Sciences,* 97**,** 11050-11055.
FISCHL, B., SERENO, M. I. & DALE, A. M. 1999. Cortical surface-based analysis: II: Inflation, flattening, and a surface-based coordinate system. *Neuroimage,* 9**,** 195-207.
FOMBONNE, E. 2009. Epidemiology of Pervasive Developmental Disorders. *Pediatr Res,* 65**,** 591-598.
HYDE, J. S. 2016. Sex and cognition: gender and cognitive functions. *Current opinion in neurobiology,* 38**,** 53-56.
IM, K., LEE, J.-M., LEE, J., SHIN, Y.-W., KIM, I. Y., KWON, J. S. & KIM, S. I. 2006. Gender difference analysis of cortical thickness in healthy young adults with surface-based methods. *Neuroimage,* 31**,** 31-38.
JOVICICH, J., CZANNER, S., GREVE, D., HALEY, E., VAN DER KOUWE, A., GOLLUB, R., KENNEDY, D., SCHMITT, F., BROWN, G. & MACFALL, J. 2006. Reliability in multi-site structural MRI studies: effects of gradient non-linearity correction on phantom and human data. *Neuroimage,* 30**,** 436-443.
LAI, M.-C., LOMBARDO, M. V., AUYEUNG, B., CHAKRABARTI, B. & BARON-COHEN, S. 2015. Sex/gender differences and autism: setting the scene for future research. *Journal of the American Academy of Child & Adolescent Psychiatry,* 54**,** 11-24.
LAI, M. C., LERCH, J. P., FLORIS, D. L., RUIGROK, A. N., POHL, A., LOMBARDO, M. V. & BARON‐COHEN, S. 2017. Imaging sex/gender and autism in the brain: Etiological implications. *Journal of Neuroscience Research,* 95**,** 380-397.
LORD, C., RISI, S., LAMBRECHT, L., COOK JR, E. H., LEVENTHAL, B. L., DILAVORE, P. C., PICKLES, A. & RUTTER, M. 2000. The Autism Diagnostic Observation Schedule—Generic: A standard measure of social and communication deficits associated with the spectrum of autism. *Journal of autism and developmental disorders,* 30**,** 205-223.
LORD, C., RUTTER, M. & COUTEUR, A. 1994. Autism Diagnostic Interview-Revised: a revised version of a diagnostic interview for caregivers of individuals with possible pervasive developmental disorders. *Journal of autism and developmental disorders,* 24**,** 659-685.
MANDY, W., CHILVERS, R., CHOWDHURY, U., SALTER, G., SEIGAL, A. & SKUSE, D. 2012. Sex differences in autism spectrum disorder: evidence from a large sample of children and adolescents. *Journal of autism and developmental disorders,* 42**,** 1304-1313.
MARQUAND, A., HOWARD, M., BRAMMER, M., CHU, C., COEN, S. & MOURÃO-MIRANDA, J. 2010. Quantitative prediction of subjective pain intensity from whole-brain fMRI data using Gaussian processes. *NeuroImage,* 49**,** 2178-2189.
MARQUAND, A. F., BRAMMER, M., WILLIAMS, S. C. & DOYLE, O. M. 2014. Bayesian multi-task learning for decoding multi-subject neuroimaging data. *NeuroImage,* 92**,** 298-311.
MCCARTHY, M. G., DE VRIES; FORGER, NANCY 2017. Sexual Differentiation of the Brain: A Fresh Look at Mode, Mechanisms, and Meaning. *Hormones, Brain and Behavior.* 3rd ed.: Oxford: Academic Press.
MCCARTHY, M. M. & KONKLE, A. T. 2005. When is a sex difference not a sex difference? *Frontiers in neuroendocrinology,* 26**,** 85-102.

MILLER, D. I. & HALPERN, D. F. 2014. The new science of cognitive sex differences. *Trends in cognitive sciences,* 18**,** 37-45.
NORDAHL, C. W., DIERKER, D., MOSTAFAVI, I., SCHUMANN, C. M., RIVERA, S. M., AMARAL, D. G. & VAN ESSEN, D. C. 2007. Cortical Folding Abnormalities in Autism Revealed by Surface-Based Morphometry. *The Journal of Neuroscience,* 27**,** 11725-11735.
PANIZZON, M. S., FENNEMA-NOTESTINE, C., EYLER, L. T., JERNIGAN, T. L., PROM-WORMLEY, E., NEALE, M., JACOBSON, K., LYONS, M. J., GRANT, M. D. & FRANZ, C. E. 2009. Distinct genetic influences on cortical surface area and cortical thickness. *Cerebral Cortex***,** bhp026.
RAKIC, P. 1995. A small step for the cell, a giant leap for mankind: a hypothesis of neocortical expansion during evolution. *Trends in neurosciences,* 18**,** 383-388.
RASMUSSEN, C. E. & WILLIAMS, C. K. I. 2006. *Gaussian processes for machine learning*, MIT press Cambridge, MA.
SCHAER, M., CUADRA, M. B., TAMARIT, L., LAZEYRAS, F., ELIEZ, S. & THIRAN, J. 2008. A surface-based approach to quantify local cortical gyrification. *Medical Imaging, IEEE Transactions on,* 27**,** 161-170.
SCHAER, M., OTTET, M.-C., SCARIATI, E., DUKES, D., FRANCHINI, M., ELIEZ, S. & GLASER, B. 2013. Decreased frontal gyrification correlates with altered connectivity in children with autism. *Frontiers in human neuroscience,* 7.
SÉGONNE, F., DALE, A., BUSA, E., GLESSNER, M., SALAT, D., HAHN, H. & FISCHL, B. 2004. A hybrid approach to the skull stripping problem in MRI. *Neuroimage,* 22**,** 1060-1075.
SOLOMON, M., MILLER, M., TAYLOR, S. L., HINSHAW, S. P. & CARTER, C. S. 2012. Autism symptoms and internalizing psychopathology in girls and boys with autism spectrum disorders. *Journal of autism and developmental disorders,* 42**,** 48-59.
SOWELL, E. R., PETERSON, B. S., KAN, E., WOODS, R. P., YOSHII, J., BANSAL, R., XU, D., ZHU, H., THOMPSON, P. M. & TOGA, A. W. 2007. Sex differences in cortical thickness mapped in 176 healthy individuals between 7 and 87 years of age. *Cerebral cortex,* 17**,** 1550-1560.
SZATMARI, P., LIU, X. Q., GOLDBERG, J., ZWAIGENBAUM, L., PATERSON, A. D., WOODBURY‐SMITH, M., GEORGIADES, S., DUKU, E. & THOMPSON, A. 2012. Sex differences in repetitive stereotyped behaviors in autism: implications for genetic liability. *American Journal of Medical Genetics Part B: Neuropsychiatric Genetics,* 159**,** 5-12.
WALLACE, G. L., DANKNER, N., KENWORTHY, L., GIEDD, J. N. & MARTIN, A. 2010. Age-related temporal and parietal cortical thinning in autism spectrum disorders. *Brain***,** awq279.
WECHSLER, D. 1999. *Wechsler abbreviated scale of intelligence*, Psychological Corporation.
WERLING, D. M. 2016. The role of sex-differential biology in risk for autism spectrum disorder. *Biology of Sex Differences,* 7**,** 58.
WERLING, D. M., PARIKSHAK, N. N. & GESCHWIND, D. H. 2016. Gene expression in human brain implicates sexually dimorphic pathways in autism spectrum disorders. *Nature communications,* 7.
WINKLER, A. M., SABUNCU, M. R., YEO, B., FISCHL, B., GREVE, D. N., KOCHUNOV, P., NICHOLS, T. E., BLANGERO, J. & GLAHN, D. C. 2012. Measuring and

comparing brain cortical surface area and other areal quantities. *NeuroImage,* 61**,** 1428-1443.
WORSLEY, K., ANDERMANN, M., KOULIS, T., MACDONALD, D. & EVANS, A. 1999. Detecting changes in nonisotropic images. *Human brain mapping,* 8**,** 98-101.

6.7 Acknowledgements: We would like to thank all of our participants and their family members for partaking in this study. The Autism Imaging Multicentre Study Consortium, members in alphabetical order are: Anthony J. Bailey (Oxford), Simon Baron-Cohen (Cambridge), Patrick F. Bolton (IoP), Edward T. Bullmore (Cambridge), Sarah Carrington (Oxford), Marco Catani (IoPPN), Bhismadev Chakrabarti (Cambridge), Michael C. Craig (IoPPN), Eileen M. Daly (IoPPN), Sean C. L. Deoni (IoPPN), Christine Ecker (IoPPN), Francesca Happé (IoPPN), Julian Henty (Cambridge), Peter Jezzard (Oxford), Patrick Johnston (IoPPN), Derek K. Jones (IoPPN), Meng-Chuan Lai (Cambridge), Michael V. Lombardo (Cambridge), Anya Madden (IoPPN), Diane Mullins (IoPPN), Clodagh M. Murphy (IoPPN), Declan G. M. Murphy (IoPPN), Greg Pasco (Cambridge), Amber N. V. Ruigrok (Cambridge), Susan A. Sadek (Cambridge), Debbie Spain (IoPPN), Rose Stewart (Oxford), John Suckling (Cambridge), Sally J. Wheelwright (Cambridge), Steven C. Williams (IoPPN), and C. Ellie Wilson (IoPPN). The EU-AIMS Consortium. Furthermore, we would like to thank the National Institute for Health Research Biomedical Research Centre for Mental Health, the Dr. Mortimer and Theresa Sackler Foundation, and the German Research Foundation (DFG).

6.8 Funding: The study represents independent research partly funded by the National Institute for Health Research (NIHR) Biomedical Research Centre at South London and Maudsley NHS Foundation Trust and King's College London. The views expressed are those of the authors and not necessarily those of the NHS, the NIHR or the Department of Health. This work was also supported by funding from the Medical Research Council UK (grant number G0400061); the Innovative Medicines Initiative Joint Undertaking (grant number 115300), which includes financial contributions from the EU Seventh Framework Programme (FP7/2007-2013) from the European Federation of Pharmaceutical Industries and Associations companies in kind; the Sackler foundation and from Autism Speaks.

6.9 Statement of Disclosure: Professor Edward Bullmore is employed half-time by GlaxoSmithKline and holds GSK shares. Dr. Meng-Chuan Lai receives financial support from the O'Brien Scholars Program within the Child and Youth Mental Health Collaborative at the Centre for Addiction and Mental Health and The Hospital for Sick Children, Toronto. None of the remaining authors have declared any conflict of interest or financial interests, which may arise from being named as an author on the manuscript.

Chapter 7: General Discussion

The studies that comprise this thesis employed structural magnetic resonance imaging (MRI) and novel analytical frameworks to address three overarching aims, namely *i*) developing novel neuroimaging features that are informative (e.g. of diagnostic or prognostic value) for the condition, *ii*) evaluating the efficacy of structural neuroimaging features to identify ASD cases within the clinical setting, and *iii*) investigating the role of normative sex differences in brain structure and their influence on the probability for ASD. Collectively these studies share the broader goal of advancing the field of neuroimaging research in a direction that provides real world translational value for ASD individuals and stakeholders. First, the present chapter aims to summarize the key findings of each of the four studies that were presented in this thesis. Second, possible interpretations of these results are provided, particularly with regards to moving neuroimaging studies in ASD closer to the development of translational imaging tools. Last, strengths and limitations of the presented studies will be discussed, followed by final conclusions.

7.1 Summary and Key Findings

7.1.1 Study 1: Tissue Contrast as a Novel Imaging Marker in Autism Spectrum Disorder

The aim of this study was to determine if previous post-mortem reports of poor definition of the grey–white matter boundary in autism spectrum disorder (ASD) (Avino and Hutsler, 2010) could be detected using a whole brain *in vivo* MRI approach. To accomplish this, we used a novel application of tissue signal intensity contrast measures sampled at and around the grey-white matter boundary (Salat et al., 2009, Andrews et al., 2017). As hypothesized, we determined that individuals with ASD had significantly less well-defined grey-white matter percent contrast (GWPC) across the grey-white matter boundary. This effect appeared to be largely driven by an increase in grey matter signal intensities in individuals with ASD. Taken together, our findings suggest that measures of GWPC sampled across cortical layers may serve as an *in vivo* proxy measure for irregular microstructural organization of the cortex in ASD.

7.1.2 Study 2: Clinical Validation of Multivariate Pattern Classification Models for Autism Spectrum Disorder

This study sought to first establish predictive models for the broader ASD phenotype based on measures of cortical neuroanatomy within a well-defined sample consisting of typically developing (TD) and ASD male adults acquired in the research setting. The second and primary aim of this study was to test the efficacy of these classification models to identify individuals with ASD within an independent clinical sample. Two different well established pattern classification algorithms, namely the support vector machine (SVM; Vapnik, 1995) and Gaussian process classifier (GPC; Rasmussen and Williams, 2006, Marquand et al., 2010), were used to establish classifiers based on the research sample utilizing measures of either cortical volume, thickness (CT), surface area (SA), the local gyrification index (*l*GI), sulcal depth (SULC), or grey-white matter percent contrast (GWPC). Based on previously reported findings (Ecker et al., 2010, Jiao et al., 2010) we hypothesized that these structural measures are able to discriminate individuals with ASD and TD controls significantly above chance levels. However, given differences in inclusion criteria between our research training and clinical testing samples, and based on previous findings of classification models showing reduced performance in the range of 10-15% when applied to independent testing sets (Sabuncu and Konukoglu, 2014), we expected a reduction in overall accuracy when predicting ASD diagnosis within the clinical sample.

While some classifiers showed modest classification accuracies (61%) within the research sample, we were not able to establish the statistical significance of these classifiers due to the small size of our training set. However, in an exploratory analysis we applied our best performing models to predict ASD diagnoses within the independent clinical sample. We established that the majority of these models showed decreased overall classification accuracies within the clinical testing set. One noteable exception to this was the GPC utilizing measures of grey-white matter percent contrast (GWPC) sampled at the grey-white matter boundary (Andrews et al. 2017), which showed high overall accuracy within the clinical sample (81%). However, given this model's initial performance in the research setting this result must be considered as preliminary at best.

7.1.3 Studies 3 and 4: Association of Normative Sex-Related Phenotypic Diversity in Brain Structure with Probability for Autism Spectrum Disorder

These two studies sought to directly investigate possible biological underpinnings of male preponderance in ASD (Lai et al., 2017, Werling, 2016). The aims of these studies were three-fold; *i*) to provide a phenotypic characterization of normative sex related diversity in brain structure, *ii*) to determine how diversity in sex based neurophenotypes is associated with probability for ASD, and *iii*) to estimate variability in ASD prevalence in the general population as a function of normative sex-related phenotypic diversity in brain structure. To accomplish this, we first established normative predictive models in male and female TD individuals for the binary classes dictated by biological sex. In study 3, we report initial findings using measures of CT (Ecker et al., 2017), and in study 4 we extended the analytical framework to include measures of SA, *l*GI, and SULC. The use of GPC (Rasmussen and Williams, 2006, Marquand et al., 2010) allowed us to effectively represent the diversity of sex based neurophenotypes along a singular axis dictated by predictive class probabilities ranging from the female- to male-typical neurophenotype. Once established, these normative models were applied to males and females with ASD.

In both studies we found that sample probabilities for ASD increased with predicative probabilities for the male-typical class. This was largely due to a statistically significant shift towards more male-typical neurophenotypes in females with ASD across all cortical measures. We then extrapolated sample probabilities for ASD among individuals with female- and male-typical neurophenotypes to estimate their association with ASD prevalence within the general population. Based on previous population prevalence estimates (Baio, 2014), we demonstrate that biological females with more male-typical brain morphology (2.6% estimated prevalence) are 26 times more likely to have ASD compared to biological females with female-typical neuroanatomical phenotypes (0.1% estimated prevalence). Biological males with male-typical brain morphometry showed an estimated population prevalence of 2.4%, which is in line with previously reported rates. In addition, males with female-typical phenotypes showed a reduced prevalence estimate for ASD (1.9%). Taken

together, these results support the notion that there is differential liability for ASD between the sexes, which increases from a female to male phenotypic presentation of the brain, and is also indicative of a 'female protective effect' for ASD in terms of brain anatomy.

7.2 Discussion

7.2.1 The Development of Imaging Features for Autism Spectrum Disorders

The past decade has seen several advances in the development of structural MRI features to study the neuroanatomical underpinnings of ASD. Studies continue to move away from investigating relatively unspecific, gross-anatomical measures, such as total brain volume, to using more advanced metrics that represent particular aspects of neuroanatomical structure and development (Ecker et al., 2015). For example, surface based morphometry (SBM) measures of CT and SA have been shown to be *i*) mediated by different sets of genes (Panizzon et al., 2009), *ii*) have different developmental trajectories (Ecker et al., 2014), and *iii*) represent distinct aspects of the cortical architecture (Rakic, 1995). Thus, these measures are well suited to explore etiological theories for ASD, which suggest that the condition arises from atypical neuronal proliferation, migration, and maturation (Casanova, 2014). The development of novel neuroimaging features that map onto specific aspects of the ASD phenotype thus offers the potential for both greater insight into the biological underpinnings of ASD, and the possibility for such features to act as imaging biomarkers.

One neuropathological finding that remained relatively underexplored *in vivo* is atypical cell patterning at the grey-white matter boundary in ASD (Avino and Hutsler, 2010). The current thesis presented a novel *in vivo* approach to quantify this specific neuroanatomical feature (Andrews et al., 2017). This was done with the purpose of investigating a critical aspect of neurodevelopment believed to contribute to poor grey-white matter boundary integrity in ASD, namely the formation and resolution of the cortical subplate (Hoerder-Suabedissen and Molnár, 2015). During neurodevelopment, cells within the subplate are critical for establishing proper cortical structure and connectivity by guiding both migrating neurons and innervating

cortico-cortico and thalamo-cortical axons (Allendoerfer and Shatz, 1994). Thus, disruptions to subplate development and apoptosis may contribute to both atypical cortical structure and connectivity observed within ASD (Hutsler and Avino, 2015).

The importance of the subplate in establishing inter-cortical connectivity is supported by reports suggesting that this structure is thicker within highly connected cortical association areas (Kostovic and Rakic, 1990). This has recently been linked to the downward dispersion of subplate cells resulting from a high degree of axonal innervation in these regions (Duque et al., 2016). Within the current study, significant increases in grey matter signal intensity in ASD were largely localized to association areas that underpin social processing and wider socio-cognitive functioning, including regions of the temporal lobe, the temporal parietal junction, and fusiform gyrus. Thus, the increased signal intensities in adults with ASD in these regions may reflect the consequences of an atypical formation of cortical connections during early brain development, potentially resulting in increased myelination and hyper local connectivity (Belmonte et al., 2004).

Moreover, our examination of grey-white matter percent tissue contrast (GWPC) at the grey-white matter boundary represents a direct attempt to quantify a specific neuropathological mechanism in ASD (i.e. poor delineation of this boundary). Accordingly, this feature is likely to have greater effects sizes within ASD individuals than other, more general measures of cortical morphometry. This is of key importance for translational studies seeking to use brain imaging features to make prognostic or diagnostic predictions within ASD. For example, in the context of pattern recognition it has been shown that the best predictor of successful classification of ASD is not the particular algorithm used but training models on imaging features with significant effects sizes in the condition (Sabuncu and Konukoglu, 2014). Thus, measures such as GWPC that map onto particular aspects of ASD neuropathology are likely to be valuable to translational research for their potential increased sensitivity to detect the condition.

7.2.2 The Development of Diagnostic Imaging Tools for Autism Spectrum Disorder

Increasingly, through applications of multivariate pattern classification, studies have provided proof of concept evidence that individuals with ASD can be identified with high accuracy in the research setting based on neuroimaging features (Ecker et al., 2010, Ingalhalikar et al., 2011, Just et al., 2014). The implementation of predictive models for ASD would offer significant benefits to patients and stakeholders. Such benefits could come through early identification of the condition allowing for intervention and treatment to begin at a younger age. Furthermore, this would provide clinicians biologically based evidence when making a diagnosis of ASD, which currently is reliant solely on behavioral assessments. However, to date no studies have tested classification models for ASD trained in the research environment on independent samples that are representative of the broader clinical population. This is important because inclusion criteria for participation in ASD research are likely to introduce several phenotypic differences between research and clinical ASD cohorts.

Within the current study, our best performing classifiers for ASD in the research setting showed modest overall accuracies (61%). While this is within the range of previous models tested on independent samples (Sabuncu and Konukoglu, 2014, Shen et al., 2017), we were not able to establish the statistical significance of these classifiers due to the small size of our research sample. However, as an exploratory step we applied the best performing classifiers within the training set to predict ASD within the clinical sample. We found a GPC based on measures of grey-white matter percent contrast (GWPC) taken at the grey-white matter boundary (Andrews et al., 2017) to have high overall accuracy within the clinical sample (81%) across all diagnostic sub-categories (74-88%). This preliminary result supports the concept that features developed to map onto particular aspects of ASD neuropathology have an increased sensitivity to detect the condition. However, given that we could not show this model performed significantly better than chance within the research setting (p=0.197), this finding must be considered as suggestive only.

A major impediment to classifying individuals with ASD at high accuracy is the highly heterogeneous nature of the phenotype. As a result, maximal classification

accuracy based on brain structure across the ASD population is likely to be modest. Thus, the development of approaches that directly address phenotypic heterogeneity within ASD will be of critical importance for the successful delivery of classification methods that have translational value in clinical settings. Several individual variables including exogenous factors and genetic disposition may contribute to neuroanatomical variance in ASD. One variable that has been shown to have strong associations with ASD is biological sex (Lai et al., 2017, Werling, 2016). Accordingly, a major theme of this thesis dealt with identifying how normative variance in brain structure associated with biological sex is associated with probability for ASD.

7.2.3 Neuro-Diversity Associated with Biological Sex and Probability for Autism Spectrum Disorder

It has been suggested that on a phenotypic level, the brain should be considered a 'mosaic' of regions that differ between degrees of relative maleness or femaleness, or not at all (i.e. unisex), resulting in a potentially infinite variety of brain phenotypes both within and between the sexes (McCarthy, 2017). The studies presented in this thesis employed a multivariate classification approach that allowed us to represent diversity in sex based neurophenotypes along a continuum ranging from typically male to female. This 'more nuanced' approach to investigating sex differentiation in the brain represents a key advancement as it can accommodate the long-standing notion that both males and females are subject to various degrees of masculinization and feminization (Whalen, 1974).

Through this normative modelling approach we were able to estimate an individual's probability of ASD based on phenotypic, rather than biological sex. Using this approach, we demonstrated that an individual's probability for developing ASD can vary from 0.1 to 2.6% in the general population depending on having a female- or male-typical neuroanatomical phenotype, while being biologically male or female. Thus, these phenotypic measures that represent variable degrees of sexual differentiation in individuals, may serve as an important factor in future multivariate disease liability models for complex neurobiological phenotypes such as ASD.

Moreover, we established that the neuroanatomical patterns associated with prediction of biological sex differed in region and sign between the sexes, and individuals with female- and male-typical neurophenotypes. This finding is consistent with the idea that sex-dependent mechanisms have region specific effects in the brain, and that the neuroanatomical patterns associated with high and low probability for ASD may be used to identify brain regions where sexual differentiation contributes to male preponderance in ASD prevalence. Given the significant association between biological sex and ASD prevalence, these findings contribute to ongoing research efforts into the etiological underpinnings of ASD, and potentially other mental health disorders with sex differences in prevalence (Cahill, 2017).

7.3 Strengths of the Current Studies

The studies that comprised this thesis have a number of benefits. First, to the best of our knowledge, we present the first study to investigate grey-white matter boundary integrity *in vivo* in ASD. In doing so we established a novel imaging feature in the form of percent contrast of grey-white matter signal intensity (GWPC) taken at and around the grey-white matter boundary. Given that GWPC potentially maps onto a specific neuropathological feature in ASD, the measure is likely to be particularly useful to future ASD researchers as it has large effect sizes (i.e. 'biological footprint') in the condition in comparison to many other cortical morphometric features. Second, through collaboration with the Autism Assessment and Behavioural Genetics Service at the Bethlem Royal Hospital, South London and Maudsley NHS Foundation Trust, we were able to recruit a highly representative sample of ASD individuals within the clinical setting. Several neuroimaging studies have sought to develop a diagnostic imaging biomarker for ASD within the research setting. However, inherent differences in the clinical phenotype between research and clinical ASD samples are likely to exist (see Chapter 4.1). Therefore, the recruitment of a clinical sample such as the one presented in the current study is of critical importance for testing the translational value of classifiers established in the research setting. Third, this thesis presents the first proof of concept studies linking normative variability in brain structure associated with biological sex to the probability for ASD. A particular strength of these studies was the use of Bayesian pattern recognition methods to effectively represent biological sex along a continuum. This nuanced approach

allowed us to move beyond simple binary sex categories and more fully capture the spectra of neurodiversity associated with differentiation between the sexes (McCarthy, 2017).

7.4 Limitations

Collectively, the presented studies face limitations common to several structural neuroimaging investigations in ASD. The high cost of MRI along with the significant amount of time, energy, and expertise needed to recruit patients to participate in imaging research presents inherent limitations on sample sizes. Furthermore, the nature of MRI acquisition also hinders the collection of samples that accurately reflect the entire spectrum of ASD phenotypes. Often, individuals with particularly severe ASD symptoms and/or comorbid learning disability are unable or unwilling to conform to the requirements that MRI acquisition demands, namely lying motionless within a confined noisy space for an extended period of time. Consequentially, so called 'low functioning' individuals with ASD are nearly absent within the neuroimaging literature.

Despite these limitations, however, our studies investigating tissue contrast and the association between biological sex and ASD probability benefit from relatively large sample sizes (n ~100), which is above what has been shown to be required for the identification of subtle group differences in cortical measures (n=50, Pardoe et al., 2013). Furthermore, inclusion of nearly 50 females with ASD represents one of the largest imaging samples of females with the condition reported to date. However, the recruitment of adult samples introduces limitations when studying a neurodevelopmental condition such as ASD that likely originates during early prenatal stages of life (Bauman and Kemper, 2005). The developmental trajectories of the variety of structural neuroimaging measures within this study are yet to be firmly established, but are likely to non-linear and complex (Ecker et al., 2014). Thus, it remains uncertain if, and how, the current results identified within adults will translate to infants, toddlers, adolescents, and elders with ASD. Ultimately, future longitudinal studies that recruit participants during the first stages of life (e.g. fetal and/or neonatal) who are followed up with across the lifespan will be invaluable to the study of ASD.

The current studies utilized state of the art MRI methods for investigating cortical structure *in vivo* within a clinical population. While these methods offer many improvements over more traditional MRI methods, such as voxel based morphometry (VBM), they are still limited in several ways. The current high end resolution of 3T structural MRI scans is roughly $1mm^3$. It has been estimated that a $1mm^3$ volume in the cerebral cortex may contain upwards of 630,000 neuron cells and as many as four times that number of glial cells (Lent et al., 2012). Therefore, the current resolution offered by structural MRI does not allow for the investigation of fine aspects of neuro-biology such as cell patterning of individual cortical layers, and is thus limited to gross volumetric and geometric measures. Accordingly, one of the greatest limitations of structural neuroimaging studies remains a lack of understanding of the underlying biological mechanisms that contribute to imaging measures. For example, atypical CT measures in ASD may reflect gross numbers of neuronal cells within the cortical sheet (Courchesne et al., 2011), degrees of dendritic arborization (Tang et al., 2014), or myelination processes (Sowell et al., 2004). Adding to the complexity, it is likely that each of these variables contribute to CT to different degrees and kind across individuals and developmental stages. Future research is thus required to investigate the specific cytoarchitectural abnormalities underlying ASD.

7.5 Future Directions

7.5.1 Large Scale Studies and Heterogeneity

The use of MRI techniques to investigate ASD is a relatively novel and rapidly growing field. In this context, it is perhaps unsurprising that many of the limitations outlined above remain to be addressed. Ongoing efforts such as the Autism Brain Imaging Database Exchange (ABIDE), Infant Brain Imaging Study (IBIS), Autism Phenome Project (APP) and European Autism Interventions Study (EU-AIMS) are currently recruiting and scanning large numbers of individuals with autism across the full spectrum of impairment, and at the earliest stages of neurodevelopment. The collection of large scale, high quality, imaging data sets that accurately reflect the phenotypic heterogeneity observed in the broader ASD population will be invaluable, and constitute an essential step towards addressing issues surrounding ASD heterogeneity.

Moreover, current efforts to better understand the biological underpinnings of ASD and develop both efficacious treatments and biomarkers for the condition are hindered by the diversity of clinical phenotypes incorporated under ASD diagnostic criteria. Thus, the stratification of the ASD phenotype into biologically more homogeneous subtypes is of critical importance for advancing studies of ASD etiology, and efforts towards developing imaging tools for translational applications. Recent applications of normative models that seek to identify deviations in particular behavioral measures within individuals from a population distribution represent a critical advancement in this area of research (Marquand et al., 2016). These methods appear to be particularly well suited for parsing ASD through their ability to infer how certain atypical behaviors map onto biology and thus identify homogenous biological subtypes in ASD associated with degrees of variation in behavioral measures when compared to a healthy cohort.

7.5.2 Development and Implementation of Multi-Modal Methods

Increasingly, neuroimaging studies of ASD incorporate several different imaging features and modalities. Such multimodal imaging studies are extremely valuable because different imaging sequences (e.g. diffusion, functional, structural) can be used to capture unique aspects of neuropathology in ASD. However, standard practice for multimodal studies still involves investigating features in a parallel (i.e. unimodal) fashion. Thus, interpretation of the relationship between results in different modalities is conducted in a post-hoc manner. In order to determine the inter-relationships between different imaging measures, and to take full advantage of the unique strengths that each modality offers, so-called multimodal 'fusion methods' are required. For example, linked independent component analysis can be used to identify components comprised of shared variance across multiple imaging features, regardless of differences in spatial dimensions between them (Groves et al., 2012). Such methods have already shown the ability to identify multimodal components associated with particular behaviors associated with ADD (Francx et al., 2016), and thus may offer value in efforts to parse the heterogeneity of ASD.

7.5.3 Linking Imaging with Biology

Lastly, the development of surface based morphometry measures that represent distinct aspects of cortical architecture and etiology has provided unique insights into

the potential underlying biological mechanisms driving differences in these measures in individuals with ASD. However, there is a critical need for establishing concrete links between macroscopic imaging measures and microscopic biology within individuals. Recent advancements in the use of cellular models based on patient-specific induced pluripotent stem cells (iPSCs) offer particular promise to address this relationship. Through a typical biopsy (e.g. skin, hair ect.), this technology allows for the delivery of in vitro neuron cells from particular patients (Takahashi and Yamanaka, 2006, Takahashi et al., 2007). Accordingly, many of the developmental events believed to be atypical in ASD can be recapitulated and observed in the culture dish (Marchetto and Gage, 2012) and then related to neuroimaging measures, all within the same individual in a safe, *in vivo*, minimally invasive fashion.

7.5 Conclusion

The studies that comprise this thesis highlight advances in the field of structural neuroimaging research in autism spectrum disorder (ASD) in areas of feature development, clinical translation, and efforts to understand the modulating role of biological sex on the prevalence of ASD. Here we first introduced a novel *in vivo* feature based on tissue contrast to measure atypical cortical microstructure that has previously been reported in histological studies. Second, we trained classification models for ASD in the research setting and then tested the ability of these models to make diagnostic predictions within a representative clinical ASD sample. Last, we established normative models of phenotypic diversity in brain structure associated with biological sex in a sample of typically developing (TD) males and females, which we subsequently applied to males and females with ASD to identify the association between sex based neurophenotypes and ASD probability. Taken together, the body of work presented within this thesis constitutes an important step forward toward establishing translational imaging tools for ASD that may one day be applied in the clinical setting. However, future studies will be required to address the large degree of phenotypic heterogeneity in ASD, develop methods that can take full advantage of multimodal imaging data, and identify the biological underpinnings of macroscopic neuroimaging measures.

7.6 References

ALLENDOERFER, K. L. & SHATZ, C. J. 1994. The subplate, a transient neocortical structure: its role in the development of connections between thalamus and cortex. *Annual review of neuroscience,* 17**,** 185-218.

ANDREWS, D. S., AVINO, T. A., GUDBRANDSEN, M., DALY, E., MARQUAND, A., MURPHY, C. M., LAI, M.-C., LOMBARDO, M. V., RUIGROK, A. N. & WILLIAMS, S. C. 2017. In Vivo Evidence of Reduced Integrity of the Gray–White Matter Boundary in Autism Spectrum Disorder. *Cerebral Cortex*.

AVINO, T. A. & HUTSLER, J. J. 2010. Abnormal cell patterning at the cortical gray–white matter boundary in autism spectrum disorders. *Brain Research,* 1360**,** 138-146.

BAIO, J. 2014. Prevalence of autism spectrum disorder among children aged 8 years - autism and developmental disabilities monitoring network, 11 sites, United States, 2010. *MMWR Surveill Summ,* 63**,** 1-21.

BAUMAN, M. L. & KEMPER, T. L. 2005. Neuroanatomic observations of the brain in autism: a review and future directions. *International Journal of Developmental Neuroscience,* 23**,** 183-187.

BELMONTE, M. K., ALLEN, G., BECKEL-MITCHENER, A., BOULANGER, L. M., CARPER, R. A. & WEBB, S. J. 2004. Autism and abnormal development of brain connectivity. *The Journal of Neuroscience,* 24**,** 9228-9231.

CAHILL, L. 2017. A New Link Between Autism and Masculinity. *Jama psychiatry,* 74**,** 318-318.

CASANOVA, M. F. 2014. Autism as a sequence: from heterochronic germinal cell divisions to abnormalities of cell migration and cortical dysplasias. *Medical hypotheses,* 83**,** 32-38.

COURCHESNE, E., MOUTON, P. R., CALHOUN, M. E., SEMENDEFERI, K., AHRENS-BARBEAU, C., HALLET, M. J., BARNES, C. C. & PIERCE, K. 2011. Neuron number and size in prefrontal cortex of children with autism. *JAMA: The Journal of the American Medical Association,* 306**,** 2001-2010.

DUQUE, A., KRSNIK, Z., KOSTOVIĆ, I. & RAKIC, P. 2016. Secondary expansion of the transient subplate zone in the developing cerebrum of human and nonhuman primates. *Proceedings of the National Academy of Sciences,* 113**,** 9892-9897.

ECKER, C., ANDREWS, D. S., GUDBRANDSEN, C. M. & ET AL. 2017. Association between the probability of autism spectrum disorder and normative sex-related phenotypic diversity in brain structure. *JAMA Psychiatry*.

ECKER, C., BOOKHEIMER, S. Y. & MURPHY, D. G. M. 2015. Neuroimaging in autism spectrum disorder: brain structure and function across the lifespan. *The Lancet Neurology,* 14**,** 1121-1134.

ECKER, C., MARQUAND, A., MOURÃO-MIRANDA, J., JOHNSTON, P., DALY, E. M., BRAMMER, M. J., MALTEZOS, S., MURPHY, C. M., ROBERTSON, D. & WILLIAMS, S. C. 2010. Describing the brain in autism in five dimensions—magnetic resonance imaging-assisted diagnosis of autism spectrum disorder using a multiparameter classification approach. *The Journal of Neuroscience,* 30**,** 10612-10623.

ECKER, C., SHAHIDIANI, A., FENG, Y., DALY, E., MURPHY, C., D'ALMEIDA, V., DEONI, S., WILLIAMS, S. C., GILLAN, N., GUDBRANDSEN, M., WICHERS, R., ANDREWS, D., VAN HEMERT, L. & MURPHY, D. G. M. 2014. The effect of age, diagnosis, and their interaction on vertex-based measures of cortical

thickness and surface area in autism spectrum disorder. *Journal of Neural Transmission,* 121**,** 1157-1170.
FRANCX, W., LLERA, A., MENNES, M., ZWIERS, M. P., FARAONE, S. V., OOSTERLAAN, J., HESLENFELD, D., HOEKSTRA, P. J., HARTMAN, C. A. & FRANKE, B. 2016. Integrated analysis of gray and white matter alterations in attention-deficit/hyperactivity disorder. *NeuroImage: Clinical,* 11**,** 357-367.
GROVES, A. R., SMITH, S. M., FJELL, A. M., TAMNES, C. K., WALHOVD, K. B., DOUAUD, G., WOOLRICH, M. W. & WESTLYE, L. T. 2012. Benefits of multi-modal fusion analysis on a large-scale dataset: life-span patterns of inter-subject variability in cortical morphometry and white matter microstructure. *Neuroimage,* 63**,** 365-380.
HOERDER-SUABEDISSEN, A. & MOLNÁR, Z. 2015. Development, evolution and pathology of neocortical subplate neurons. *Nature Reviews Neuroscience,* 16**,** 133-146.
HUTSLER, J. J. & AVINO, T. 2015. The Relevance of Subplate Modifications to Connectivity in the Cerebral Cortex of Individuals with Autism Spectrum Disorders. *Recent Advances on the Modular Organization of the Cortex.* Springer.
INGALHALIKAR, M., PARKER, D., BLOY, L., ROBERTS, T. P. L. & VERMA, R. 2011. Diffusion based abnormality markers of pathology: Toward learned diagnostic prediction of ASD. *NeuroImage,* 57**,** 918-927.
JIAO, Y., CHEN, R., KE, X., CHU, K., LU, Z. & HERSKOVITS, E. H. 2010. Predictive models of autism spectrum disorder based on brain regional cortical thickness. *Neuroimage,* 50**,** 589-599.
JUST, M. A., CHERKASSKY, V. L., BUCHWEITZ, A., KELLER, T. A. & MITCHELL, T. M. 2014. Identifying autism from neural representations of social interactions: Neurocognitive markers of autism. *PloS one,* 9**,** e113879.
KOSTOVIC, I. & RAKIC, P. 1990. Developmental history of the transient subplate zone in the visual and somatosensory cortex of the macaque monkey and human brain. *Journal of Comparative Neurology,* 297**,** 441-470.
LAI, M. C., LERCH, J. P., FLORIS, D. L., RUIGROK, A. N., POHL, A., LOMBARDO, M. V. & BARON-COHEN, S. 2017. Imaging sex/gender and autism in the brain: Etiological implications. *Journal of Neuroscience Research,* 95**,** 380-397.
LENT, R., AZEVEDO, F. A., ANDRADE-MORAES, C. H. & PINTO, A. V. 2012. How many neurons do you have? Some dogmas of quantitative neuroscience under revision. *European Journal of Neuroscience,* 35**,** 1-9.
MARCHETTO, M. C. & GAGE, F. H. 2012. Modeling brain disease in a dish: really? *Cell stem cell,* 10**,** 642-645.
MARQUAND, A., HOWARD, M., BRAMMER, M., CHU, C., COEN, S. & MOURÃO-MIRANDA, J. 2010. Quantitative prediction of subjective pain intensity from whole-brain fMRI data using Gaussian processes. *NeuroImage,* 49**,** 2178-2189.
MARQUAND, A. F., REZEK, I., BUITELAAR, J. & BECKMANN, C. F. 2016. Understanding heterogeneity in clinical cohorts using normative models: beyond case-control studies. *Biological psychiatry,* 80**,** 552-561.
MCCARTHY, M. G., DE VRIES; FORGER, NANCY 2017. Sexual Differentiation of the Brain: A Fresh Look at Mode, Mechanisms, and Meaning. *Hormones, Brain and Behavior.* 3rd ed.: Oxford: Academic Press.

PANIZZON, M. S., FENNEMA-NOTESTINE, C., EYLER, L. T., JERNIGAN, T. L., PROM-WORMLEY, E., NEALE, M., JACOBSON, K., LYONS, M. J., GRANT, M. D. & FRANZ, C. E. 2009. Distinct genetic influences on cortical surface area and cortical thickness. *Cerebral Cortex*.

RAKIC, P. 1995. A small step for the cell, a giant leap for mankind: a hypothesis of neocortical expansion during evolution. *Trends in neurosciences,* 18**,** 383-388.

RASMUSSEN, C. E. & WILLIAMS, C. K. I. 2006. *Gaussian processes for machine learning*, MIT press Cambridge, MA.

SABUNCU, M. R. & KONUKOGLU, E. 2014. Clinical Prediction from Structural Brain MRI Scans: A Large-Scale Empirical Study. *Neuroinformatics***,** 1-16.

SALAT, D. H., LEE, S. Y., VAN DER KOUWE, A., GREVE, D. N., FISCHL, B. & ROSAS, H. D. 2009. Age-associated alterations in cortical gray and white matter signal intensity and gray to white matter contrast. *Neuroimage,* 48**,** 21-28.

SHEN, M. D., KIM, S. H., MCKINSTRY, R. C., GU, H., HAZLETT, H. C., NORDAHL, C. W., EMERSON, R. E., SHAW, D., ELISON, J. T., SWANSON, M. R., FONOV, V. S., GERIG, G., DAGER, S. R., BOTTERON, K. N., PATERSON, S., SCHULTZ, R. T., EVANS, A. C., ESTES, A. M., ZWAIGENBAUM, L., STYNER, M. A., AMARAL, D. G. & PIVEN, J. 2017. Increased Extra-axial Cerebrospinal Fluid in High-Risk Infants who Later Develop Autism. *Biological Psychiatry*.

SOWELL, E. R., THOMPSON, P. M., LEONARD, C. M., WELCOME, S. E., KAN, E. & TOGA, A. W. 2004. Longitudinal mapping of cortical thickness and brain growth in normal children. *The Journal of neuroscience,* 24**,** 8223-8231.

TAKAHASHI, K., TANABE, K., OHNUKI, M., NARITA, M., ICHISAKA, T., TOMODA, K. & YAMANAKA, S. 2007. Induction of pluripotent stem cells from adult human fibroblasts by defined factors. *cell,* 131**,** 861-872.

TAKAHASHI, K. & YAMANAKA, S. 2006. Induction of pluripotent stem cells from mouse embryonic and adult fibroblast cultures by defined factors. *cell,* 126**,** 663-676.

TANG, G., GUDSNUK, K., KUO, S.-H., COTRINA, MARISA L., ROSOKLIJA, G., SOSUNOV, A., SONDERS, MARK S., KANTER, E., CASTAGNA, C., YAMAMOTO, A., YUE, Z., ARANCIO, O., PETERSON, BRADLEY S., CHAMPAGNE, F., DWORK, ANDREW J., GOLDMAN, J. & SULZER, D. 2014. Loss of mTOR-Dependent Macroautophagy Causes Autistic-like Synaptic Pruning Deficits. *Neuron*.

VAPNIK, V. 1995. *The Nature of Statistical Learning Theory,* New York, Springer-Verlag.

WERLING, D. M. 2016. The role of sex-differential biology in risk for autism spectrum disorder. *Biology of Sex Differences,* 7**,** 58.

WHALEN, R. E. 1974. Sexual differentiation: Models, methods, and mechanisms. *Sex differences in behavior***,** 467-481.

Appendix I: ICD-10 Criteria for "Childhood Autism"

A. Abnormal or impaired development is evident before the age of 3 years in at least one of the following areas:

1. receptive or expressive language as used in social communication;

2. the development of selective social attachments or of reciprocal social interaction;

3. functional or symbolic play.

B. A total of at least six symptoms from (1), (2) and (3) must be present, with at least two from (1) and at least one from each of (2) and (3)

1. Qualitative impairment in social interaction are manifest in at least two of the following areas:

a. failure adequately to use eye-to-eye gaze, facial expression, body postures, and gestures to regulate social interaction;

b. failure to develop (in a manner appropriate to mental age, and despite ample opportunities) peer relationships that involve a mutual sharing of interests, activities and emotions;

c. lack of socio-emotional reciprocity as shown by an impaired or deviant response to other people's emotions; or lack of modulation of behavior according to social context; or a weak integration of social, emotional, and communicative behaviors;

d. lack of spontaneous seeking to share enjoyment, interests, or achievements with other people (e.g. a lack of showing, bringing, or pointing out to other people objects of interest to the individual).

2. Qualitative abnormalities in communication as manifest in at least one of the following areas:

a. delay in or total lack of, development of spoken language that is not accompanied by an attempt to compensate through the use of gestures or mime as an alternative mode of communication (often preceded by a lack of communicative babbling);

b. relative failure to initiate or sustain conversational interchange (at whatever level of language skill is present), in which there is reciprocal responsiveness to the communications of the other person;

c. stereotyped and repetitive use of language or idiosyncratic use of words or phrases;

d. lack of varied spontaneous make-believe play or (when young) social imitative play

3. Restricted, repetitive, and stereotyped patterns of behavior, interests, and activities are manifested in at least one of the following:

a. An encompassing preoccupation with one or more stereotyped and restricted patterns of interest that are abnormal in content or focus; or one or more interests that are abnormal in their intensity and circumscribed nature though not in their content or focus;

b. Apparently compulsive adherence to specific, nonfunctional routines or rituals;

c. Stereotyped and repetitive motor mannerisms that involve either hand or finger flapping or twisting or complex whole body movements;

d. Preoccupations with part-objects of non-functional elements of play materials (such as their oder, the feel of their surface, or the noise or vibration they generate).

C. The clinical picture is not attributable to the other varieties of pervasive developmental disorders; specific development disorder of receptive language (F80.2) with secondary socio-emotional problems, reactive attachment disorder (F94.1) or disinhibited attachment disorder (F94.2); mental retardation (F70-F72) with some associated emotional or behavioral disorders; schizophrenia (F20.-) of unusually early onset; and Rett's Syndrome (F84.12).

World Health Organization. (1992). *International classification of diseases: Diagnostic criteria for research* (10th edition). Geneva, Switzerland

Appendix II: Chapter 3 Supplementary Materials

Chapter 3 Supplementary Methods

Surface deformation procedure to place the grey-white matter boundary (i.e. white matter surface)

Within this study we refer to the white matter surface (i.e. the surface that defines the transition from grey to white matter) as the grey-white matter boundary. The surface deformation procedure that places the white matter surface has previously been described by Dale et al. (1999) and is detailed bellow.

First white matter voxels are labeled through a segmentation procedure. Contiguous white matter voxels are identified through a connected components algorithm resulting in a filled white matter labeled volume. This volume is then tessellated using two triangles to define each voxel composing the surface of the white matter volume. Deformation of this "jagged" white matter tessellation to the grey-white matter boundary is accomplished by a minimization of an energy functional. The first two terms of this energy functional act to smooth the surface and regularize the tessellation by introducing a spring like property to the surface. This spring property is decomposed into two terms given as,

$$J_n = \frac{1}{2V}\left(\sum_{i=1}^{V}\sum_{j\in N_1 i}(\mathbf{n}(i)\cdot(\mathbf{x}_i-\mathbf{x}_j))^2\right)$$

$$J_t = \frac{1}{2V}\left(\sum_{i=j}^{V}\sum_{j\in N_1 i}(\mathbf{e}_0(i)\cdot(\mathbf{x}_i-\mathbf{x}_j))^2+(\mathbf{e}_1(i)\cdot(\mathbf{x}_i-\mathbf{x}_j))^2\right)$$

where $N_1(i)$ denotes the set of nearest neighbors of the i^{th} vertex, V is the total number of vertices in the tessellation, $\mathbf{n}(i)$ is the unit normal vector to the surface at the i^{th} vertex, $[\mathbf{e}_0(i),\mathbf{e}_1(i)]$ is an orthonormal basis for the tangent plane at the i^{th} retex, and $\mathbf{x}_k$ regers to the (x,y,z) position of the k^{th} vertex in the tessellation. The term J_i results in the redistribution of vertices to regions where they are needed, encouraging a uniform spacing of vertices without requiring prohibitive numbers of elements. The term J_n imposes a smoothness constraint on the surface deformation by penalizing nodes that distance themselves from the direction normal to surface from its neighboring nodes. The third term of the energy functional is based on intensity values. The volume intensity at position x_i can be written as $I(x_i)$ and this term given as,

$$J_I = \frac{1}{2V}\left(\sum_{i=1}^{V}(T(i) - I(x_i))^2\right)$$

where T(i) is the mean white matter value of border voxels within a 5mm neighborhood of each vertex, within the segmented white matter volume. The value of I(x) is computed on a subvoxel basis using trilinear interpolation. The placement of the grey-white matter boundary is achieved by minimizing an energy function that is a weighted sum of the three terms presented above,

$$J = J_t + \lambda_n J_n + \lambda_I J_I$$

where the coefficients λ_n and λ_I specify the strength of the smoothness and regularization constraints in relation to the intensity term. The gradient of this functional defines the movement of the surface tessellation such as the movement of the k^{th} vertex is given by the negative of the directional derivative with respect to $\mathbf{x}_{k,,}$

$$-\frac{\partial J}{\partial \mathbf{x}_k} = \lambda_I\big(T(k) - I(\mathbf{X}_k)\big)\nabla I(\mathbf{x}_k) + \sum_{j\in N_1(k)}(\lambda_n\big(\mathbf{n}(k)\cdot\mathbf{x}_j\big) + \mathbf{e}_0(k)\cdot\mathbf{x}_j + \mathbf{e}_1(k)\cdot\mathbf{x}_j)$$

where the volume gradient $\nabla I(\mathbf{x}_k)$ is computed using a Gaussian blurred ($\sigma = 1$) version of the MRI volume.

These automated methods for determining the grey-white matter boundary have been previously validated using scans of postmortem brains and have found FreeSurfer based measures of cortical thickness to be on average only 0.077mm different than manual measures performed on dissected tissue samples (Rosas et al. 2002). Within group systematic errors in the placement of the grey-white matter boundary using these methods would result in whole brain differences in cortical thickness that are not observed in our study. These findings thus indicate a high degree of accuracy for FreeSurfer in placing the white matter surface (i.e. the grey-white matter boundary).

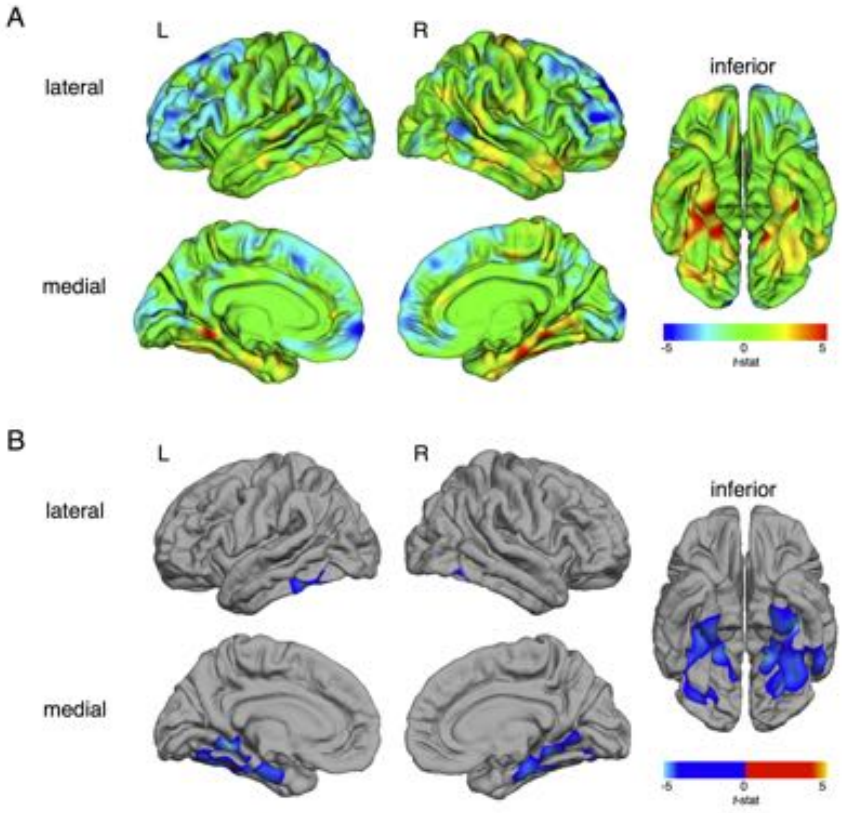

Supplementary Figure 1, Regions of decreased cortical thickness (CT) in autism spectrum disorder (ASD): A.) Between group differences in CT (uncorrected). B.) Individuals with ASD showed significantly decreased CT (RFT $p<0.5$) bilaterally in the parahippocampal, fusiform, and lingual gyri (highlighted in blue). See supplementary Table 1 for statistical details of these clusters.

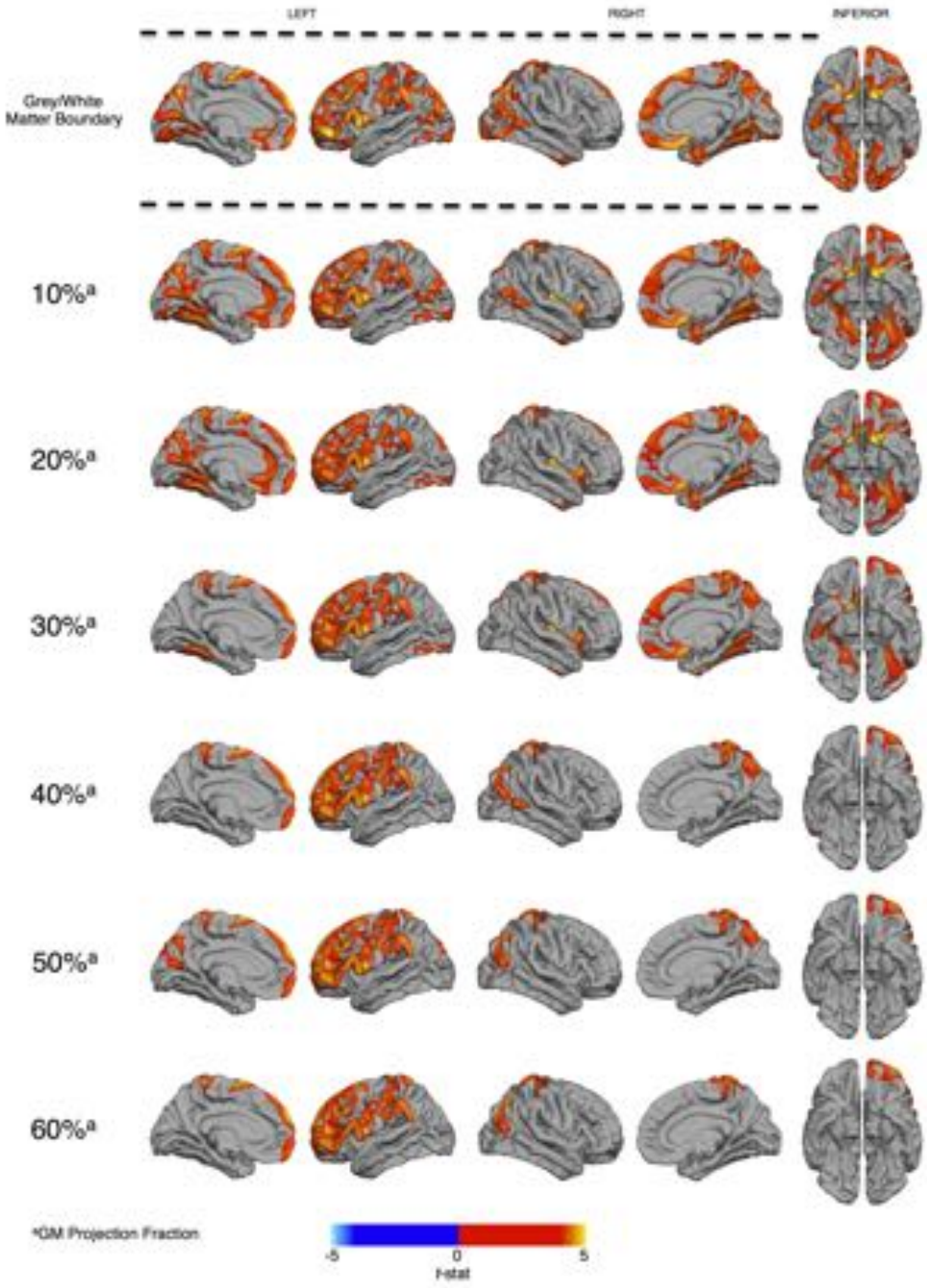

Supplementary Figure 2, Sex differences in grey-white matter signal intensity percent contrast (GWPC): Regardless of diagnosis males showed significantly greater GWPC (RFT $p<0.5$) compared to females across all grey matter sampling depths (a). These increases are highlighted in red and include predominantly fronto-parietal regions of the left hemisphere, and bilateral inferior temporal regions (see supplementary Table 2 for statistical details of these clusters).

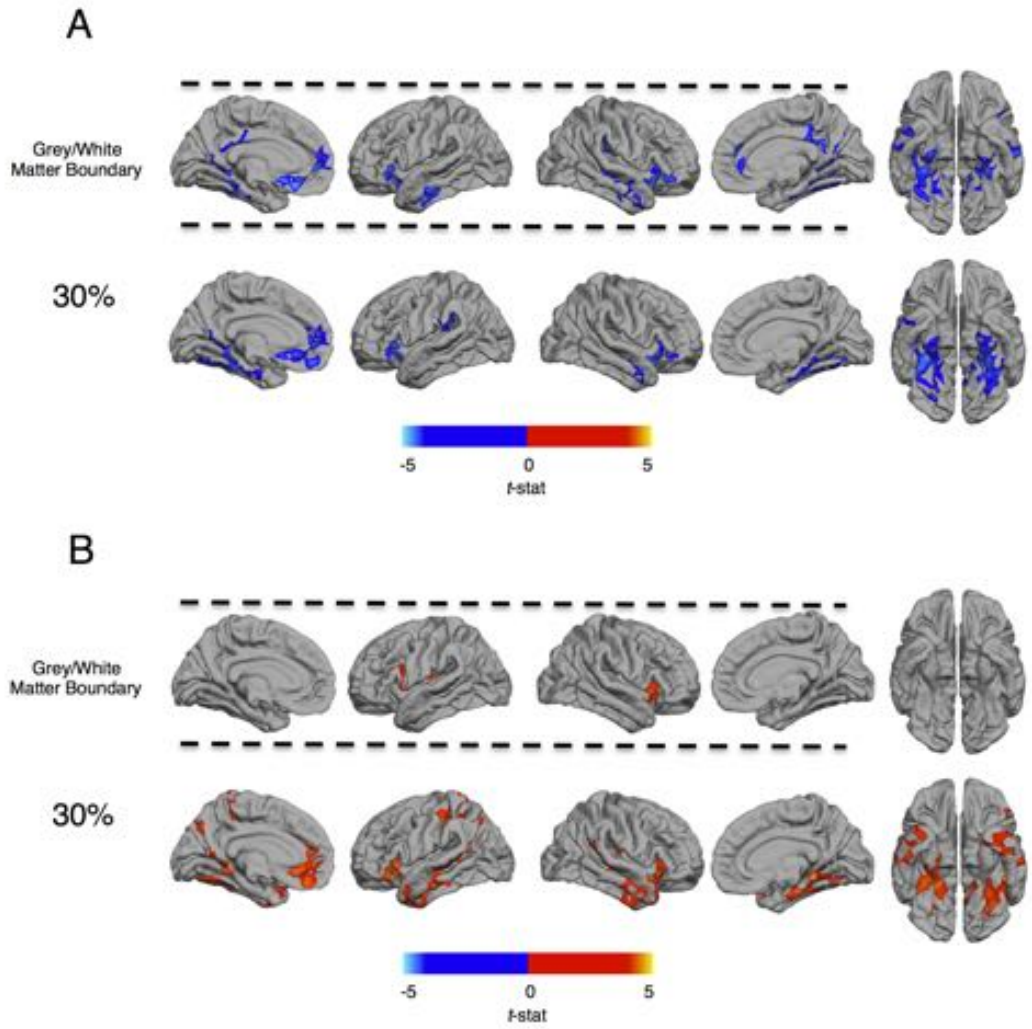

Supplementary Figure 3, Regional differences in grey-white matter signal intensity percent contrast (GWPC) and grey matter intensities (GMI) in Autism Spectrum Disorder (ASD) (5mm FWHM smoothing kernel): Between group differences in (A) GWPC and (B) GMI intensities are shown when GMI was sampled at the grey-white matter boundary (i.e. white matter surface, projection fraction 10%) and a projection fraction of 30% into the cortical sheet. Individuals with ASD showed (A) significantly decreased GWPC (RFT $p<0.5$), indicating less definition between grey and white matter, in several regions highlighted in blue. In several of these regions (B) increases in GMI, highlighted in red were also observed. These results using a 5mm FWHM smoothing kernel were largely similar to those using a 10mm FWHM smoothing kernel (Figures 2 and 3, Table 2). For statistical details of these clusters see supplementary Table 3.

Supplementary Table 1

Cluster	Region Labels	Hemisphere	BA(t_{max})	No vertices	Talairach			t_{max}	$p_{cluster}$
					x	y	z		
1	parahippocampal gyrus, entorhinal cortex, fusiform gyrus, inferior temporal gyrus, lingual gyrus	L	19	6191	-17	-48	-3	-4.46	4.89 x 10-6
2	parahippocampal gyrus, fusiform gyrus, lingual gyrus	R	36	3728	21	-42	-5	-3.35	1.73 x 10-4

Supplementary Table 1, Clusters of Decreased Cortical Thickness in Autism Spectrum Disorder (ASD): Broadmann area (BA), left (L), right (R), *Vertices* indicates the number of vertices within the cluster, t_{max} represents the maximum *t*-statistic within the cluster located at the x y z Talairach coordinates listed, $p_{cluster}$ is the cluster corrected *p* value.

Supplementary Table 2

Cluster	Region Labels	Hemisphere	BA(t_{max})	No. vertices	Talairach x	Talairach y	Talairach z	t_{max}	$p_{cluster}$
1	**precentral gyrus**, frontal pole, pars opercularis, pars orbitalis, pars triangularis, rostral middle frontal gyrus, superior frontal gyrus	L	44	11867	-49	10	6	5.35	4.38×10^{-6}
2	**inferior parietal cortex**, lateral occipital cortex, lingual gyrus, middle temporal gyrus, superior parietal cortex	R	7	10199	39	-63	44	4.82	4.38×10^{-6}
3	**middle temporal gyrus**, inferior parietal cortex, lateral occipital cortex, postcentral gyrus, superior parietal cortex, supramarginal gyrus	L	19	9991	-38	-78	25	4.49	4.38×10^{-6}
4	**precuneus**, inferior temporal gyrus, isthmus-cingulate cortex, lateral occipital cortex, lingual gyrus, pericalcarine cortex, superior parietal cortex	L	7	9359	-6	-67	41	4.53	4.38×10^{-6}
5	**postcentral gyrus**, paracentral lobule, precentral gyrus, precuneus cortex, superior parietal cortex	R	3	7611	36	-30	61	4.54	4.38×10^{-6}
6	**parahippocampal gyrus**, entorhinal cortex, fusiform gyrus, inferior temporal gyrus	R	36	4001	34	-27	-15	3.42	1.16×10^{-3}
7	**lateral orbital frontal cortex**, medial orbital frontal cortex, rostral anterior cingulate cortex	L	47	3563	-24	12	-16	5.71	1.14×10^{-3}
8	**superior frontal gyrus**	R	6	3139	9	20	54	4.59	8.45×10^{-4}
9	**lateral orbital frontal cortex**, medial orbital frontal cortex	R	47	2824	26	10	-14	5.29	1.06×10^{-2}
10	**middle frontal gyrus**, precentral gyrus	L	9	2246	-37	32	25	4.31	1.81×10^{-3}
11	**paracentral lobule**, precentral gyrus, superior parietal cortex	L	6	1988	-9	-25	67	3.79	2.20×10^{-2}

Supplementary Table 2, Clusters of Increased Grey-White Matter Signal Intensity Percent Contrast (GWPC) in Males: Broadmann area (BA), left (L), right (R), *Vertices* indicates the number of vertices within the cluster, t_{max} represents the maximum *t*-statistic within the cluster located at the x y z Talairach coordinates listed, $p_{cluster}$ is the cluster corrected *p* value.

Supplementary Table 3

Measure	Cluster	Region Labels	Hemisphere	BA(*t*max)	Vertices	Talairach x	Talairach y	Talairach z	*t*max	*p*clust
Grey-White Matter Percent Contrast										
	1	fusiform gyrus, lingual gyrus, parahippocampal gyrus	L	36	4027	-27	-39	-7	-3.66	1.33 x 1
	2	parahippocampal gyrus, fusiform gyrus, lingual gyrus	R	20	3447	33	-35	-18	-3.8	1.33 x 1
	3	medial orbital frontal cortex, rostral anterior cingulate cortex, superior frontal gyrus	L	10	2342	-10	39	-4	-3.68	1.45 x 1
	4	insula, lateral orbital frontal cortex	R	47	1671	26	18	-14	-4.02	1.76 x 1
	5	posterior-cingulate cortex, isthmus-cingulate cortex, lingual gyrus, precuneus cortex	L	30	1348	-19	-53	9	-3.72	3.52 x 1
	6	insula, lateral orbital frontal cortex	L	13	1267	-30	19	-2	-3.58	1.05 x 1
	7	middle temporal gyrus, superior temporal gyrus	R	21	1068	55	-13	-17	-3.74	1.01 x 1
	8	insula	L	13	1132	-38	-4	16	-2.97	4.43 x 1
	9	supramarginal gyrus	R	13	926	-45	-32	23	-4.13	1.24 x 1
Grey Matter Signal Intensity										
	1	insula, lateral orbital frontal cortex, superior temporal gyrus	R	38	4370	37	0	-12	4.01	7.28 x 1
	2	banks superior temporal sulcus, inferior parietal cortex, middle and superior temporal gyrus	L	21	4021	-50	-26	-2	3.64	7.89 x 1
	3	banks superior temporal sulcus, inferior parietal cortex, inferior, middle, and superior temporal gyri	R	41	3735	46	-36	7	2.95	1.05 x 1
	4	fusiform gyrus, lingual gyrus, parahippocampal gyrus	R	30	3522	18	-38	-6	3.90	7.40 x 1
	5	isthmus-cingulate cortex, precuneus cortex	L	29	2694	-14	-49	7	3.38	3.39 x 1
	6	fusiform gyrus, inferior temporal gyrus, lingual gyrus	L	19	2410	-29	-56	-3	3.56	2.22 x 1
	7	medial orbital frontal cortex, rostral anterior cingulate cortex, superior frontal gyrus	L	32	2165	-11	42	2	3.40	2.96 x 1
	8	postcentral gyrus, superior parietal cortex	L	2	1868	-46	-23	43	3.56	1.66 x 1
	9	insula, lateral orbital frontal cortex	L	13	1654	-30	18	-2	3.79	4.09 x 1
	10	paracentral lobule, superior parietal cortex,	L	5	1458	-16	-35	50	3.11	4.85 x 1
	11	superior temporal gyrus	L	21	1228	-45	-9	-13	2.78	2.73 x 1
	12	inferior temporal gyrus	L	20	1085	-48	-10	-23	3.47	3.34 x 1

Supplementary Table 3, Significant Reductions in Grey-White Matter Signal Intensity Percent Contrast (GWPC) and Increases in Grey Matter Intensity (GMI) in ASD (FWHM 5mm): Broadmann area (BA), left (L), right (R), *Vertices* indicates the number of vertices within the cluster, t_{max} represents the maximum *t*-statistic within the cluster located at the x y z Talairach coordinates listed, $p_{cluster}$ is the cluster corrected *p* values

Appendix III: Chapter 5 Supplementary Materials

Supplementary Online Content

Ecker C, Andrews DS, Gudbrandsen CM, et al; Medical Research Council Autism Imaging Multicentre Study (MRC AIMS) Consortium. Association between the probability of autism spectrum disorder and normative sex-related phenotypic diversity in brain structure. *JAMA Psychiatry*. Published online February 8, 2017. doi:10.1001/jamapsychiatry.2016.3990

eTable 1. Frequency Ratios of ASD Cases to TD Controls, and Males to Females, Acquired Within and Across the Different Acquisition Sites

eTable 2. Population Prevalence of ASD for Biological Males and Females With Male or Female Neuroanatomical Brain Phenotype

eTable 3. Differences in Neuroanatomical Patterns Associated With High Probability of ASD Between Men and Women

eTable 4. Results of the Vertex-wise Analysis of CT Utilizing a General Linear Model (GLM)

eTable 5. Differences in Demographic Measures Between Diagnostic Groups and Biological Sexes

eMethods. Supplementary Methods

eFigure 1. Sex-Related Pattern of Neuroanatomical Variability in Cortical Thickness

eFigure 2. Significant Differences in CT Between Male and Female TD Controls

eFigure 3. Sample Probability of ASD for Females (A) and Males (B) as a Function of Normative Sex-Related Phenotypic Variability in CT

eFigure 4. Clusters With Significant Differences in the Neuroanatomical Pattern of CT Associated With High Probability of ASD Between Males and Females (i.e. Product of *w* and CT)

eFigure 5. Clusters With Significant Group-by-Sex Interactions Following a Non-parametric Clustering Approach With *n*=10,000 Permutations of Group (i.e. Sex) Labels (Permutation-Based Cluster-Corrected, $p<0.05$)

eFigure 6. Group-by-Sex Interaction Graph Based on Mean CT in the Left-Hemisphere Cluster That Extended Into the Hippocampal/Entorhinal Cortex, the Fusiform and Lingual Gyrus, and the Inferior/Middle Temporal Lobe

eFigure 7. Differences in Full-Scale, Verbal and Non-verbal (i.e. Performance) IQ Between Individual Subgroups of ASD vs. TD Individuals, and Males vs. Females, Examined Using *t* Tests for Independent Samples

eFigure 8. Spatially Distributed Pattern of Negative (Blue) and Positive (Red) Correlations Between Verbal IQ Measures and CT Assessed Across Male and Female Neurotypical Controls

eAppendix. Supplementary Appendix

eReferences. Supplementary References

This supplementary material has been provided by the authors to give readers additional information about their work.

eTable 1. Frequency Ratios of ASD Cases to TD Controls, and Males to Females, Acquired Within and Across the Different Acquisition Sites

		Group		
		ASD	Control	total
Cambridge	female	28	28	56
	male	25	26	51
London	female	21	19	40
	male	24	25	49

eTable 2. Population Prevalence of ASD for Biological Males and Females With Male or Female Neuroanatomical Brain Phenotype

	S = 1		S = 0	
	N = 1	N = 0	N = 1	N = 0
D = 1	0.025	0.017	0.013	0.002
D = 0	0.975	0.983	0.987	0.998

Note. D: diagnosis of ASD (0=no, 1=yes), S: biological sex/gender (0=female, 1=male), N: neuroanatomical brain phenotype (0=female, 1=male); Notably, the probability of receiving a diagnosis of ASD appears to increase for male participants with N=0. This is due to the fact that the probability of being classified as N=0 for biological males is relatively low, thereby inflating the conditional probability of having ASD.

eTable 3. Differences in Neuroanatomical Patterns Associated With High Probability of ASD Between Men and Women

				Talairach				
ID	Region Labels	Side	BA	*x*	*y*	*z*	t_{max}	$p_{cluster}$
Females > Males								
1	banks superior temporal sulcus, caudal middle frontal gyrus, inferior parietal cortex, insula, lateral, orbital frontal cortex, middle temporal gyrus, pars opercularis, pars triangularis, postcentral gyrus, precentral gyrus,rostral middle frontal gyrus, superior temporal gyrus	R	11/22/44/45/46	34	-25	14	4.96	6.09×10^{-6}
2	cuneus cortex, fusiform gyrus, isthmus-cingulate cortex, lingual gyrus, precuneus cortex	L	18/19/20/30/31/37	-32	-48	-16	3.78	6.29×10^{-6}
3	insula, lateral orbital frontal cortex, pars opercularis, pars triangularis, postcentral gyrus, precentral gyrus, supramarginal gyrus	L	11/45/47	-38	-18	16	4.57	1.37×10^{-5}
4	inferior parietal cortex, supramarginal gyrus	R	19/39/40	41	-66	43	4.54	1.35×10^{-5}
5	fusiform and lingual gyrus, parahippocampal gyrus	R	19/20/37	24	-44	-7	3.47	1.09×10^{-4}
6	caudal anterior-cingulate cortex, medial orbital frontal cortex, rostral anterior cingulate cortex, superior frontal gyrus	L	25/32/24	-12	42	8	4.45	1.27×10^{-4}
7	caudal anterior-cingulate cortex, paracentral lobule, posterior-cingulate cortex, precuneus cortex, superior frontal gyrus	L	24	-13	-15	38	3.97	1.34×10^{-4}

8	postcentral gyrus, superior parietal cortex	L	7	-27	-55	60	3.25	4.05×10^{-2}

Note. BA, Brodman Area; tmax, maximum absolute t value within cluster, x,y,z, Talairach coordinates at tmax; pcluster, cluster probability; R, right; L, left

eTable 4. Results of the Vertex-wise Analysis of CT Utilizing a General Linear Model (GLM)

				Talairach				
ID	Regional Labels	Side	BA	*x*	*y*	*z*	t_{max}	$p_{cluster}$
Group-by-Sex Interaction								
(1)	fusiform gyrus, inferior/middle temporal gyrus, lingual gyrus, parahippocampal gyrus	L	19/20/34/35/37/38	-29	-71	-5	3.29	3.5×10^{-6}
(2)	fusiform gyrus, inferior temporal gyrus, lateral occipital cortex, lingual gyrus, parahippocampal gyrus	R	18/19/34/35/37	26	-27	-18	3.42	5.49×10^{-5}
(3)	superior temporal sulcus, middle temporal gyrus	R	21/22	60	-33	-6	3.51	2.13×10^{-2}
Contrast: ASD males > TD males								
(1)	fusiform gyrus, inferior/middle temporal gyrus	L	18/19/20/37	-52	27	-19	2.61	1.04×10^{-2}
(2)	fusiform gyrus, lateral occipital cortex, lingual gyrus, parahippocampal gyrus	R	18/19/37	29	-60	-8	2.71	2.90×10^{-2}
Contrast: ASD females < TD females								
(1)	entorhinal cortex, fusiform gyrus, inferior/middle temporal gyrus, lingual gyrus, parahippocampal gyrus	L	18/19/20/34/35/37/38	-30	-69	-6	-3.90	2.23×10^{-6}
(2)	entorhinal cortex, fusiform gyrus, inferior/middle temporal gyrus, lateral occipital cortex, lingual gyrus, parahippocampal gyrus	R	18/19/20/34/35/36/37	25	-26	-18	-4.13	1.08×10^{-6}
(3)	superior temporal sulcus/gyrus, inferior parietal cortex, middle/superior temporal gyrus	R	21/22/39	62	-33	-6	-3.61	1.08×10^{-3}

(4)	insula, pre-/post-central gyrus, supramarginal gyrus	L	40/41	-44	-18	16	-3.96	1.23×10^{-2}
(5)	insula, pre-/post-central gyrus, superior temporal gyrus, supramarginal gyrus	R	40/41	46	-14	20	-3.67	4.17×10^{-2}

Note. ID, cluster number; BA, approximate Brodman Area; t_{max}, maximal *t* test statistic within cluster, *x,y,z*, Talairach coordinates at t_{max}; $p_{cluster}$, cluster probability; R, right; L, left

eTable 5. Differences in Demographic Measures Between Diagnostic Groups and Biological Sexes

	Groups			
	ASD (n=98)	Control (n=98)	$F(df=1)$	p
Age [years]	26.88 ± 7.18	27.39 ± 6.44	0.099	0.585
Full-scale IQ (WASI)	113.74 ± 12.31	116.44 ± 9.48	3.142	0.078
Verbal IQ	113.52 ± 12.89	113.68 ± 10.75	0.027	0.871
Performance IQ	111.28 ± 14.02	115.61 ± 9.75	6.179	0.014*
Mean Cortical Thickness [mm]	2.41 ± 0.01	2.34 ± 0.09	0.010	0.921
Total Grey Matter Volume [litre]	0.72 ± 0.08	0.72 ± 0.07	0.003	0.955
Total Intracranial Volume [litre]	1.45 ± 0.24	1.45 ± 0.21	0.000	0.994
	Biological Sex			
	Males (n=100)	Females (n=96)	$F(df=1)$	p
Age [years]	26.70 ± 6.41	27.60 ± 7.21	0.875	0.351
Full-scale IQ (WASI)	113.66 ± 11.57	116.59 ± 10.32	3.673	0.057
Verbal IQ	110.18 ± 11.98	117.21 ± 10.59	18.685	0.001*
Performance IQ	114.42 ± 12.49	112.45 ± 11.92	1.211	0.272
Mean Cortical Thickness [mm]	2.34 ± 0.085	2.33 ± 0.11	0.898	0.345
Total Grey Matter Volume [litre]	0.763 ± 0.06	0.677 ± 0.10	82.690	0.001*
Total Intracranial Volume [litre]	1.58 ± 0.19	1.32 ± 0.17	100.730	0.001*

Note. Data expressed as mean ± standard deviation; F,p resulting from a general linear model (GLM) including a main effect of diagnostic group and biological sex. * statistically significant based on $p < 0.05$ (two-sided)

eMethods. Supplementary Methods

Gaussian Process Classification of biological sex based on normative variability in CT

Gaussian process models were used for the probabilistic prediction of biological sex based on patterns of neuroanatomical variability in CT. Gaussian process classification (GPC) has previously been applied to MRI data [1,2], and a detailed description can be found in [3]. Briefly, we begin with a set of training data $X_{train}=\{X,y\}$, where X is an m x d matrix consisting of input vectors x_i (i.e. m training samples with d features each), and y is a column vector of target variables or class labels where $y_i \in \{-1, +1\}$. Training samples are indexed by $i = 1, \ldots, m$. The training data are used to estimate a probability distribution that allows us to predict a target y^* for a new data sample x^* as accurately as possible. For binary GPC, predictions take the form of predictive or 'class' probabilities, where the probability for a class results from $(y^*=1|x^*,X_{train})$. These predictions are computed by first estimating the posterior distribution of a set of vertex weights using the rules of probability, then passing the output through a sigmoid function to constrain the output to the unit interval, ensuring a valid probabilistic interpretation. The mode of the distribution of weights, $\mathbf{w}$, can be understood as providing a spatial representation of the decision boundary. If GPC is applied to neuroimaging data, $\mathbf{w}$ has the same number of elements as the feature vector $\mathbf{x}$, and can subsequently be used to create a map of the most important brain regions underlying the prediction (analogous to Support Vector Machine (SVM) discrimination maps).

Here, we initially employed GPC to establish (i.e. train) a predictive model of biological sex based on normative phenotypic variability in CT. Thus, the input matrix X was an m x d matrix of CT measures where m was defined as the number of typically developing (TD) controls (i.e. 51 males and 47 females), and d was defined as the number of vertices across the cortical surface. As target variable y, we used the class labels of -1 and +1 for neurotypical females and males respectively. This allowed us to

make probabilistic predictions for individuals based on the binary categories dictated by biological sex, utilizing their neuroanatomical brain phenotype. Class probabilities ranged from 0 to 1, wherein those being most confidently classified as phenotypically female (i.e. class probability=0) or male (i.e. class probability=1) representing the most prototypical (i.e. characteristic) male or female neurophenotype respectively. The GP classifier was trained by maximizing the logarithm of the marginal likelihood, which measures the total probability of the data given the Gaussian process prior and the model's hyperparameters [2]. The performance of the normative model was subsequently validated using cross validation, which provides robust parameter estimates of generalisation ability. Here, the classifier is trained repeatedly using all but one participant from each class label. This procedure was repeated *n* times, where *n* is the number of participants per class label. The accuracy of the classifier was measured by the proportion of observations that were correctly classified, e.g. the number of biological males (or females) correctly classified as male (or female) based on their brain phenotype. Permutation testing was used to assess the statistical significance of the model performance relative to chance level. To achieve this, we permuted the class (i.e. sex) labels 1000 times without replacement. Each time, the model was retrained and the accuracy was computed. All Gaussian process models were estimated using the GPML toolbox (www guassianprocess.org/gpml/code).

The normative predictive model of biological sex was subsequently used to predict biological sex for the independent sample of ASD individuals. To visualize the spatially-distributed patterns of neuroanatomical variability in CT carrying high and low risk of ASD in males and females, we employed a recently proposed approach for mapping the contribution of each vertex to the classifier decision [1]. This approach has two advantages over the more conventional appeoach of mapping the weight vector: (1) it indicates the total contribution of each vertex to the prediction for each individual, i.e. not just the contribution from the training set; and (2) it can be used to map the neural constituents

for the predictions based on a second sample, independent from the training set (i.e. the clinical and normative samples respectively). To achieve this, we calculated the element-wise product of $\mathbf{w}$ and each individual's CT measures (i.e. x_i*CT) for (1) all males (or all females) classified as phenotypically male (i.e. class probability > 0.5), (2) all males (or all females) classified as phenotypically female (i.e. class probability < 0.5), and (3) across biological males and females with a class probability < 0.5 (or a class probability > 0.5). Within each of these groups and at each cerebral vertex, the resulting maps were then summarized by the mean value across individuals.

Estimation of ASD probability based on normative sex-related phenotypic variability of the brain

To determine whether normative sex-related variability in CT measures modulates the probability of ASD, we initially examined the (absolute) probability of ASD as a function of predictive probabilities for the TD male or female brain phenotype within our sample. The sample probability of ASD for females (or males) was determined as the ratio of females (or males) with ASD divided by the total number of females (or males) falling within eight bins (i.e. from 0 to 1 in steps of 0.125) along the axis of predictive class probabilities for the male neuroanatomical phenotype (M). Let D and S denote binary variables representing a diagnosis of ASD and biological sex respectively. This equals the posterior probability of having ASD (i.e. $D=1$) under the condition of being biologically female or male (i.e. $S=0$ or $S=1$, respectively), and given a neuroanatomical phenotype M quantified by class probabilities, so that $\mathbb{P}(D=1|M, S=s)$, for every $s \in \{0,1\}$.

Furthermore, this data allowed us to estimate the population risk of having a diagnosis of ASD, given that an individual exhibits a male or female neuroanatomical phenotype. In our notation, this may be expressed as $\mathbb{P}(D=1|M=m, S=s)$, for every $m \in \{0,1\}$ and $s \in \{0,1\}$ where 0 denotes female and 1 denotes male. Using Bayes theorem, such a conditional probability can be expressed as

$$\mathbb{P}(D = 1|M = m,\ S = s) = \frac{\mathbb{P}(M=m|D=1,S=s)\mathbb{P}(D=1|S=s)}{\mathbb{P}(M=m|S=s)}, \qquad (1)$$

in which the normalizing constant is obtained by integrating out D, so that $\mathbb{P}(M|D,S) = \mathbb{P}(M|D = 1,S)\mathbb{P}(D = 1|S) + \mathbb{P}(M|D = 0,S)\mathbb{P}(D = 0|S)$ for every realization of M and S. The probabilities in the numerator of the right-hand side of equation (1) are readily obtained from our sample, and from previous epidemiological studies (e.g. [4]). Indeed, the term $\mathbb{P}(M = m|D = 1,S = s)$ corresponds to the number of biological males or females with a diagnosis of ASD, who have been identified as having a male or female neuroanatomical phenotype by our GPC model.

Moreover, the prevalence rates of ASD for males and females in the general population (i.e. $\mathbb{P}(D=1|S=s)$) are known from epidemiological priors (i.e. 1:42 for males, 1:189 for females [4]). Based on these previous priors, and the sample estimates resulting from our study, we were therefore able to estimate the population risk of ASD given a male/female neuroanatomical phenotype for biological males and females, i.e. $\mathbb{P}(D|M,S)$. Note that the estimation of $\mathbb{P}(D = 1|M,S)$ presented here is analogous to the correction usually applied to a sensitivity test in order to compute the probability of having a disease, given a positive test result. In our context, the probability of a particular neuroanatomical phenotype can thus be regarded as a 'test' for disease status.

eFigure 1. Sex-Related Pattern of Neuroanatomical Variability in Cortical Thickness

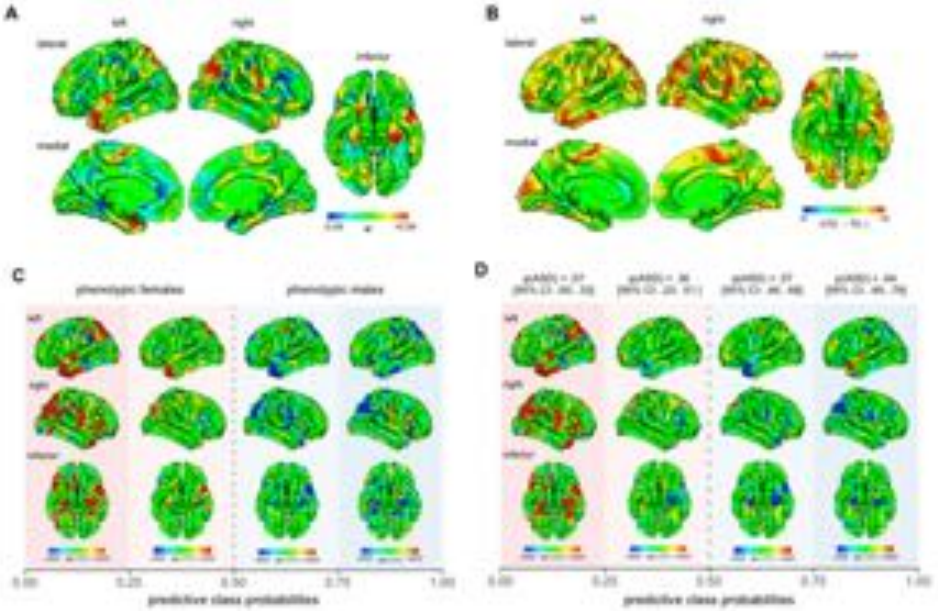

(A) Spatial distribution of the weight vector w resulting from the Gaussian Process Classification of biological sex in TD controls. **(B)** Un-thresholded statistical difference map representing t-test statistics resulting from the GLM-comparison between TD males and females using CT measures. Positive t-values (yellow to red colormap) indicate increased CT in TD females relative to males, while negative t-values (cyan to blue colormap) indicate decreased CT in females. Clusters with significant differences in CT following statistical thresholding are shown in eFigure 2 in the Supplement. **(C)** Patterns of normative neuroanatomical variability in CT associated with a phenotypic shift of the brain from a characteristic female to male presentation. These patterns were derived using a predictive mapping approach, which quantifies the extent to which the individual's neuroanatomy interacts with the weight vector **w**. At each vertex, the color-scale therefore represents the product of **w** and CT, averaged across all individuals falling within four bins along the normative axis of predictive probabilities. **(D)** Patterns of sex-related neuroanatomical CT variability associated with high and low risk for ASD across sex categories. The risk of ASD was determined as the number of males and females with ASD relative to the total number of individuals falling within four intervals of predictive class probabilities. At each vertex, the color-scale indicates the product of **w** and CT, averaged across all individuals within the four risk groups. Brackets indicate the 95% confidence interval associated with the risk for ASD.

eFigure 2. Significant Differences in CT Between Male and Female TD Controls

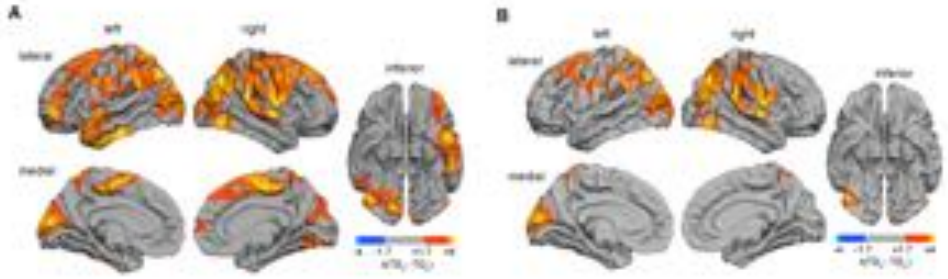

A) Clusters with significant between-group differences using random-field theory (RFT)-based clustering with a cluster threshold of 0.5 (two-tailed). The orange to yellow colormap indicates brain regions where CT is significantly increased in females relative to males. **(B)** Clusters with significant between-group differences using a non-parametric clustering approach with n=10,000 permutations at the same cluster-threshold and colormap.

eFigure 3. Sample Probability of ASD for Females (**A**) and Males (**B**) as a Function of Normative Sex-Related Phenotypic Variability in CT

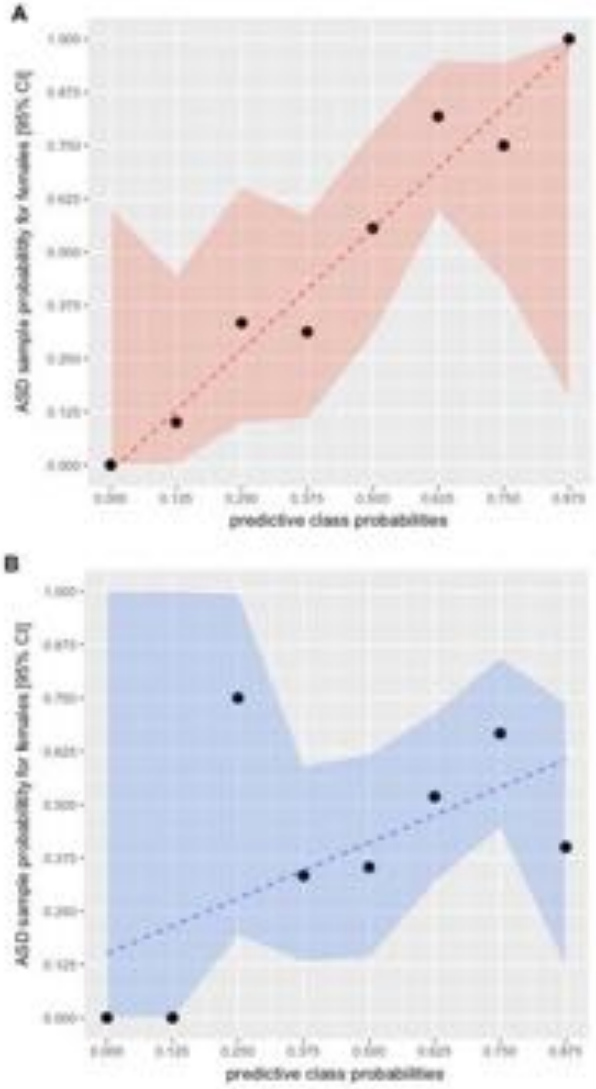

The sample probability of ASD was determined as the ratio of females (or males) with ASD relative to the total number of females (or males) falling within eight bins (i.e. from 0 to 1 in steps of 0.125) along the normative axis of predictive probabilities. The colored area around the regression line indicates the 95% confidence interval (CI) resulting from a binomial test, based on the hypothesis that the probability of having ASD is larger (or smaller) than the probability of not having ASD.

eFigure 4. Clusters With Significant Differences in the Neuroanatomical Pattern of CT Associated With High Probability of ASD Between Males and Females (i.e. Product of w and CT; See Figure 2 Right Panel)

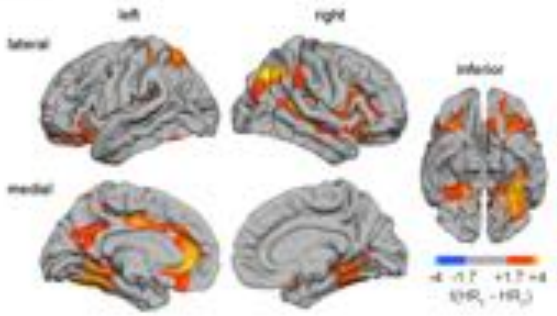

The red colormap indicates regions where females had a significant increased w x CT as compared to males (RFT-based cluster-corrected, $p<0.05$). There were no significant between-sex differences in the low ASD probability maps.

eFigure 5. Clusters With Significant Group-by-Sex Interactions Following a Non-parametric Clustering Approach With n=10,000 Permutations of Group (i.e. Sex) Labels (Permutation-Based Cluster-Corrected, p<0.05) (**A**). (**B**) Clusters where CT was significantly reduced in females with ASD relative to female controls (permutation-based cluster-corrected, p<0.05). No significant clusters remained when comparing ASD males with male TD controls using a permutation-based cluster correction.

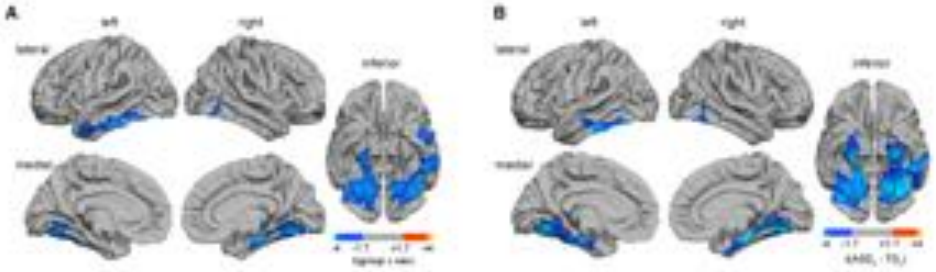

eFigure 6. Group-by-Sex Interaction Graph Based on Mean CT in the Left-Hemisphere Cluster That Extended Into the Hippocampal/Entorhinal Cortex, the Fusiform and Lingual Gyrus, and the Inferior/Middle Temporal Lobe (see cluster ID 1 in eTable 4)

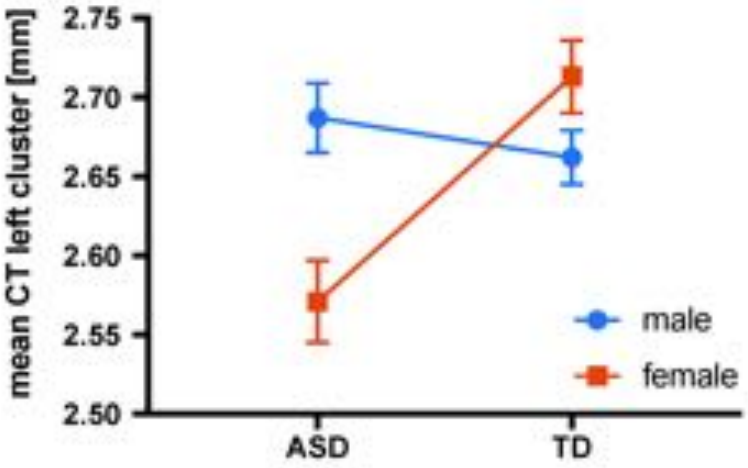

eFigure 7. Differences in Full-Scale, Verbal and Non-verbal (i.e. Performance) IQ Between Individual Subgroups of ASD vs. TD Individuals, and Males vs. Females, Examined Using *t* Tests for Independent Samples

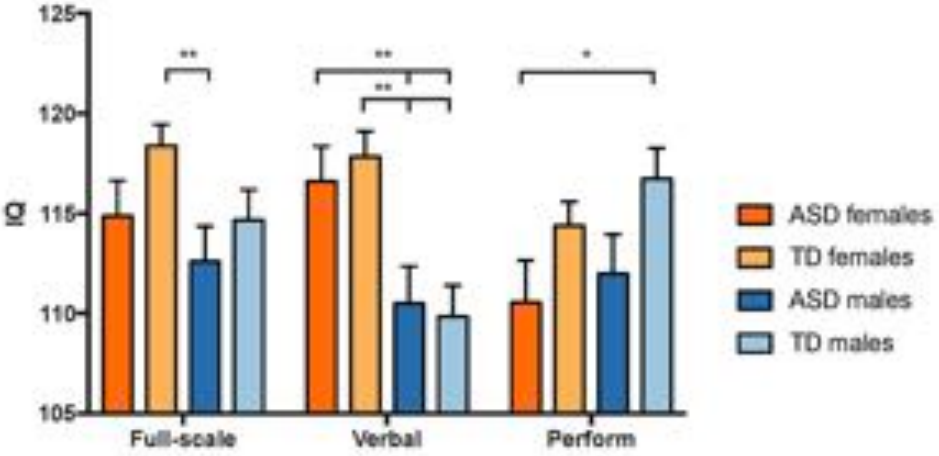

Note. ** indicates $p<0.01$, * indicates $p<0.05$.

eFigure 8. Spatially Distributed Pattern of Negative (Blue) and Positive (Red) Correlations Between Verbal IQ Measures and CT Assessed Across Male and Female Neurotypical Controls

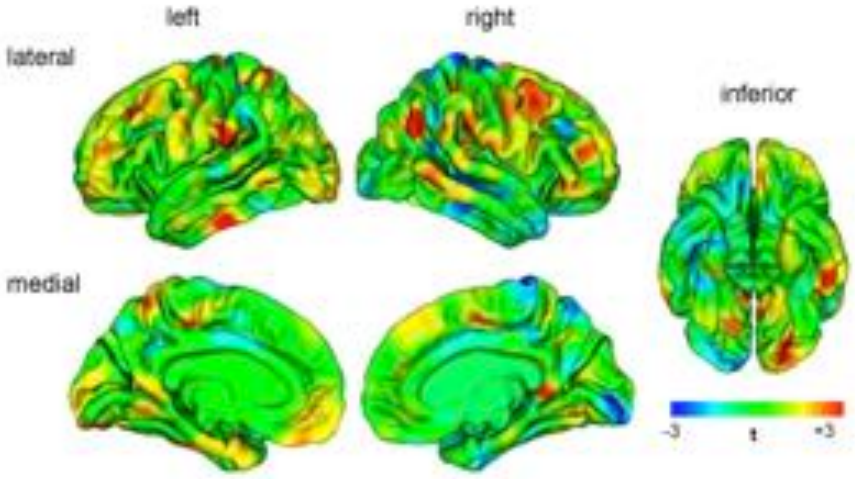

The colourmap indicates the *t* test statistics for vertex-wise correlation coefficients.

eAppendix. Supplementary Appendix

Relationship between sex-related neuroanatomical differences and inter-individual variability in clinical and or neurocognitive measures

To determine how the observed sex-related differences in brain structure may be related to variability in clinical or neurocognitive measures, we also examined if differences in verbal and non-verbal (i.e. performance) IQ between diagnostic groups and biological sexes could explain the phenotypic shift of the brain in females. For example, neurotypical females tend to have a significantly higher verbal IQ than neurotypical males, which has previously been suggested to be a 'protective' factor for ASD (e.g. [5]). It is therefore possible that females with ASD display a neurocognitive profile that is more similar to the neurotypical male rather than female behavioral phenotype, which in turn could account for a more male-typic pattern of brain anatomy.

However, when examining similarities and differences in IQ measures between females with ASD, and male and female controls, we found that ASD females differed significantly from neurotypical males in both verbal ($t(97)=-2.993$, $p<0.01$) and performance IQ ($t(97)=2.406$, $p<0.05$). Moreover, ASD females were not statistically different from female controls ($p>0.05$, two-tailed) (see eFigure 7 in the Supplement). Based on IQ profiles, the ASD females assessed in our sample therefore seem functionally closer to female rather than male TD controls. Thus, based on IQ measures exclusively, our finding of increased predictive probabilities for the male neuroanatomical brain phenotype in ASD females seems to reflect a sex- rather than function-related difference in brain anatomy. Moreover, there was no significantly correlation between predictive probabilities for a male neuroanatomical brain phenotype and variability in verbal or performance IQ in females ($p>0.05$, two-tailed), as would be expected based on the absence of a significant difference between females with ASD and female controls. Given that females tend to have a significantly increased verbal IQ compared to males, we also compared the

normative patterns of neuroanatomical variability indicative of biological sex (i.e. the weight vector w, eFigure 1a) with the spatially distributed pattern of correlations between CT measures and verbal IQ (see eFigure 8 in the Supplement). Overall, however, the distributed patterns indicative of biological sex, and the patterns associated with high and low ASD probability, are quite different from the spatial distribution of high/low correlations between CT and verbal IQ. Based on these findings, it seems unlikely that the results of our multivariate prediction of biological sex are driven by sex-dependent differences in verbal IQ, rather than by biological sex itself.

Last, we also explored the relationship between autistic symptoms and CT variability in the two main clusters with significant sex-by-group interactions (see Figure 3a) within the ASD group. Here, we utilized a GLM predicting CT variability using separate effects of biological sex and measures of symptom severity to (1) examine whether CT in these clusters is significantly correlated with measures of symptom severity within the ASD group, and to (2) disentangle the effect of biological sex from the effect of inter-individual variability in symptom severity. We examined these relationships in two separate statistical models, one including the three ADI-R subdomains, and one including the ADOS total and repetitive domain. Overall, we found that CT measures in the right-hemisphere cluster correlated with ADOS total scores exclusively ($r(97)=0.283$, $p<0.05$, two-tailed). No significant correlations were observed in the left-hemisphere cluster. However, when predicting CT by biological sex and ADOS total scores, both effects remained statistically significant in the right hemisphere ($p<0.05$, two-tailed). In the left hemisphere, only the effect of biological sex exceeded the level of statistical significance ($p<0.05$, two-tailed). Thus, while measures of symptom severity may explain some CT variability in addition biological sex, it seems that both effects are statistically separable. Although a more thorough investigation of this issue is required in the future, these preliminary results

indicate that our findings reflect neuroanatomical differences related to biological sex, and having a diagnosis of ASD, rather than functional differences in specific clinical or neurocognitive features.

eReferences. Supplementary References

1. Marquand AF, Brammer M, Williams SCR, Doyle OM. Bayesian multi-task learning for decoding multi-subject neuroimaging data. *Neuroimage*. 2014;92:298-311. doi:10.1016/j.neuroimage.2014.02.008.

2. Marquand A, Howard M, Brammer M, Chu C, Coen S, Mourão-Miranda J. Quantitative prediction of subjective pain intensity from whole-brain fMRI data using Gaussian processes. *Neuroimage*. 2010;49(3):2178-2189. doi:10.1016/j.neuroimage.2009.10.072.

3. Rasmussen C, Williams C. *Gaussian Processes for Machine Learning. Massachusetts Institute of Technology*. 2006.

4. Baio J. *Prevalence of Autism Spectrum Disorder Among Children Aged 8 Years—Autism and Developmental Disabilities Monitoring Network, Surveillance Summaries*, March 28, 2014, 63(SS02):1-21

5. Skuse DH, Mandy W, Steer C, Miller LL, Goodman R, Lawrence K, Emond A, Golding J. *Social communication competence and functional adaptation in general population of children: preliminary evidence for sex-by-verbal IQ differential risk*. J Am Acad Child Adolesc Psychiatry. 2009;48(2):128-137. doi:10.1097/CHI.0b013e3181919176b8.

Appendix IV: Chapter 6 Supplementary Materials

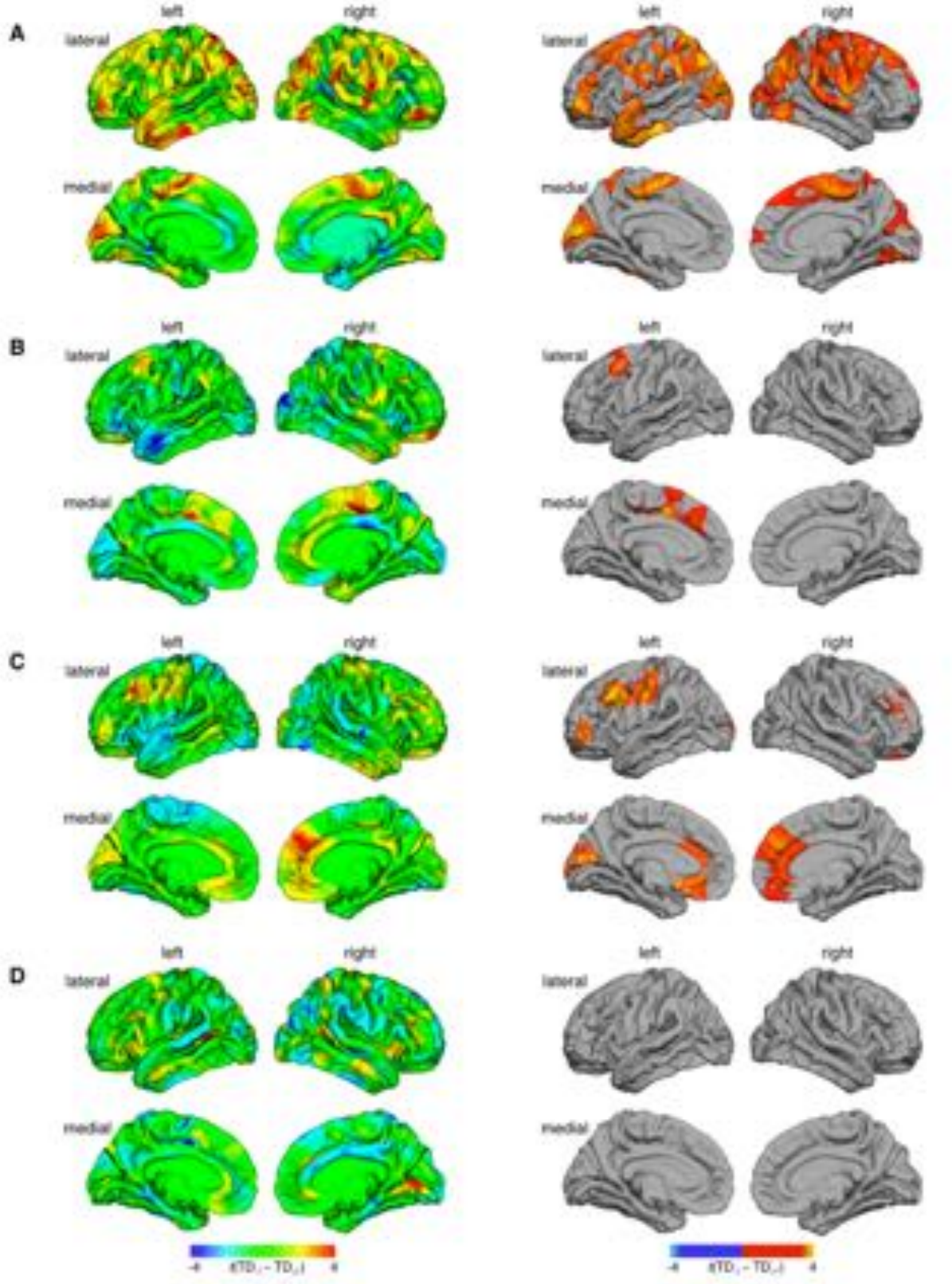

Supplementary Figure 6, Morphological Differences Between Typically Developing (TD) Females and Males as Identified Using a General Linear Model: Sex differences between TD males and females for (A) cortical thickness, (B) surface area, (C) the local gyrification index, and (D) sulcal depth. Uncorrected *t*-maps are shown in the left panel, random field theory cluster corrected (p<0.5) maps are shown in the right panel.

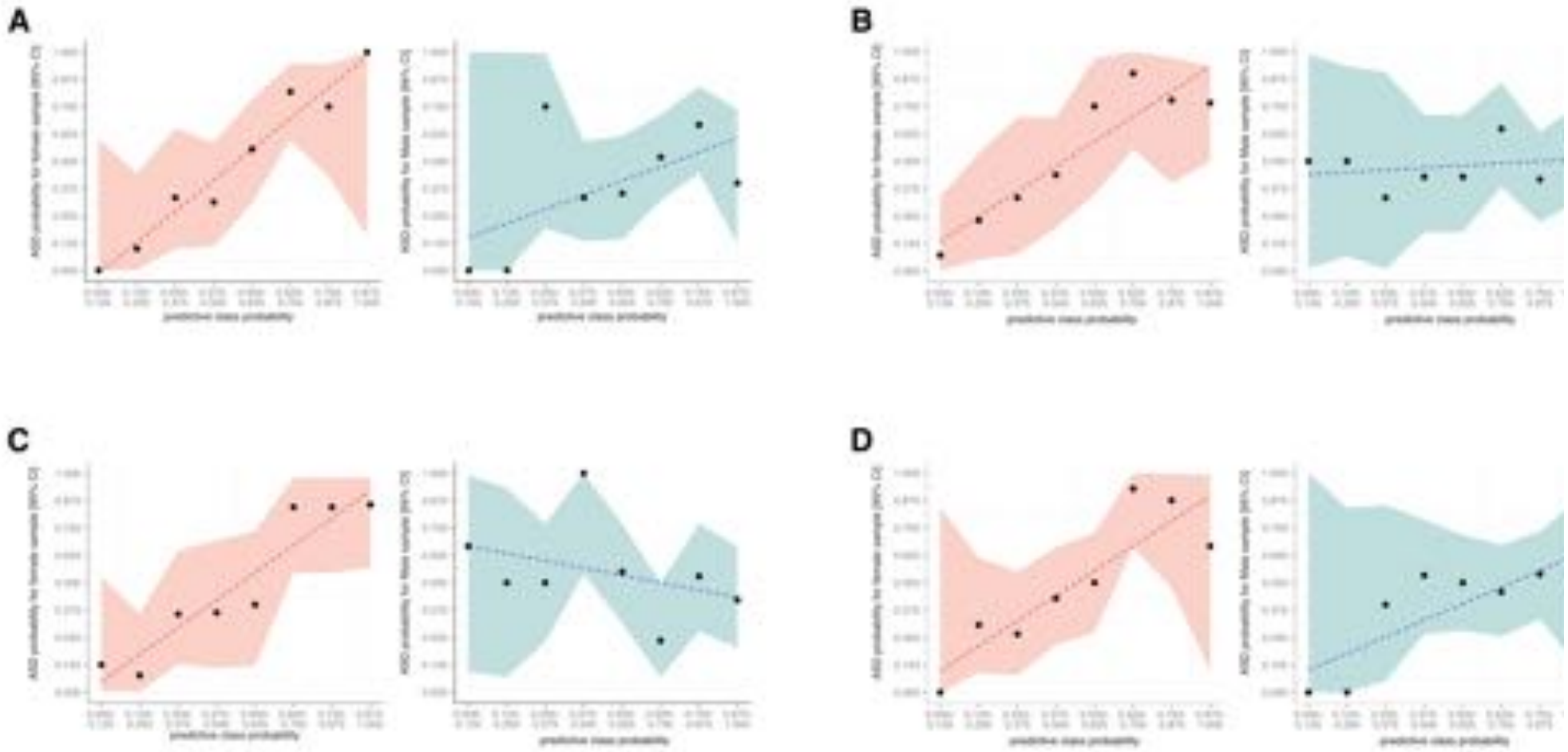

Supplementary Figure 3. Probability for ASD as a Function of Normative Sex-Related Phenotypic Variability in Brain Morphology: Probability estimates for ASD across eight discrete bins along the axis of predictive class probabilities for biological sex are plotted for (A) cortical thickness, (B) surface area, (C) the local gyrification index, and (D) sulcal depth for biological females and males (left and right panel respectively). For each model (excluding local gyrification index measures in biological males) probability for ASD was seen to increase along with increasingly male-typical class predictions. This relationship was particularly apparent in females due to the statistically significant shift in females with ASD towards male-typical neuroanatomical phenotypes.

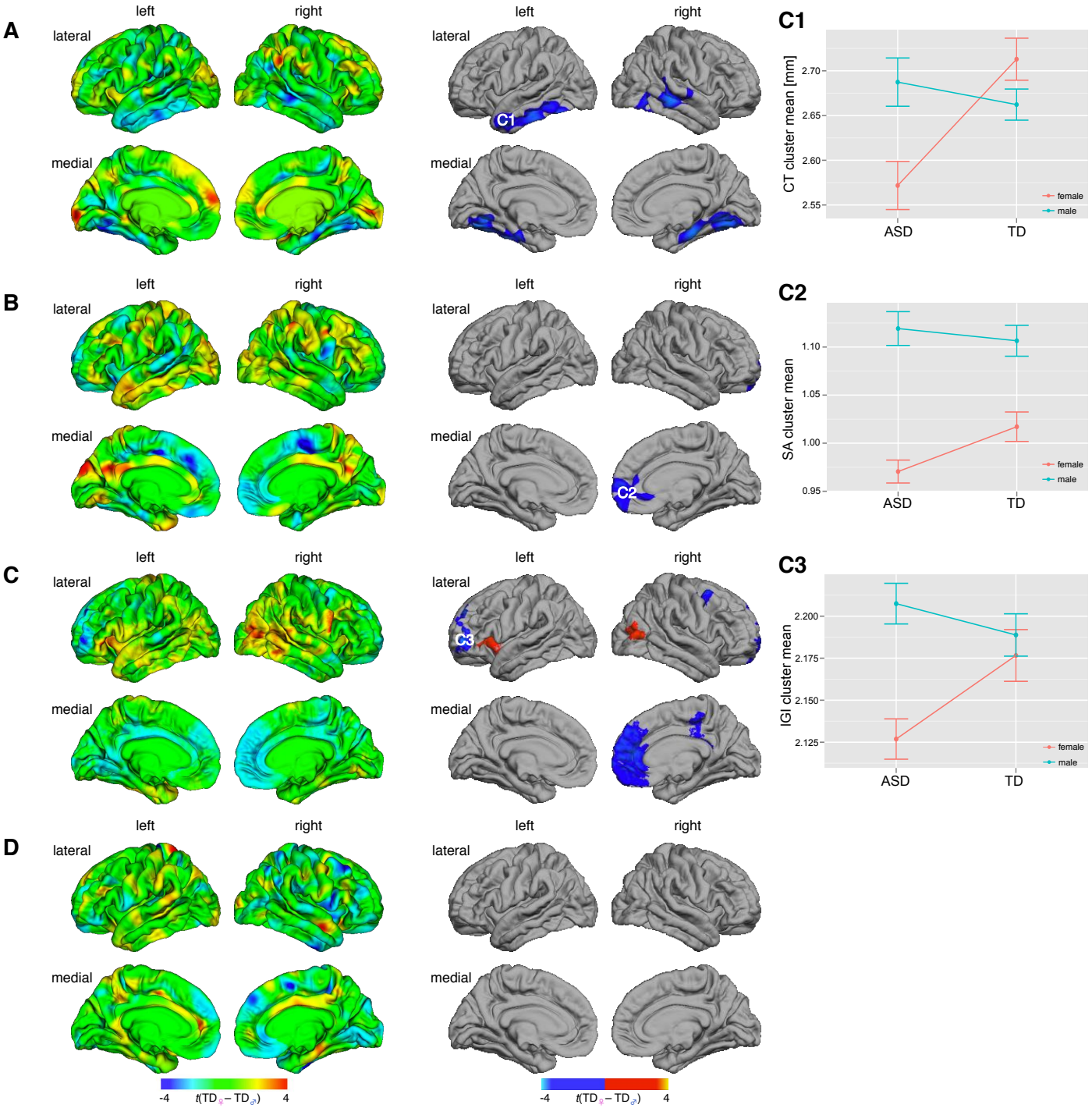

Supplementary Figure 2, Group x Sex Interaction Effects Identified Using a General Linear Model: Uncorrected *t* maps of group x sex interaction effects are shown in the left panel for (A) cortical thickness, (B) surface area, (C) the local gyrification index, and (D) sulcal depth. Significant clusters after random field theory (RFT) correction ($p<0.05$) are shown in the middle panel. Plots of the mean values from cortical thickness cluster C1, surface area cluster C2, and local gyrification index cluster C3 are shown in the right panel.

Supplementary Table 1

Measure	Cluster	Region Labels	Hemisphere	Vertices	Talairach x	Talairach y	Talairach z	t_{max}	$p_{cluster}$
Cortical Thickness									
	1	superior temporal sulcus, middle frontal gyrus, cuneus, fusiform gyrus, inferior parietal cortex, inferior temporal gyrus, lateral occipital cortex, lingual gyrus, middle temporal gyrus, paracentral lobule, postcentral gyrus, precentral gyrus, precuneus cortex, rostral middle frontal gyrus, superior frontal gyrus, superior parietal cortex, superior temporal gyrus, supramarginal gyrus	R	130855	62	-11	1	3.95	3.32×10^{-6}
	2	caudal middle frontal gyrus, inferior parietal cortex, lateral orbital frontal cortex, paracentral lobule, pars orbitalis, postcentral gyrus, precentral gyrus, precuneus cortex, rostral middle frontal gyrus, superior frontal gyrus, superior parietal cortex, supramarginal gyrus	L	29647	-36	-69	41	3.82	3.32×10^{-6}
	3	cuneus cortex, inferior parietal cortex, lateral occipital cortex, pericalcarine cortex, superior parietal cortex	L	7447	-36	-76	14	3.76	1.12×10^{-4}
	4	inferior temporal gyrus, middle temporal gyrus, superior temporal gyrus	L	4744	-53	-28	-21	3.69	6.64×10^{-3}
Surface Area									
	1	caudal middle frontal gyrus, paracentral lobule, superior frontal gyrus	L	6382	-10	4	43	4.42	2.33×10^{-4}

local Gyrification Index								
	1	caudal middle frontal gyrus, postcentral gyrus, precentral gyrus, rostral middle frontal gyrus, supramarginal gyrus	L	10280	-41	20	36	4.35	1.55×10^{-5}
	2	caudal anterior-cingulate cortex, lateral orbital frontal cortex, medial orbital frontal cortex, rostral anterior cingulate cortex, superior frontal gyrus	R	6450	10	38	23	3.56	1.55×10^{-5}
	3	lateral orbital frontal cortex, rostral middle frontal gyrus	L	1144	-37	43	-2	3.18	5.79×10^{-5}
	4	cuneus cortex, lateral occipital cortex, pericalcarine cortex	L	1599	-4	-73	18	3.28	2.87×10^{-4}
	5	rostral middle frontal gyrus	R	1377	37	41	19	3.44	2.24×10^{-3}
	6	caudal anterior-cingulate cortex, rostral anterior cingulate cortex, superior frontal gyrus	L	1941	-8	37	9	2.58	5.22×10^{-3}
	7	medial orbital frontal cortex, rostral anterior cingulate cortex	L	1335	-6	11	-9	3.36	7.11×10^{-3}
	8	caudal middle frontal gyrus, postcentral gyrus, precentral gyrus, rostral middle frontal gyrus, supramarginal gyrus	L	929	-42	-28	21	-3.33	2.84×10^{-4}

Supplementary Table 1, Clusters of Significant Differences in Cortical Morphometry Utilizing a General Linear Model (TD Females – TD Males): left (L), right (R), *Vertices* indicates the number of vertices within the cluster, t_{max} represents the maximum *t*-statistic within the cluster located at the x y z Talairach coordinates listed, $p_{cluster}$ is the cluster corrected *p* value.

Supplementary Table 2

		S = 1		S = 0	
Mean		N = 1	N = 0	N = 1	N = 0
	D = 1	0.024	0.019	0.026	0.001
	D = 0	0.976	0.981	0.974	0.999

		S = 1		S = 0	
CT		N = 1	N = 0	N = 1	N = 0
	D = 1	0.025	0.017	0.013	0.002
	D = 0	0.975	0.983	0.987	0.998

		S = 1		S = 0	
SA		N = 1	N = 0	N = 1	N = 0
	D = 1	0.025	0.019	0.019	0.002
	D = 0	0.975	0.981	0.981	0.998

		S = 1		S = 0	
*l*GI		N = 1	N = 0	N = 1	N = 0
	D = 1	0.019	0.04	0.016	0.002
	D = 0	0.981	0.96	0.984	0.998

		S = 1		S = 0	
SULC		N = 1	N = 0	N = 1	N = 0
	D = 1	0.024	0.02	0.012	0.003
	D = 0	0.976	0.98	0.988	0.998

Supplementary Table 2, Population Prevalence of ASD for Biological Males and Females with Male- or Female-typic Neuroanatomical Brain Phenotypes: Population estimates are given based on the predictive class probabilities for each morphological feature (i.e. cortical thickness [CT], surface area [SA], the local gyrification index [*l*GI], and sulcal depth [SULC]) as well as the average of these class probabilities across features (mean). D: diagnosis of ASD (0=no, 1=yes), S: biological sex (0=female, 1=male), N: neuroanatomical brain phenotype (0=female-typical, 1=male-typical).

Supplementary Table 3

Measure	Cluster	Region Labels	Hemisphere	Vertices	Talairach x	Talairach y	Talairach z	t_{max}	$p_{cluster}$
Cortical Thickness									
	1	fusiform gyrus, inferior temporal gyrus, lingual gyrus, middle temporal gyrus, parahippocampal gyrus	L	9368	-29	-71	-5	-3.29	3.55×10^{-6}
	2	fusiform gyrus, inferior temporal gyrus, lateral occipital cortex, lingual gyrus, parahippocampal gyrus	R	6835	26	-27	-18	-3.42	5.49×10^{-4}
	3	banks superior temporal sulcus, middle temporal gyrus, superior temporal gyrus	R	4412	60	-33	-6	-3.51	2.13×10^{-2}
Surface Area									
	1	medial orbital frontal cortex, rostral anterior cingulate cortex, superior frontal gyrus	R	2985	14	37	11	-2.88	2.48×10^{-2}
local Gyrification Index									
	1	frontal pole, medial orbital frontal cortex, rostral anterior cingulate cortex, superior frontal gyrus	R	5715	15	39	8	3.05	1.02×10^{-5}
	2	caudal middle frontal gyrus, precentral gyrus, superior frontal gyrus	R	2415	31	9	48	3.89	4.42×10^{-5}
	3	rostral middle frontal gyrus	L	918	-37	49	-2	3.5	1.49×10^{-3}
	4	isthmus-cingulate cortex, paracentral lobule, posterior-cingulate cortex	R	1922	7	-27	52	2.48	3.14×10^{-3}
	5	superior frontal gyrus	L	584	-19	48	24	3.29	3.92×10^{-2}
	6	frontal pole, medial orbital frontal cortex, rostral anterior cingulate cortex, superior frontal gyrus	L	1791	-47	29	-2	-3.01	9.73×10^{-4}
	7	caudal middle frontal gyrus, precentral gyrus, superior frontal gyrus	R	1224	45	-70	8	-2.73	9.91×10^{-3}

Supplementary Table 3, Clusters of Significant Group-by-Biological Sex Interaction Effects: left (L), right (R), *Vertices* indicates the number of vertices within the cluster, t_{max} represents the maximum *t*-statistic within the cluster located at the x y z Talairach coordinates listed, $p_{cluster}$ is the cluster corrected *p* value.

Appendix V: Chapter 6 Manuscript Proof

The American Journal of Psychiatry

The American Journal of Psychiatry

Normative Sex-Related Phenotypic Diversity Across Multiple Measures of Brain Anatomy is Associated with Probability for Autism Spectrum Disorder

Journal:	*The American Journal of Psychiatry*
Manuscript ID	Draft
Manuscript Type:	Article
Date Submitted by the Author:	n/a
Complete List of Authors:	Andrews, Derek; King's College London. Institute of Psychiatry, Psychology & Neuroscience, Forensic and Neurodevelopmental Sciences Marquand, Andre; Radboud Universiteit Donders Institute for Brain Cognition and Behaviour; King's College London. Institute of Psychiatry, Psychology & Neuroscience, Centre for Neuroimaging Sciences Ginestet, Cedric; King's College London. Institute of Psychiatry, Psychology & Neuroscience, Biostatistics Gudbrandsen, Maria; King's College London. Institute of Psychiatry, Psychology & Neuroscience, Forensic and Neurodevelopmental Sciences Daly, Eileen; King's College London. Institute of Psychiatry, Psychology & Neuroscience, Forensic and Neurodevelopmental Sciences Lai, Meng; University of Toronto, Child and Youth Mental Health Collaborative at the Centre for Addiction and Mental Health and The Hospital for Sick Children, Department of Psychiatry; Cambridge University, Autism Research Centre, Department of Psychiatry; National Taiwan University Hospital, Department of Psychiatry Murphy, Clodagh; King's College London. Institute of Psychiatry, Psychology & Neuroscience, Forensic and Neurodevelopmental Sciences; Bethlem Royal Hospital, South London and Maudsley NHS Foundation Trust, National Autism Unit Lombardo, Michael; University of Cyprus, Department of Psychology & Center for Applied Neuroscience; Cambridge University, Autism Research Centre, Department of Psychiatry Ruigrok, Amber; Cambridge University, Autism Research Centre, Department of Psychiatry Williams, Steven; King's College London. Institute of Psychiatry, Psychology & Neuroscience, Centre for Neuroimaging Sciences Bullmore, Edward; University of Cambridge, Brain Mapping Unit, Department of Psychiatry Suckling, John; University of Cambridge, Brain Mapping Unit, Department of Psychiatry Baron-Cohen, Simon; University of Cambridge, Autism Research Centre, Department of Psychiatry Craig, Michael; King's College London. Institute of Psychiatry, Psychology & Neuroscience, Forensic and Neurodevelopmental Sciences; Bethlem Royal Hospital, South London and Maudsley NHS Foundation Trust, National

	Autism Unit Murphy, Declan; King's College London. Institute of Psychiatry, Psychology & Neuroscience, Forensic and Neurodevelopmental Sciences; Bethlem Royal Hospital, South London and Maudsley NHS Foundation Trust, National Autism Unit Ecker, Christine; University Hospital, Goethe University Frankfurt am Main, Department of Child and Adolescent Psychiatry, Psychosomatics and Psychotherapy; King's College London. Institute of Psychiatry, Psychology & Neuroscience, Forensic and Neurodevelopmental Sciences
Keywords:	Gender Differences - A3P0089, Autism - A3P0006, Brain Imaging Techniques - A3P0068

WORD COUNT: **3796**

ABSTRACT WORD COUNT: **241**

FIGURES: **4**

TABLES: **1**

SUPPLEMENTARY FIGURES: **3**

SUPPLEMENTARY TABLES: **3**

Title

Normative Sex-Related Phenotypic Diversity Across Multiple Measures of Brain Anatomy is Associated with Probability for Autism Spectrum Disorder

Authors: Derek S. Andrews[a] MSc, Andre Marquand[b,c] PhD, Cedric E Ginestet[a] PhD, Maria Gudbrandsen[a] MSc, Eileen Daly[a] PhD, Clodagh M. Murphy[a,d] MBBS PhD, Meng-Chuan Lai[1,e,g] MD PhD, Michael V. Lombardo[h,i] PhD, Amber N.V. Ruigrok[a] PhD, the MRC AIMS Consortium[*], Steven C. Williams[a] PhD, Edward T. Bullmore[j], MBBS PhD, John Suckling[j] PhD, Simon Baron-Cohen[f] PhD, Michael C. Craig[a,d] MBBS PhD, Declan G.M. Murphy[a,d**] MBBS MD, & Christine Ecker[a,d**] PhD

Affiliations:

[a] Department of Forensic and Neurodevelopmental Sciences, and the Sackler Institute for Translational Neurodevelopment, Institute of Psychiatry, Psychology and Neuroscience, King's College London, UK

[b] Donders Institute for Brain, Cognition and Behaviour, Radboud University, Nijmegen, Netherlands

[c] Centre for Neuroimaging Sciences, Institute of Psychiatry, Psychology and Neuroscience, King's College, London, UK

[d] National Autism Unit, Bethlem Royal Hospital, South London and Maudsley NHS Foundation Trust, UK

[e] Autism Research Centre, Department of Psychiatry, University of Cambridge, Cambridge, UK

[f] Child and Youth Mental Health Collaborative at the Centre for Addiction and Mental Health and The Hospital for Sick Children, Department of Psychiatry, University of Toronto, Toronto, Canada

[g] Department of Psychiatry, National Taiwan University Hospital and College of Medicine, Taiwan

[h] Department of Psychology & Center for Applied Neuroscience, University of Cyprus, Nicosia, Cyprus

[i] Brain Mapping Unit, Department of Psychiatry, University of Cambridge, UK

[j] Department of Child and Adolescent Psychiatry, Psychosomatics and Psychotherapy, Universitätsklinikum Frankfurt am Main, Goethe-University Frankfurt am Main, Germany

[*] The Medical Research Council Autism Imaging Multicentre Study Consortium (MRC AIMS Consortium) is a UK collaboration between the Institute of Psychiatry, Psychology and Neuroscience at King's College, London, the Autism Research Centre, University of Cambridge, and the Autism Research Group, University of Oxford. The Consortium members in alphabetical order are: Anthony J. Bailey (Oxford), Simon Baron-Cohen (Cambridge), Patrick F. Bolton (IoP), Edward T. Bullmore (Cambridge), Sarah Carrington (Oxford), Marco Catani (IoPPN), Bhismadev Chakrabarti (Cambridge), Michael C. Craig (IoPPN), Eileen M. Daly (IoPPN), Sean C. L. Deoni (IoPPN), Christine Ecker (IoPPN), Francesca Happé (IoPPN), Julian Henty (Cambridge), Peter Jezzard (Oxford), Patrick Johnston (IoPPN), Derek K. Jones (IoPPN), Meng-Chuan Lai (Cambridge), Michael V. Lombardo (Cambridge), Anya

Madden (IoPPN), Diane Mullins (IoPPN), Clodagh M. Murphy (IoPPN), Declan G. M. Murphy (IoPPN), Greg Pasco (Cambridge), Amber N. V. Ruigrok (Cambridge), Susan A. Sadek (Cambridge), Debbie Spain (IoPPN), Rose Stewart (Oxford), John Suckling (Cambridge), Sally J. Wheelwright (Cambridge), Steven C. Williams (IoPPN), and C. Ellie Wilson (IoPPN).

** These authors contributed equally to the manuscript

Corresponding Author:

Mr. Derek Sayre Andrews, BA MSc

PhD Candidate

Department of Forensic & Neurodevelopmental Science

Institute of Psychiatry, Psychology & Neuroscience

King's College London

PO Box 50

16 De Crespigny Park, Denmark Hill

London, England, SE5 8AF

Email: Derek.Andrews@KCL.ac.uk

Work Phone: 02078485701 (UK)

Acknowledgements: We would like to thank all of our participants and their family members for partaking in this study. The Autism Imaging Multicentre Study Consortium, members in alphabetical order are: Anthony J. Bailey (Oxford), Simon Baron-Cohen (Cambridge), Patrick F. Bolton (IoP), Edward T. Bullmore (Cambridge), Sarah Carrington (Oxford), Marco Catani (IoPPN), Bhismadev Chakrabarti (Cambridge), Michael C. Craig (IoPPN), Eileen M. Daly (IoPPN), Sean C. L. Deoni (IoPPN), Christine Ecker (IoPPN), Francesca Happé (IoPPN), Julian Henty (Cambridge), Peter Jezzard (Oxford), Patrick Johnston (IoPPN), Derek K. Jones (IoPPN), Meng-Chuan Lai (Cambridge), Michael V. Lombardo (Cambridge), Anya Madden

(IoPPN), Diane Mullins (IoPPN), Clodagh M. Murphy (IoPPN), Declan G. M. Murphy (IoPPN), Greg Pasco (Cambridge), Amber N. V. Raigrok (Cambridge), Susan A. Sadek (Cambridge), Debbie Spain (IoPPN), Rose Stewart (Oxford), John Suckling (Cambridge), Sally J. Wheelwright (Cambridge), Steven C. Williams (IoPPN), and C. Ellie Wilson (IoPPN). The EU-AIMS Consortium. Furthermore, we would like to thank the National Institute for Health Research Biomedical Research Centre for Mental Health, the Dr. Mortimer and Theresa Sackler Foundation, and the German Research Foundation (DFG).

Funding: The study represents independent research partly funded by the National Institute for Health Research (NIHR) Biomedical Research Centre at South London and Maudsley NHS Foundation Trust and King's College London. The views expressed are those of the authors and not necessarily those of the NHS, the NIHR or the Department of Health. This work was also supported by funding from the Medical Research Council UK (grant number G0400061), the Innovative Medicines Initiative Joint Undertaking (grant number 115300), which includes financial contributions from the EU Seventh Framework Programme (FP7/2007-2013) from the European Federation of Pharmaceutical Industries and Associations companies in kind, the Sackler foundation and from Autism Speaks.

Statement of Disclosure: Professor Edward Bullmore is employed half-time by GlaxoSmithKline and holds GSK shares. Dr. Meng-Chuan Lai receives financial support from the O'Brien Scholars Program within the Child and Youth Mental Health Collaborative at the Centre for Addiction and Mental Health and The Hospital for Sick Children, Toronto. None of the remaining authors have declared any conflict of interest or financial interests, which may arise from being named as an author on the manuscript.

KEY WORDS: ASD, FreeSurfer, Sex, Gender, MRI

Abstract

Objective: Males are 2 to 5 times more likely to be diagnosed with Autism spectrum disorder (ASD) than females. The reasons for this bias are not fully understood. However, normative diversity in brain structure associated with biological sex is one possible mediator for ASD risk. The authors therefore examined the probability of ASD as a function of sex-related variability in multiple measures of brain anatomy.

Method: 98 adults with ASD (49 males, 49 females) and 98 typically developing controls (51 males, 47 females) underwent structural MRI scanning. Measures of cortical morphometry (i.e. cortical thickness, surface area, the local gyrification index, and sulcal depth) were used to establish normative models of biological sex. These models were subsequently applied to males and females with ASD. Sample probabilities for ASD were calculated across features according to sex-based neuroanatomical phenotypes and extrapolated to estimate ASD risk within the general population.

Results: Across morphometric features, females with ASD displayed a statistically significant neuroanatomical shift towards more male-typical presentations ($p<0.001$). Moreover, within both biological males and females sample probabilities for ASD increased with predicted probabilities for male-typical brain phenotypes. For biological females, this translated to an estimated variability in population prevalence ranging from 0.01 to 2.6% depending on having either a female- or male-typical neurophenotype.

Conclusions: Male-typical neurophenotypes are associated with higher probability for having an ASD diagnosis than female-typical neurophenotypes across a range of neuroanatomical features. In addition to genetic and environmental factors, normative sex-related phenotypic diversity in brain structure should be considered when investigating risk and resilience for ASD.

Introduction

Autism spectrum disorder (ASD) is a complex neurodevelopmental condition estimated to be 2-5 times more common in males than females (1, 2). While the preponderance of males with ASD has partially been attributed to sex differences in clinical phenotypes (3-7), etiological models propose that factors inherent to normative sex differences may modulate ASD liability (for review see (8)). However, it remains unknown what "male risk" and/or "female protective" factors may contribute to the male preponderance of ASD, and how these factors may affect the biological underpinnings of the condition.

To identify potential sex-related risk (and protective) factors, we recently examined the probability of ASD as a function of normative sex-related phenotypic diversity in brain structure (9). To do so, we initially developed a multivariate predictive model of biological sex based on differential patterns of brain structure in a sample of typically developing (TD) males and females. This model of normative sex differences was subsequently applied to males and females with ASD, which allowed us to (*i*) examine the probability of ASD along a phenotypic axis, ranging from the characteristic female to male brain phenotype, and (*ii*) identify patterns of sex-related neuroanatomical variability associated with low and high probability of ASD. In this previous study we reported that normative sex-related phenotypic diversity in brain structure significantly affects the risk of ASD in addition to biological sex alone, with male-typical neuroanatomical characteristics carrying a higher intrinsic risk for ASD than female-typical characteristics. This increased risk was predominantly driven by a phenotypic shift of the brain in females with ASD for a male-typical rather than female-typical presentation. Moreover, using a mapping approach that enabled us to estimate patterns of atypicality at the level of each individual subject (10), we demonstrated that high and low risk of ASD is associated with particular patterns of neuroanatomical variability that included many of the brain regions where males typically differ from females on average (e.g. (11, 12)). Taken together, these findings highlight the need for considering normative sex-related

phenotypic diversity in addition to genetic and environmental factors when estimating an individual's risk for ASD.

However, in this prior 'proof-of-concept' study, our analysis was based exclusively on measures of cortical thickness (CT) as previous neuroimaging studies have shown CT to be highly variable between TD males and females (11, 12), and significantly altered in individuals with ASD (13, 14). Thus, as has been raised by others (15), it is unknown whether or how our initial findings generalize to other morphometric features that have been reported to be atypical in ASD. These include vertex-wise estimates of surface area (SA; (14)), the local gyrification index (lGI; (16, 17)), and sulcal depth (SULC; (18)). Here, we extended these findings to consider multiple aspects of brain anatomy including both volumetric and geometric cortical features in order to (*i*) provide a more comprehensive characterization of normative sex related differences in brain structure, (*ii*) determine how diversity in sex based neurophenotypes are associated with ASD probability, and (*iii*) estimate how much ASD prevalence in the general population might vary as a function of normative sex-related phenotypic diversity. We expect that our initial finding of a phenotypic shift of the brain in ASD females towards a more male-typical neurophenotype generalizes to other morphometric features, and for sex differences in cortical morphometry to be associated with population risk for ASD.

Methods

Participants

98 right-handed adults with ASD (49 males and 49 females) and 98 age and IQ matched TD controls (51 males and 47 females) aged 18-42 years were recruited by advertisement and assessed at the Institute of Psychiatry, Psychology and Neuroscience (IoPPN), London, and the Autism Research Centre, Cambridge. Approximately equal ratios of cases to controls, and males to females, were recruited within sites (Table 1). Exclusion criteria included a history

of major psychiatric disorder (e.g. psychosis), head injury, genetic disorder associated with ASD (e.g. fragile-X syndrome, tuberous sclerosis), or any other medical condition affecting brain function (e.g. epilepsy). We also excluded participants on antipsychotic medication, mood stabilizers or benzodiazepines.

All participants with ASD were diagnosed according to International Statistical Classification of Diseases, 10th Revision (ICD-10) research criteria. Clinical diagnoses were confirmed using the Autism Diagnostic Interview Revised (ADI-R; (19)) or the Autism Diagnostic Observation Schedule (ADOS; (20)). All ADI-R diagnosed participants reached algorithm cut-offs in the three domains of the ADI-R, although failure to reach cut-off in one domain by maximally two points was permitted. Due to reliable informants being unavailable, we were unable to obtain ADI-R diagnostic data from five females with ASD, for whom diagnostic status was confirmed using ADOS-G cut-offs for ASD. In all other participants, ADOS-G scores were used to assess the severity of current symptoms and were not used as an inclusion criterion. One female with ASD fell short one point on the ADI-R communication and repetitive domain but met ADOS-G criteria. Overall intellectual ability was assessed using the Wechsler Abbreviated Scale of Intelligence (21). All participants had a full-scale IQ greater than 80 and gave informed written consent in accordance with ethics approval by the National Research Ethics Committee, Suffolk, UK.

Structural MRI Data Acquisition

Scanning took place at the IoPPN, London, and the Addenbrooke's Hospital, Cambridge, using matched 3T GE Signa systems (General-Electric, Milwaukee, USA). A quantitative T_1-mapping sequence was used to ensure standardization of structural MRI scans across scanner platforms (22, 23), which resulted in high-resolution structural T_1-weighted inversion-recovery images, with 1x1x1mm resolution, a 256x256x176 matrix, TR=1800ms, TI=50ms, FA=20°, and FOV=25cm.

Cortical Reconstruction using FreeSurfer

FreeSurfer v5.3.0 software (http://surfer.nmr.mgh.harvard.edu/) was used to derive tessellated models of the cortical surface for each T_1-weighted image. These well-validated and fully automated procedures have been extensively described elsewhere (e.g. (24-28)). Resulting surface models were visually inspected for reconstruction errors. Surface reconstructions with visible inaccuracies were further excluded from the statistical analysis and are not described in this study. Dropout rates were equal across groups and were <10% of the total sample.

From each individual's surface reconstructions four separate vertex based morphometric cortical features were calculated. (*i*) Cortical thickness (CT), i.e. the closest distance between corresponding vertices between the grey-white matter and gray matter-cerebrospinal fluid boundaries (28); (*ii*) vertex-wise estimates of pial (i.e. grey matter) surface area (SA) (29). And measures of cortical geometry including (*iii*) the local gyrification index (*I*GI) (30) and (*iv*) sulcal depth (SULC, i.e. average convexity, the depth/height of each vertex above the average cortical surface). Prior to further analysis all features (excluding *I*GI) were smoothed using a 15mm surface-based FWHM Gaussian kernel. As *I*GI utilizes SA values sampled within spherical regions on interest with a 15mm diameter, no additional smoothing was performed for this measure.

Gaussian Process Classification

Gaussian Process Classification (GPC) (31, 32) models were employed to discriminate biological sex among TD participants on the basis of each of the four cortical features (i.e. CT, SA, *I*GI, SULC) separately. These classifiers provide a predictive class probability (y_p) for each individual ranging from 0 to 1 for the characteristic female to male brain phenotype, with y_p=0.5 serving as the binary cut-off between classes. The overall classification accuracy of each model was estimated using leave-one-out cross validation and tested for significance by repeating the cross-validation procedure n=1,000 times after randomly permuting the class labels. Subsequently, we applied these four classifiers for biological sex in TD participants to

predict the sex of males and females with ASD. The resulting classification accuracies for the ASD cases were tested for statistical significance using permutation testing as outlined above.

To visualize the patterns of brain regions representative of normative sex differences, we present spatial representations of the maximum a-posteriori estimate of each model's weight vector ($\mathbf{w}$), which is indicative of the regional contribution to the overall prediction of biological sex (32). For each classifier, $\mathbf{w}$ was derived by training the GPC on all TD individuals. As individuals with ASD were not included in the initial training of the classifiers they do not contribute to $\mathbf{w}$, thus we used a "predictive mapping" approach (10) to determine which cortical features are driving sex related differences in ASD among groups of males and females with high and low probability for ASD. Here, groups of high and low ASD probability were determined according to predicted class probabilities, with y_i>0.5 (i.e. male-typical phenotype) representing high and y_i<0.5 (i.e. female-typical phenotype) representing low probability. For each test example i in both male (and female) high (and low) probability groups j, we calculated the element-wise (i.e. Hadamard) product of each individuals data (x_i) and the corresponding weights ($\mathbf{w}$), so that $(x_i)^*\mathbf{w}$ (10). For each group (i.e. male and female, high and low ASD probability) brain regions contributing the most to the classification were summarized by taking the mean of the $(x_i)^*\mathbf{w}$ values at each vertex.

Estimating ASD Probability

To examine how normative sex based phenotypic diversity in brain structure is associated with probability for ASD we first calculated the mean of each individual's predictive class probabilities across the four classification models. This provided a single class probability for each individual that takes into account normative sex variability across all four cortical features. We then converted the continuous axis of class probabilities into a set of discrete bins (e.g., from 0 to 1 in steps of 0.125). Within each bin, the sample probability of ASD was calculated as the ratio of the number of individuals with ASD relative to the total number of individuals within the bin. Confidence intervals for these sample probabilities were determined using an exact binomial test implemented in R Project for Statistical Computing

(https://www.r-project.org). Furthermore, these data allowed us to estimate the population prevalence of ASD given a male- or female-typical neuroanatomical phenotype in addition to being biologically male or female. Details of these methods are provided in the supplementary materials. In brief, using Bayes theorem, we combined our sample prevalence estimates with previously published prevalence rates of ASD for biological male and female individuals in the general population (i.e., 1:42 for male and 1:189 for female individuals; (33)). In this way, we were able to estimate the population prevalence of ASD diagnosis (D = 1) given an individual's predicted neuroanatomical sex phenotype (M) and biological sex (S), that is P(D = 1 | M, S).

Vertex-wise between-group comparison of cortical measures

Vertex-wise statistical analyses of each cortical feature were conducted using the SurfStat toolbox (www.math.mcgill.ca/keith/surfstat/) for MATLAB (R2014a, The Mathworks, Massachusetts). For the comparisons between TD males and females, parameter estimates were obtained by regression of a GLM at each vertex i with biological sex and center as categorical fixed-effects factors, and total grey matter (GM) volume as a continuous covariate. To examine whether the neuroanatomy of ASD is significantly modulated by biological sex, we also included a main effect of diagnostic group and a group-by-sex interaction, i.e.

$$Y_i = \beta_0 + \beta_1 Group + \beta_2 Sex + \beta_3 (Group \times Sex) + \beta_4 GM_{total} + \beta_5 Center + e_i$$

where e_i is the residual error. Additionally, total SA was used as a continuous covariate for analyses of SA. Effects of interest were estimated from the coefficients β_{1-3} normalized by the corresponding standard error. Corrections for multiple comparisons were performed using a 'random field theory' (RFT)-based cluster analysis for non-isotropic images at a cluster-threshold of $p<0.05$ (two-tailed) (34).

Results

Participant Demographics and Global Brain Measures

There were no significant differences between all individuals with ASD and TD controls in age ($t(194)=-0.53$, $p=0.598$), full-scale IQ ($t(194)=-1.72$, $p=0.086$), mean CT ($t(194)=0.08$, $p=0.936$), mean SA ($t(194)=0.03$, $p=0.976$), mean *I*Gl ($t(194)=0.24$, $p=0.810$), mean SULC ($t(194)=0.67$, $p=0.499$), and total GM volume ($t(194) = -0.20$, $p=0.839$). There were also no significant differences between males and females in age ($t(194)=-0.93$, $p=0.356$), full-scale IQ ($t(194)=-1.87$, $p=0.063$), mean CT ($t(194)=0.95$, $p=0.344$), or mean SULC ($t(194)=-2.80$, $p=0.006$) across diagnostic groups. As expected, total grey matter volume was significantly larger in males than in females ($t(194)=9.11$, $p<0.001$). Furthermore, across the entire sample males showed significantly greater mean SA ($t(194)=9.43$, $p<0.001$) and mean *I*Gl ($t(194)=5.56$, $p<0.001$) than females. There were no significant differences in any of these measures between TD and ASD males, or between TD and ASD females ($p<0.05$, 2-tailed).

Prediction of Biological Sex Based on Normative Variability in Cortical Morphometry

Across all four vertex based cortical features GPC was able to separate male from female TD controls at cross validated accuracies significantly above what would be expected by chance (SA 78%, $p<0.001$; CT 71%, $p<0.001$; SULC 74%, $p<0.001$; *I*Gl 77%, $p<0.001$). Using each classifiers predictive class probabilities for individuals we were able to represent normative sex based variability in brain phenotypes along a singular phenotypic axis, ranging from the female- to male-typical neurophenotype (Figure 1). For each morphological measure, the GPC model weights (w) followed a spatial pattern similar to the distribution of group differences observed between TD males and females as determined via a conventional GLM (Figure 1, Supplementary Figure 1, Supplementary Table 1).

Prediction of Biological Sex Among Individuals with ASD

When predicting biological sex for individuals with ASD we found that females with ASD were more frequently allocated to the male rather than the female class in all four models (SA 71%, p=0.002; CT 80%, p=0.002; SULC 65%, p=0.009; *I*GI 78%, p=0.001). Females with ASD were significantly allocated to the male class more frequently than would be expected based on the typical rates of misclassification for female controls (SA χ^2=26.41, p<0.001; CT χ^2=22.15, p<0.001; SULC χ^2=13.65, p<0.001; *I*GI χ^2=26.01, p<0.001). Furthermore, the mean across the predicted class probabilities for ASD females was significantly increased in females with ASD relative to female controls, indicating a shift towards male-typical morphological patterns in the brain (SA t=6.158, p<0.001; CT t=6.13, p<0.001; SULC t=4.44, p<0.001; *I*GI t=6.85, p<0.001). Across all four models there were no significant differences (p<0.05) between the predicted class probabilities for TD and ASD males, or between males and females with ASD.

ASD Probability as a Function of Normative Sex Variability in Cortical Morphometry

Within our sample we found that the number of individuals with ASD significantly increased along the female to male phenotypic axis (i.e. from female to male) as defined by predicted class probabilities. This effect was predominantly driven by the shift of females with ASD towards a more male-typical neuroanatomical brain phenotype (See Figure 2, Supplementary Figure 2). When these sample probabilities were combined with previously reported ASD prevalence rates in the general population among males (1/43, i.e. 2.3%) and females (1/190, i.e. 0.5%) (33), we found that biological females with male-typical brain morphology (0.1% estimated prevalence) were twenty six times more likely to have ASD compared to biological females with female-typical neuroanatomical phenotypes (2.6% estimated prevalence). Biological males with male-typical brain morphometry showed an estimated population prevalence of 2.4% in line with previously reported rates. However, males with female-

typical phenotypes showed a reduced prevalence estimate for ASD (1.9%) indicative of a 'female protective effect' in relation to brain anatomy (see Supplementary Table 2).

Predictive maps identifying patterns of neuroanatomical variability associated with high and low probability of ASD across sexes are shown in Figure 3. While a similar set of brain regions conferred high (and low) probability for ASD in men and women within features, certain brain regions were unique to or differed in sign between particular risk groups and sexes. For example, negative predictive mapping values for CT in the left parahippocampal gyrus and SULC in the superior temporal gyrus were observed across all males and high-probability females, while low probability females showed positive values in these regions. For predictive mapping measures of SA and fGI, regions of the inferior and superior temporal gyri appear to show a sex-specific relationship with high probability males showing negative values compared to positive values amongst females and low probability males. This indicates that morphometric measures in particular brain regions that are important for classifying sex differences differ between individuals with high and low risk for ASD and may be sex-specific.

Cortical Morphometry in ASD is Modulated by Biological Sex

Lastly, we used a conventional GLM to test for significant between-group differences and diagnosis-by-group interactions in the four examined morphometric features. Overall, we found that measures of CT, SA, and fGI in ASD were significantly modulated by biological sex (Figure 4, also Supplementary Figure 3). Such group-by-sex interactions therefore need to be taken into account when interpreting main effects of group. Significant group-by-sex interactions in measures of CT were observed across the temporal lobe, including the fusiform and parahippocampal gyri. Across this cluster the degree of CT abnormality in females with ASD exceeded those of males, despite no differences in measures of ASD

symptom severity (9). Additionally, group-by-sex interactions were observed for measures of SA and *G*yi in the medial orbital frontal cortex showing decreases in females with ASD and increases in males with ASD. Statistical details of these clusters are provided in Supplementary Table 3.

Discussion

The present study builds upon a previous 'proof-of-concept' suggesting that probability of ASD increases significantly from a characteristic female to male neuroanatomical brain phenotype (9). In this prior study, which examined measures of cortical thickness (CT) only, the increase in ASD probability was predominantly driven by a phenotypic shift of the brain in females with ASD towards a male-typical neurophenotype (9). In the current study, we show that this phenotypic shift is not restricted to measures of CT, but generalizes to other cortical features including vertex-wise estimates of surface area (SA), the local gyrification index (*G*yi), and sulcal depth (SULC). The findings of the present study therefore not only support our original report in suggesting that male-typical neuroanatomical characteristics carry a higher probability for ASD than female-typical characteristics, but further show this effect to be broadly and consistently related across multiple measures of cortical morphometry.

The extension of our approach to include multiple morphometric features is of crucial importance as there is evidence to suggest that different cortical features are etiologically and phenotypically distinct. For example, it has been shown that measures of CT and SA (*i*) are mediated by different sets of genes (35), (*ii*) have different developmental trajectories (36), and (*iii*) represent distinct aspects of the cortical architecture (37). Therefore, the observation that the phenotypic shift of the brain in ASD females is consistent across morphometric features may indicate the existence of a common underlying mechanism, such as atypical

cortical neurogenesis and migration (38), that steers multiple aspects of brain anatomy towards a similar phenotypic endpoint overall. Yet, the neuroanatomical patterns associated with the prediction of biological sex, and the patterns carrying high/low ASD probability in males and females, differed in sign and regional distribution between the cortical features. Thus, while there may be a common etiology for the phenotypic differences in brain anatomy in ASD within the sexes, our findings are consistent with the notion that sex differentiation mechanisms in the brain have region specific effects (for review see (39, 40)). Therefore, differences in these neuroanatomical patterns associated with high probability for ASD may be beneficial in identifying brain regions where sexual differentiation may contribute to male preponderance in ASD.

Moreover, we established that the neuroanatomy of ASD in some regions of the brain is modulated by biological sex by examining sex-by-diagnosis interactions for multiple cortical features. This suggests that in these brain regions (*i*) there are not only quantitative differences in the degree of neuroanatomical abnormality between males and females with ASD and their respective normative population, but also that (*ii*) ASD potentially interacts with sexually-differential neurobiological phenotypes to give rise to qualitative differences in brain anatomy between males and females with the condition. This is also relevant in view of a recent genetic study, suggesting that while ASD risk genes are expressed at similar levels in males and females, the impact of these genes is likely modulated by their interactions with sex-differential processes (e.g. in cortical microglia and/or astrocytes) that may play a critical role in setting males at a greater risk for ASD (41). An individual's risk or probability of ASD is therefore not only dependent on genetic load itself, but also on naturally occurring sex-differential biological pathways.

With respect a biological organ as complex as the brain it has been suggested that on a phenotypic level, the brain should be considered a 'mosaic' of regions that differ between

degrees of relative maleness or femaleness, or not at all (i.e. unisex), resulting in a potentially infinite variety of brain phenotypes both within and between sexes (39, 40). In order to identify an individual's position on such a multi-dimensional 'spectrum' of sex-related phenotypic variability, it is important to develop analytical frameworks that can accommodate inter-individual phenotypic diversity within and across the binary categories dictated by biological sex, such as the probabilistic multivariate pattern classification approach utilized in the present study (see also (9)). In this way we were able to estimate an individual's risk of ASD based on phenotypic, rather than biological sex and in doing so demonstrated that an individual's probability for developing ASD may vary from as much as 0.1 to 2.6% in the general population depending on having a female- or male-typical neuroanatomical phenotype, in addition to being biologically male or female. Our approach to modeling normative sex-related phenotypic diversity may therefore be extended to various additional phenotypic features in the future, and to contribute to the development of multivariate disease liability models for complex neurobiological phenotypes.

Despite the advantages of the current approach over the original proof-of-concept study, a number of limitations remain. Most importantly, it is crucial to highlight that while we were able to show a statistical association between normative sex-related phenotypic diversity in brain structure and ASD probability, this relationship should not be interpreted as being 'causal'. Future studies will be needed to uncover the genetic and/or neurobiological mechanisms underpinning this relationship (e.g. (41-43)). Second, due to the limited range of clinical/behavioral measures acquired in the current study, we were unable to determine the functional relevance of our findings. In the future it will be crucial to identify how diversity in normative sex-related morphometric phenotypes relates to sex-differences in general cognitive and/or behavioral profiles (44, 45), or to different clinical ASD phenotypes (3, 4, 6, 7). Last, our study was based on a sample of adults with ASD without learning disability using a cross-sectional study design. The fact that our sample is not representative of the

entire ASD population limits the generalizability of our sample probability estimates for ASD to the general population. Furthermore, our population estimations are based on previously reports of male preponderance in ASD being roughly a 4:1 male to female ratio (33), however other studies have shown this ratio may actually to be closer to 2:1 (8). The nature of our sample means farther studies will thus be required to (*i*) replicate our findings in other subgroups on the autism spectrum (e.g. in children and adolescents, or individuals with a learning disability), and (*ii*) to identify how stable (or variable) our neuroanatomical indicators of biological sex are across different stages of development.

Conclusions

Taken together, our findings suggest that the male-typical neurobiological brain phenotype carries a higher probability for ASD than the female-typical phenotype across the binary categories dictated by biological sex, and across a range of neuroanatomical features that include both volumetric as well as geometric measures. In addition to genetic and environmental factors, multiple morphometric features characteristic of normative phenotypic diversity in brain structure should therefore be considered when investigating risk and resilience for ASD.

Table 1. Participant Demographics and Global Brain Measures

	ASD (n = 98)	TD Control (n = 98)
Male Participants (n = 100)	n = 49	n = 51
Age [years]	26.16 ± 7.2 (18 - 41)	27.22 ± 5.58 (18 - 42)
Full-scale IQ (WASI)	112.61 ± 12.27 (89 - 135)	114.67 ± 10.88 (93 - 137)
Verbal IQ	110.51 ± 13.01 (83 - 137)	109.86 ± 11.03 (88 - 137)
Performance IQ	112.00 ± 13.65 (85 - 138)	116.74 ± 10.90 (93 - 133)
ADI-R Social	17.57 ± 5.50 (10 - 28)	-
ADI-R Communication	13.86 ± 4.16 (8 - 24)	-
ADI-R Repetitive Behavior	4.96 ± 2.37 (1 - 10)	-
ADOS Social + Communication	9.43 ± 4.39 (1 - 21)	-
ADOS Stereotypic Behaviour	1.27 ± 1.27 (0 - 5) *	-
Mean Cortical Thickness [mm]	2.35 ± 0.10	2.33 ± 0.10
Mean Surface Area	0.7680 ± 0.71	0.7683 ± 0.05
Mean local Gyrification Index	3.04 ± 0.12	3.04 ± 0.10
Mean Sulcal Depth	0.0341 ± 0.007	0.0356 ± 0.006
Total Grey Matter Volume [litre]	0.76 ± 0.08	0.76 ± 0.05
Total Intracranial Volume [litre]	1.59 ± 0.21	1.58 ± 0.17

Female Participants (n = 96)	n = 49	n = 47
Age [years]	27.60 ± 7.12 (18 - 48)	27.60 ± 7.31 (19 - 52)
Verbal IQ*	116.60 ± 12.15 (76 - 144)	117.83 ± 8.81 (96 - 135)
Performance IQ*	110.56 ± 14.50 (67 - 138)	114.38 ± 8.26 (96 - 128)
Full-scale IQ (WASI)	114.88 ± 12.36 (84 - 136)	118.38 ± 7.32 (99 - 129)
ADI-R Social	16.32 ± 4.24 (10 - 26)	-
ADI-R Communication	12.43 ± 3.96 (7 - 22)	-
ADI-R Repetitive Behavior	4.36 ± 1.98 (1 - 9)	-
ADOS Social + Communication	7.71 ± 5.28 (0 - 19)	-
ADOS Stereotypic Behaviour	0.75 ± 0.97 (0 - 3) *	-
Mean Cortical Thickness [mm]	2.32 ± 0.11	2.34 ± 0.10
Mean Surface Area	0.6895 ± 0.05	0.6865 ± 0.06104
Mean local Gyrification Index	2.95 ± 0.09	2.96 ± 0.10
Mean Sulcal Depth	0.0378 ± 0.008	0.0380 ± 0.007
Total Grey Matter Volume [litre]	0.67 ± 0.06	0.68 ± 0.06
Total Intracranial Volume [litre]	1.32 ± 0.18	1.32 ± 0.17

Note. Data expressed as mean ± standard deviation (range). There were no significant between-group differences in age, FSIQ, mean cortical thickness, total grey matter volume, or

total intracranial volume ($p<0.05$, two-sided). ADI-R values based on 49 males and 44 females with ASD. ADOS values based on 49 males and 48 females. * statistically significant between males and females based on $p<0.05$, two-sided ($t(95)=2.23$, $p=0.028$). ^ verbal and performance IQ data was not available for one ASD female

Figure 1. Gaussian Process Classification of Biological Sex: The results of Gaussian Process Classification (GPC) according to biological sex categories are shown for each of the four cortical features investigated: (A) cortical thickness (CT), (B) surface area (SA), (C) the local gyrification index (lGI), and (D) sulcal depth (SULC). Each model was able to separate TD males from females at accuracies significantly above what would be expected by chance (top left). When these models of normative sex differences in cortical morphology where applied to males and females with ASD, females with ASD were more frequently classified to the male class (bottom left) indicating a male-typic morphological presentation amongst females with ASD. Spatial representations of each discriminative model (i.e. weight vectors) are shown (right). These patterns largely corresponded with brain regions that differed between TD males and females as identified using a conventional general linear model (see supplementary Figure 1).

Figure 2. Probability for ASD as a Function of Normative Sex-Related Phenotypic Variability in Brain Morphology: Probability estimates for ASD across eight discrete bins along the axis of probabilistic class predictions for biological sex are plotted for (A) biological females and (B) males. Each individual's probabilistic class prediction was calculated as the mean prediction across all four classification models. Probability for ASD was seen to increase along with increasingly male-typic class predictions. This relationship was particularly apparent in females due to the statistically significant shift in females with ASD towards the male-typic neuroanatomical phenotype.

Figure 3. Prediction Maps for High and Low ASD Probability Males and Females: Prediction maps highlighting brain regions most relevant to classifying biological sex among high and low risk males and females are shown for each cortical feature. (A) cortical thickness (CT), (B) surface area (SA), (C) local gyrification index (lGI), and (D) sulcal depth (SULC). For male and female individuals high and low probability groups were determined according to class probabilities with <0.5 (i.e. female-typic) indicating low and >0.5 (i.e.

male-typic) indicating high probability. For each subgroup the product of the decision function for classifying biological sex (w) and each individual's data (x_i) was calculated. Mean values at each vertex were then used to summarize maps within subgroups.

Figure 4. Group by Sex Interaction Effects in Cortical Morphometry: Clusters of significant (RFT $p<0.5$) group x sex interactions in (A) cortical thickness (CT), (B) surface area (SA), and (C) the local gyrification index (*l*GI). No significant group x sex interactions were observed in measures of sulcal depth (SULC). Statistical details of these clusters are provided in Supplementary Table 3.

References

1. Lai M-C, Lombardo MV, Auyeung B, Chakrabarti B, Baron-Cohen S. Sex/gender differences and autism: setting the scene for future research. Journal of the American Academy of Child & Adolescent Psychiatry. 2015; 54(1):11-24.

2. Fombonne E. Epidemiology of Pervasive Developmental Disorders. Pediatr Res. 2009; 65(6):591-598.

3. Szatmari P, Liu XQ, Goldberg J, Zwaigenbaum L, Paterson AD, Woodbury-Smith M, et al. Sex differences in repetitive stereotyped behaviors in autism: implications for genetic liability. American Journal of Medical Genetics Part B: Neuropsychiatric Genetics. 2012; 159(1):5-12.

4. Bölte S, Duketis E, Poustka F, Holtmann M. Sex differences in cognitive domains and their clinical correlates in higher-functioning autism spectrum disorders. Autism. 2011; 15(4):497-511.

5. Dworzynski K, Ronald A, Bolton P, Happe F. How different are girls and boys above and below the diagnostic threshold for autism spectrum disorders? J Am Acad Child Adolesc Psychiatry. 2012; 51(8):788-797.

6. Mandy W, Chilvers R, Chowdhury U, Salter G, Seigal A, Skuse D. Sex differences in autism spectrum disorder: evidence from a large sample of children and adolescents. Journal of autism and developmental disorders. 2012; 42(7):1304-1313.

7. Solomon M, Miller M, Taylor SL, Hinshaw SP, Carter CS. Autism symptoms and internalizing psychopathology in girls and boys with autism spectrum disorders. Journal of autism and developmental disorders. 2012; 42(1):48-59.

8. Werling DM. The role of sex-differential biology in risk for autism spectrum disorder. Biology of Sex Differences. 2016; 7(1):58.

9. Ecker C, Andrews DS, Gudbrandsen CM, et al. Association between the probability of autism spectrum disorder and normative sex-related phenotypic diversity in brain structure. JAMA Psychiatry. 2017; 74(4):329-338.

10. Marquand AF, Brammer M, Williams SC, Doyle OM. Bayesian multi-task learning for decoding multi-subject neuroimaging data. NeuroImage. 2014; 92:298-311.

11. Sowell ER, Peterson BS, Kan E, Woods RP, Yoshii J, Bansal R, et al. Sex differences in cortical thickness mapped in 176 healthy individuals between 7 and 87 years of age. Cerebral cortex. 2007; 17(7):1550-1560.

12. Im K, Lee J-M, Lee J, Shin Y-W, Kim IY, Kwon JS, et al. Gender difference analysis of cortical thickness in healthy young adults with surface-based methods. Neuroimage. 2006; 31(1):31-38.

13. Wallace GL, Dankner N, Kenworthy L, Giedd JN, Martin A. Age-related temporal and parietal cortical thinning in autism spectrum disorders. Brain. 2010; 133(12):3745-3754.

14. Ecker C, Ginestet C, Feng Y, Johnston P, Lombardo MV, Lai M-C, et al. Brain Surface Anatomy in Adults With Autism - The Relationship Between Surface Area, Cortical Thickness, and Autistic Symptoms. JAMA psychiatry. 2013; 70(1):59-70.

15. Cahill L. A New Link Between Autism and Masculinity. Jama psychiatry. 2017; 74(4):318.

16. Ecker C, Andrews D, Dell'Acqua F, Daly E, Murphy C, Catani M, et al. Relationship Between Cortical Gyrification, White Matter Connectivity, and Autism Spectrum Disorder. Cerebral Cortex. 2016; 26(7): 3297-3309.

17. Schaer M, Ottet M-C, Scariati E, Dukes D, Franchini M, Eliez S, et al. Decreased frontal gyrification correlates with altered connectivity in children with autism. Frontiers in human neuroscience. 2013; 7:161-173.

18. Nordahl CW, Dierker D, Mostafavi I, Schumann CM, Rivera SM, Amaral DG, et al. Cortical Folding Abnormalities in Autism Revealed by Surface-Based Morphometry. The Journal of Neuroscience. 2007; 27(43):11725-11735.

19. Lord C, Rutter M, Couteur A. Autism Diagnostic Interview-Revised: a revised version of a diagnostic interview for caregivers of individuals with possible pervasive developmental disorders. Journal of autism and developmental disorders. 1994; 24(5):659-685.

20. Lord C, Risi S, Lambrecht L, Cook Jr EH, Leventhal BL, DiLavore PC, et al. The Autism Diagnostic Observation Schedule—Generic: A standard measure of social and communication deficits associated with the spectrum of autism. Journal of autism and developmental disorders. 2000; 30(3):205-223.

21. Wechsler D. Wechsler abbreviated scale of intelligence: Psychological Corporation; 1999.

22. Deoni SC, Williams SC, Jezzard P, Suckling J, Murphy DG, Jones DK. Standardized structural magnetic resonance imaging in multicentre studies using quantitative T1 and T2 imaging at 1.5 T. Neuroimage. 2008; 40(2):662-671.

23. Ecker C, Suckling J, Deoni SC, Lombardo MV, Bullmore ET, Baron-Cohen S, et al. Brain Anatomy and Its Relationship to Behavior in Adults With Autism Spectrum Disorder. Archives of General Psychiatry. 2012; 69(2):195-209.

24. Dale AM, Fischl B, Sereno MI. Cortical surface-based analysis: I. Segmentation and surface reconstruction. Neuroimage. 1999; 9(2):179-194.

25. Fischl B, Sereno MI, Dale AM. Cortical surface-based analysis: II: Inflation, flattening, and a surface-based coordinate system. Neuroimage. 1999; 9(2):195-207.

26. Ségonne F, Dale A, Busa E, Glessner M, Salat D, Hahn H, et al. A hybrid approach to the skull stripping problem in MRI. Neuroimage. 2004; 22(3):1060-1075.

27. Jovicich J, Czanner S, Greve D, Haley E, van der Kouwe A, Gollub R, et al. Reliability in multi-site structural MRI studies: effects of gradient non-linearity correction on phantom and human data. Neuroimage. 2006; 30(2):436-443.

28. Fischl B, Dale AM. Measuring the thickness of the human cerebral cortex from magnetic resonance images. Proceedings of the National Academy of Sciences. 2000; 97(20):11050-11055.

29. Winkler AM, Sabuncu MR, Yeo B, Fischl B, Greve DN, Kochunov P, et al. Measuring and comparing brain cortical surface area and other areal quantities. NeuroImage. 2012; 61(4):1428-1443.

30. Schaer M, Cuadra MB, Tamarit L, Lazeyras F, Eliez S, Thiran J. A surface-based approach to quantify local cortical gyrification. Medical Imaging, IEEE Transactions on. 2008; 27(2):161-170.

31. Rasmussen CE, Williams CKI. Gaussian processes for machine learning: MIT press Cambridge, MA; 2006.

32. Marquand A, Howard M, Brammer M, Chu C, Coen S, Mourão-Miranda J. Quantitative prediction of subjective pain intensity from whole-brain fMRI data using Gaussian processes. NeuroImage. 2010; 49(3):2178-2189.

33. Baio J. Prevalence of autism spectrum disorder among children aged 8 years - autism and developmental disabilities monitoring network, 11 sites, United States, 2010. MMWR Surveill Summ. 2014; 63(2):1-21.

34. Worsley K, Andermann M, Koulis T, MacDonald D, Evans A. Detecting changes in nonisotropic images. Human brain mapping. 1999; 8(2-3):98-101.

35. Panizzon MS, Fennema-Notestine C, Eyler LT, Jernigan TL, Prom-Wormley E, Neale M, et al. Distinct genetic influences on cortical surface area and cortical thickness. Cerebral Cortex. 2009; 19(11):2728-2735.

36. Ecker C, Shahidiani A, Feng Y, Daly E, Murphy C, D'Almeida V, et al. The effect of age, diagnosis, and their interaction on vertex-based measures of cortical thickness and surface area in autism spectrum disorder. Journal of Neural Transmission. 2014; 121(9):1157-1170.

37. Rakic P. A small step for the cell, a giant leap for mankind: a hypothesis of neocortical expansion during evolution. Trends in neurosciences. 1995; 18(9):383-388.

38. Casanova MF. Autism as a sequence: from heterochronic germinal cell divisions to abnormalities of cell migration and cortical dysplasias. Medical hypotheses. 2014; 83(1):32-3

39. McCarthy MG, De Vries; Forger, Nancy. Sexual Differentiation of the Brain: A Fresh Look at Mode, Mechanisms, and Meaning. Hormones, Brain and Behavior. 5. 3rd ed. Oxford: Academic Press; 2017. p. 3-32.

40. McCarthy MM, Konkle AT. When is a sex difference not a sex difference? Frontiers in neuroendocrinology. 2005; 26(2):85-102.

41. Werling DM, Parikshak NN, Geschwind DH. Gene expression in human brain implicates sexually dimorphic pathways in autism spectrum disorders. Nature communications. 2016;7.

42. Baron-Cohen S, Auyeung B, Norgaard-Pedersen B, Hougaard D, Abdallah M, Melgaard L, et al. Elevated fetal steroidogenic activity in autism. Molecular psychiatry. 2015; 20(3):369-376.

43. Lai MC, Lerch JP, Floris DL, Ruigrok AN, Pohl A, Lombardo MV, et al. Imaging sex/gender and autism in the brain: Etiological implications. Journal of Neuroscience Research. 2017; 95(1-2):380-397.

44. Miller DI, Halpern DF. The new science of cognitive sex differences. Trends in cognitive sciences. 2014; 18(1):37-45.

45. Hyde JS. Sex and cognition: gender and cognitive functions. Current opinion in neurobiology. 2016; 38:53-56.

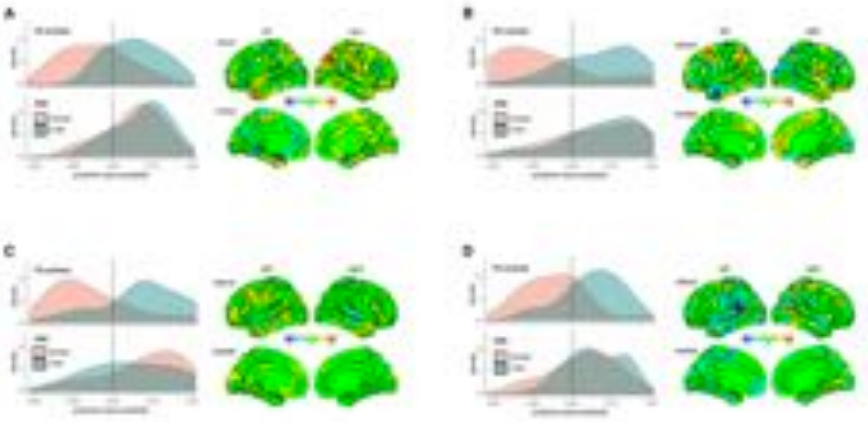

296x209mm (300 x 300 DPI)

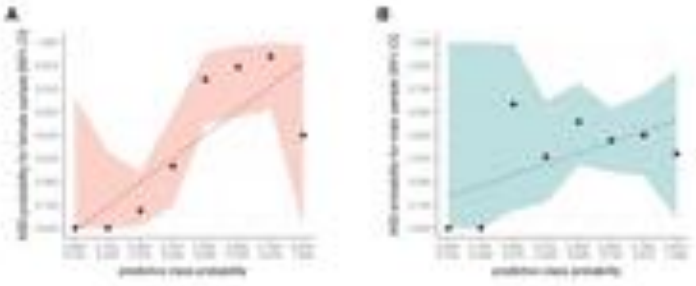

296x209mm (300 x 300 DPI)

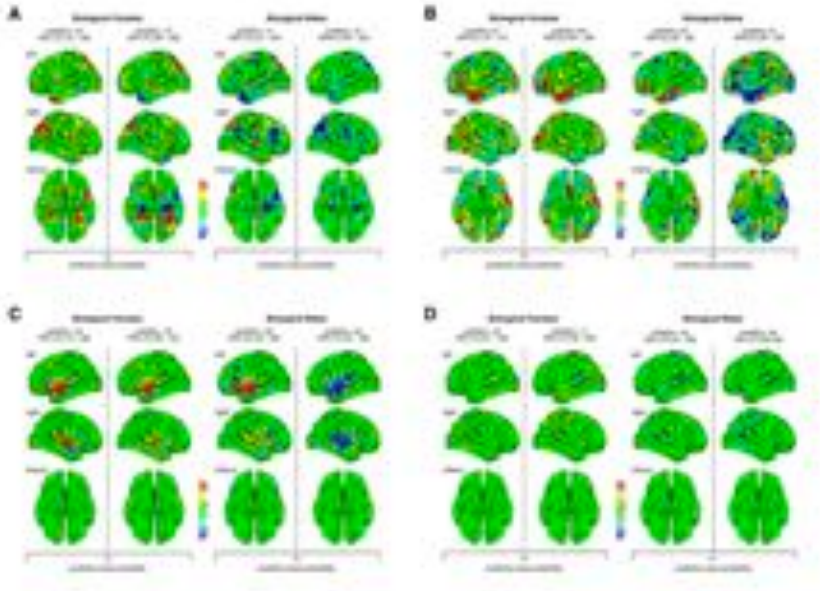

296x209mm (300 x 300 DPI)

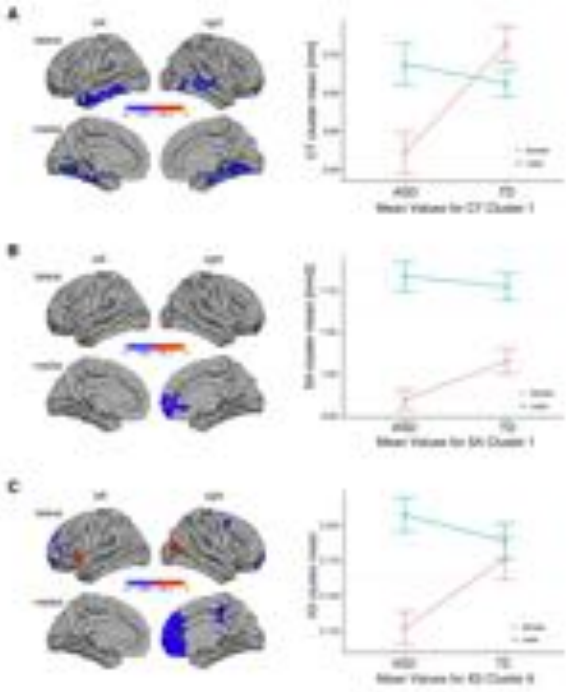

209x296mm (300 x 300 DPI)